

PONTIFÍCIA UNIVERSIDADE CATÓLICA DO PARANÁ

MARCELO PINTO DA SILVA

**ENRICHED MODIFIED LOCAL GREEN'S FUNCTION METHOD
APPLIED TO ELASTO STATIC PROBLEMS**

**CURITIBA
August 2018**

PONTIFÍCIA UNIVERSIDADE CATÓLICA DO PARANÁ

MARCELO PINTO DA SILVA

**ENRICHED MODIFIED LOCAL GREEN'S FUNCTION METHOD
APPLIED TO ELASTO STATIC PROBLEMS**

Tese apresentada como requisito parcial à obtenção do grau de Doutor em Engenharia Mecânica, Curso de Pós-Graduação em Engenharia Mecânica, Escola Politécnica, Pontifícia Universidade Católica do Paraná.

Orientador:

Prof. João Elias Abdalla Filho, Ph. D

Coorientador:

Prof. Roberto Dalledone Machado, Ph. D

**CURITIBA
August 2018**

Dados da Catalogação na Publicação
Pontifícia Universidade Católica do Paraná
Sistema Integrado de Bibliotecas – SIBI/PUCPR
Biblioteca Central
Luci Eduarda Wielganczuk – CRB 9/1118

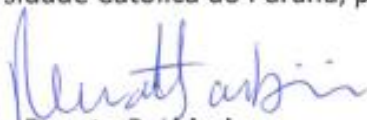
S586e 2018	<p>Silva, Marcelo Pinto</p> <p>Enriched modified local Green's function method applied to elasto static problems / Marcelo Pinto da Silva ; orientador: João Elias Abdalla Filho ; coorientador: Roberto Dalledone Machado. – 2018. 250 f. f. : il. ; 30 cm</p> <p>Tese (doutorado) – Pontifícia Universidade Católica do Paraná, Curitiba, 2018 Bibliografia: f. 198-227</p> <p>1. Engenharia Mecânica. 2. Green, Funções de. 3. Método dos elementos finitos, I. Abdalla Filho, João Elias. II. Machado, Roberto Dalledone. III. Pontifícia Católica do Paraná. Programa de Pós-Graduação em Engenharia Mecânica. IV. Título.</p> <p>CDD 22. ed. 620.1</p>
---------------	----------------------------------------------------------------------------------------------------------------------------------------------------------------------------------------------------------------------------------------------------------------------------------------------------------------------------------------------------------------------------------------------------------------------------------------------------------------------------------------------------------------------------------------------------------------------------------------------------------------------------------------------------------------------

TERMO DE APROVAÇÃO

MARCELO PINTO DA SILVA

Enriched Modified Local Green's Function Method Applied to Elasto Static Problems

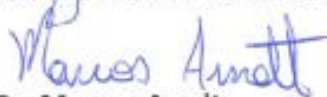
Tese aprovada como requisito parcial para obtenção do grau de doutor no Curso de Doutorado em Engenharia Mecânica, Programa de Pós-Graduação em Engenharia Mecânica, da Escola Politécnica da Pontifícia Universidade Católica do Paraná, pela seguinte banca examinadora:



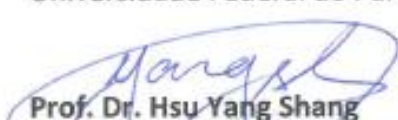
Prof. Dr. Renato Barbieri
Universidade do Estado de Santa Catarina, UDESC



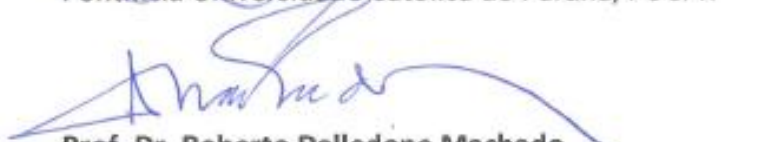
Prof. Dr. Jucélio Tomás Pereira
Universidade Federal do Paraná, UFPR



Prof. Dr. Marcos Arndt
Universidade Federal do Paraná, UFPR



Prof. Dr. Hsu Yang Shang
Pontifícia Universidade Católica do Paraná, PUCPR



Prof. Dr. Roberto Dalledone Machado
Universidade Federal do Paraná, UFPR, Co-Orientador



Presidente: **Prof. Dr. João Elias Abdalla Filho**
Pontifícia Universidade Católica do Paraná, PUCPR - Orientador

Curitiba, 27 de agosto de 2018



Abstract

The aim of this work is to present and apply “The Enriched Modified Local Green’s Function Method” (EMLGFM). Its precursor, “The Modified Local Green’s Function Method” (MLGFM) has been extensively employed during last decades to solve a large number of solid mechanics problems. The MLGFM is an integral method that uses projections of appropriate Green’s functions on subspaces generated by finite and boundary interpolation functions instead of a fundamental solution to be applied in a boundary system. Standard Lagrange shape functions are commonly used as these interpolation functions to approximate the solution space. In parallel, many efforts have been made in last decades to improve the well-established technique called “The Finite Element Method” (FEM). Among those improvements and enriched methods, the Hierarchical Finite Element Method and the Generalized Finite Element Method deserve to be highlighted. This work applies Hierarchical and Generalized Finite Element techniques into the Modified Local Green’s Function Method aiming to enrich the solution space of this new method now named as “The Enriched Modified Local Green’s Function Method”. Some two-dimensional (2D) elasto static problems are employed to test and investigate this new technique. This novel method is compared to some well-established methods, such as MLGFM and FEM as well as the analytical solution, presenting good displacement, stresses and convergence rate results.

Keywords: Modified local Green’s function method; Hierarchical finite element method; Generalized finite element method; Lobatto shape functions; Trigonometric shape functions; Two-dimensional elasto static problems.

*To my dad, Edvaldo.
To my mom, Conceição.*

*“Know thyself, accept thyself, overcome thyself”.
Saint Augustine*

Acknowledgments

First and above everything, I would like to thank you, God! “There is nothing I cannot do in the One who strengthens me”. *Phillippians 4, 13*.

I wish to thank my brilliant mentors and advisors, Prof. Roberto Dalledone Machado and Prof. João Elias Abdalla Filho. To my dear Prof. Roberto, you are a mentor, a friend, a great inspiration. Thank you very much for your attention, patience and dedication with me. To my dear Prof. João Elias, thank you very much for accepting me at NuPES! Because of that, I’m here right now writing these few words! And, thank you for accepting me as your doctoral student. Both of you are remarkable professionals, teachers, persons.

I would like to thank CAPES that supported this study financing it in part by the Coordenação de Aperfeiçoamento de Pessoal de Nível Superior - Brasil (CAPES) - Finance Code 001!

To my mom and my dad, Conceição and Edvaldo, how can I thank you for being the instrument in giving me life? There is nothing I can do to compensate that! Despite being far from me (in a space context only), you have always supported me with your prayers, supportive words, with your own life’s experience and example.

I would like to give special thanks to my family, firstly my sisters Karina and Larissa for your prayers and supportive words. My aunt Maria and my cousins here in Curitiba, thank you for listening to me in all desperate moments and for always supporting me.

I want to thank my wonderful girlfriend Débora, for your patience (and patience and more patience) and, mainly, for your love. You are my safe harbor, my blue sky, and the best of my days! Everything is gonna be “allys-brown” with

you! To all your family, Mr. Zatoni and Mrs. Déda, your sister Ana Paula e your brother-in-law Marcelão, and little Maria Alice, you are part of my accomplishment. Thank you very much for your prayers, your care, and your support.

I offer my deepest gratitude to all my friends from Volvo, in special; I would like to express my gratitude to Elpídio Narde and Maurício Capucho. Elpídio, thank you! You have always supported me. You are a great leader and an inspiring person. Maurício, you supported me in one of the most difficult periods of my life. I know you overcame yourself, looked at me with all kindness, more than a manager but as a friend. Thank you very much for your support and comprehension. And now, almost in the end, I need to express my gratitude also to Jones Gioppo for your support and comprehension (and still representing all my friends from the worldwide band “GlobeRockers”). Without that, this thesis wouldn’t be completed.

I am also very thankful to my friends from PUC-PR, specially my dear PPGEM, I would like to thank you, Prof. Yang Shang Hsu, for your precious advices and Mrs. Jane Marques da Rocha, representing all the great people from this noble department!

Besides, I would like to thank my coach and friend Divina Marisa. You shed some light along my very rough road and guided me in one of my most challenging fight, against the most arduous competitor: myself. You fought difficult battles and won every single of them too. You are a being of light!

And the last but not the least, I feel deeply fortunate to have had the company of my wonderful friend Serena. I know you are not a human being. Actually, you are an angel, sent by God to protect me, to be my loyal companion. There is no other better dog in the Universe, absolutely!

Table of Contents

Abstract	iv
Table of Contents	ix
List of Figures	xii
List of Tables	xvi
Abbreviation and Acronyms	xviii
List of Symbols	xxi

Chapter 1

Introduction

1.1	OPENING DISCUSSION.....	1
1.2	OBJECTIVES AND METHODOLOGY	5
1.2.1	Main Objective	5
1.2.2	Specific Objectives and Methodology.....	5
1.3	OUTLINE OF THIS WORK.....	6

Chapter 2

Literature Review

2.1	INTRODUCTION	8
2.2	REVIEW OF THE ENRICHED METHODS.....	9
2.3	REVIEW OF THE MODIFIED LOCAL GREEN'S FUNCTION METHOD ...	47

Chapter 3

Enriched Finite Element Methods: HFEM and GFEM

3.1	Introduction	53
3.2	ENRICHED METHODS.....	55
3.2.1	The Hierarchical Finite Element Method (HFEM)	55
3.2.2	The Generalized Finite Element Method (GFEM)	60
3.2.2.1	The partition of unity method (PUM)	61
3.2.2.2	GFEM generalization	66
3.3	THE ELEMENT'S ENRICHMENT: 1D LINEAR ELEMENT AND 2D BILINEAR ELEMENT	71

Chapter 4

The Modified Local Green's Function Method

4.1	INTRODUCTION	79
4.2	THE MLGFM: ABSTRACT ANALYSIS	81
4.2.1	Notations and Preliminary Concepts	81
4.2.2	The MLGFM Abstract Formulation	86
4.3	THE MLGFM VARIATIONAL FORMULATION.....	89
4.4	THE FORMALISM OF THE MLGFM	92
4.4.1	Integral Equations	92
4.4.2	Integral Equations Approximation.....	96
4.4.3	The Green's Function Projections Determination.....	101
4.4.4	Matrices Implementation and Equation System Calculation.....	108

Chapter 5

Enriched Modified Local Green's Function Methodology for Elasto Static

5.1	INTRODUCTION	111
5.2	EMLGFM FORMALISM TO ELASTO STATIC	112
5.3	GREEN'S FUNCTION PROJECTIONS DETERMINATION.....	115
5.3.1	Green's Matrices General Characteristics.....	115
5.3.2	Green's Function Projections Approximation.....	120
5.4	MLGFM's MATRICES FOR THE ENRICHED CASE	130
5.5	DISPLACEMENTS, REACTION FORCES AND STRESSES CALCULATION	133

Chapter 6

Enriched Modified Local Green's Function Method Applications for Elasto Static Problems

6.1	INTRODUCTION	135
6.2	APPLICATIONS, RESULTS AND DISCUSSIONS	136
6.2.1	Straight Cantilever Beam.....	139
6.2.2	Curved Cantilever Beam.....	154
6.2.3	Thick-Walled Cylinder	160
6.2.4	Rectangular Plate with a Center Hole.....	164
6.2.5	Rectangular Plate with a Center Crack	170
6.2.6	L-Shaped Domain with a Singularity.....	178

Chapter 7

Conclusions and Recommendations for Future Work

7.1	SUMMARY	193
-----	---------------	-----

References	198
-------------------------	-----

Appendix A

A.1	SOME TOPICS IN FUNCTIONAL ANALYSIS	228
A.2	BOUNDARY-VALUE PROBLEMS (BVP).....	233
A.3	VARIATIONAL BOUNDARY-VALUE PROBLEMS (VBVP)	235
A.4	APPROXIMATED METHODS FOR BOUNDARY-VALUE PROBLEMS	237
A.4.1	The Finite Element Method.....	240
A.4.2	The Boundary Element Method.....	242
A.4.3	The Modified Local Green's Function Method	242

Appendix B

B.1	ELASTO STATIC CLASSIC RELATIONS	244
B.1.1	Plane Strain Problems	247
B.1.2	Plane Stress Problems	248

Appendix C

C.1	THE EMLGFM ALGORITHM FLOWCHART.....	250
-----	-------------------------------------	-----

List of Figures

Figure 1.1 – Pythagoras in a detail of Raphael's fresco “The School of Athens”. SOURCE: Wikipedia (2018).....	2
Figure 3.1 – HFEM shape functions used in this work: first six Lobatto shape functions (Šolín <i>et al.</i> , 2004).	60
Figure 3.2 – FEM linear hat functions as a partition of unity – PoU. SOURCE: Adapted from Torii (2012).	65
Figure 3.3 – Construction of an enriched shape function (also known as a “generalized FEM shape function”) using the Partition of Unity Method (PUM): schematic representation. SOURCE: Duarte and Kim (2008).	67
Figure 3.4 – GFEM enriched shape functions for $\beta = \pi$	70
Figure 3.5 – A non-compatible and a compatible edge shared by two finite elements.	72
Figure 3.6 – A 1D linear element with local coordinate $\xi = [-1, 1]$	73
Figure 3.7 – An example of the vertex and bubble shape functions for a 1D element, $k = 2$	74
Figure 3.8 – A 2D quadrilateral finite element with local coordinates $\xi = [-1, 1]$ and $\eta = [-1, 1]$	75
Figure 3.9 – An example of the vertex, edge and bubble shape functions for a 2D element, $k = 2$	77
Figure 4.1 – Spaces, differential operators and bilinear forms. SOURCE: Adapted from Machado (1992).	84
Figure 4.2 – Dirac Delta excitation: a) in domain; b) on boundary. SOURCE: Adapted from Machado (1992).	87
Figure 4.3 – Physical interpretation of the modified auxiliary problem. SOURCE: Adapted from Barbieri (1992).	94

Figure 4.4 – Approximation of a real domain: a) a real domain Ω ; b) the finite elements mesh Ω^k and c) the boundary elements mesh $\partial\Omega^k$. SOURCE: Adapted from Machado (1992).....	97
Figure 4.5 – Projections determination: physical interpretation of the solution in two distinct steps (by FEM). SOURCE: Adapted from Barbieri (1992).	104
Figure 4.6 – MLGFM equation system: simplified calculation steps flowchart. .	110
Figure 5.1 – Boundary conditions for an arbitrary domain Ω . SOURCE: Adapted from Barbieri (1992).	114
Figure 5.2 – A conventional and enriched MLGFM problem discretized with only 1 finite element in domain and 4 boundary elements on boundary.	130
Figure 5.3 – A conventional and enriched MLGFM problem discretized with 4 finite elements in domain and 8 boundary elements on boundary.	131
Figure 5.4 – Standard $[K_{\text{FEM}}]$ and enriched $[K_{\text{ENR}}]$ stiffness matrix.	132
Figure 6.1 – Type of elements used in this work: 2D bilinear and biquadratic as well as 1D linear and quadratic elements.....	137
Figure 6.2 – The straight cantilever beam: geometric properties.	140
Figure 6.3 – Domain and boundary meshes for straight cantilever beam. Double node considered at corners.	142
Figure 6.4 – Straight cantilever beam: problem (a) - regular shape elements; problem (b) - trapezoidal shape elements; problem (c) - parallelogram shape elements. Length = 6.0; width (height) = 0.2; depth (thickness) = 0.1; $E = 1.0 \times 10^7$; $\nu = 0.30$; mesh = 6 x 1. Loading: unit forces at free end (tip). Constraint: fixed support.	143
Figure 6.5 – Maximum displacement for cases 1 and 2 due to forces at free end.	145
Figure 6.6 – Domain meshes and geometries for different number of elements. .	150
Figure 6.7 – Error in energy norm $(e_r)_E$ for different Degrees of Freedom - DOF (logarithmic scale).....	151
Figure 6.8 – The curved beam: geometric properties.	156
Figure 6.9 – Domain and boundary meshes for curved beam. Double node considered at corners.	157
Figure 6.10 – Curved beam: inner radius = 4.12; outer radius = 4.32; arc = 90°; depth (thickness) = 0.1; $E = 1.0 \times 10^7$; $\nu = 0.25$; mesh = 6 x 1. Loading: unit forces at free end (tip). Constraint: fixed support.	157
Figure 6.11 – Maximum displacement for case 2 due to forces at free end.	158

Figure 6.12 – The thick-walled cylinder: geometric properties.....	160
Figure 6.13 – Thick-walled cylinder. Inner radius = 3.0; outer radius = 9.0; thickness = 1.0; $E = 1000$; $\nu = 0.49, 0.499, 0.4999$; plane strain condition; mesh = 5 x 6. Loading: unit pressure at inner radius.....	161
Figure 6.14 – Domain and boundary meshes for thick-walled cylinder. Double node considered at corners.	162
Figure 6.15 – Thick-walled cylinder: undeformed and deformed geometry with the maximum displacement representation.....	163
Figure 6.16 – Tension plate with a center hole application: geometric properties.	165
Figure 6.17 – The rectangular plate with a center hole boundary condition, geometry and properties: $\alpha = 1$; $W = H/2 = 4$; $L = 28$; $E = 1.0 \times 10^5$; $\nu = 0.3$; $\sigma = 10$.	167
Figure 6.18 – The rectangular plate with a center hole: stress field representation for coarse mesh.	168
Figure 6.19 – FEM meshes: a) coarse and b) refined.....	169
Figure 6.20 – Domain and boundary meshes for the rectangular plate with a center hole. Coarse mesh: a quarter of the domain. Double node considered at corners.....	169
Figure 6.21 – The rectangular plate with a center crack: geometric properties $\alpha = 7$ and $W = 14$	171
Figure 6.22 – The rectangular plate with a center crack boundary conditions, geometry and properties: $l = 1.4$; $E = 1.0 \times 10^5$; $\nu = 0.3$; state of plane strain; graded mesh = 62 elements. Loading: $\sigma = 10$	172
Figure 6.23 – Domain and boundary meshes for the rectangular plate with a center crack. Mesh: a quarter of the domain with graded mesh at the crack tip. Double node considered at corners.	173
Figure 6.24 – Definition of the coordinate axis ahead of a crack tip.....	174
Figure 6.25 – The rectangular plate with a center crack: stress field representation.	175
Figure 6.26 – Stress distribution along singular side: Stress σ_y versus distance r from Crack tip.	177
Figure 6.27 – The L-shaped domain geometric and boundary condition definition: $\alpha = 1$	179
Figure 6.28 – The L-shaped domain: stress field representation with the stress singularity at the re-entrant corner.	180

Figure 6.29 – Domain and boundary meshes for the L-shaped domain: uniform mesh. Double node considered at corners including the re-entrant corner.	181
Figure 6.30 – Domain and boundary meshes for the L-shaped domain: graded mesh. Double node considered at corners including the re-entrant corner. ..	181
Figure 6.31 – The L-shaped domain: boundary condition, $E = 1.0 \times 10^5$; $\nu = 0.3$; plane strain condition; uniform mesh = 12 elements. Loading: tractions computed from Equations 6.46 to 6.48 applied on boundary mesh nodes.	182
Figure 6.32 – The L-shaped domain: boundary condition, $\alpha = 1.0$; $E = 1.0 \times 10^5$; $\nu = 0.3$; plane strain condition; graded mesh = 24 elements. Loading: tractions computed from Equations 6.46 to 6.48 applied on boundary mesh nodes.....	183
Figure 6.33 – Stress curve: stress σ_x versus distance r from stress singularity for uniform and graded meshes.	189
Figure 6.34 – Stress curve: stress σ_y versus distance r from stress singularity for uniform and graded meshes.	190
Figure C.1 – EMLGFM approximate solution implementation.....	250

List of Tables

Table 3.1	– First six Lobatto shape functions and their polynomial order.	59
Table 3.2	– GFEM enriched functions and their level of enrichment.	69
Table 6.1	– Boundary conditions: constraint symbols and degree of freedom definition.	138
Table 6.2	– Displacements results and analytical solution for straight cantilever beam.	146
Table 6.3	– Normalized tip displacements results in direction of load.	147
Table 6.4	– Displacement error (%) for different L/h aspect ratio.	148
Table 6.5	– Stress error (%) for different L/h aspect ratio.	148
Table 6.6	– Computational cost evaluation versus displacement u_y error.	152
Table 6.7	– Condition number study for straight cantilever beam.	153
Table 6.8	– Displacements results, error (%) and elapsed time (s) for curved beam.	159
Table 6.9	– Normalized tip displacements results in direction of load.	159
Table 6.10	– Thick-walled cylinder displacement results for different Poisson's ratio values.	163
Table 6.11	– Thick-walled cylinder normal stress results for different radial positions.	164
Table 6.12	– Stress Concentration Factor Comparison for Lobatto Shape Functions.	170
Table 6.13	– Stress Intensity Factor Comparison.	176
Table 6.14	– Stress Intensity Factor Comparison: error (%).	176
Table 6.15	– Resultant displacement results for uniform and graded meshes in domain.	184
Table 6.16	– Resultant displacement results for uniform and graded meshes on boundary.	184

Table 6.17 – Resultant displacement results for uniform and graded meshes in domain: error (%).	185
Table 6.18 – Resultant displacement results for uniform and graded meshes on boundary: error (%).	185
Table 6.19 – Stress values for uniform and graded meshes in domain.	186
Table 6.20 – Stress error (%) for uniform and graded meshes in domain.	187
Table 6.21 – K_I error (%) calculated from displacements on boundary: graded mesh.	191
Table 6.22 – Condition number for K matrix.	192

Abbreviation and Acronyms

AMM	Admissible Modes Method
BEM	Boundary Element Method
BVP	Boundary-value Problem
EMLGFM	Enriched Modified Local Green's Function Method
CEM	Composite Element Method
CFM	Cutoff Function Method
CIM	Contour Integral Method
C^k -GFEM	Arbitrarily Smooth Generalized Finite Element Method
DBEM	Direct Boundary Element Method
DCM	Displacement Correlation Method
DE-FEM	Discontinuity-Enriched Finite Element Method
DOF	Degrees of Freedom
DQFEM	Differential Quadrature Finite Element Method
DQHFEM	Differential Quadrature Hierarchical Finite Element Method
FCM	Face Compensation Method
FEM	Finite Element Method
FFEM	Fourier Finite Element Method
FVM	Finite Volume Method
GBEM	Generalized Boundary Element Method
GFEM	Generalized Finite Element Method
GFEM ^{gl}	Global-local Generalized Finite Element Method
GFM	Green's Function Method
GFp	Green's Function Projections
HCE	Hybrid Cracking Element

HFEM	Hierarchical Finite Element Method
HNA	Hierarchical Non-Intrusive Algorithm
HSDT	Higher Order Shear Deformation Theory
IGFEM	Interface-Enriched Generalized Finite Element Method
Is-XFEM	Improved Stable Extended Finite Element Method
LOD	Localized Orthogonal Decomposition
MAT-MI	The Magneto Acoustic Tomography with Magnetic Induction
MFS	Method of Finite Spheres
MLS	Moving Least Squares Method
MLGFM	Modified Local Green's Function Method
MS-GFEM	Multiscale Generalized Finite Element Method
<i>nec</i>	Number of boundary elements
<i>nef</i>	Number of finite elements.
<i>ngln</i>	Number of degrees of freedom per node
<i>ngle</i>	Number of enriched degrees of freedom in domain
<i>nglec</i>	Number of enriched degrees of freedom on boundary
<i>nnec</i>	Number of nodes in a boundary element
<i>nnef</i>	Number of nodes in a finite element
<i>ntn</i>	Total number of finite element nodes
<i>ntnc</i>	Total number of boundary element node
NDOF	Total number of degrees of freedom
NURBS	Non-Uniform Rational B-Splines
OGFEM	Orthonormalized Generalized Finite Element Method
PNM	Phantom Node Method
PoU	Partition of Unity
PPUM	Particle-Partition of Unity Method
PUFEM/PUM	The Partition of Unity Finite Element Method or only Partition of Unity Method
ROM	Reduced Order Modeling
RVE	Representative Volume Element
SFEM	Special Finite Element Method
SGFEM	Stable Generalized Finite Element Method

SIF	Stress Intensity Factor
SMAHC	Shape Memory Alloy Hybrid Composites
SRI	Selective reduced integration
VBVP	Variational Boundary-value Problem
V-GFEM	Vademecum GFEM
XFEM	Extended Finite Element Method

List of Symbols

$A, B, C, D,$	
E, F or $[A],$	
$[B], [C], [D],$	
$[E], [F]$	MLGFM matrices
a	Inner radii
α_i	Resulting coefficients of linear equations
$a_0, \alpha_{11}, \alpha_{22}$	Scalars or real numbers
A, B_k	Linear differential operator
b_j	Arbitrary coefficients of linear equations or components of the body forces vector
$B(\cdot, \cdot), b(\cdot, \cdot)$	Bilinear form
\mathbf{B}	Strain-displacement matrix
\mathcal{B}_i	Basis functions of a hierarchic basis
\mathcal{B}^n	A hierarchic basis of order “ n ”
$A(x)$	Cross-sectional area
b	Outer radii
\mathbf{b}	Nodal body forces vector
b_{ij}	Field degrees of freedom related to the enrichment functions
$\text{cond}(K)$	Condition number
c	Half-width (height)
C_G	Constant
C_∞	Constant

C^m	The space of functions all of whose derivatives are continuous up to order “ m ”
$C^\infty(\cdot)$	The space of functions all of whose derivatives are continuous
$\text{card}\{\cdot\}$	Cardinality of a set (a measure of the "number of elements of a set")
$\text{closure}(\cdot)$	Closure of a domain
d	Diameter
\mathbf{d}	Degrees of freedom per node vector (displacement in one node)
\mathbf{D}	Elasticity matrix
\mathbf{D}_ε	Elasticity matrix normal strain part
\mathbf{D}_γ	Elasticity matrix shear strain part
$D(T)$	Domain of T
$\mathcal{D}_j, \mathcal{D}^*$	Trace operator (Dirichlet’s generalized operator)
$\mathcal{D}_K, \mathcal{D}_H$	Trace operator (Dirichlet’s generalized operator)
\mathcal{D}^{-1}	Inverse of trace operator \mathcal{D}
$\text{diag}(\cdot)$	Diagonal matrix
$\text{diam}(\cdot)$	Diameter of a metric space
$\text{dim}(\cdot)$	Dimension of a vector space (set)
$(e_r)_E$	Relative error in energy norm
E	Young’s Modulus
f	A function or a domain excitation
f_h	Approximate function of f
\mathbf{f}	Nodal boundary generalized forces vector
$\bar{\mathbf{f}}$	Prescribed nodal boundary generalized forces vector
\mathcal{F}	MLGFM variable defined as $\mathcal{F} = \mathcal{N}(u)$
\mathcal{F}	Functional
\mathcal{F}_h	Approximate variable of \mathcal{F}
$g, u, r,$ s, v, w	Elements of a topological space or functions (polynomials, for instance)

g_{jk}^{CP}	The value in the node “ k ” of the “ j -th” column of the “ i -th” component $\mathbf{G}_c^i(P)$ of the projection $\mathbf{G}_c(P)$
g_{jk}^{DP}	The value in the node “ k ” of the “ j -th” column of the “ i -th” component $\mathbf{G}_d^i(P)$ of the projection $\mathbf{G}_d(P)$
g_k	Functions
G	Shear modulus or modulus of rigidity
$\mathbf{G}(\cdot, \cdot)$	Green’s function
$\mathbf{G}_c(\cdot), \mathbf{G}_d(\cdot)$	Green’s function $\mathbf{G}(\cdot, \cdot)$ projections
\mathbf{G}_{cj}^i	A vector $\{\mathbf{G}_{cj}^i\}$ correspond to “ j -th” column (or degree of freedom) of $\mathbf{G}_c^i(P)$
\mathbf{G}_{dj}^i	A vector $\{\mathbf{G}_{dj}^i\}$ corresponding to “ j -th” column (or degree of freedom) of $\mathbf{G}_d^i(P)$
\mathbf{G}^{DP} or $[\mathbf{G}^{DP}]$	A tensor obtained from nodal values of $\mathbf{G}_d(P)$
\mathbf{G}^{Dp} or $[\mathbf{G}^{Dp}]$	A tensor obtained from nodal values of $\mathbf{G}_d(p)$
\mathbf{G}^{CP} or $[\mathbf{G}^{CP}]$	A tensor obtained from nodal values of $\mathbf{G}_c(P)$
\mathbf{G}^{Cp} or $[\mathbf{G}^{Cp}]$	A tensor obtained from nodal values of $\mathbf{G}_c(p)$
h	Height or parameter related to the dimension of a finite-dimensional space
H	Plate width (height)
$H, K, U, V,$	
$\partial H, \partial K$	Infinite-dimensional topological spaces (Hilbert spaces)
$H', K_0', U',$	
$V', \partial H', \partial K'$	Topological dual spaces
H_0, K_0	Kernel of the trace operator \mathcal{D}
H^m	Sobolev space (Hilbert space of functions with derivatives of order up to “ m ” and square integrable in Lebesgue sense L_2)
I	An interval of real line or the area moment of inertia
\mathbf{I}	Identity tensor
k_i	A non-zero real constant

K or $[K]$	Stiffness matrix
K' or $[K']$	Matrix whose the boundary operator \mathcal{N}' coefficients are placed
K_{ENR} or $[K_{\text{ENR}}]$	Finite Element Method enriched stiffness matrix
K_{FEM} or $[K_{\text{FEM}}]$	Finite Element Method standard stiffness matrix
K_h	Finite-dimensional topological spaces (trial space)
K_h^e	A closed subset of \mathbb{R}^n (a domain in \mathbb{R}^n) or finite element domain
K_{ha}	Parametric interval for the one-dimensional (1D) case
K_{hq}	Parametric domain for the two-dimensional (2D) case
K_I	Stress intensity factor
$[K_{\max}]$	The highest value of the standard stiffness matrix
K_{tg}	Stress concentration factor based on gross cross-sectional area
K_{tn}	Stress concentration factor based on net (nominal) stress
K_ε	Stiffness matrix normal strain part
K_γ	Stiffness matrix shear strain part
$\text{Ker}(\cdot)$	Kernel of operators \mathcal{D}_j collection
le	Level of enrichment
$l_0, l_1, l_2,$	
l_3, l_4, l_5	Lobatto or GFEM shape functions
$L(x)$	Length
$L(\cdot, \cdot)$	The set of all linear operators
L, T	Linear operator or map L , map T
L_p	Lebesgue space of order up to “ p ”
L^∞	The space of all measurable functions which are bounded almost everywhere
$\ell(\cdot)$	A linear functional (operator associated to the bilinear form B)
$\ell^*(\cdot)$	Adjoint operator
\mathcal{L}	Differential operator
m	Sobolev (Hilbert) space order
M	Constant
n -tuple	And ordered set with n elements

N_p	Vector space dimension or hierarchic basis order
N_e	Total number of nodes in the element
N_j	Number of used enrichment functions
$\mathcal{N}, \mathcal{N}^*$	Neumann's generalized operator
\mathcal{N}'	MLGFM auxiliary operator defined as $\mathcal{N}' = k_i(x - x_i)$
p	Point “ p ” on boundary $\partial\Omega$ or Lobatto shape function polynomial order
q	Point on boundary $\partial\Omega$
O, P, Q, R, S	Point in domain Ω
P_p	Finite-dimensional space of real-valued functions (e.g. polynomial functions)
$P(\mathbf{x})$	Load
r, θ	Polar coordinates
$R(T)$	Range of T
\mathbb{R}	Set of real numbers
\mathbb{R}^n	Set of all ordered n -tuples of real numbers (n -dimensional space)
$\text{span}\{\cdot\}$	Vector space spanned by basis
$\text{sup}(\cdot)$	Support of a function
t	Thickness
T_i	Components of the traction vector
\mathbf{T}	Traction vector
\mathbf{u}	Resultant displacement
\mathbf{u}	Nodal displacement vector
\mathbf{u}_C	Nodal displacement vector on boundary
$\bar{\mathbf{u}}_C$	Prescribed nodal displacement vector on boundary
\mathbf{u}_D	Nodal displacement vector in domain
\mathbf{u}^e	Nodal displacement vector of an element
\mathbf{u}_D^e	Approximate nodal displacement vector in element domain
\mathbf{u}_B^e	Approximate nodal displacement vector on element boundary
$\mathcal{U}_{ENRICHED}$	Enrichment part of the approximate solution

u_{FEM}	Standard FEM part of the approximate solution
u_h	Approximate functions (approximate solution)
u_h^{bubble}	Approximate solution of the displacement nodal variables located in the interior of the element
u_h^{edge}	Approximate solution of the displacement nodal variables located on edges
u_h^{vertex}	Approximate solution of the displacement nodal variables located at vertices
u_h^e	Approximate solution in an element
u_i	Nodal displacement components (nodal degrees of freedom)
u_x, u_y, u_z	Components of the displacement vector
$U(\mathbf{u})$	Strain energy of the exact solution
$U(\mathbf{u}_h)$	Strain energy of the approximate solution
U_{SE}	Strain energy
v_h	Approximate functions (test function)
V_i	Local basis spaces (approximate spaces)
V_{PUM}	PUM space
V_{WD}	The total work done by external forces
\mathbf{w}_j	Vector containing boundary shape functions originated from $\mathcal{F}(\mathbf{G}_{c_j}^i)$ minimization
\mathbf{W}_j	Vector containing domain shape functions originated from $\mathcal{F}(\mathbf{G}_{d_j}^i)$ minimization
x, y, z	Cartesian coordinates
x_i	An arbitrary node (coordinate)
α, β	Scalars or real numbers.
β_i	Hierarchical enrichment parameter
δ_{ij}	Kronecker delta (discrete cases)
$\delta(\cdot, \cdot)$	Dirac delta distribution (continuous cases)
ε or ε_{ij}	Strain Tensor

$\varepsilon_x, \varepsilon_y, \varepsilon_{xy},$	
$\varepsilon_{xz}, \varepsilon_{yz}, \varepsilon_{zz}$	Components of the strain tensor ε_{ij}
ϵ	Constant
$\varepsilon_1(i), \varepsilon_2(i)$	Dependent values of a PoU “ i -th” cover
$\Phi(\cdot), \Psi(\cdot)$	Shape functions matrix
ϕ_i, ψ_i	Linearly independent functions or basis functions (shape functions)
ϕ_k	Enriched shape function in a 1D domain
$\phi_k^{bubble}(\xi)$	1D <i>bubble</i> functions
$\phi^{vertex}(\xi)$	1D <i>vertex</i> shape functions
Φ_e	Element boundary shape functions matrix with dimension [$ngln$ x ($ngln$ x $nnef$)]
Φ	Global boundary shape functions matrix with dimension [$ngln$ x ($ngln$ x $ntnc$)]
Γ^k	The boundary of a boundary finite element “ k ”
φ_i	Partition of Unity
γ_{ij}	Enrichment functions
\mathcal{K}	Finite element triad $(K_h^e; P; \Sigma)$
λ	Lamé constant
λ_i	Real coefficients
ν	Poisson’s ratio
\mathcal{G}	MLGFM variable used in functional minimization
Π	The total potential energy
σ or σ_{ij}	Stress Tensor
$\sigma_x, \sigma_y, \sigma_{xy},$	
$\sigma_{xz}, \sigma_{yz}, \sigma_{zz}$	Components of the stress tensor σ_{ij}
Σ	A set of N_p linear forms $\zeta_i, 1 \leq i \leq N_p$
Ω	An open and bounded domain
$\overline{\Omega}$	The closure of Ω

Ω_h	Approximate domain
$\{\Omega_i\}$	An open cover of Ω
ξ, η	Finite element natural coordinates (or local coordinates)
ψ_k	Enriched shape function in a 2D domain
$\psi_{n_1, n_2}^{bubble}(\xi, \eta)$	2D <i>bubble</i> functions
$\psi_k^{edge}(\xi, \eta)$	2D <i>edge</i> functions
$\psi^{vertex}(\xi, \eta)$	2D <i>vertex</i> shape functions
Ψ_e	Element domain shape functions matrix with dimension [$n_{gl}n$ x $(n_{gl}n \times n_{nef})$]
Ψ	Global domain shape functions matrix with dimension [$n_{gl}n$ x $(n_{gl}n \times n_{tn})$]
ζ_i	Linear forms (called degrees of freedom – DOF)
$\partial\Omega$	A boundary, sufficiently regular
$\partial\Omega_h$	Approximate boundary
∇	Del or nabla, differential operator
$\ \cdot\ $	Norm
(\cdot, \cdot)	Inner product
$\langle \cdot, \cdot \rangle$	Duality pairing

Chapter 1

Introduction

1.1 OPENING DISCUSSION

From the beginning of the humankind, man argues himself: “From where does everything come? From what is everything created?” During a very long period of the humanity, mankind answered these and various others questions by myths and unnatural explanations. But something unusual happened in Greece almost two thousand and five hundred years ago: man started using the reason instead of mythological and unnatural explanations. Instead of reading various ancient scriptures or poems, they began to use reason, contemplation, and sensory observation to make sense of reality. Among of these giants of humankind, one of these lovers of wisdom, declared: “All things are number”. A strong statement assigned to Pythagoras (Figure 1.1). His famous “Pythagoras’ Theorem” is fantastic. It simply tells us that the geometry of objects embodies hidden numerical relationships. It says something very important about physical reality, namely the “*sizes*” and “*shapes*” of the objects that inhabit it. Mathematical relations underlie reality! Countless philosophers studied the nature and/or the man’s nature afterwards (including Socrates, Plato and Aristotle whose Pythagora’s ideas found fertile soil). The Pythagoras’ Theorem is nowadays really easy to understand and almost seen as silly if compared to the advances of the natural philosophy or what we call nowadays “science”. But it is

Introduction

worth mentioning: Philosophy is the mother of all sciences we currently know. Imagine those human giants like Copernicus, Galileo, Descartes, Kepler, Leibniz, Newton, Hooke or even Einstein seeing the computers we have nowadays and how far humankind has gone. Each contribution, each effort led the mankind to this. Of course, there were a boost of new technologies from 20th's century but these technologies couldn't be created without each endeavor, each new discovery, each new method developed so far.

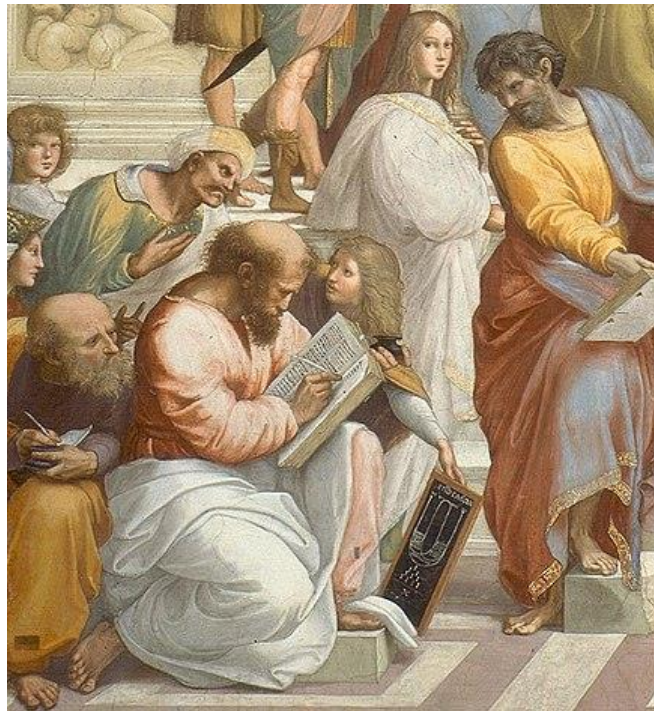


Figure 1.1 – Pythagoras in a detail of Raphael's fresco “The School of Athens”.

SOURCE: Wikipedia (2018).

From the first mathematical relations found out by man to the highest technology such as nanotechnology, robots, GPS and so on, there were countless hours of brave men leaning over calculations and more calculations until they reached their ultimate goal: an explanation of reality by reason, a new discovery! It is not different when concerning the physics and one of its branches: solid mechanics. With the advent of the differential and integral calculus, mankind discovered a powerful mathematical tool to describe physical phenomena and predict them. The same occurred with the advent of the computers. But, there are

Introduction

always bounds in all theories and methods created by mankind. And, overcoming these limits, new formulations, and new methods are created.

Describing and predicting natural events are not an easy task. If an exact solution is available then we have essentially completed our task; there is enough information about the studied system and how to solve it. But, for a great part of physical problems, the task of finding an exact solution can prove fruitless. Eventually it is necessary to make some assumptions and simplify the system to be studied. Otherwise, several problems couldn't be solved by man with current mathematical and physics/chemical tools. That is exactly what an approximate method does: to approximate a solution for a given problem. There might be a huge introduction describing all approximate methods developed by man but here, in this work, we are aiming to focus on two of them: the Finite Element Method (FEM) and its extensions as well as the Modified Local Green's Function Method (MLGFM) and also its extensions (including the novelty of this work).

The Finite Element Method (ODEN; REDDY, 1976; BECKER *et al.*, 1981; BATHE, 1996; ZIENKIEWICZ *et al.*, 2005) is proven one of the most widespread techniques used for the approximate solution of partial differential equations. However, several authors observed that low polynomial order of the finite elements may give poor results for some applications and improvements have been proposed (PEANO, 1976; ZIENKIEWICZ *et al.*, 1983; CAMPION; JARVIS, 1996; BESLIN; NICOLAS, 1997; RIBEIRO, 2001). Most improvements in FEM involve the enrichment of the approximation space by some set of functions such as seen in hierarchical formulations (Hierarchical Finite Element Method – HFEM) and the Partition of Unity (PoU) methods named by Arndt (2009) as “enriched methods”. In the hierarchical enrichment case, the approximation space is populated by a set of shape functions with order “ $p + 1$ ” where the space of order “ p ” is a sub-space of the space of order “ $p + 1$ ”. In other words, the approximation space with order “ p ” is “enriched” by shape functions of space with order “ $p + 1$ ”. One example of polynomials used to enrich an approximation space in terms of hierarchical basis is the Lobatto shape functions (ŠOLÍN *et al.*, 2004). Further developments in this field originated the Generalized Finite Element Method (GFEM) and its improvements (STROUBOULIS *et al.*, 2000; BABUŠKA;

Introduction

BANERJEE, 2012; ZHANG *et al.*, 2014; BABUŠKA *et al.*, 2017; FILLMORE; DUARTE, 2018). This method is based on the Partition of Unity Method – PUM – (MELENK; BABUŠKA, 1996) where the partition of unity can be provided by the Lagrange FEM shape functions or other shape functions that can be created as a partition of unity

The Modified Local Green's Function Method (MLGFM) is an integral technique that explores the main benefits from three techniques: the Finite Element Method – FEM, the Boundary Element Method – BEM (BREBBIA *et al.*, 1984; BREBBIA; DOMINGUEZ, 1992) and the Green's Function Method – GFM (BURNS, 1975; HORAK, 1980). The method was first proposed by Barcellos and Silva (1987) which applied MLGFM to the case of elastic membranes problems. Opposite to the BEM, the MLGFM does not use an explicitly fundamental solution. The matrices of the integral equation system are determined directly without the explicit knowledge of the Green Function. The MLGFM uses finite elements in domain to create discrete projections of the Green's Functions, which correspond to the fundamental solutions to be used in integral equations system associated with the boundary approximation. When FEM and BEM are associated, the Modified Local Green's Function Method become as efficient as the former ones, making possible to apply it at any Continuum Mechanics problem, with any geometry and boundary condition (BARBIERI; BARCELLOS, 1991a; 1991b; BARCELLOS; BARBIERI, 1991; MACHADO; BARCELLOS, 1993; MALDANER; BARCELLOS, 1992; FILIPPIN *et al.*, 1992a; 1992b; 1992c; BARBIERI *et al.*, 1993a; 1993b; MACHADO *et al.*, 2008; MACHADO *et al.*, 2012).

In this work, for the first time, the Modified Local Green's Function Method is enriched using the formulation proposed by Šolín *et al.* (2004) in the context of the Hierarchical Finite Element Method and its concept extended in the context of the Generalized Finite Element Method using, as partition of unity, the standard Lagrange shape functions.

1.2 OBJECTIVES AND METHODOLOGY

1.2.1 Main Objective

The novelty and main goal of this work is to present the Enriched Modified Local Green's Function Method (EMLGFM).

1.2.2 Specific Objectives and Methodology

In order to achieve the main objective one intends to present HFEM and GFEM formulations and develop them appropriately to this work as well as the MLGFM is described and developed for elasticity.

The MLGFM approximation space is then enriched using hierarchical concepts into the Modified Local Green's Function Method, such that:

- a. For a Hierarchical Finite Element Method (HFEM) context it is used the Lobatto shape functions as described by Šolín *et al.* (2004);
- b. For a Generalized Finite Element Method (GFEM) it is used an extension of the hierarchical concept but employing trigonometric basis functions (BABUŠKA *et al.*, 1994).

The Modified Local Green's Function Method is a powerful method especially when it concerns boundary flow variables (for example, stresses). But the MLGFM has never been experienced an improvement in its capabilities by using latest techniques such as enrichment methods so far. Since the Green's function projections are approximated using the Finite Element Method, it is expected an improvement in Green's function projections approximation and, consequently, in displacements results. Afterwards, when calculating strain and stress values, it is also expected a higher performance.

In order to investigate the accuracy and potential of this new method, some 2D elasto static problems are presented and compared with:

- a. The standard FEM (without enrichment);

- b. The conventional MLGFM (without enrichment);
- c. The available analytical solutions presented by Timoshenko and Goodier (1951), MacNeal and Harder (1985), Szabó (1986), Anderson (2005) and Pilkey and Pilkey (2008).

All results for the Enriched Modified Local Green's Function Method (EMLGFM), the scope of this work, were pre-processed, processed and post-processed from an own algorithm developed here and implemented in a FORTRAN platform.

1.3 OUTLINE OF THIS WORK

Following this Introduction ([Chapter 1](#)), in [Chapter 2](#) it is given a deep literature review of the enriched methods, especially the Hierarchical Finite Element Method and the Generalized Finite Element Method showing in a timeline its beginning from the Finite Element Method up to nowadays their advances employed in several areas of physics. Also, in this chapter, it is reserved a special section for the Modified Local Green's Function Method demonstrating its application and advances so far.

In [Chapter 3](#), it is presented an introduction of the Enriched Methods focusing on methods employed in this work: the Hierarchical Finite Element Method (HFEM) and the Generalized Finite Element Method (GFEM). In this chapter it is discussed their mathematical approach and how it is possible to enrich a one-dimensional (1D) and a two-dimensional (2D) element using higher-order finite element methods.

In [Chapter 4](#), the Modified Local Green's Function Method (MLGFM) is introduced, going through its abstract formulation and variational approach, moving into the discretization of the problem by it, the Green's function projections determination and how to implement the involved matrices and solve the equations system of this method.

In [Chapter 5](#), the methodology of the Enriched Modified Local Green's Function Method (EMLGFM) is presented, demonstrating its formalism and

Introduction

detailing how the Green's functions projections are figured out for 2D elasticity problems. In the end, it is explained how to calculate the displacements, reaction forces and stresses in this new method.

Chapter 6 is devoted to the applications of the EMLGFM for 2D elasto static problems, as following: a straight cantilever beam, a curved cantilever beam, a thick-walled cylinder, a rectangular plate with a center hole, a rectangular plate with a center crack and closing the application section, a L-shaped domain with singularity, including results and discussions of each one of them.

Finally, in Chapter 7 it is presented the conclusion where it is discussed the performance of the EMLGFM for 2D elasto static analysis and suggestions are presented for future applications of this new method.

Chapter 2

Literature Review

2.1 INTRODUCTION

In this chapter, it is done a review of the Finite Element Method (FEM) and some extensions of this method called by Arndt (2009) as “Enriched Methods” in a timeline structure. There has been a lot of FEM contributions since late 50’s so there is a limitation of the scope focusing on main characteristics of the Hierarchical Finite Element Method (HFEM) and Generalized Finite Element Method (GFEM) since they are based on the Finite Element Method. Some other enriched methods share the same attributes and because of that, they are also quoted here in this revision. Also, in the second and last part of this chapter, there is a literature review of the Modified Local Green’s Function Method (MLGFM). The MLGFM has been successfully used during the last two decades and here, in this review, the focus is in its main contributions for engineering problems. The main objective of this thesis is to ally the major characteristics of both methodologies: the Enriched Methods (HFEM and GFEM) and the Modified Local Green’ function Method (MLGFM). Therefore, this literature review is so important in order to extract the central attributes of these methods.

2.2 REVIEW OF THE ENRICHED METHODS

There is no way to begin a review of the literature on the enriched methods exploring the Hierarchical Finite Element Method (HFEM) and the Generalized Finite Element Method (GFEM) without first mentioning, even briefly, the precursor of it: the Finite Element Method (FEM) itself.

The Finite Element Method (FEM) is a mathematical technique using numerical resolutions with the purpose of calculating an approximate solution of boundary-value problems. It is also considered as a generalization of the Rayleigh-Ritz Method being a well-known and powerful method for solving problems with any geometry and degree of complexity (ZIENKIEWICZ *et al.*, 2005).

It is possible to increase the accuracy of FEM through certain refinements called in literature of “ h ”, “ p ”, “ hp ” and/or adaptive refinements (ARNDT, 2009).

The simplest technique, called h -refinement, corresponds to the increase of the number of elements that compose the mesh whereas the p -refinement technique corresponds to increase the order (or degree) of the polynomial interpolator, as those used in standard (or conventional) FEM. The combination of the refinement techniques of the mesh h with the variation of the order of the polynomial approximation p is called the hp -refinement. All of these techniques can be adaptive as long as the mesh of elements, shape functions, or both, depending on the type of refinement, are adjusted during the analysis process in order to improve the solution.

As quoted in Zienkiewicz *et al.* (1983), in a p -refinement, if the set of the approximate shape functions of an order “ p ” constitutes a subset of the approximate shape functions of an order “ $p + 1$ ”, this approach is termed “hierarchical”.

It is difficult to trace the origin of HFEM (Hierarchical Finite Element Method), but it seems to have been Peano (1976) who first presented the basic idea of the method. Subsequently, the concept was appropriately employed in Zienkiewicz *et al.* (1983), where it was shown that there is no need to completely

change the existing nodal interpolation functions, but only add enrichment functions.

In Guo and Babuška (1986), it was shown that the *hp*-version leads to an exponential convergence rate by solving problems with analytical data by piecewise functions.

A pioneer concept of hierarchical finite element adaptive meshes for 2D elliptic problems of second order (linear scalar) was presented in Deuffhard *et al.* (1989). It was shown that this approach allows a balance among the iterative algorithm, the local error estimator and the local mesh refinement mechanism that represent the main components of an adaptive partial differential equation code.

In Leung and Au (1990), it was proposed to use other shape functions like spline functions (B_3 -spline) and not the standard polynomial shape functions used in standard FEM for beam and plate elements. This methodology was known as the “Spline Finite Element Method”. The disadvantage is that with this approach the function does not vanish at each node (i.e., this condition is not respected as it is in FEM) making necessary special procedures to be taken into account to apply boundary conditions.

Ganesan and Engels (1992) developed a model for dynamic analysis of Bernoulli-Euler beams called the “Admissible Modes Method” (AMM) where it was used as the approximation space the union between a space that represents static displacements and another space that represents dynamic displacements. For the static displacements, FEM space is used, while in order to generate the space for the dynamic displacements, the admissible modes of vibration of the structure are used, canceling out at nodes of the elements (non-polynomial shape functions) and also their first derivatives.

A special treatment of FEM was developed in Babuška *et al.* (1994) where it was considered the approximate solution of a class of elliptic second-order equations with coefficients that change abruptly or that are highly oscillating. This method was called “Special FEM” (SFEM) because it employs special shape functions chosen precisely to model the unknown solution.

In 1995, in a report of Duarte and Oden (1995), the concept of the “*hp*

Cloud Method” was presented, based on the “Partition of Unity Method” (PUM), the method uses radial base functions by varying the size of the supports and reproducing polynomial properties of arbitrary order. Together with Melenk and Babuška (MELENK, 1995; BABUŠKA *et al.*, 1995; MELENK; BABUŠKA, 1996; BABUŠKA; MELENK, 1997), it is considered the precursor of GFEM. In Melenk's PhD thesis (MELENK, 1995), the method was formally presented and called the Generalized Finite Element Method. In Babuška *et al.* (1995), GFEM was applied to solve boundary-value problems governed by the Helmholtz equation. In Melenk and Babuška (1996) and Babuška and Melenk (1997) the "Partition of Unity Finite Element Method" (PUFEM) was presented, being the main mathematical foundation of the “Generalized Finite Element Method” (GFEM) and it is still one of the pioneering works to introduce concepts of Meshless Method in finite element formulation.

Belytschko and others (BELYTSCHKO *et al.*, 1995) proposed a new method for crack propagation analysis. The new method, called by the authors as “Galerkin's Meshless Method”, was one of the pioneers in the study of meshless methods and its application in crack propagation.

In 1996, several papers dealing with the *hp* Cloud Method were published in literature, such as, Lyszka *et al.* (1996), analyzing stresses close to a singularity, Duarte's PhD thesis (DUARTE, 1996), where the formalism of the method was presented, Duarte and Oden (1996a) and Duarte and Oden (1996b), developing this method.

Beslin and Nicolas (1997) used a trigonometric functions approach that is similar to the polynomial functions but which has better numerical manipulation characteristics in a HFEM context. It was shown that for high-order polynomials a locking behavior can occur. It was verified that in trigonometric functions approach, one has the advantage of causing smaller locking errors. Results for rectangular plate vibrations under bending were studied.

Concurrently, Houmat (1997) proposed the use of trigonometric functions that resemble the polynomials that would be obtained from HFEM. Again, better results were obtained when using high order approximations.

An extension of the *hp* cloud method for fracture mechanics problems as

an example of the custom cloud functions development was studied in Oden and Duarte (1997). Some applications for boundary-value problems were presented in that paper.

In 1998, Taylor, Zienkiewicz and Oñate (TAYLOR *et al.*, 1998) deduced hierarchical enrichment functions based on the partition of unity technique, applying the methodology to linear elasticity.

The "Partition of Unity Method" (PUM) was again used in the work of Babuška and Zhang (1998) for analysis of Timoshenko's beam under elastic support. Also, the "*hp* Cloud Method" was again used in Oden's work (Oden *et al.*, 1998) showing its advantages with severely distorted meshes and its exponential convergence rates.

Another method presented in 1998 was the Composite Element Method – CEM (ZENG, 1998) where the proposal was to use the standard element of FEM together with functions enriched by the addition of non-polynomial functions related to the analytical solutions of the problem. It was shown that the results presented a great superiority compared to the FEM with constant order.

This enrichment technique – the Composite Method – was used in Arndt *et al.* (2003), proving to have better results than those obtained by the *h*-refinement of the standard FEM for the analysis of Euler-Bernoulli bars and beams in free-vibration.

In Cramer *et al.* (1999), an adaptive finite element procedure for the analysis of elastoplastic problems was developed. Special attention was given to the essential ingredients of the adaptive process and the mapping of history-dependent state variables between different meshes. The hierarchical strategy facilitated the simple definition of transfer operators for history-dependent variables. Some numerical examples demonstrated the applicability of the approach to general elastic-plastic problems including associated as well as non-associated plasticity.

In 2000, Babuška's work (BABUŠKA; SAUTER, 2000) showed that by carrying out a Galerkin Method modification based on GFEM, one can eliminate the so-called "pollution effect" in one dimension. However, in two or more dimensions, the "pollution effect" cannot be eliminated completely, but

substantially reduced.

A new finite element method for elliptic problems called “Generalized p -FEM in Homogenization” was developed and analyzed by Matache *et al.* (2000). It was demonstrated, through numerical experiments, its feasibility and the theoretical results were confirmed.

Strouboulis, Babuška and Copps (STROUBOULIS *et al.*, 2000; 2001) defined GFEM as simply a combination of the Finite Element Method and the Partition of Unity. Strategies for solving linear dependence and numerical integration were described as well as discussions on computational code architectures, feasibility and capacity of GFEM.

The main ideas of the Generalized Finite Element Method (GFEM) were described in Duarte *et al.* (2000) and some of its advantages were demonstrated against the standard FEM in solutions of three-dimensional structural mechanics complex problems. These include the ability to produce finite element hp -refinements with non-uniform h and p , and to generate subspaces of particular approximations for specific applications.

In Sukumar *et al.* (2000), it was discussed another method based on the Partition of Unity (PoU) called the “Extended Finite Element Method” (XFEM) that afterwards it would be concluded to be very similar to GFEM. This work was based on the three-dimensional modeling of cracks and on presenting a study using discontinuous functions and crack tip displacement fields to enrich the standard finite element method. Good results were shown and compared to the literature. The XFEM was also applied in Daux *et al.* (2000) work for cracks with arbitrary intercepting branches.

Ribeiro (2001) examined the Hierarchical Finite Element Method (HFEM) using trigonometric (non-polynomial) functions to analyze vibrations in beams and plates. The results were compared with polynomial shape functions.

The Extended Finite Element Method (XFEM) was used to model arbitrary holes and material interfaces (inclusions) without the need of meshing within internal bounds in Sukumar *et al.* (2001). Numerical examples were presented for the case of linear elasticity in two dimensions (2D).

Also in 2001, De and Bathe's work (DE; BATHE, 2001) suggested the

“Method of Finite Spheres” (MFS) based on the “Partition of Unity Method” (PUM) as a truly meshless technique with the objective of achieving a better computational efficiency. Numerical rules with an emphasis on reducing computational cost were shown in this paper.

In Duarte *et al.* (2001), it was again applied the technique of Partition of Unity (PoU) through the Generalized Finite Element Method (GFEM), but here for three-dimensional analysis of the dynamic crack propagation using a couple of enrichment functions in elements where the crack is crossed by.

Duarte and Babuška (2002) continued working on the Generalized Finite Element Method proposing a simple but effective process of implementing an independent mesh p -orthotropic enrichment.

One of the pioneering texts on the selection of shape functions for GFEM is the work of Babuška *et al.* (2002). Some theorems based on the mathematical principles of functional analysis were presented and shape functions selections in Sobolev space for one-dimensional problems were discussed.

In Barros' PhD thesis (BARROS, 2002) a non-linear analysis of structures was presented using the meshless methods and GFEM, where some enrichment functions were applied in the study and simulation of the propagation of discontinuities. It was enumerated some proposals for the application of GFEM in propagation of defects problems.

Another contribution in the Generalized Finite Element Method (GFEM) was presented in 2003 by Torres' PhD thesis (TORRES, 2003). There, it was applied GFEM in three-dimensional non-linear analysis of solids considering three constitutive models: plasticity, fragile damage and damage with coupled plasticity.

Garcia's PhD thesis (GARCIA, 2003) addressed two fundamental aspects of GFEM: the construction of local spaces on curved surfaces and the imposition of strong boundary conditions. Examples were given for composite and homogeneous materials with linear elastic behavior.

Strouboulis *et al.* (2003) described a new version of the Generalized Finite Element Method (GFEM) that is well suited for problems in domains with large

number of inclusions, voids and cracks using different constructions of known functions in literature.

In Zhang's PhD thesis (ZHANG, 2003), it was described a new version of the Generalized Finite Element Method called GFEM for multiscale analysis. The robustness of the method was illustrated by several model problems defined in domains with a large number of closely spaced voids and/or inclusions with various shapes, including the heat conduction problem defined on domains with porous media and/or a real composite material.

A review of meshless methods and methods closely related to GFEM for solving elliptic linear equations using variational principles was addressed in Babuška *et al.* (2003). The intention was to show a unified mathematical theory, some aspects of implementation and numerical examples.

In 2004, Góis (2004) proposed a discussion in his Master's dissertation of the combination of "Mixed Hybrid Volumetric Formulation" and the Generalized Finite Element Method (GFEM). It was accurately possible to calculate stresses for this formulation using several enrichment functions in analysis, among them, polynomial functions and trigonometric functions.

Pereira's work (PEREIRA, 2004) showed a study on the method of stress intensity factor (SIF) using GFEM. Several methods of fracture mechanics were presented in his work addressing them in the context of GFEM and applying this method to the pure and mixed modes of classic fracture mechanics problems.

The characteristics of the meshless and GFEM methods are investigated in Santana (2004), their advantages and limitations in the application of computational fracture mechanics. Numerical tests for plane problems were presented.

A book (ŠOLÍN *et al.*, 2004) dealing with the higher-order finite element methods where several categories of hierarchical functions could be used as enrichment functions was published in 2004. In this work the basic principles of high-order FEM, adaptive discretization and refinement techniques were presented.

GFEM was applied for non-linear analysis where it was proposed a p -adaptive strategy motivated by the problem of the reinforced concrete beam in

Barros *et al.* (2004). The p -adaptive scheme consists of multiplying the functions of the partition of unity by a set of polynomials. The effectiveness of the error estimator index proposed in this paper was exemplified by a numerical example.

The “Fourier Finite Element Method” (FFEM) was again revisited in 2004 through the work of Leung and Zhu (LEUNG; ZHU, 2004) applied to the vibration problem of in plane thin and thick curved beams with p -elements. Fourier trigonometric functions were used as enrichment functions, showing the numerical stability of this method. This method was first employed in 1998 by Leung and Chan (1998).

A general overview of the main ideas of the Generalized Finite Element Method was presented in Babuška *et al.* (2004), presenting the basic results, experiences and potentials of the method so far, proving that the Finite Element Method (FEM) is actually a particular case of GFEM.

In 2005, Nirschl's master dissertation (NIRSCHL, 2005) studied GFEM applied to the analysis of cylindrical tubes and spherical shells. For this purpose polynomial and trigonometric functions were used as enrichment functions and the results were compared with FEM and analytical solutions.

A method of extracting stress intensity factors (SIF) using GFEM was studied in Pereira and Duarte (2005). Several methods such as the contour integral, *cutoff* function and the “ J ” integral were used in the fracture mechanics scope. Numerical experiments showed that the contour integral and *cutoff* functions were more robust than the “ J ” integral method and the *cutoff* function is the most accurate.

Nicolazzi and others (NICOLAZZI *et al.*, 2005) discussed another meshless approach called the “Generalized Boundary Element Method” (GBEM). This work can be understood as an extension of the BEM using enrichment approach. The “Moving Least Square Method” – (MLS) – was used to build a partition of unity but now on boundary and then applied to Galerkin's boundary element formulations. Numerical solutions were reported in this work, verifying good accuracy and convergence.

GFEM technique of “grouping elements” was used in Duarte *et al.* (2005a) making possible to combine neighbor elements and to generate correct and

smooth approximation solutions for these groups. Some examples were presented illustrating the reduction of the processing time and proposing future improvements.

Duarte *et al.* (2005b) was focused on a marriage of the Finite Element Method and any approximation based on the Partition of Unity (PUM). It was emphasized the combination of the shape functions from finite element and from meshless methods like those of the *hp* cloud method. This work also contributed showing a procedure of building shape functions with any degree of regularity using the so-called “*R*-functions”. Some numerical experiments were reported demonstrating the proposed technique.

One of the pioneering works on the concept of isogeometric analysis was presented by Hughes and others (HUGHES *et al.*, 2005) where the base functions were generated from the NURBS (*Non-Uniform Rational B-Splines*) to build an exact geometric model. This technique was applied to problems of linear elasticity with extremely satisfactory results and it was much more efficient compared to other methods using a new refinement technique called “*k*-refinement”.

A classification of numerical formulations divided into methods by standard finite elements and methods without mesh (meshless) was proposed in Idelsohn and Oñate (2006). It was argued, using some numerical examples, what would be the best choice for each studied case.

Strouboulis *et al.* (2006a) applied GFEM to the Helmholtz equation using meshes that may overlap the boundaries of the problem domain and enriching the approximation by wave functions based on the discontinuous Galerkin with Lagrange multipliers (based on the Partition of Unity Method). Subsequently, in Strouboulis *et al.* (2006b), a methodology to estimate errors a posteriori was developed and the reliability of these estimators was examined. It was shown that the proposed algorithm is as efficient as an adaptive mesh strategy.

In Mangini’s master dissertation (MANGINI, 2006), GFEM was applied to the analysis of shells of revolution structures exploring its axisymmetric geometry. Polynomial enrichment functions were used for this analysis. The obtained results were compared to analytical and numerical solutions generated by FEM.

An analysis of polycrystal structures with explicit treatment of grain boundaries by GFEM was proposed in Simone *et al.* (2006). This methodology allows the finite element mesh does not need to conform to the polycrystalline topology. The potential and precision of the method was demonstrated by a numerical example.

Chessa and Belytschko (2006) developed a locally enriched space-time finite element method for solving hyperbolic problems with on move discontinuities. The space-time scheme in which the discontinuities were explicitly obtained with enrichment was combined with classical formulations of finite elements for hyperbolic problems. The enriched space-time formulation was coupled with semi-discrete finite elements outside the discontinuity region. Results were presented for two examples: linear wave equation and Burgers equation.

In Duarte *et al.* (2006), it was intended to show a procedure to construct C^k , with k arbitrarily large, shape functions for the generalized finite element defined in unstructured finite element meshes. The so-called R -functions were used to build C^k partition of unity functions based on finite elements with non-convex support. This technique is quite similar to GFEM except by the arbitrarily smooth shape functions. The method was applied for solving a linear elasticity problem with good results and low computational cost.

The use of GFEM is dealt with an arbitrary degree of smoothness called the p -adaptive technique in Barros *et al.* (2007). The weight functions were obtained from R -functions where one could construct approximations C^k , with k arbitrarily large, similar to that employed by Duarte *et al.* (2006). Error indicators were used taking into account the typical scheme of the nodal enrichment method. It was presented some numerical examples of in plane elasticity problems where the performance was investigated.

The concept of grouping nodes and elements where in this group a partition of unity in the modified finite element is enriched through GFEM by any desired order was proposed in Duarte *et al.* (2007a). Some numerical experiments were presented as well as some implementation details.

Duarte, Reno and Simone (DUARTE *et al.*, 2007b) dedicated themselves

to present high order implementations of GFEM for three-dimensional through-the-thickness branching cracks. Discontinuities such as triple joints in polycrystalline materials and branched cracks are accurately represented independently by the mesh in use. The combination of local refinement at the crack tip and the higher order of nodal enrichment proved to be an excellent alternative.

Duarte *et al.* (2007c) proposed a development of enrichment functions in a global-local approach using a fixed global mesh around the crack front, being especially attractive for non-linear problems and/or time dependent problems. Numerical experiments were reported demonstrating the accuracy and efficiency of the method.

A method for treatment of Dirichlet boundary conditions for the Laplacian under GFEM was proposed in Babuška *et al.* (2007a). The method is based on using approximate Dirichlet boundary conditions and polynomial approximations of the boundary. Quasi-optimal convergence rates are obtained for GFEM approximations sequence. The results were extended for the problem of the non-homogeneous Dirichlet boundary value, including the case when the boundary data has low regularity (i.e., it is a distribution, in the functional analysis context).

Babuška, Banerjee and Osborn discussed in Babuška *et al.* (2007b) the problem of the super convergence points existence obtained from GFEM approximate solutions for an elliptic boundary-value problem of Neumann type. It was shown that the super convergence points for the approximate solution gradient were the zero values of a system of nonlinear equations; not depending on the solution of the boundary-value problem. It was observed that the smoothed generalized finite element approximation is easy to be built.

An application of the PUM to the problem of the thick sandwich plates vibration with viscoelastic layers, taking polynomial functions as basis functions for a Mindlin's plate element was proposed in Hazard and Bouillard (2007). Their results were compared with available numerical and experimental results.

Gracie, Ventura and Belytschko (GRACIE *et al.*, 2007) showed a technique based on XFEM (similar to GFEM) where plasticity phenomena were

modeled directly by interior discontinuities and the tangential enrichment was applied. Some examples were examined and it was found that the method exhibits excellent accuracy.

The hybrid cracking element (HCE) combined with the XFEM was implemented in Xiao and Karihaloo (2007). Studies showed that the HCE element was one of the most accurate and convenient for obtaining stress intensity factors (SIF) and higher order terms. This work presented the technique to implement the HCE in a general mesh of FEM, maintaining the advantages of both methods: HCE and XFEM. Some numerical results were reported to validate the proposal.

Lu and Law (2007) addressed the Composite Element Method (CEM) in beam free vibration analysis with the use of different analytical functions, according to the beam's boundary conditions and considering the coupling terms of the nodal coordinates and coordinates "c" in the stiffness matrix. It was shown that the Composite Element Method was improved with the proposed modifications, and the solutions had better results than the former approach.

It was analyzed the propagation of cracks in a structure under dynamic loading based on the numerical implementation of the Extended Finite Element Method (XFEM) in Nistor *et al.* (2008). Also, in Khoei *et al.* (2008), a new computational technique was presented based on the Finite Element Method called as arbitrary Lagrangean-Eulerian for problems of solid mechanics with large deformations. This technique captured the advantages of both the Lagrangian and Eulerian methods.

Abdelaziz and Hamouine's work (ABDELAZIZ; HAMOUINE, 2008) reported a global vision and the progress of the Extended Finite Element Method (XFEM) up to that moment, proving that the technique was an alternative to problems that could not be solved by the standard FEM.

Some aspects of the Generalized Finite Element Method (GFEM) and the classic p -refinement in the hybrid-Trefftz stress formulation for the two-dimensional elasticity was introduced in Souza (2008). It was also preliminary discussed a study of plate with multiple cracks by the Partition of Unity Method in Hybrid-Trefftz formulation with selective enrichment that revealed an

excellent performance of the numerical analyzes.

Babuška *et al.* (2008) elaborated a method for approximation of the essential boundary conditions (Dirichlet type conditions) within GFEM where the results were applied to elliptic general boundary-value problems.

A work related to the application of GFEM for cracking analysis, with special attention focused on local and global enrichment functions was presented in Duarte and Kim (2008). Local enrichment functions were used in the region near the crack, or even at the crack border, while global enrichment functions were applied to the rest of the solid observing a major improvement in this approach.

In Strouboulis *et al.* (2008), it was published a GFEM approach applied to solution of Helmholtz equation. Enrichment functions involving exponential and trigonometric functions for the propagation of two-dimensional waves were demonstrated. It was considered in the choice of these functions, solution already tested and studied in literature and, in addition to that, GFEM criteria, previously established, was also met.

A general formulation of GFEM to solve two-dimensional problems characterized with continuity C^0 with gradient jumps such as those found in thermal analyzes and heterogeneous structures was demonstrated in Aragón *et al.* (2008). It was shown that the introduction of the enrichment functions led to accurate solutions with meshes that did not conform to the geometry of the discontinuity lines. The convergence was studied by demonstrating that quadratic approximations did not require corrections and they had better performance than linear approximations by investigating them with the available literature.

The effectiveness of the Global-Local Finite Element Method versus the Generalized Finite Element Method with enrichment functions in a global-local approach to three-dimensional fracture mechanics problems was compared in Kim *et al.* (2008). It was demonstrated through numerical experiments that interactions among cracks with different sizes are taken into account by GFEM even when all cracks in the global domain are not modeled.

The technique of enriching the partition of unity was developed and

extended in Góis' PhD thesis (GÓIS, 2009) to two non-conventional formulations in plane elasticity: the hybrid stress formulation and the hybrid-mixed stress formulation. Polynomial functions were used to enrich the approximations. Some numerical examples were demonstrated to illustrate the performance of both approaches, especially when the enrichment technique is applied.

The multilevel hp -adaptive solution of elliptic second-order partial differential equations using the meshfree method – “Particle-Partition of Unity Method” (PPUM) was treated in Schweitzer (2009). New discretization points (or particles) were automatically created in the proposed refinement scheme, the analogue of an adaptive meshfree h -refinement method. For local approximation spaces it was employed a better local resolution similar to a p -refinement. It was presented some numerical results that showed the efficiency of the proposed scheme.

Kim, Duarte and Proença in 2009 (Kim *et al.*, 2009a) and Pereira, Duarte, Guoy and Jiao (Pereira *et al.*, 2009a; 2009b) focused on the topic of generalized enrichment functions but now for 3D non-planar cracks. The representation preserved continuity of the crack surface while it was able to represent non-planar, non-smooth, crack surfaces inside of elements of any size. It was illustrated some numerical experiments to show the accuracy and robustness of the proposed approaches.

The problems of three-dimensional fracture mechanics using GFEM based on the solution of the global (structure) and local (crack) interdependent problems was developed in Kim *et al.*, 2009b. The effect of the local boundary condition on the performance of the proposed method was studied and several problems of the three-dimensional fracture mechanics were investigated to test the accuracy and performance.

In Barcellos *et al.* (2009), GFEM based on the Partition of Unity (PoU) with smooth approximation functions was employed by modeling anisotropic laminated plates under the Kirchhoff hypothesis. The enriched shape functions were obtained by the product of Shepard's partition of unity and the polynomial enrichment functions. Different edge functions were investigated to generate the C^k functions.

A mapping method to integrate weak singularities that result from GFEM/XFEM enrichment functions for bi- and three-dimensional problems (2D and 3D) was developed in 2009, Park *et al.* (2009). The accuracy and convergence of the proposed method were demonstrated by 2D and 3D numerical examples.

Heat transfer problems in steady state with strong thermal gradients by both the standard finite element method and GFEM were analyzed in O'Hara *et al.* (2009). The robustness and feasibility of the heat transfer method was investigated in order to generate accurate approximations. It was shown that the global problem converges at least as fast as the local problems and in many cases the enriched global problem could offer much more accurate solutions than the local ones.

GFEM continued to be explored in Arndt (2009) for free vibration analysis of straight bars, beams, trusses and frames, specifically in the determination of natural frequencies of structures. In his work, the h -, p - and adaptive refinement methods were analyzed and compared. Enriched formulations for free vibration dynamics problems were inspected as well as a detailed convergence analysis using h - and p - refinements where it were developed adaptive methods to improve the determination of eigenvalue and eigenvector pairs.

Belytschko *et al.* (2009) exposed a review of GFEM and XFEM, verifying the application of these methods in engineering and proving both methods are practically the same. It was emphasized in this work the application of numerical techniques in fracture mechanics problems, dislocations, grain boundaries and phases interface.

In Alves' PhD thesis (ALVES, 2010), the Partition of Unity Method (PUM) was applied in the analysis of problems with multiple cracks, one of the main objectives being to check the ability of the method to obtain stress intensity factors (SIF). Later on, GFEM was applied in the analysis of the local sub-problem. Numerical examples were presented, proving that the use of GFEM allows good approximate results even with poorly refined meshes.

Argôlo (2010) used the Partition of Unity Method in the analysis of problems with multiple distributed cracks. Here, in addition to GFEM, the

Hybrid-Trefftz Stress formulation was also used. Numerical examples were reported in order to prove the efficiency of the proposed method.

It was discussed the link between two methods: GFEM and the “Face Compensation Method” (FCM) in Pereira *et al.* (2010). Applying GFEM at each step of the crack growth, the higher order approximations were locally refined in the mesh while controlling the evolution of the crack front in the explicit crack surface representation by the Face Compensation Method. The robustness and precision of the proposed methodology were illustrated by numerical simulations.

Improvements in simulation of three-dimensional crack propagation by GFEM were presented in Garzon *et al.* (2010). In particular, new updated algorithms suitable for explicit crack surface representations and simulations in which the initial crack surfaces grow significantly in size (one order of magnitude or more) were also included in this paper. Numerical examples were provided illustrating the robustness and capability of the proposed approaches and some of their potential applications in engineering.

Kim, Pereira and Duarte (Kim *et al.*, 2010), using GFEM, applied it to the study of fracture in a global (structural) and local (crack) interdependent solution approach. A number of three-dimensional fracture mechanics problems were proposed to investigate the accuracy of the method and its computational performance, both in terms of problem size and computational processing time.

In Yu *et al.* (2010), it was shown the formulations of a multivariable hierarchical beam element for static analysis and vibration analysis based on the generalized variational principle. Two forms of hierarchical Legendre polynomials were used as basic interpolation functions. The method was applied to several cases of static analysis and the results were satisfactory while further development is still required for dynamic analysis.

It was developed a first application of the adaptive GFEM for free vibration analysis of straight bars and trusses applying adaptive refining strategies with generalized enrichment functions in Arndt *et al.* (2010). The frequencies obtained by the adaptive GFEM were compared with those obtained by the analytical solution, by the Composite Element Method (CEM) and by the h - version of the Finite Element Method.

In Lins' master dissertation (LINS, 2011), the question of a posteriori estimation of discretization errors and particularly the retrieval of numerical solutions gradients obtained with the Finite Element Method (FEM) and the Generalized Finite Element Method (GFEM) was dealt with. The schemes presented through numerical examples were illustrated to evaluate the efficiency of each estimator.

Soghrati *et al.* (2011) presented a new GFEM scheme based on the interface for solving problems with discontinuous gradient fields. The method is based on enrichment functions associated with generalized degrees of freedom at nodes generated from the intersection of the phase interface with the elements edges. A convergence study for heat transfer problems was illustrated and compared with FEM.

The intergranular brittle cracking of polycrystalline aggregates by means of GFEM with cohesive grain boundaries and linear elastic grains was analyzed in Shabir *et al.* (2011). It was shown that the resulting crack path is insensitive to the key cohesive law parameters such as maximum cohesive strength and critical fracture energy.

Kim *et al.* (2011) looked over a "parallel" simulation of GFEM where custom enrichment functions were used for applications which a priori solution is known. The parallel solution of local boundary-value problems was involved in the procedure using the boundary conditions of a coarse global problem. Problems of the three-dimensional fracture mechanics were analyzed in order to investigate the precision and performance of the proposed GFEM.

GFEM was applied with global-local enrichment but for transient heat transfer problems with solutions exhibiting abrupt, highly localized thermal gradients in O'Hara *et al.* (2011). It was required, with the use of time-dependent functions, that the system of equations were discretized temporally first, and then spatially, in order to adequately account for the dependence of time. Applications were provided for heterogeneous materials and moving heat sources as well as a convergence analysis was done for the proposed method.

Babuška and Lipton (2011) were engaged in a numerical method to solve second-order elliptic partial differential equations describing fields inside

heterogeneous media such as micro-structures and media with multiple non-separated length scales. It was shown that the homogenization theory could be used to construct local approximation spaces with errors decaying exponentially in a pre-asymptotic regime.

In Yang *et al.* (2011), it was conceived an h -hierarchical adaptive mesh strategy based on finite element method (FEM) and boundary element method (BEM) for transient elastodynamic problems. It was shown that this mixed formulation is efficient to determine displacement fields, stresses, velocities and accelerations using semi-analytical functions.

GFEM was applied in framed structures by examining the convergence rates for natural frequencies in comparison to a reference situation in Arndt *et al.* (2011). In the study, it was shown that GFEM is efficient to determine natural frequencies of higher orders compared to other methods.

A procedure to generate, numerically, adequate enrichment functions for three-dimensional problems, with confined plasticity where the plastic evolution is gradual was proposed in Kim *et al.* (2012). It was shown that with this procedure it was possible to produce precise nonlinear solutions with reduced computational effort. Numerical three-dimensional nonlinear problems based on the rate-independent J_2 plasticity theory with isotropic hardening were studied to demonstrate the robustness, precision and efficiency of the proposed method.

Pereira *et al.* (2012) again looked over the topic of crack growth by GFEM but based on two-scale decomposition (global-local) – a smooth coarse-scale component and a singular fine-scale component. The fine-scale component was approximated by discretizations defined on coarse finite element meshes while the fine-scale component was approximated by the solution of local problems defined in neighborhoods of cracks. Numerical examples demonstrating the approximation properties of proposed enrichment functions and the computational performance of the methodology were illustrated.

Gupta *et al.* (2012) demonstrated that GFEM with global-local enrichment functions (named as GFEM^{gl}) could be implemented in a non-intrusive way in finite element closed-source codes as an add-on module. The global problem was solved through commercial finite element analysis software

(Abaqus) while the local problem containing three-dimensional fractures were solved by *hp*-adaptive GFEM. The applicability and accuracy of the methodology were investigated through several problems of three-dimensional fracture mechanics.

Ozer *et al.* (2012) used GFEM/XFEM to deal with discontinuities arbitrarily located within a finite element mesh with the intention of formulating and implementing a three-dimensional and high order integral method of domain for the calculation of the energy release rate. Numerical examples were reported to verify the convergence rates where the results were compared with numerical solutions available in literature.

The use of GFEM based on the global interdependent solution (structure) and on a fine scale (local problems) – GFEM^{gl} – was exploited in Garzon *et al.* (2012). Local problems were treated using the adaptive *hp*-GFEM considering fine-scale features, such as areas with cracking process, while the overall problem is addressed by the structural behavior of the macro-scale. Numerical examples of crack growth and high fatigue cycle were illustrated as well as problems exhibiting localized nonlinear responses.

In Amorim's master dissertation (AMORIM, 2012), it was studied hybrid-mixed and purely mixed formulations, both combined with techniques to enrich the solutions provided by GFEM. The numerical methodology was applied to problems of the solid mechanics modeled by damage mechanics. The results were compared to simulated and non-linear complete strategies, proving that the simplified model could be used in localized damage situations in small domain regions.

GFEM global-local approach (GFEM^{gl}) was also studied in Alves (2012). In this scheme, the enrichment functions for a certain region of the mesh are numerically constructed from the solution of a local problem restricted to that region allowing the use of coarse meshes around the domain with complex stress field distribution. The proposed methodology was applied in two numerical examples, validating its results: beam under simple bending and wedge/plate with cracks.

The formulation and implementation of an interface-based GFEM scheme

for solving thermal problems in discontinuous gradient fields in a 2D model has been presented in Soghrati *et al.* (2012), allowing the accurate and efficient capture of the discontinuity gradient along the solid-fluid interface without the need for meshes that conform to the geometry of the problem. The method was validated by comparison with infrared measurements of the polymeric fin thermal response with an embedded sinusoidal microchannel.

Three-dimensional GFEM applied to discontinuous gradient fields was discussed in Soghrati and Geubelle (2012), showing that the method yields similar rate of convergence and accuracy level with non-conforming meshes as that of the standard FEM with conforming meshes at a computational cost similar to or lower than that of conventional GFEM. It has been demonstrated the potential of the method by solving some heat transfer problems.

The application of GFEM to the problem of structural dynamic analysis of bars subject to axial displacements and trusses for the evaluation of the time response of the structure was presented in Torii and Machado (2012). Trigonometric functions were used as enrichment functions and the Newmark method and modal superposition method were used as algorithms for solution. The results were compared with available analytical solutions, FEM and HFEM.

In Torii's PhD thesis (TORII, 2012), the GFEM formulation was developed for the dynamic transient analysis problems for: bars subjected to axial displacements, beams subject to transverse displacements, two-dimensional wave equation and plane stress state. Studies were performed for time response and modal analyses. The results were compared with those obtained with the polynomial Hierarchical Finite Element Method (HFEM), being allowed to develop the formulation of higher order elements.

The issue of ill-conditioning of the stiffness matrix and a proposal of modification in GFEM, being referred as the "Stable GFEM" (SGFEM) was presented in Babuška and Banerjee (2012). It was shown that the conditioning of the SGFEM stiffness matrix is not worse than the standard FEM in addition to being very robust in relation to the enrichment parameters. Several examples were performed applying the new SGFEM strategy.

A heat transfer study using GFEM was presented in Soghrati *et al.*

(2013). In this work, a computational design of a three-dimensional microvascular mesh of actively-cooled composite material with sinusoidal and straight microchannels was developed. The aim was to minimize the maximum composite temperature, the volume fraction of the microchannels and the pressure drop required for the circulation of the fluid in microchannels. GFEM with enriched interface was used to calculate the temperature field and also a GFEM based solver was included to simplify the Petrov-Galerkin stabilization scheme in order to eliminate the spurious oscillations of the temperature field due to the heat transfer in microchannels be dominated by convection.

An alternative to approach the free and forced vibrations in elastic bi-dimensional problems using the high regularity GFEM to avoid the singularity of stiffness and mass matrices was discussed in Mazzochi *et al.* (2013). The approximation space was obtained from the high regularity explicit enrichment of the partition of unity (PoU) with complete polynomial functions. It was illustrated some examples where one investigates the influence of the regularity of the approximation spaces in obtaining relatively high frequencies. The modal superposition method was employed together with Newmark method for time integration.

In Barros *et al.* (2013), GFEM was adapted to four types of error measures with particular attention to the two-dimensional elasticity problems with singular stress fields. The first error estimator was obtained by using the equilibrated element residual method, while the other three estimators overcame the necessity of equilibrating the residue by employing a subdomain strategy. The goal of this study was to investigate the performance of the four estimators in two-dimensional elasticity problems with geometries that produce singularities in the stress field and concentration of the error in the numerical solution.

GFEM was applied to predict the potential of crack propagation in concrete slabs using a two-scale global-local approach (GFEM^{gl}) in Evangelista *et al.* (2013). The main contribution of this work was the extension of GFEM^{gl} approach to a class of three-dimensional multi-site cracking problems involving realistic boundaries conditions and existence of multiple cracks spanning

different orders of magnitude in size within the domain.

The problems of heat transfer with sharp thermal gradients by GFEM with global-local enrichment functions (GFEM^{gl}) were again analyzed in O'Hara *et al.* (2013). With this approach, the enrichment functions were generated in real time, providing enrichment functions tailored to the problem to be analyzed without a priori knowledge of the exact solution. Some simulations and convergence studies were performed.

An adaptive mesh strategy was applied to analyze crack propagation using the hierarchical finite element method (HFEM) in Murotani *et al.* (2013). Like other strategies, an error estimator was presented as a first step and then an error value estimator using the deformations (Zienkiewicz-Zhu method, Wu *et al.* 1990) and, thereafter, the mesh was refined where need.

Non-linear solid mechanics problems were analyzed by GFEM in Piedade Neto's PhD thesis (PIEADADE NETO, 2013). It was discussed the development of a generalized contact element "segment-to-segment" based on the "mortar method" – a Lagrange multipliers method. The results were validated with some numerical examples.

In Gupta *et al.* (2013a), it was conceived an extension of the global-local GFEM (GFEM^{gl}) for problems of three-dimensional fracture mechanics involving again confined plasticity. The effectiveness of the proposed method was demonstrated by means of nonlinear numerical examples.

The accuracy and conditioning of the stable GFEM (SGFEM) was analyzed and compared to the standard GFEM for problems of two-dimensional fracture mechanics in Gupta *et al.* (2013b). It was presented an additional set of enrichment functions yielded accurate results while not deteriorating the conditioning of the stiffness matrix and some rules of selection of the optimal set of nodes for enrichment. A simple strategy for implementing the stable GFEM in existing software was described too. The results presented in this paper showed that SGFEM delivered optimal convergence rates while the conditioning of the method is comparable to the standard FEM even when geometrical enrichments were adopted.

The formulation of GFEM for analysis of free and transient vibration of

bars was looked over in Arndt *et al.* (2014). The efficiency and convergence of the proposed method for analysis of vibration of bars were studied. The results obtained by GFEM were also compared to those obtained by the analytical solution, some enrichment methods and the h - and p - versions of the Finite Element Method (FEM).

The hydraulic fracturing was investigated in Gupta and Duarte (2014) to complex-layered naturally fractured reservoirs, modeled in three-dimension using the adaptive GFEM to simulate the non-planar fracture propagation. An efficient technique to numerically integrate boundary conditions on crack surfaces was also proposed and implemented. In this method, stress intensity factors (SIF) with pressure on crack faces were extracted using the “Contour Integral Method” (CIM). Various non-planar crack geometries were investigated to demonstrate the robustness and flexibility of the proposed simulation methodology.

In Malagù *et al.* (2014), the application and performance of high-order approximation techniques to one-dimensional nonlocal elastic rods was investigated. A set of one-dimensional integral-differential formulations and boundary-value problems with strain gradients were studied using the finite element method equipped with classic and high order basis functions. The accuracy and convergence properties of the approximation schemes against analytical solutions were evaluated. It was concluded that the B -spline basis functions were the most efficient at modeling problems in the presence of nonlocal and gradient constitutive law.

A general construction of finite-dimensional approximation spaces leading to quasi-optimal convergence rates for Galerkin's approximation of solutions and elliptic equations in the polygonal domain when mixed Dirichlet-Neumann boundary conditions are in place were presented in Mazzucato *et al.* (2014). The construction is quite general and depends on the choice of a sequence of spaces with good approximation on a certain subdomain that is some distance from the vertices. Several theorems, propositions and mathematical proofs were presented in this paper.

Simulations of electromagnetic problems using a hybrid technique called

the “Vector-Generalized Finite Element Method” (VGFEM) allied to the standard Finite Element Method (FEM) was studied in Tuncer *et al.* (2014). This allowed the analysis of non-homogeneous problems without the definition of additional constraints in basis functions. The method was tested in several analyzes demonstrating the advantages in some applications as well as convergence characteristics.

Zhang *et al.* (2014) showed GFEM has excellent approximation properties, but its conditioning can be much worse than that of FEM. It was exposed that the conditioning may not be worse than the standard FEM if some properties for the enrichments are satisfied. This is the principle of the already mentioned Stable GFEM (SGFEM). It was discussed the higher-order SGFEM in which higher order convergence occurs and suggested a specific modification of the enrichment function where the required conditioning was guaranteed, obtaining a robust implementation of this method.

The objective in Cervelin's master dissertation (CERVELIN, 2014) was to develop an enrichment formulation of a polynomial high-order beam element that was able to improve the numerical results of the conventional methods. Different levels of enrichment were tested as well as the selection of elements to be enriched. Some examples were modeled by showing the performance of GFEM and the results were compared to commercial software's and analytical solutions. It was reported that better results were obtained in analyzes with considerations of material non-linearity.

In Shang's PhD thesis (SHANG, 2014), it was developed elastodynamic analyzes in solid media aimed to problems of propagation of mechanical waves. The bar, beam and plane stress quadrilateral elements were implemented by discretizing the time with different algorithms, such as Newmark, Hilbert - Hughes – Taylor and generalized alpha methods. The solution space was discretized by standard and enriched elements using hierarchical enrichment and the partition of unity method. The performance of standard and enriched elements with different run-time algorithms including plastification was analyzed.

Kim and Duarte (2015) worked with the global-local GFEM (GFEM^{gl}) by

simulating the propagation of three-dimensional fracture mechanics. A non-linear cohesive law was adopted to capture objectively the dissipated energy during the process of material degradation without the need of adaptive remeshing at the macro scale or artificial regularization parameters. The robustness, efficiency and accuracy of the approach were demonstrated by the results obtained in numerical experiments.

An extension of the stable GFEM (SGFEM) for problems of 3-D fracture mechanics problems was developed in Gupta *et al.* (2015). It was shown an enrichment scheme based on singular bases and linear polynomials to recover the optimal convergence of the SGFEM. The accuracy and conditioning obtained with the SGFEM was compared with GFEM for different types of singular enrichment bases. The convergence of stress intensity factors (SIF) extracted from GFEM and SGFEM solutions and the effect of the size of enrichment sub-domains on the accuracy of extracted stress intensity factors (SIF) were also studied.

GFEM was developed with enriched interface based on NURBS (*Non-Uniform Rational B-Spline*) in Tan *et al.* (2015). This method was able to efficiently handling branched and curved microchannels. Almost optimal convergence rates were achieved with this method by demonstrating the capability of this numerical scheme using problems with complex microchannel configurations.

Kim *et al.* (2015) elaborated GFEM with global-local enrichment functions (GFEM^{gl}) using numerical experiments to confirm its effectiveness and showed that it was computationally more efficient than the analysis utilizing direct methods. The proposed methodology was capable of generating enrichment functions for problems where a priori knowledge of the solution was limited. Numerical experiments were developed to confirm the effectiveness and efficiency of this methodology.

GFEM was introduced for three-dimensional solid analysis of physical problems exhibiting localized heating and its corresponding thermomechanical effects in Plews and Duarte (2015a). It was demonstrated the method in several applications, with localized thermal and mechanical characteristics and studied the accuracy and relative efficiency of traditional direct modeling approaches.

Plews and Duarte (2015b) modeled local heating problems where complex temperature gradients in materials caused three-dimensional, localized, intense stress and strain variation. To address them, the authors introduced a generalized FEM (GFEM) approach for analyzing three-dimensional solid, coupled physics problems exhibiting localized heating and corresponding thermomechanical effects. The capabilities of traditional hp-adaptive FEM or GFEM as well as GFEM with global-local enrichment functions were extended to one-way coupled thermo-structural problems. The method was demonstrated on some example thermal problems, and accuracy as well as computational efficiency relative to traditional direct modeling approaches was discussed.

An adaptive refinement scheme to reduce geometry discretization errors and provide high-order enrichment function for interface-enriched GFEM was studied in Soghrati *et al.* (2015). The proposed method is based on h -adaptive and p -adaptive refinement techniques to reduce the discrepancies between the exact and discrete geometries of the curved materials interfaces. Several examples were presented to demonstrate the application of GFEM with interface-enrich by modeling thermo-mechanical problems with complex geometries. The accuracy and convergence rates of the proposed method were also studied.

An “Interface-Enriched Generalized Finite Element Method” (IGFEM) for efficient 3-D electromagnetic analysis of heterogeneous materials was introduced in Zhang *et al.* (2015). To eliminate the requirement of generating conformal meshes for geometrically complex domains, FEM solution space was enriched at material interfaces to capture the discontinuities of the field and its derivatives. It was presented three application problems with complex internal structures to demonstrate the ability of the proposed method to analyze efficiently highly inhomogeneous composite materials, without a need to create multiple meshes for problems with randomly distributed inclusions.

In Meschke and Leonhart (2015), a “novel” Generalized Finite Element Method (GFEM) was proposed for the approximation of the liquid pressure in hydro-mechanically coupled finite element analyses of hydraulic fracturing problems. While for the approximation of propagating cracks an enrichment of the displacement field according to the XFEM, adopting the Signum function

$\text{sgn}(x) - (\text{sgn}(x) = +1, \text{ if } x > 0; \text{sgn}(x) = 0, \text{ if } x = 0; \text{sgn}(x) = -1, \text{ if } x < 0)$ – in association with crack tip functions, was employed, problem specific and physically motivated enrichment functions for the liquid pressure field in the vicinity of pressurized cracks were proposed. The performance of the proposed GFEM model in the analysis of propagating, hydraulically induced cracks was demonstrated by means of a benchmark problem.

A gradient-based shape optimization over a fixed mesh based on the recently introduced Interface-Enriched Generalized Finite Element Method (IGFEM) has been developed in Najafi *et al.* (2015), taking advantage of both Eulerian and Lagrangian approaches to eliminate mesh distortion issues as well as to represent geometrical features accurately. It was solved various numerical examples to demonstrate the capability of the method including the computational design of particulate and microvascular composites.

A new formulation for the imposition of Dirichlet boundary conditions for problems with complex boundary geometries was proposed in Ramos *et al.* (2015). The Interface-Enriched Generalized Finite Element Method (IGFEM) was combined with the Lagrange multiplier method, and the results showed that the optimal rate of convergence was preserved. The new formulation yielded a symmetric stiffness matrix and through the solution of linear elastic problems, it was shown that the optimal rate of convergence was preserved for piecewise linear finite elements.

Wu and Li (2015) aimed to remove, or at least, alleviate, the ill-conditioning or even the singularity issue vulnerability to the system matrix of standard XFEM/GFEM while preserving accuracy of the solution as much as possible. Their objective was achieved by introducing a “novel” enrichment function, defined as the linear combination of the shifted Heaviside function (with respect to the node value) and the residual one (with respect to its linear interpolants). Several representative numerical simulations of element and structure benchmark tests were presented to validate the so called “Improved stable XFEM” (Is-XFEM), regarding both accuracy of the solution and conditioning of the system matrix.

Torres *et al.* (2015) sought to identify and understand the advantages of

better capturing the information provided by singular enrichments over mesh-based smooth partitions of unity. The purpose herein was to investigate some possible advantages of mesh-based smooth partition of unity for modeling discontinuities and singularities, in two-dimensional problems of linear elastic fracture mechanics, in such a way that the discretization error associated to stress discontinuities inherent in standard C^0 -continuous GFEM/XFEM approximations could be eliminated. The special instance of GFEM/XFEM that furnishes smooth approximations, C^k -GFEM, was applied to modeling singular stress fields that occur in problems of two-dimensional linear elastic fracture mechanics.

It was shown an application of the Generalized Finite Element Method (GFEM) for modal analysis of 2D wave equation in Torii *et al.* (2015). The proposed GFEM approach was based on trigonometric functions, since these functions commonly appear in analytical solutions of wave propagation problems. The results were compared with the ones obtained with the polynomial FEM using higher order elements.

A stable and flexible generalization of PUM that they called “Orthonormalized Generalized Finite Element Method” (OGFEM) was presented in Sillem *et al.* (2015). The method could construct a well-conditioned constrained stiffness matrix from an arbitrary basis. Partial or full orthonormalization could be applied, and every instance of PUM could be expressed in OGFEM framework, including GFEM and SGFEM. The method was demonstrated for the one-dimensional modified Helmholtz, Poisson equations and compared to FEM, GFEM and SGFEM.

Liu *et al.* (2015) applied the “Differential Quadrature Hierarchical Finite Element Method” (DQHFEM) to thickness-shear vibration of quartz circular crystal plate. The DQHFEM uses a reformulated differential quadrature rule (DQFEM) added to a Gauss-Lobatto quadrature rule and hierarchical finite element method to construct the shape functions. It overcame the numerical stability problem in the Hierarchical Finite Element Method (HFEM) and it was as accurate as the previous quoted method DQFEM. Numerical results of the DQHFEM were compared with the results of other methods, which validated the

high accuracy of the DQHFEM.

Liu *et al.* (2016a) again looked over the differential quadrature hierarchical finite element method (DQHFEM) but now applied to vibration and bending of Mindlin's plates. A numerical comparison and convergence studies of the DQHFEM were carried out by comparing the DQHFEM results with available exact or highly accurate approximate results in literatures.

A generalized finite element method for linear elasticity equations with highly varying and oscillating coefficients was proposed in Henning and Persson (2016). The proposed GFEM was based on ideas often referred to as "Localized Orthogonal Decomposition" (LOD). It was considered linear elasticity equations with mixed inhomogeneous Dirichlet and Neumann boundary conditions. The theoretical a priori error estimate was confirmed by numerical examples.

Arndt *et al.* (2016) developed an accurate assessment for determine natural frequencies for uniform and non-uniform Euler-Bernoulli beams and frames by an adaptive generalized finite element method (GFEM). In this adaptive GFEM, trigonometric and exponential enrichment functions were added to FEM shape functions by the partition of unity approach. Numerical examples were used to verify the accuracy of the iterative proposed method.

An interface-enriched generalized finite element method (IGFEM) was presented for analyzing electromagnetic problems involving highly inhomogeneous materials in Zhang *et al.* (2016a). In order to avoid creating conformal meshes within a complex computational domain and prepare multiple meshes during optimization, it was introduced the enrichment vector basis functions concept. Two examples, involving multiple microvascular channels and circular inclusions of different radii, were analyzed to illustrate the capability of the proposed approach in handling complicated inhomogeneous geometries.

It was developed a coupled hydro-mechanical formulation for the simulation of non-planar three-dimensional hydraulic fractures in Gupta and Duarte (2016a). A Generalized/eXtended Finite Element Method (G/XFEM) was adopted for the discretization of the coupled system of equations. Several three-dimensional numerical verification examples were solved illustrating the generality and accuracy of the proposed coupled formulation and discretization

strategies.

Shang *et al.* (2016) presented dynamic analyses of one-dimensional bar and Euler–Bernoulli beam problems with Generalized Finite Element Method (GFEM). This new enriched finite element formulation for one-dimensional bar and Euler–Bernoulli beam were enriched by trigonometric and exponential functions. Results of a beam free vibration analysis, of a bar elastodynamic analysis, and of a beam elastoplastic dynamic analysis were presented and compared to results from a standard FEM formulation.

A free vibration analysis of Timoshenko beam models by using enriched finite element approaches was presented in Shang (2016). It was performed some analysis of free vibration of Timoshenko enriched by a C^0 element formulated by GFEM and HFEM. The shear locking was briefly investigated in static analysis as well as a normalized discrete spectra analysis was examined.

Zhang *et al.* (2016b) aimed to achieve more computational accuracy, especially on the conductivity boundaries and interfaces of inclusions, developing a forward solver in MAT-MI to compute the electromagnetic field and the induced acoustic field with generalized finite-element method (GFEM). The magneto acoustic tomography with magnetic induction (MAT-MI) is an emerging imaging approach. The aim of MAT-MI is to image the electrical conductivity distribution of biological tissue. The results demonstrated the feasibility of the forward solver in MAT-MI.

Serdoun and Cherif (2016) developed a new C^1 HSDT p -element with eight degrees of freedom per node and used it to find natural frequencies of laminated composite and sandwich thick plates in conjunction with Reddy's higher order shear deformation theory (HSDT). This proposal was made to overcome the well-known C^1 continuity requirement in with Reddy's HSDT. Monotonic and uniform convergence occurred as the number of trigonometric shape functions was increased. The effects of the boundary conditions, core to face sheet thickness ratio, Young's modulus ratio on natural frequencies were investigated through the analysis of these numerical results.

The Interface-Enriched Generalized Finite Element Method (IGFEM) using a thermal solver combined with a gradient-based shape optimization

scheme to obtain optimal designs of a set of branched microchannel networks was analyzed in Tan *et al.* (2016). The aim of utilizing IGFEM was to make easy the discretization of the many configurations analyzed in the design process, and to avoid issues associated with mesh distortion presented in standard finite element shape optimization studies. The IGFEM solver has been verified against nonlinear, fluid/thermal 3D FLUENT solutions, and validated against experimental measurements.

The challenge of a direct extension of the singular crack tip enrichment to dynamic/time dependent problems in the development history of XFEM was addressed in Wen and Tian (2016). Based on earlier works (TIAN, 2013; TIAN; WEN, 2015), an extra-dof-free (DOF = degree of freedom) partition of unity enrichment technique improved XFEM through a crack tip enrichment without extra dof (DOF). Numerical tests showed that the new XFEM was not only straightforward in implementation in dynamic problems, also provided the most accurate dynamic stress intensity factor in benchmark problems and it was orders of magnitude faster with an iterative solver.

Liu *et al.* (2016b) worked again with the differential quadrature hierarchical finite element method (DQHFEM) to analyze the interface of composite structures. The micro/macro-mechanical analysis of the interface of composite structures was very convenient for this method in which both the interfaces of grains and grain boundaries and the interfaces of nanoparticle and the matrix were analyzed. Numerical comparison of the DQHFEM results for the plane static problems with exact and approximated analytical results showed the high accuracy and efficiency of the DQHFEM.

It was suggested a modified intrinsic extended finite element method (XFEM) for one-dimensional and two dimensional elliptic equations with discontinuous coefficients and interfaces in Zhao *et al.* (2016). The shape functions on critical subdomains were special functions that reflected the discontinuous information of the interface. The Gauss integration in special elements crossed by interfaces was also changed. Numerical experiments were presented to verify the feasibility and superiority of the modified intrinsic XFEM compared with the standard FEM and extrinsic XFEM for this type of problem.

Gupta and Duarte (2016b) continued working with the Generalized/eXtended Finite Element Methods (G/XFEM) specifically in this paper studying an a priori estimate for the minimum size of the enrichment zone required for optimal convergence rate of GFEM/XFEM. Detailed numerical verification of these findings was also presented.

Kergrene *et al.* (2016) expanded the study of the Stable Generalized Finite Element Method (SGFEM) presenting a numerical study that showed that if the “angle” between the finite element space and the enrichment space was bounded away from 0, uniformly with respect to the mesh, then GFEM is stable, i.e., the conditioning of GFEM is not worse than that of the standard FEM. It was explored some iterative methods and discussions about this approach with a solid mathematical background.

A generalized finite element method based on the use of parametric solutions as enrichment functions was proposed in Canales *et al.* (2016). They called as V-GFEM (vademecum GFEM) aiming for efficient simulations of manufacturing processes. Its main advantage consists in adapting the trial space in real-time to approximate the solution of the problem optimally. Some numerical examples related to the simulation of thermal models encountered in welding processes were studied.

A hierarchical beam finite element based on the p -version of FEM, using the kinematics of the Tessler's refined zigzag theory (TESSLER *et al.* 2007), for the analysis of laminated composite beams was developed in Nallim *et al.* (2017). The hierarchical finite element proposed allowed taking into account all coupling effects in an efficient and unified procedure. This approach was validated in the analysis of laminated beams with some sequences of symmetric and asymmetric stacking, studying in each case its accuracy and stability.

Son *et al.* (2017) proposed a generalized finite element technique that could accurately approximate the solution of the flexural-shear cantilever model of wall-frame structures proposed by Heidebrecht and Stafford Smith (1973). This approach adopted scaled monomials as enrichment functions inasmuch it consists of smooth functions such as polynomials, hyperbolic and trigonometric functions. Static and modal analyses of the flexural-shear cantilever wall-frame

structures were performed using the proposed GFEM, and their accuracies were compared with those obtained using the standard FEM to investigate the effectiveness and robustness of the proposed method.

The development of isogeometric analysis (IGA) for the free vibration problem of usual structures was presented in Rauen *et al.* (2017). According the frequency spectra results, IGA showed a higher amount of accurate frequencies for bar and beam problems, in which accuracy was improved when the NURBS (*Non-Uniform Rational B-Splines*) degree increases. The results were compared to FEM, GFEM and some of enriched methods.

The aim of Lazzari's master dissertation (LAZZARI, 2017) was to propose a NURBS-based enhancement to the Discontinuity-Enriched Finite Element Method (DE-FEM) in two dimensions. The capabilities of the NURBS-enhanced DE-FEM to solve several weakly discontinuous problems were assessed for composites of different complexities. The accuracy, convergence properties and numerical efficiency of the proposed method were investigated, in particular in comparison with the standard DE-FEM.

Gupta *et al.* (2017) continued studying extraction methods of three stress intensity factor (SIF) but in this paper adopting the Generalized/eXtended Finite Element Method (G/XFEM), the Cutoff Function Method (CFM), the Contour Integral Method (CIM), and the Displacement Correlation Method (DCM). Several problems aimed at investigating the applicability and accuracy of the various extraction methods was solved. The study presented in this paper showed that the DCM is a competitive extraction method for the G/XFEM.

The effects of temperature in the "Shape Memory Alloy Hybrid Composites" (SMAHC) cylindrical stiffened panels' aero elastic stability using the hierarchical Rayleigh–Ritz method combined with the micromechanical model was investigated in Matos *et al.* (2017). The implementation of hierarchical functions proved to be very important in parametric studies, since it allowed improving accuracy without changing the mesh usually employed in standard finite element analysis. Different geometric configurations, laminate stacking sequences, boundary conditions and radii of curvature were investigated.

Iqbal *et al.* (2017) proposed the study of a posteriori error estimates for

time-dependent generalized finite element simulations of heat transfer problems. It was investigated the estimate both for problems with a known exact solution, for which it was compared the indicator with the known error, and in cases where the exact solution was not known. The results provided the basis for space–time adaptive GFEMs for the heat equation.

The determination of the stress intensity factors (SIF) of cracked homogeneous specimens using a low-order accurate eXtended Finite Element Method (XFEM) was studied in Benvenuti (2017). The XFEM was considered not only in relation with a functional space but also with a variational principle, where the singular part of the strain was regarded as an equivalent eigenstrain. The proposed XFEM has been tested on some plane strain examples that demonstrated the approach is generally computationally more robust and accurate than existing comparable XFEMs, while keeping a minimal implementation effort.

Komijani and Gracie (2017) proposed a new numerical method based on enriched finite element methods to analyze wave propagation in fractured media, modeling cracks independently of the mesh. The numerical method combines the Phantom Node Method (PNM) to model fractures and a Generalized Finite Element Method (GFEM) to accurately model wave phenomena. Through three numerical examples it was demonstrated that the spurious oscillations that appear in propagation pattern of high-frequency transient waves in PNM simulations can be effectively suppressed by including harmonic enrichment functions (PNM-GFEM).

It was again considered the differential quadrature hierarchical finite element method (DQHFEM) to analyze the dynamic response of sandwich laminated plates with a viscoelastic core and laminated anisotropic face layers in Liu *et al.* (2017a). The DQHFEM presented good results using a few nodes on the boundary of an element and only several clamped modes inside the element. The response of the model has also been compared with approximated results available in literature, showing excellent agreement.

Liu *et al.* (2017b) also again carried out a study involving the differential quadrature hierarchical finite element method (DQHFEM) but now, for the first

time, for hexahedral, triangular prism and tetrahedral domains were applied to three dimensional analyses of the interfaces of composites. A representative volume element (RVE) was built considering a continuum-based analytical model. This model of grains and their boundaries allied to a two-scale RVE model of nanoparticles and the matrices were analyzed. Numerical results showed the high efficiency and accuracy of the DQHFEM in three dimensional analyses of the two-scale problems for the interfaces of composite structures.

Pinheiro *et al.* (2017) studied the C^k , with k arbitrarily large, partition of unity function, built over a finite element mesh to simulate the non-linear behavior of structures with quasi-brittle materials. The numerical simulation of a plain concrete L-shaped panel was adopted with different kinds of polynomial enrichments in order to test the implemented resources and evaluate its performance on the analysis of damaged quasi-brittle media, comparing with the experimental results.

A systematic approach using GFEM to determine the optimal number of plane waves for a given problem was proposed in Mahdinejad *et al.* (2017). Actually, this work addressed the methodology to identify the best number of enrichment functions for GFEM solution. The results indicated that the adopted strategy could guarantee accurate and converging responses for GFEM in complex problems, along with remarkable reductions of the computational cost.

In Kim *et al.* (2017), a robust and efficient strategy was proposed to simulate mechanical problems involving cohesive fractures in the context of h -adaptive generalized and standard finite element methods. The proposed approach was based on the division of a simulation into a suitable number of sub-simulations where adaptive mesh refinement was performed only once based on refinement window around crack front process zone. Furthermore, a simplified strategy without the need of any data transfer between sub-simulations was proposed so that it could be readily employed in existing FEM software. The computational efficiency, accuracy, and robustness of the proposed strategies were demonstrated by an application to cohesive fracture simulations.

A direct extension of the multiscale GFEM (MS-GFEM) was carried out in Friderikos *et al.* (2017) where damage and fracture mechanisms were now

taken into account. A methodology to enrich the global computational domain with numerically constructed enrichment functions of cracks was presented. The multiscale approach was implemented inside commercial finite element software in order to use the existing infrastructure of the object oriented code for the development of MS-GFEM. Preliminary numerical results showed that with a proper selection of enrichment functions based on the physics associated with the problem, it could be possible to predict the local microstructure interactions that cause damage.

Shang *et al.* (2017) proposed a study with C^0 quadrilateral enriched element by the Generalized Finite Element Method (GFEM), both trigonometric and exponential functions as enrichment functions, applied in free vibration analysis with distorted mesh. The enriched 2D quadrilateral element was employed for static bending problem and some free vibrations analyses providing accurate results with low level of enrichment and few degrees of freedom in several applications. The results were compared with other numerical formulations and showed that the proposed element had good performance.

Some numerical tests in order to implement the latest stable GFEM (SGFEM) improvements were investigated in Sato (2017). Some aspects about integration when using higher order SGFEM were taken into account too. The numerical examples involved 2D panels that presented favorable geometries to explore the advantages of the method comparing it with standard FEM. The results showed the higher order SGFEM was more robust and reliable among the versions of GFEM tested.

The study of NURBS Interface-Enriched GFEM (IGFEM) for a gradient-based shape optimization over a fixed mesh was addressed in Najafi *et al.* (2017). It was combined the advantages of Eulerian approaches in eliminating mesh distortion issues with the accurate representation of the interface geometry in NURBS-based shape optimization. The analytical sensitivity developed in this work introduced new terms involved in the sensitivity of the shape functions and their derivatives for GFEM-based approaches. The method has been verified by solving two benchmark problems, and three application problems demonstrated the capabilities of the shape optimization scheme.

In Babuška *et al.* (2017), it was presented the theoretical justification for the Stable Generalized Finite Element Method (SGFEM) when applied to smooth interface problems. It was proven that a Generalized Finite Element Method (GFEM) is stable, i.e., its conditioning is not worse than that of the Finite Element Method, and it is robust with respect to the mesh, if the enrichment space of GFEM satisfies two axioms. The idea of a strongly stable GFEM associated with one of the two axioms was introduced. This work was the continuation of Kergrene *et al.* (2016), where the stability of GFEM, when applied to interface problems, was established through numerical experiments. The numerical results in Kergrene *et al.* (2016) indicated that GFEM is indeed strongly stable.

A new methodology for modeling problems with both weak and strong discontinuities independently of the finite element discretization as a variance of eXtended/Generalized Finite Element Method (X/GFEM) was introduced in Aragón and Simone (2017). This method so called “Discontinuity-Enriched Finite Element Method” (DE-FEM), added enriched degrees of freedom only to nodes created at the intersection between a discontinuity and edges of elements in the mesh. Emphasis has been placed on the solution of problems in fracture mechanics but the formulation is general and could therefore be applied to solve other partial differential equations. This approach was compared to X/GFEM showing the same convergence rate as the standard FEM with matching meshes.

Liu *et al.* (2017c) continued studying the differential quadrature hierarchical finite element method (DQHFEM) but applied for free in-plane vibration analysis of plates. The NURBS geometries were first transformed into differential quadrature hierarchical geometries and then the solutions field also used the differential quadrature hierarchical basis for analysis. Both curvilinear quadrilateral plates in several platforms and structures composed of several curvilinear quadrilateral elements were analyzed. The accuracy and convergence of the DQHFEM were validated through comparison with exact and approximate results in literature.

An algorithm for non-intrusively coupling commercial finite element software with a research code implementing a hierarchical enrichment of finite

element spaces was discussed in Fillmore and Duarte (2018). The proposed algorithm could be used with any method that hierarchically enriches a finite element space. Examples showing the application of the hierarchical non-intrusive algorithm (HNA) to the coupling of Abaqus with tridimensional GFEM^{gl} software were presented.

Gupta and Duarte (2018) worked with three-dimensional no-planar hydraulic fracture propagation proposing an algorithm and a fully coupled hydro mechanical-fracture formulation in a GFEM approach. The proposed algorithm extended the work of Gupta and Duarte (2016ab nm,) previously quoted by coupling a new fracture propagation model, so called “the GD model”, based on a regularization of Irwin’s criterion with the fluid flow in the fracture and the mechanical deformation of the rock. Examples demonstrating the accuracy and robustness of the proposed formulation and algorithm were presented.

The reduced order modeling (ROM) of structures with local defects undergoing large deformations, i.e., within the nonlinear geometric range was the object of study in Wang *et al.* (2018). The aim was to develop this ROM as an enhancement of its counterpart for the virgin structure so that it could be easily adapted as the defects change and/or new defects appear. In order to numerically implement that, it was used the generalized finite element (GFEM). Validation results on the finite element model of a beam-like panel with a notch confirmed the appropriateness of these basis enrichments.

Chen *et al.* (2018) proposed to compute elliptic equations with rough coefficients using random sampling strategies in the context of Generalized Finite Element Method (GFEM). It was addressed a quantitative criterion to analyze and compare these sampling strategies. Numerical evidence showed that the optimal basis functions could be well approximated by a random projection of generalized eigenvalue problem onto subspace of α -harmonic functions.

And, the last but not the least, Weinhardt *et al.* (2018) dealt with two proposals to minimize the problem of sensitivity of GFEM in the dynamic analysis: an adaptation of the Stable Generalized Finite Element Method (SGFEM) and a stabilization strategy based on preconditioning of enrichment. Examples of one-dimensional modal and transient analysis were presented as

bars with cross section area variation. The results of this work pointed out that there are ways to overcome instability problems in GFEM applied to dynamic analysis, since simple proposals were able to positively impact the approaches.

2.3 REVIEW OF THE MODIFIED LOCAL GREEN'S FUNCTION METHOD

The Modified Local Green's Function was developed by Barcellos and Silva (1987) and Silva (1988) after studies and modifications of the technique used by Burns (1975), Horak (1980) and Horak and Dorning (1981) called the "Local Green Function Method".

The initial conception of the Modified Local Green's Function was to explore the main advantages of three other techniques: the Finite Element Method (FEM), the Boundary Element Method (BEM) and the Green's Function Method (GFM). Through the MLGFM, the matrices of the integral equations system are determined directly without the explicit knowledge of the Green's Function. This is one of the greatest advantages compared to the original method.

The first applications (BARCELLOS; SILVA, 1987; SILVA, 1988) of this new technique were based on solutions of membranes problems, rods and beams. Later on, publications such as Barbieri and Barcellos (1993a; 1991a; 1991b; 1993b) and Barcellos and Barbieri (1991) used this method to solve problems of nonhomogeneous potential, three-dimensional potential, Mindlin's plate and singular potential, with good results.

The new method then turned over to the case of bending in orthotropic laminated plate by first order theory through the work of Machado and Barcellos (1993) investigating the MLGFM in problems not adequately solved by other numerical techniques.

In Barbieri's PhD thesis (BARBIERI, 1992), a generalization of the MLGFM to problems of structural mechanics was exposed, presenting the problems of homogeneous and nonhomogeneous potential, two-dimensional elasticity, including fracture problems and Mindlin's plate bending.

The performance of the MLGFM in static and dynamic analyzes (modal analysis) concerning potential problems was examined in Fillipin, Barbieri and Barcellos' paper (FILLIPIN *et al.*, 1992a) as well as the " p -" and " h -" convergence rates.

Other works also used this new numerical technique, reinforcing the good numerical performance of this integral method, such that

- Barbieri *et al.* (1992) applied to elasto static problems;
- Machado *et al.* (1992), in the case of laminated plates analyzed by higher order theory (KANT; PANDYA, 1988);
- Filippin *et al.* (1992c), to dynamic problems governed by the Helmholtz Equation, as free vibrations in membranes and propagation of waves in acoustic cavities;
- Filippin *et al.* (1992b) presented the MLGFM as a computational tool, to exemplify membrane-free vibration problems. It was suggested the use of adaptive techniques to maximize the potential of the method;
- Filippin (1992), in his master's dissertation, presented more details and cases for problems of membrane-free vibration and acoustic cavities;
- Maldaner and Barcellos (1992) for two-dimensional fracture problems.

Several laminated plate problems with first order and higher order theories employing the MLGFM were shown in Machado's PhD thesis (MACHADO, 1992) where the results were compared with the available literature.

In Barcellos *et al.* (1992a; 1992b) papers, it was consolidated a review of the method until that moment, with some of its latest applications.

A new application of the MLGFM was presented in Barbieri *et al.* (1993a), where the problem of shells was treated through the one-cell approach.

In 1993, other works based on MLGFM were developed and published such as

- Barbieri and Barcellos (1993a), for potential problems in which the properties of the medium vary continuously or continuously in parts;

- Barbieri and Barcellos (1993b), advancing in studies of Mindlin's plates with emphasis on numerical applications;
- Maldaner *et al.* (1993), amplifying the range of the MLGFM for two-dimensional fracture using the "quarter-point" element;
- Maldaner and Barcellos (1993) presenting a comparison of the special fracture elements performance based on the family of Akin and Stem, applying the MLGFM;
- Machado *et al.* (1993) comparing the performance of MLGFM with some Finite Element formulations to solve the problem of orthotropic laminated plates;
- Filippin *et al.* (1993), more results were presented for free-vibration of membrane and acoustic cavities problems emphasizing the excellent convergence of results for the high frequencies;
- Barbieri *et al.* (1993b) presenting a study of mesh distortion sensitivity and punctual convergence in Mindlin's plate problems;
- Munoz *et al.* (1993), was devoted to a first free-vibration analysis of Mindlin's plate problem.

In Maldaner's master dissertation MALDANER (1993), the MLGFM was studied, implementing special non-isoparametric fracture elements, comparing its performances with those of conventional elements.

Muñoz (MUÑOZ, 1994) dealt with the application of the Modified Local Green's Function Method (MLGFM) to problems of bending and free-vibration of Reissner-Mindlin's plates. A general alternative formulation of the method was presented, demonstrating that the approximate solution error is minimized only in domain, within each Green cell. Particular attention was assigned to the analysis of the locking phenomenon when approaching Green's function with finite elements based on displacements.

The Modified Local Green's Function (MLGFM) was adopted to solve problems of three-dimensional elastostatics in Meira Junior's work (MEIRA JUNIOR, 1994). The MLGFM was used to solve some examples of three-dimensional elasticity applications, such as: prismatic bar under uniform traction, block subjected to simple shear, bending of a short beam uniformly

loaded, thick-walled cylinder with internal pressure, bending of a beam curve by a load at its extremity and pure bending of a prismatic beam.

A comparative analysis of the MLGFM performance versus FEM for bending and free-vibration Mindlin's plate solution was presented in Muñoz and Barcellos (1994a). Comparisons were made for displacements, reactions and natural frequencies (vibration).

Muñoz and Barcellos (1994b) presented more results of the MLGFM application in the free-vibration Mindlin's plate solution. It was shown the MLGFM formulation for free-vibration Mindlin's plate problems and numerical results for plates with some boundary conditions.

A detailed review of the MLGFM can be found in Muñoz (1994) and Meira (1994) works, up to 1994.

In Barbieri *et al.* (1998), it was formally introduced the mathematical basis of MLGFM. In fact, this work is split into two parts (two publications). Although many researchers have presented numerical results using this technique, no attempt had been made until at the time of this work to demonstrate the solid mathematical basis of this method. These publications were sought to close this gap.

Barbieri and Muñoz (1998) published this second paper commented above showing a compilation of significant results obtained by the application of the MLGFM to the potential problems and Mindlin's plate. Numerical examples were given explaining the main points of the method, for example, convergence rate, processing time, application to the problems of one-cell and multi-cell two-dimensional potential, two-dimensional elasticity problems and Mindlin's plates under bending with one-cell approach.

After a long period, in Silva (2004), the application of MLGFM was resumed, applying this technique to laminated composite plates previously explored by Machado (1994) but including the damage within these structures. The damage was modeled as transverse cracks distributed in the matrix and some configurations of cracked laminated plates were studied.

Continuing the studies of laminated composite plates with cracks in their matrices, Silva *et al.* (2005) proposed an investigation of strain-displacement

relations for damaged structures and, subsequently, including the cracks in the matrix. The MLGFM was used to approximate the final solution. Some results were shown by varying the stacking sequence of the plates, number of laminated layers, orientation of the fibers and the extension of damage compared to other publications.

With Tassini's master dissertation (TASSINI, 2005), the studies of laminated composite plates with cracks in the matrix were extended, but now considering the evolution of the damage being clearly the continuity of the studies developed by Silva (2004). In this work, it was shown that the strength of the laminated plates is affected by the damage process when subjected to some loading in time. The strain energy criterion was used to calculate the evolution of the damage.

It was shown a comparison between the MLGFM for the evaluation of the heat flow in anisotropic media with finite volumes and finite elements in Muñoz and Vaz (2007). In this paper, the heat flow was approached by using a super convergent recovery scheme, while the former flow quantities were calculated directly at nodes. Linear elements were used in the numerical example. Non-homogeneous temperature and flow boundary conditions were included.

Again, MLGFM was used in Machado *et al.* (2008) to solve problems of laminated composite plates with generalized transversal cracks. The effect of the damage was considered as an additional loading vector and no modification was necessary in the stiffness matrix of the problem.

Machado *et al.* (2012) dealt with laminated composite plates with generalized transversal cracks in the matrix by applying the Mechanical Damage Theory (LEMAITRE, 1992) where the loss of stiffness in laminated composite plates was calculated when the cracks were formed into the matrix and the consequent evolution of the damage based on time and loading. This work was presented in the form of a chapter of a book.

It was presented a review of the main applications of the Modified Local Green's Function Method in the context of the structural mechanics of plates in Machado *et al.* (2013). This contribution was part of the celebration of the 70th Prof. Clovis Sperb of Barcellos' anniversary.

Barbieri and Machado (2015) resumed the local strategy (multiple cells) for calculating the projections of Green's function using the Finite Element Method (FEM). The numerical examples showed some aspects of the method that had not yet been observed and good results for the flow in all nodes of the mesh as expected in the multi-cell approach.

In 2017, two conference papers were published dealing with the enrichment of the MLGFM. In Silva *et al.* (2017a) and Silva *et al.* (2017b), the first application of this approach was employed to solve some 2D elasticity problems both in plane strain and stress states. The results showed the great potential of this application and further developments are expected with this new concept.

In next chapter, in order to properly prepare the mathematical formulation of the Enriched Modified Local Green's Functions Method, the enriched methods used in this work – HFEM and GFEM – are presented and developed.

Chapter 3

Enriched Finite Element Methods: HFEM and GFEM

3.1 Introduction

Since the 1950s, with the computational advance fomented mainly by the spatial race, several approximate methods of solving equations that govern physical problems have been developed. These methods are able to solve approximately problems where analytical solutions are not feasible. One of these methods widely used until now is the Galerkin Method (REDDY, 1986). The Galerkin Method is an established procedure of converting a continuous operator problem (such as a differential equation) to a discrete problem, seeking an approximate solution of a boundary-value problem in a finite-dimensional space. Actually, the determination of suitable basis functions for use in the Galerkin method can be extremely difficult. The Finite Element Method (FEM) overcomes this difficulty by providing a systematic means for generating basis functions on domains of fairly arbitrary shape. There are several methods that have the basic characteristics of FEM in addition to some kind of modification or enrichment. Arndt (2009) was one of works that classified a group of methods based on FEM as “Enriched Finite Element Methods”. The main feature of the enriched methods is the enrichment of the shape functions space from the classical FEM by adding

other polynomial or non-polynomial functions related to the solution of the governing differential equation of the problem. The approximated solution of these methods – the finite element approximation of displacements – in element domain, for example, is obtained adding the FEM displacement u_{FEM} and the enriched displacement $u_{ENRICHED}$. This concept will be further detailed in this chapter.

Different sets of enrichment functions can produce different enriched methods as quoted by Arndt (2009) such as: Assumed Modes Method (ENGELS, 1992; GANESAN; ENGELS, 1992), Composite Element Method (ZENG, 1998) and p -Fourier Finite Element Method (LEUNG; CHAN, 1998). These methods classified by Arndt as “enriched methods” have also in common another important characteristic: the approximation functions are reused when the order of the approach is increased. This characteristic is known as “Hierarchical”. Although these concepts were applied by Arndt (2009) in a vibration/dynamic analysis context, this idea was firstly employed in static and singular problems analysis (PEANO, 1976; ZIENKIEWICZ *et al.*, 1983). The Hierarchical Finite Element Method (HFEM) is the subject of the first part of this chapter.

Among the enriched formulations, the Generalized Finite Elements has to be highlighted. GFEM described by Babuška and Melenk (1997) has been presented as a way of generating approximation spaces from any basis functions by multiplying these basis functions and a partition of unity (PoU). GFEM is based on the Partition of Unity Method (PUM) presented by Melenk and Babuška (1996) that showed that the space obtained from PUM was able to inherit the approximation properties of the original space and moreover the conformity and regularity properties. For instance, the conventional Lagrangian FEM shape functions form a partition of unity.

Independently, similar concepts were presented by Duarte and Oden (1995) – the hp Cloud Method. According to Babuška *et al.* (2003), several other methods are strictly related to GFEM, because they are based on PUM, such as, The Method of Finite Spheres – MFS – (DE; BATHE, 2001) and the Extended Finite Element Method – XFEM – (BELYTSCHKO *et al.*, 2009). Anyway, the concept developed by Duarte and Oden (1995) as well as Babuška and Melenk

(1997) are very similar, being unified later on as the name GFEM. This is the concept explored here in this work and the subject of the second part of this chapter.

Wrapping up this chapter, the element's enrichment is established following the procedure proposed by Šolín *et al.* (2004). It is important to point out that the element's enrichment for both approaches, HFEM and GFEM, are implemented according to the developments described in last section of this chapter.

3.2 ENRICHED METHODS

3.2.1 The Hierarchical Finite Element Method (HFEM)

The standard finite element formulation uses polynomials as shape functions. Furthermore, the coefficients of these polynomials are determined by using mathematical boundary conditions, related to nodal positions. This type of formulation presents several difficulties in the case where element order increase is desired, thus the quantity of nodes should be increased. Therefore, a serious drawback exists with this “standard” shape functions (for example, Lagrange shape functions) since when element refinement is made totally new shape functions have to be generated and hence all calculations repeated. In other words, it is necessary to generate new shape functions to increase the element order, without possibilities to reuse those from previous order. It represents a difficulty in computational code implementation, thus there is not hierarchical characteristic in this type of mesh refinement. From a computational cost point of view, it will be advantageous to have a solution that permits increasing the mesh refinement order without necessity to recalculate the matrices created from previous orders. The finite element formulations with hierarchical enrichment present this characteristic. When the enrichment level is augmented, it increases the element order, but without the necessity to reconstruct the terms in matrices

obtained from previous level. The new enrichment functions increase the matrix size, however, reuse integrally those terms generated from previous level.

It seems that the hierarchical functions were introduced by Zienkiewicz, Irons, Scott and Campbell around the year 1971, according to the work of Zienkiewicz *et al.* (1983). Campion and Jarvis (1996) highlighted the main advantages of hierarchical methods: the retention of the coefficients of the stiffness matrix when the order of the interpolation increases and the achievement of high convergence rates without the need to refine the mesh, besides resulting in improved conditioning of the involved system equation. It is difficult to trace the origin of the name “*Hierarchical Finite Element Method – HFEM*”, but it seems that Peano (1976) was the first to use it.

The idea of HFEM is to utilize approximation spaces that are hierarchical. That is, by increasing the order of an approximation space from “ p ” to “ $p+1$ ” the functions used for order “ p ” are kept. In traditional form, HFEM employs the Lagrange polynomials as hierarchical functions, due to the fact that these polynomials are relatively easy to be obtained, and they respect the features of conventional FEM, that makes easier the application of boundary conditions and determination of stiffness matrix. This is cited by Beslin and Nicolas (1997) as “a particular class of the p -version of the finite element method”. But a hierarchical basis doesn't necessarily need to be a polynomial form since it is found developments in trigonometric basis too, for instance (RIBEIRO, 2001).

In this work, the context of HFEM employs hierarchical polynomials as “*enrichment functions*”. These functions are developed and incorporated into standard finite element shape functions. A special attention has been taken in handling these hierarchical functions to avoid compromising the nodal physical meanings, in finite element mesh. It is desirable to employ the hierarchical shape functions that assume zero value in nodal points and any other values in other points in element domain. That is exactly the case of Lobatto shape functions! Hence, the Lobatto shape functions are referred as enrichment functions with hierarchical characteristics.

The construction of hierarchical mathematical spaces by polynomials is described in detail by Šolín *et al.* (2004) as mentioned before but we can summarize the concept in such way (see Appendix “A”):

According to Ciarlet (1991) and Šolín *et al.* (2004), a finite element in \mathbb{R}^n is a triad $K = (K_h^e; P_p; \Sigma)$, where

- K_h^e is a closed subset of \mathbb{R}^n with a nonempty interior and a Lipschitz-continuous boundary;
- P_p is a finite-dimensional space of real-valued functions defined over the set K_h^e of dimension $N_p = \dim(P_p)$;
- Σ is a set of N_p linear forms ζ_i , $1 \leq i \leq N_p$, defined over the space P_p and, by definition, it is assumed that the set Σ is P_p -unisolvent, in the following sense: given any real scalars α_i , $1 \leq i \leq N_p$, there exists a unique function $l \in P_p$ that satisfies

$$\zeta_i(l) = \alpha_i \quad \text{for } 1 \leq i \leq N_p, \quad (3.1)$$

in particular

$$\zeta_j(l_i) = \delta_{ij} \quad \text{for } 1 \leq j \leq N_p, \quad (3.2)$$

and the following identity holds

$$l = \sum_{i=1}^{N_p} \zeta_i(l) l_i \quad \text{for all } l \in P_p. \quad (3.3)$$

Here δ_{ij} is the standard “*Kronecker delta*” (for discrete cases), $\delta_{ij} = 1$ if $i = j$ and $\delta_{ij} = 0$ otherwise. The linear forms ζ_i , $1 \leq i \leq N_p$, are called the *degrees of freedom* (DOF) of the finite element, and the functions l_i , $1 \leq i \leq N_p$, are called the *basis functions* of the finite element. The basis functions are also called the *shape functions* in engineering literature. The set K_h^e itself is often called a *finite*

element. What makes the method especially attractive is the fact that these basis functions are piecewise polynomials that are non-zero only a relatively small part of the domain

Now, consider a domain K_h^e and a space P_p of polynomials of the order at most “ n ” of dimension N_p . Consider a hierarchic basis $\mathcal{B}^n = \{\mathcal{B}_1, \mathcal{B}_2, \dots, \mathcal{B}_{N_p}\}$ in the space P_p . By hierarchic we mean that

$$\mathcal{B}^n \subset \mathcal{B}^{n+1} \quad (3.4)$$

for every “ n ”. Every polynomial $g \in P_p$ can be uniquely expressed as a linear combination

$$g = \sum_{i=1}^{N_p} \lambda_i \mathcal{B}_i = \sum_{i=1}^{N_p} L_i(g) \mathcal{B}_i \quad (3.5)$$

where λ_i are real coefficients and $L_i(g) = \lambda_i$ linear forms

$$L_i : P_p \rightarrow \mathbb{R}, \quad i = 1, 2, \dots, N_p. \quad (3.6)$$

Obviously, the choice $\mathcal{B}^n = \Sigma = \{\zeta_1, \zeta_2, \dots, \zeta_{N_p}\}$ yields a unisolvent finite element $(K_h^e; P_p; \Sigma)$ as defined in Šolín *et al.* (2004), and by the definition, the hierarchic basis \mathcal{B} has the “*delta-property*”¹. “*Unisolvency*” here is another expression for compatibility of the set of degrees of freedom Σ with the polynomial space P_p . So, the standard Lagrange interpolation in FEM has now to be combined with *projection* onto hierarchically constructed subspaces of the space P_p , technique also known as “*projection-based interpolation*” (ŠOLÍN *et al.*, 2004). This nontrivial technique extends the standard nodal interpolation to hierarchic higher-order elements and forms an essential part of higher-order finite element methods. It is not the objective of this work to explore it and for

¹ *delta-property*: only one shape function is non-null at each node.

further details, please see Šolín *et al.* (2004). In there, the developments of the projection-based interpolant is constructed as a sum of a vertex and bubble interpolants in a 1D element and a sum of a vertex, edge and bubble interpolants in a 2D element. This concept will be better developed further in this work in last section named “The Element’s Enrichment”.

One way of constructing the hierarchical mathematical space, among any other ones, is to use the Lobatto shape functions. The first six Lobatto shape functions used in this work can be visualized on Table 3.1.

Table 3.1 – First six Lobatto shape functions and their polynomial order.

HFEM ENRICHED SHAPE FUNCTIONS	
Polynomial Order	Lobatto Shape Functions
$p = 1$	$l_0 = \frac{1-\xi}{2}$ $l_1 = \frac{1+\xi}{2}$
$p = 2$	$l_2 = \frac{1}{2}\sqrt{\frac{3}{2}}(\xi^2 - 1)$
$p = 3$	$l_3 = \frac{1}{2}\sqrt{\frac{5}{2}}(\xi^2 - 1)\xi$
$p = 4$	$l_4 = \frac{1}{8}\sqrt{\frac{7}{2}}(\xi^2 - 1)(5\xi^2 - 1)$
$p = 5$	$l_5 = \frac{1}{8}\sqrt{\frac{9}{2}}(\xi^2 - 1)(7\xi^2 - 3)\xi$

Observe that $\xi = [-1, 1]$ is the finite element natural coordinate known as local coordinates. These shape functions can be plotted in a graph as shown in Figure 3.1. Also, note that the boundary conditions can be easily set for Lobatto shape functions with $p > 2$ where “ p ” is the Lobatto shape function polynomial order since they have null values at the end of the interval $\xi = [-1, 1]$.

It was observed by Torii (2012) there are only diagonal terms added to the

stiffness matrix when increasing the element order “ p ” of a one-dimensional approximation using Lobatto shape functions. This characteristic is due to the fact that the Lobatto shape functions are “orthogonal polynomials” with respect to the bilinear operator norm of the problem’s weak form. But it is important to emphasize that this attribute may not be kept for bi-dimensional problems.

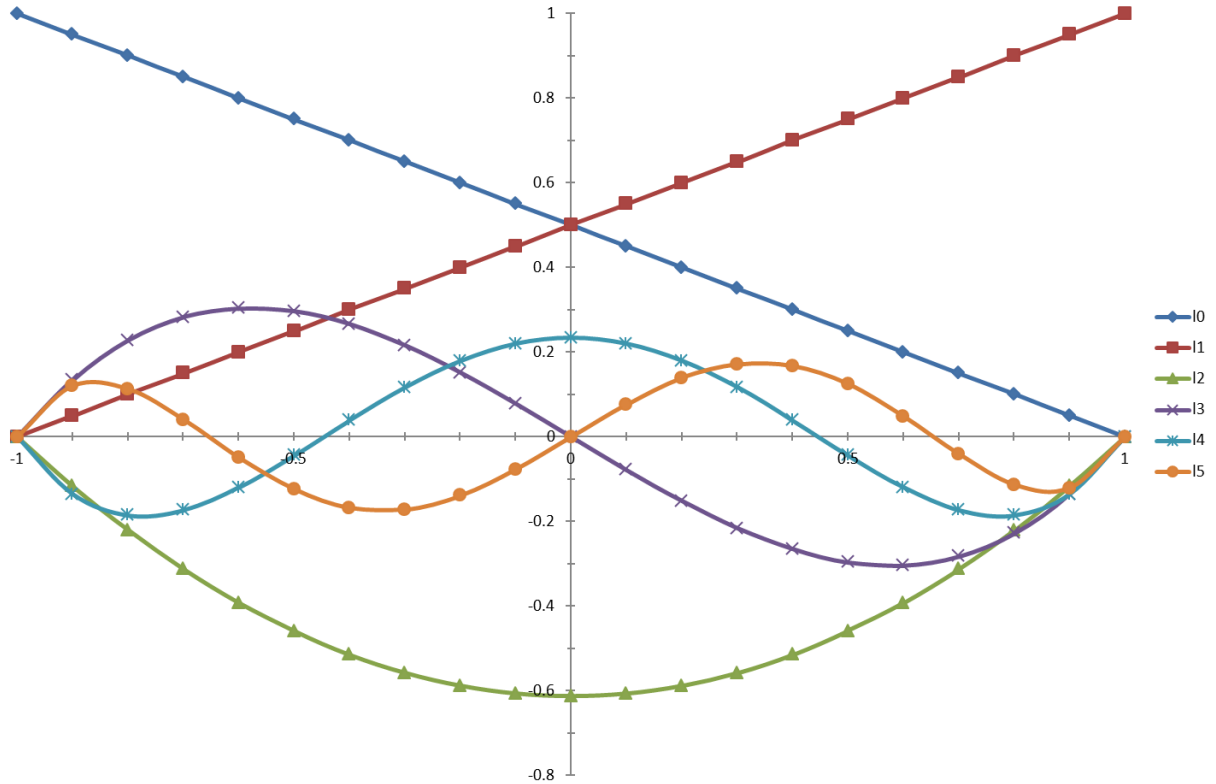


Figure 3.1 – HFEM shape functions used in this work: first six Lobatto shape functions (ŠOLÍN *et al.*, 2004).

3.2.2 The Generalized Finite Element Method (GFEM)

According to Barros (2002), “*The Generalized Finite Element Method – GFEM*” was independently proposed by Babuška, Caloz and Osborn as “Special Finite Element Method - SFEM” (BABUŠKA *et al.*, 1994) and further by Babuška and Melenk as “The Partition of Unity Finite Element Method – PUFEM or simply PUM” (MELENK; BABUŠKA, 1996) at the same time that Duarte and

Oden established “The hp Cloud Method” (DUARTE; ODEN, 1995) as a hybrid FEM formulation.

The GFEM is nowadays understood as an extension of the standard Finite Element Method (FEM) in the sense that it allows us to incorporate into the basis of the approximation any special functions which are known to well approximate the solution locally. These special functions are pasted into the standard FEM basis of mapped polynomials by employing the Partition of Unity Method (PUM). So, the key feature of these methods is the use of a partition of unity (PoU).

It is important to emphasize the distinction proposed by Torii (2012) and also used here in this work: we named PUM the methodology of obtaining local approximate functions from any PoU plus a basis function that represent the physical phenomenon to be studied. On the other hand, the name “GFEM” is adopted in the case of the obtained functions from PUM are added with the standard FEM functions.

Next section will deal with the definition of the PUM and it will make clear that it is a generalization of a partition of unity given by the standard FEM.

3.2.2.1 The partition of unity method (PUM)

The most prominent features of PUM according to Melenk and Babuška (1996) are:

1. The ability to include a priori knowledge about the local behavior of the solution in the finite element space;
2. The ability to construct finite element spaces of any desired regularity (as may be important for the solution of higher order equations);
3. The fact that the PUM falls into the category of “meshless” methods; a mesh in the classical sense does not have to be created and thus the complicated meshing process is avoided;
4. The fact that the PUM can be understood as a generalization of the classical h , p , and hp versions of the Finite Element Method.

The main technical notion in the construction of the PUM spaces is the

(M, C_∞, C_G) partition of unity. The mathematical foundation of the Partition of Unity Method will be then further examined (MELENK; BABUŠKA, 1996).

Definition 3.1 (Partition of Unity). Let $\Omega \subset \mathbb{R}^n$ be an open set, $\{\Omega_i\}$ be an open cover of Ω satisfying a pointwise overlap condition

$$\exists M \in \mathbb{N} \quad \forall x \in \Omega \quad \text{card}\{i \mid x \in \Omega_i\} \leq M. \quad (3.7)$$

Let $\{\varphi_i\}$ be a Lipschitz partition of unity subordinate to the cover $\{\Omega_i\}$ satisfying

$$\text{supp}(\varphi_i) \subset \text{closure}\{\Omega_i\} \quad \forall i, \quad (3.8)$$

$$\sum_i \varphi_i \equiv 1 \text{ on } \Omega, \quad (3.9)$$

$$\|\varphi_i\|_{L^\infty(\mathbb{R}^n)} \leq C_\infty, \quad (3.10)$$

$$\|\nabla \varphi_i\|_{L^\infty(\mathbb{R}^n)} \leq \frac{C_G}{\text{diam}\Omega_i} \quad (3.11)$$

where C_∞, C_G are two constants and L^∞ is the space of all measurable functions which are bounded almost everywhere. Then $\{\varphi_i\}$ is called a (M, C_∞, C_G) partition of unity subordinate to the cover $\{\Omega_i\}$. The partition of unity $\{\varphi_i\}$ is said to be of degree $m \in \mathbb{N}_0$ if $\{\varphi_i\} \subset C^m(\mathbb{R}^n)$. The covering sets $\{\Omega_i\}$ are called “patches”.

From the Definition 3.1, the constant M from expression 3.7 controls the overlap of the patches. In particular, not more than M patches overlap in any given point $x \in \Omega$ of the domain. The expression 3.8 express that the functions $\{\varphi_i\}$ must be non-null only inside their patches. The expression 3.9 points out the fact that the functions $\{\varphi_i\}$ of a PoU must have the unit value when added with. And, finally, the expression 3.10 denote that the functions $\{\varphi_i\}$ must be bounded and the expression 3.11 that $\{\varphi_i\}$ possess bounded derivatives, i.e., it expresses the fact that we need to control the gradient of the partition of unity functions

$\{\varphi_i\}$ if we are interested in H^1 estimates.

Definition 3.2 (PUM space). Let $\{\Omega_i\}$ be an open cover of $\Omega \subset \mathbb{R}^n$ and let $\{\varphi_i\}$ be a (M, C_∞, C_G) partition of unity subordinate to the cover $\{\Omega_i\}$. Let $V_i \subset H^1(\Omega_i \cap \Omega)$ be given. Then the space

$$V_{PUM} = \sum_i \varphi_i V_i = \left\{ \sum_i \varphi_i v_i \mid v_i \in V_i \right\} \subset H^1(\Omega) \quad (3.12)$$

is called the PUM space. The PUM space V_{PUM} is said to be of degree $m \in \mathbb{N}$ if $V_{PUM} \subset C^m(\mathbb{R}^n)$. The spaces V_i are referred to the local basis (approximate) spaces.

Theorem 3.1 (PUM approximation). Let $\Omega \subset \mathbb{R}^n$ be given. Let $\{\Omega_i\}$, $\{\varphi_i\}$ and $\{V_i\}$ be as in Definitions 3.1 and 3.2. Let $u \in H^1(\Omega)$ be the function to be approximated. Assume that the local basis (approximate) spaces V_i have following approximation properties: On each patch $\Omega_i \cap \Omega$, u can be approximated by a function $v_i \in V_i$ such that

$$\|u - v_i\|_{L^2(\Omega_i \cap \Omega)} \leq \varepsilon_1(i), \quad (3.13)$$

$$\|\nabla(u - v_i)\|_{L^2(\Omega_i \cap \Omega)} \leq \varepsilon_2(i). \quad (3.14)$$

where $\varepsilon_1(i)$ and $\varepsilon_2(i)$ are dependent values of an “ i -th” cover that confine $(u - v_i)$ and their derivatives according to a convenient norm.

Then the function

$$u_h = \sum_i \varphi_i v_i \in V \subset H^1(\Omega) \quad (3.15)$$

satisfies

$$\|u - u_h\|_{L^2(\Omega)} \leq \sqrt{M} C_\infty \left(\sum_i \epsilon_1^2(i) \right)^{1/2}, \quad (3.16)$$

$$\|\nabla(u - u_h)\|_{L^2(\Omega)} \leq \sqrt{2M} \left(\sum_i \left(\frac{C_G}{\text{diam}\Omega_i} \right) \epsilon_1^2(i) + C_\infty^2 \epsilon_2^2(i) \right)^{1/2}. \quad (3.17)$$

The Theorem 3.1 demonstrates that the PUM space is similar to the base spaces V_i . From expression 3.16 it is observed that the difference between the original solution u and the approximate one u_h depends on a constant and the individual differences of the chosen functions $v_i \in V_i$. That is the same for the gradient of the approximate function in expression 3.17. Consequently, it is expected the PUM space V_{PUM} is able to give similar results as the local basis space V_i once the $v_i \in V_i$ is a good approximation of u .

There is an advantage on using the PUM space: it is possible to employ non polynomial functions $v_i \in V_i$ once these functions represent the physical phenomenon to be studied. This aspect allows enlarging the approximate spaces. It is possible to build several kinds of PoU using, for instance: Lagrange and Legendre polynomials, Lobatto and Shepard functions, B-Splines and trigonometric functions (SHANG *et al.*, 2017).

As a matter of fact, the usual FEM piecewise linear hat functions on a regular mesh in two dimensions satisfy the above conditions of a (M, C_∞, C_G) partition of unity; and condition 3.11 is satisfied because of the regularity of the mesh, i.e., the minimum angle condition satisfied by the triangulation. For instance, the classical bilinear finite element functions on quadrilateral meshes form a (M, C_∞, C_G) partition of unity ($M = 4, C_\infty = 1$).

Actually, the partition of unity generated by the usual FEM linear hat functions can be better visualized in a one-dimensional finite elements example as in Figure 3.2. In this case, each global approximate function ϕ_i is a PoU φ_i given by Definition 3.1. Examining this definition: the cover $\{\Omega_i\}$ is the finite element mesh and each patch Ω_i corresponds to a subdomain of Ω formed by the union of the elements that share an arbitrary node x_i . Each function ϕ_i is defined by two neighboring elements except by the functions ϕ_1 and ϕ_4 . For example, the

function ϕ_2 is defined by the union of the first and second elements. Hence, each patch is given by two adjacent elements as previously mentioned and, in this case, the number of patches in each finite element is 2; thus, $M = 2$. From expression 3.9, the sum of all functions ϕ_i results in unity across the domain. Moreover, both the functions ϕ_i and their first derivatives are bounded from expressions 3.10 and 3.11. Finally, it is observed that ϕ_i acts only under its patch Ω_i as enunciated by expression 3.8. In other words, the support of each PoU ϕ_i is constrained in the closure of each patch Ω_i ; ϕ_i is different of zero only inside the patch Ω_i .

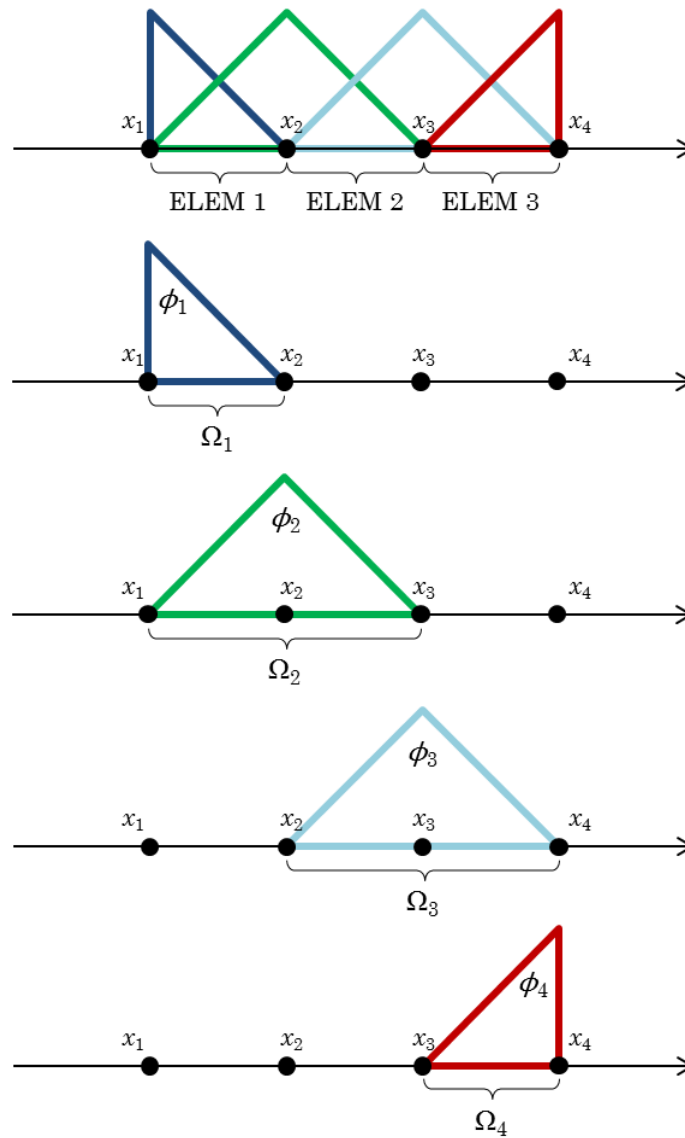


Figure 3.2 – FEM linear hat functions as a partition of unity – PoU. **SOURCE:** Adapted from Torii (2012).

For GFEM employed in this work, the standard FEM shape functions are taken as the partition of unity (PoU). For example, for 1D problems, the standard FEM uses the already mentioned linear “hat functions” as well as for the 2D problems, the standard FEM uses the bilinear Lagrangian functions. The original element domain is then enriched by appropriated enrichment local functions.

3.2.2.2 GFEM generalization

Taking the *hp* cloud method (DUARTE; ODEN, 1995) as reference, the element domain can then be enriched by multiplying the standard shape function of finite elements by a new set of linearly independent functions called here as “enrichment functions”. These enrichment functions can be selected arbitrarily or even can be set from the analytical solutions, since they are in accordance with mathematical condition previously established by GFEM. This *a priori* knowledge is introduced by the PUM into the local approximate space to generate the “generalized finite element functions” or simply the “enriched shape functions”. They can range from polynomials to very sophisticated handbook functions (STROUBOULIS *et al.*, 2001). These are local approximations and they should represent the solution on the associated support in its own patch Ω_i . So, using the PUM to generate local approximation spaces in patches Ω_i , it is possible to represent the overall approximation in the cover Ω (BABUŠKA *et al.*, 2002).

A generalization of GFEM formulation in \mathbb{R}^2 can be understood as an overlap of an arbitrary enrichment function and a partition of unity (PoU), as can be seen in Figure 3.3. For the linear standard element (hat function), the PoU is a polynomial function of order $p = 1$ (bilinear function), which generates an approximation C^0 (Figure 3.3a). The enrichment function is an arbitrary special function, polynomial or non-polynomial form (Figure 3.3b). The appropriate combination of these two functions, the enrichment function and the PoU (in this case, the hat function from the standard FEM), provides the enriched shape function (Figure 3.3c) which has special characteristics of the approximating chosen function and, at the same time, incorporates the compact support from the PoU. Thus, the overall approximation is constructed without penalizing the

continuity between the elements.

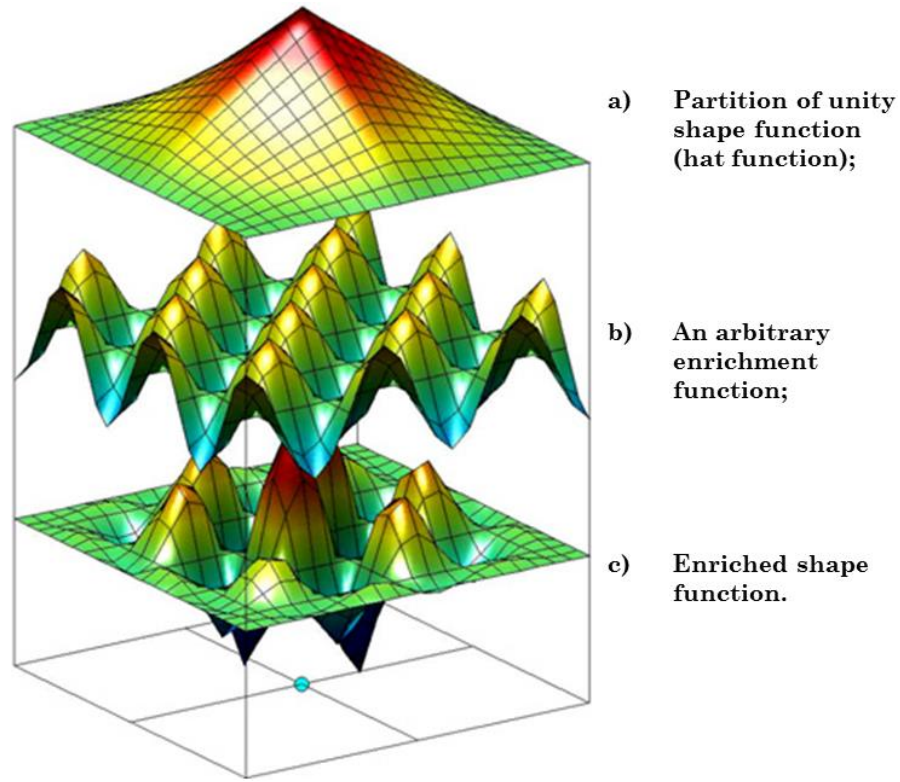


Figure 3.3 – Construction of an enriched shape function (also known as a “generalized FEM shape function”) using the Partition of Unity Method (PUM): schematic representation. **SOURCE:** Duarte and Kim (2008).

Note that an approximate solution proposed by GFEM in element domain may be written as an Enriched Method, i.e., as the sum of two parts:

$$u_h^e = u_{FEM} + u_{ENRICHED} \quad (3.18)$$

where u_{FEM} is the standard Finite Element Method (FEM) part based on nodal degrees of freedom and $u_{ENRICHED}$ is the enrichment part produced by the partition of unity approach based on field degrees of freedom. In this sense, the nodal displacement $u_h^e(\xi)$ for an element can be expressed by

$$u_h^e(\xi) = \sum_{i=1}^{N_e} \varphi_i(\xi) \left\{ u_i + \sum_{n=1}^{N_j} \gamma_{jn}(\xi) b_{jn} \right\} \quad (3.19)$$

where φ_i are the partition of unity functions, γ_{jn} are the enrichment functions, N_e is the total number of nodes in the element, N_j is the number of used enrichment functions, u_i are the nodal displacements (nodal degrees of freedom) and b_{jn} are the field degrees of freedom related to the enrichment functions γ_{jn} without a physical meaning.

Hence, for a given one-dimensional domain Ω_{1D} , the set of functions ϕ_i constitutes a partition of unity ϕ_i in Ω_{1D} and it has the unity value in one node of element and zero in all other nodes, such as

$$\sum_{i=1}^{N_e} \phi_i(\xi) = 1 \quad (3.20)$$

and for a given two-dimensional domain Ω_{2D} , the set of functions ψ_i constitutes a partition of unity ϕ_i in Ω_{2D} and it has the unity value in one node of element and zero in all other nodes, such as

$$\sum_{i=1}^{N_e} \psi_i(\xi, \eta) = 1 \quad (3.21)$$

where $\xi = [-1, 1]$ and $\eta = [-1, 1]$ are the finite element natural (local) coordinate.

The enrichment functions (also named in literature as basis functions) used in this work are the trigonometric functions firstly proposed by Arndt (2009) and adapted by Torii (2012), such that

$$\gamma_{j1} = \sin\left(\frac{\beta_j(\xi+1)}{2}\right) \quad (3.22)$$

$$\gamma_{j2} = \cos\left(\frac{\beta_j(\xi+1)}{2}\right) - 1 \quad (3.23)$$

$$\gamma_{j3} = \sin\left(\frac{\beta_j(\xi-1)}{2}\right) \quad (3.24)$$

$$\gamma_{j4} = \cos\left(\frac{\beta_j(\xi-1)}{2}\right) - 1 \quad (3.25)$$

which in $\beta_j = j\alpha\pi$ is a hierarchical enrichment parameter proposed by Arndt (2009) for “j” levels of functions and α is an adaptable parameter that can involve the material parameters, e.g., length, density and Young's modulus (only for adaptive GFEM). Multiplying the partition of unity by the trigonometric shape functions described in Equations 3.22 to 3.25 we can find GFEM enriched shape functions used in this work. They can be visualized in Table 3.2 and can be plotted in a graph as shown in Figure 3.4.

Table 3.2 – GFEM enriched functions and their level of enrichment.

GFEM ENRICHED SHAPE FUNCTIONS	
Level of Enrichment	GFEM Functions
$le = 0$	$l_0 = \frac{1-\xi}{2}$
	$l_1 = \frac{1+\xi}{2}$
$le = 1$	$l_2 = \left(\frac{1-\xi}{2}\right) \sin\left(\frac{\beta_j(\xi+1)}{2}\right)$
$le = 2$	$l_3 = \left(\frac{1+\xi}{2}\right) \sin\left(\frac{\beta_j(\xi-1)}{2}\right)$
$le = 3$	$l_4 = \left(\frac{1-\xi}{2}\right) \left[\cos\left(\frac{\beta_j(\xi+1)}{2}\right) - 1 \right]$
$le = 4$	$l_5 = \left(\frac{1+\xi}{2}\right) \left[\cos\left(\frac{\beta_j(\xi-1)}{2}\right) - 1 \right]$

Afterwards, Torii (2012) proposed a modification of trigonometric enrichment functions, removing the influence of the parameter β_j from the

material parameters (length, density and Young's modulus) and rewriting it for the elementary domain $\xi = [-1, 1]$, resulting in expressions from 3.22 to 3.25 used in this work. It is interesting to observe that Arndt (2009) subtracted the unity from some basic functions to ensure that these functions in PUM space could always be cancelled at element nodes, avoiding the use of special procedures to impose boundary conditions.

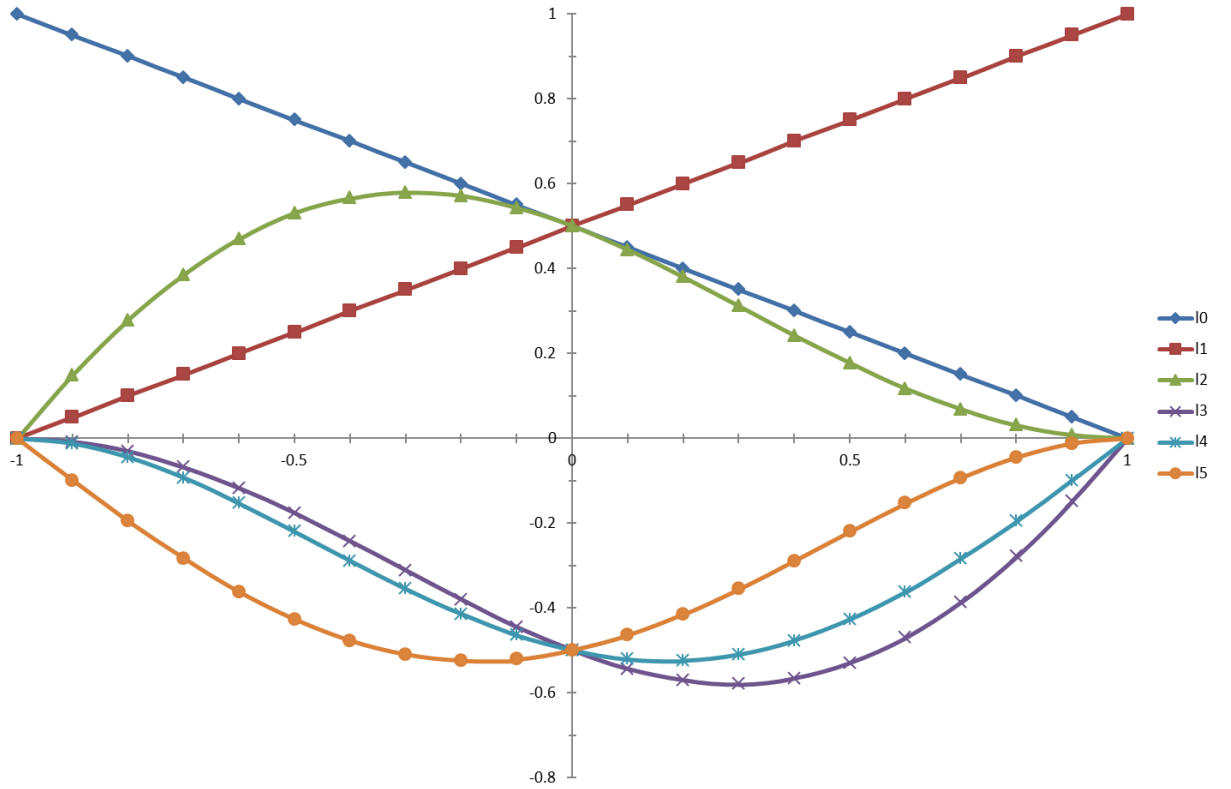


Figure 3.4 – GFEM enriched shape functions for $\beta = \pi$.

These functions were already successfully tested by Arndt (2009), Torii (2012) and Shang (2014) but in vibration and dynamic analysis cases moreover the analytical solution of the proposed studied problems in this work present trigonometric terms. So, because of that, these shape functions have been chosen. For all applications where these functions are used, it is assumed the $\beta = \pi$ (constant). The level of enrichment is increased adding new enriched shape functions as further described in next session.

3.3 THE ELEMENT'S ENRICHMENT: 1D LINEAR ELEMENT AND 2D BILINEAR ELEMENT

As described in previous section, an enriched shape function (generalized finite element function), named henceforth as ϕ_k in a 1D domain or ψ_k in a 2D domain, can be obtained by multiplying the PoU, φ_i by an enrichment (basis) functions, γ_{jn} . The sub-index “ k ” indicates the polynomial order (in case of HFEM) or the order of enrichment level (in case of GFEM). A set of functions define a polynomial order or an enrichment level. So, functions l_0 and l_1 expressed in Tables 3.1 and 3.2 are associated to level zero or indicate the conventional C^0 element (hat functions) for a 1D element. For the first enrichment level, function l_2 is included, and so on. As the level of enrichment increases, the value of sub-index “ k ” is added, while the value β_j remains the same. It is easily possible to increase the level of enrichment in an approximate solution only changing the parameter β_j and adding the new resulting function to the approximate space in GFEM. So, when all enriched shape functions are used, new enriched shape functions can be generated by changing the value of β_j , $\beta_j = j\pi$. But this is not the case in this work: the value of β_j is kept constant ($\beta = \pi$) and the level of enrichment is only increased by adding new enrichment functions. It is relevant to point out again that the enriched shape functions generated by GFEM should assume null values at nodal points to make it easier for the application of boundary conditions. An important aspect to be considered on boundary of the enriched elements regards to the continuity across the border, where there should have a compatibility of mathematical functions between neighbor elements as seen in Figure 3.5. It means neighbor elements sharing same side have linked edge shape functions with each other. It is a crucial fundament that will be further detailed in the construction of mathematical space.

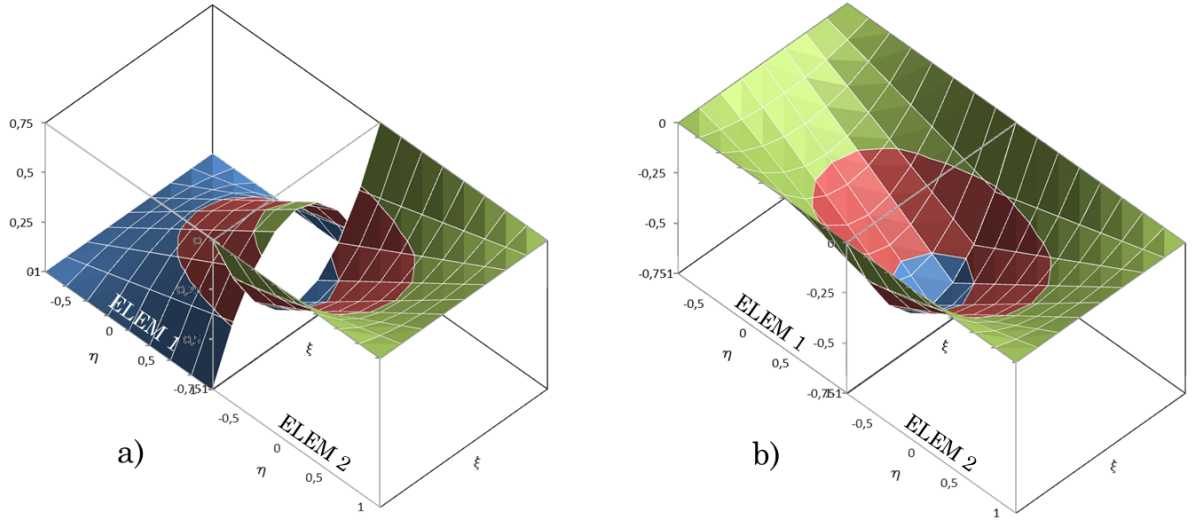


Figure 3.5 – A non-compatible and a compatible edge shared by two finite elements.

After the enriched shape functions are generated, these functions can be used to produce a one-dimensional enriched element and a two-dimensional quadrilateral enriched element. The construction of mathematical space of enriched elements (both for HFEM and GFEM approaches) is as following: consider a parametric interval for the one-dimensional (1D) case K_{ha} and a parametric domain for the two-dimensional (2D) case K_{hq} such that

$$K_{ha} = \{ \xi \in \mathbb{R}; -1 < \xi < 1 \}, \quad (3.26)$$

$$K_{hq} = \{ \xi, \eta \in \mathbb{R}^2; -1 < \xi, \eta < 1 \} \quad (3.27)$$

where ξ is the natural coordinate of a 1D finite element and ξ, η represent the natural coordinates of a square 2D finite element.

The enriched mathematical space in an elementary element (a “master” element) is constructed by functions related to the vertices and its interior for a 1D element and to the vertices, its edges and its interior for a 2D element according to Šolín *et al.* (2004). We will firstly begin investigating the enriched mathematical space for a 1D element.

In the case of the 1D isoparametric element used in this work on boundary (Figure 3.6), the *vertex* shape functions $\phi^{vertex}(\xi)$ are given by

$$\phi^{vertex,1}(\xi) = l_0(\xi), \quad (3.28)$$

$$\phi^{vertex,2}(\xi) = l_1(\xi) \quad (3.29)$$

and the interior functions, called *bubble* functions, are expressed by

$$\phi_k^{bubble}(\xi) = l_k(\xi), \quad 2 \leq k \leq p^{bubble} \quad (3.30)$$

where $p^{bubble} \geq 2$ is the local order of approximation in element interior.

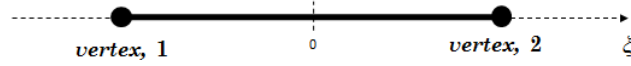


Figure 3.6 – A 1D linear element with local coordinate $\xi = [-1, 1]$.

In Figure 3.7, it is possible to visualize an example of the vertex and bubble shape functions in the case of the boundary 1D element used in this work for $k = 2$.

In the case of the 2D isoparametric quadrilateral element used in domain (Figure 3.8), it is firstly important to emphasize the *minimum rule* for conforming approximation according to Šolín *et al.* (2004). In order to compose an enriched shape function for a quadrilateral element, the polynomial order (in the context of HFEM) for edge and bubble functions must comply with the minimum requirement of the Hilbert space H^1 , such that the polynomial order of the edge functions must be less than or equal to the order of the bubble functions, that is

$$p^{edge,2}, p^{edge,4} \leq p^{bubble,1} \text{ and } p^{edge,1}, p^{edge,3} \leq p^{bubble,2} \quad (3.31)$$

where $p^{edge,1}, p^{edge,2}, p^{edge,3}$ and $p^{edge,4}$ are related to the polynomial order, here in this work, the four edges of a quadrilateral element whereas $p^{bubble,1}$ and $p^{bubble,2}$ are related to the polynomial order of the element interior, i.e., the directions ξ and η . This concept is easily extended to GFEM approach replacing from

polynomial order “ p ” to level of enrichment “ le ”.

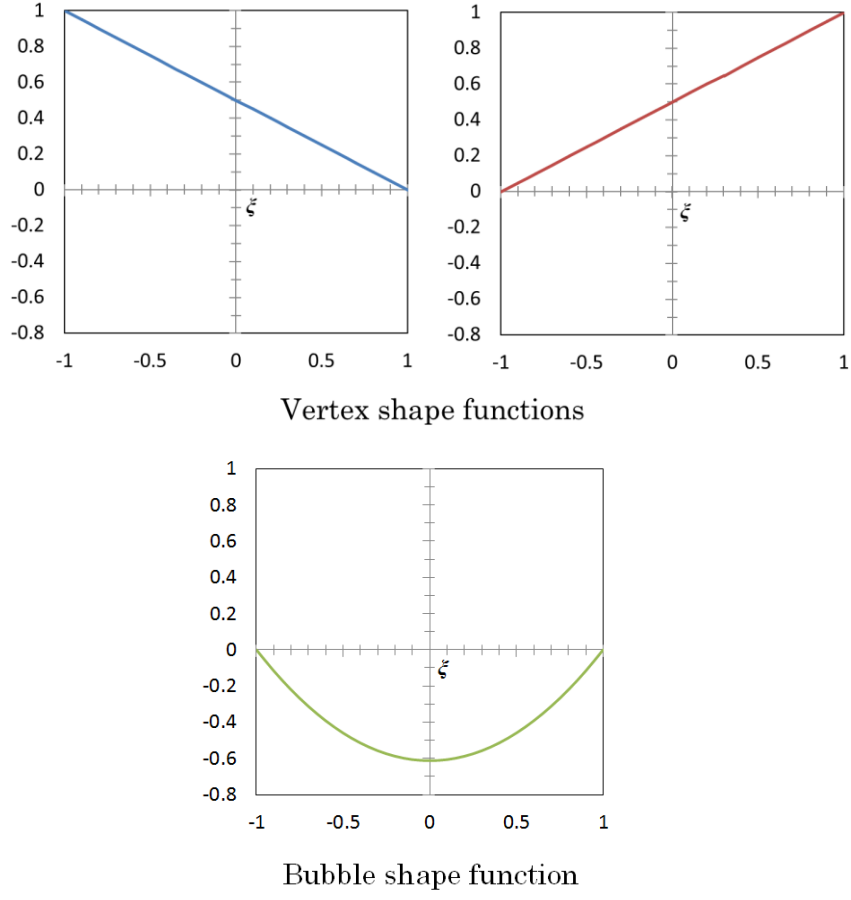


Figure 3.7 – An example of the vertex and bubble shape functions for a 1D element, $k = 2$.

So, starting by the 2D quadrilateral element *vertex* shape functions $\psi^{vertex}(\xi, \eta)$, we have

$$\psi^{vertex,1}(\xi, \eta) = l_0(\xi)l_0(\eta), \quad (3.32)$$

$$\psi^{vertex,2}(\xi, \eta) = l_1(\xi)l_0(\eta), \quad (3.33)$$

$$\psi^{vertex,3}(\xi, \eta) = l_1(\xi)l_1(\eta), \quad (3.34)$$

and

$$\psi^{vertex,4}(\xi, \eta) = l_0(\xi)l_1(\eta). \quad (3.35)$$

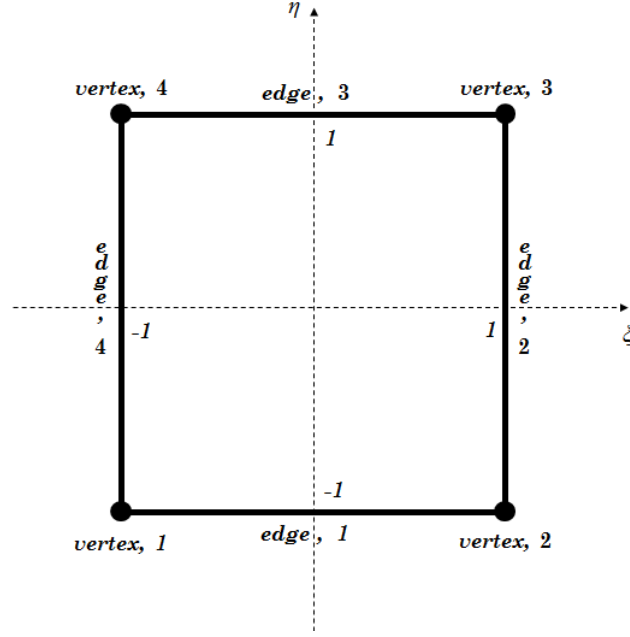


Figure 3.8 – A 2D quadrilateral finite element with local coordinates $\xi = [-1, 1]$ and $\eta = [-1; 1]$.

Note that the previous functions generate conventional C^0 bilinear shape functions for a 2D quadrilateral element (hat functions, as we can see in Figure 3.9), i.e., $\psi^{vertex,j}$ is equal to one at v_j (where j can assume the values 1, 2, 3 or 4) and it vanishes at all remaining vertices.

In addition, the *edge* functions are expressed by

$$\psi_k^{edge,1}(\xi, \eta) = l_0(\xi)l_k(\eta), \quad 2 \leq k \leq p^{edge,1}, \quad (3.36)$$

$$\psi_k^{edge,2}(\xi, \eta) = l_1(\xi)l_k(\eta), \quad 2 \leq k \leq p^{edge,2}, \quad (3.37)$$

$$\psi_k^{edge,3}(\xi, \eta) = l_k(\xi)l_1(\eta), \quad 2 \leq k \leq p^{edge,3}, \quad (3.38)$$

$$\psi_k^{edge,4}(\xi, \eta) = l_k(\xi)l_0(\eta), \quad 2 \leq k \leq p^{edge,4} \quad (3.39)$$

and, the *bubble* functions that vanish everywhere on boundary (the edges) of the domain (2D quadrilateral element) are

$$\psi_{n_1, n_2}^{bubble}(\xi, \eta) = l_{n_1}(\xi)l_{n_2}(\eta), \quad 2 \leq n_1 \leq p^{bubble,1}, \quad 2 \leq n_2 \leq p^{bubble,2} \quad (3.40)$$

where n_1 and n_2 , used in the context of bubble functions, represent indices k , for directions ξ and η .

In Figure 3.9 it is possible to visualize an example of the vertex, edge and bubble shape functions for a 2D element used in this work with $k = 2$.

As previously mentioned, in order to properly build a hierarchic higher-order element for a regular function, e.g., an approximate displacement field $u_h^e(\xi, \eta)$ in an element, it is necessary to consider the developments of the projection-based interpolant that states the interpolant can be constructed as a sum of a vertex and bubble interpolants in a 1D element and a sum of a vertex, edge and bubble interpolants in a 2D element. We will consider a 2D case to elucidate this concept since it is used both for HFEM (polynomial order “ p ”) and GFEM (only replacing from polynomial order “ p ” to level of enrichment “ le ”) explored in this work.

According to Šolín *et al.* (2004) the variables to be determined can be expressed as a sum of the standard shape functions (vertex shape functions) and enriched functions on edges and in interior of the element such that

$$u_h^e(\xi, \eta) = u_h^{vertex}(\xi, \eta) + u_h^{edge}(\xi, \eta) + u_h^{bubble}(\xi, \eta); \quad (3.41)$$

where $u_h^e(\xi, \eta)$ is the approximate solution of a displacement field $u(\xi, \eta)$ in element local coordinates; $u_h^{vertex}(\xi, \eta)$ are nodal variables located at vertices (used both for 1D and 2D elements); $u_h^{edge}(\xi, \eta)$ are variables situated on edges (used only for 2D element); and $u_h^{bubble}(\xi, \eta)$ are variables located in interior of the element (used both for 1D and 2D elements).

To be clear, the expression 3.41 for a 1D element contains the terms $u_h^{vertex}(\xi, \eta) + u_h^{bubble}(\xi, \eta)$ whereas for a 2D element it contains complete terms $u_h^{vertex}(\xi, \eta) + u_h^{edge}(\xi, \eta) + u_h^{bubble}(\xi, \eta)$.

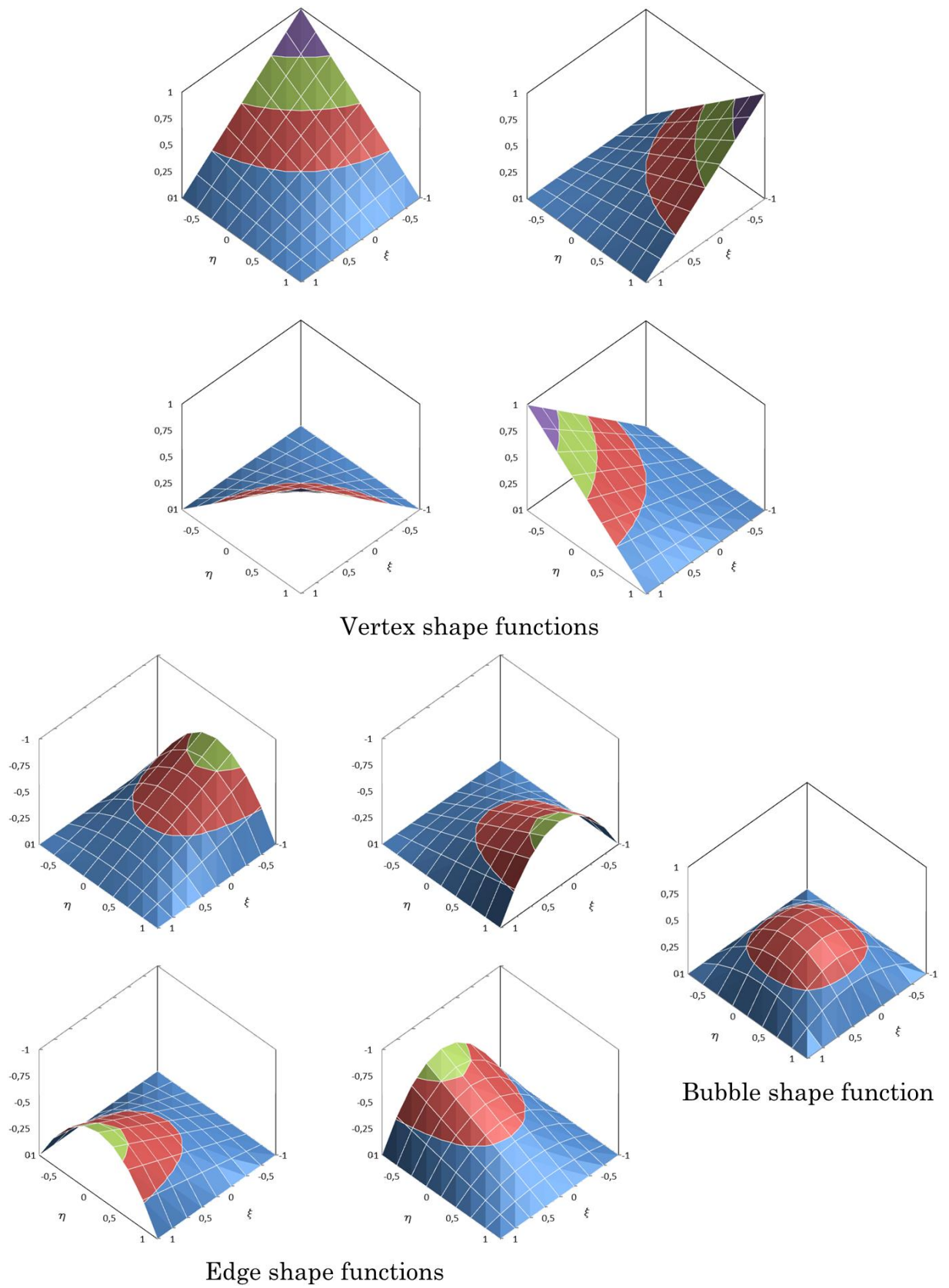


Figure 3.9 – An example of the vertex, edge and bubble shape functions for a 2D element, $k = 2$.

In this way, $u_h^{vertex}(\xi, \eta)$ can be determined knowing values of standard FEM bilinear shape functions whereas $u_h^{edge}(\xi, \eta)$ and $u_h^{bubble}(\xi, \eta)$ can be figured out in such way

$$u_h^{edge}(\xi, \eta) = \sum_{j=1}^4 u_h^{edge,j}(\xi, \eta),$$

$$\text{which in } u_h^{edge,j}(\xi, \eta) = \sum_{k=2}^{p^{edge,j}} b_k^{edge,j} \psi_k^{edge,j}, \text{ with } j = 1, 2, 3 \text{ and } 4 \quad (3.42)$$

and

$$u_h^{bubble}(\xi, \eta) = \sum_{n_1=2}^{p^{bubble,1}} \sum_{n_2=2}^{p^{bubble,2}} b_{n_1,n_2}^{bubble} \psi_{n_1,n_2}^{bubble} \quad (3.43)$$

where $\psi_k^{edge,j}$ are edge enriched functions, ψ_{n_1,n_2}^{bubble} are bubble enriched functions, $b_k^{edge,j}$ and b_{n_1,n_2}^{bubble} are field degrees of freedom generate by these enriched functions. The “ b ” variables associated with these enriched functions are calculated without any physical meaning. The determination of the displacement field for one-dimensional case is straightforward considering only the natural coordinate ξ of a 1D finite element and its development it will be omitted here. One point deserves to be highlighted here: all enriched degrees of freedom on boundary conditions are set null.

Now, the MLGFM can be enriched once endowed with these concepts discussed in this chapter. But, before applying them, it is necessary to properly present the robust mathematical foundation of the MLGFM in order to further discuss its domain and boundary spaces' enrichment. This is exactly the scope of the next chapter.

Chapter 4

The Modified Local Green's Function Method

4.1 INTRODUCTION

The Modified Local Green's Function Method (MLGFM) was proposed by Barcellos and Silva (1987) as an alternative to extend the Boundary Element Method (BEM) methodologies to problems which have no known fundamental solution in its explicit form or are very intricate. One of the most important features of the MLGFM is the advantage of taking the Green's function adjoint operator properties without the knowledge of its explicit form, but by evaluating its projections on appropriate subspaces spanned by domain and boundary interpolation functions. This allows the solution of problems where the fundamental solution is unknown. These projections can be calculated with appropriate numerical techniques. The Finite Element Method (FEM) is an interesting technique to obtain discrete values for the “*Green's Function Projections*” (GFp) because it does not use fundamental solutions and/or Green's Functions. However, it is necessary to use an additional operator, \mathcal{N}' prescribed on boundary by the user in order to avoid the singularity of the final system of equations. To analyze a continuum mechanics problem through the MLGFM, two meshes are necessary: one for the domain and another one for the boundary. In

the domain elements, the method generates a set of domain equations, which are used to generate automatically the domain Green's functions projections. Later on, a set of boundary equations are also generated and the boundary Green's functions projections can be determined with the domain projections former developed. At the end, the system is solved only for boundary equations, where the main variables are calculated. Domain values may be obtained once the boundary values are known after the solution of the boundary equation system.

The MLGFM, in a global approach, is known as “*unicell-multielement*”. This is the approach used in this work. It has been used by several authors in last decades and its implementation has been extensively studied. Some examples of this approach are: for membranes, Barcellos and Silva (1987); for Mindlin's plate, Barbieri and Barcellos (1991b; 1993b); for singular potential, Barcellos and Barbieri (1991a); for h - and p - convergence, Filippin *et al.* (1992a); for semi-thick shell, Barbieri *et al.* (1993a), for non-homogenous potentials problems, Barbieri and Barcellos (1993a); for laminated plates with and without cracks, Machado *et al.* (1993; 2008; 2012); for 3D elasticity, Barcellos *et al.* (1995) and for details in mathematical formulation, Barbieri *et al.* (1998a; 1998b).

This chapter is divided in three sections: the first one deals with the abstract formulation of the MLGFM where a robust mathematical foundation based on functional analysis is described. The second part is devoted to the variational formulation of the MLGFM where the concepts of variational boundary-value problems are employed (see Appendix “A”). The third and last part is dedicated to the formalism of MLGFM where the integral equations are postulated; the discretization, Green's functions projections, the MLGFM's matrices and system of equations are developed.

4.2 THE MLGFM: ABSTRACT ANALYSIS

4.2.1 Notations and Preliminary Concepts

One of the most important aspects for the definition of the mathematical basis of the MLGFM is the one related to the adopted bilinear form and the identification of the differential operator and its formal adjoint. These concepts are in the scope of the functional analysis whose will be not treated here. Some very basic concepts can be seen in appendix “A” but for a deeper description in functional analysis and boundary-value problems, see Reddy (1986) and/or Oden and Reddy (1976).

In next developments, Ω is an open and bounded domain, in the n -dimensional space \mathbb{R}^n and $\partial\Omega$ is a boundary, sufficiently regular, i.e., it allows the existence of a normal vector in almost every points (except by in sets of zero measures, possibly).

Since the MLGFM is based on boundary formulation (SILVA, 1988), it is important to extend the sought functions space to the boundary. In other words, these extensions must possess the “*trace property*” (ODEN; REDDY, 1976).

Therefore, let $u(\mathbf{x})$ be a function defined on an arbitrary Hilbert space $H^m(\Omega)$ with order “ m ”, i.e. $u(\mathbf{x}) \in H^m(\Omega)$. The normal derivatives of $u(\mathbf{x})$ on boundary $\partial\Omega$ will be represented by:

$$\mathcal{D}_j u(\mathbf{x}) = \frac{\partial^j u(\mathbf{x})}{\partial \mathbf{n}^j} \quad \text{for } \forall \mathbf{x} \in \Omega, \quad 0 \leq j \leq m-1 \quad (4.1)$$

where \mathbf{n} is the normal to the boundary $\partial\Omega$ at \mathbf{x} . The operator \mathcal{D}_j is known as the “*trace operator*”. It is a linear and continuous mapping such that

$$\mathcal{D}_j : H^m(\Omega) \rightarrow H^{m-j-1/2}(\partial\Omega) \quad (4.2)$$

wherein the exponent “ m ” may assume an integer or fraction value, without any

generality loss. Another property of this operator is

$$\text{Ker}(\mathcal{D}_0, \mathcal{D}_1, \mathcal{D}_2, \mathcal{D}_3, \dots, \mathcal{D}_{m-1}) \equiv H_0^m(\Omega) \quad (4.3)$$

where $\text{Ker}(\cdot)$ denotes the kernel of the collection of operators \mathcal{D}_j . Still, $\text{Ker}(\cdot)$ is dense in space $L_2(\Omega)$.

Let H , U and ∂H be Hilbert spaces such that

$$\mathcal{D} : H \rightarrow \partial H \quad (4.4)$$

with \mathcal{D} being the trace operator as former quoted. The space H has the trace property if it satisfies the following conditions:

a) H is a subset of U , with U having a weaker topology than H . Here, “weak topology” is meant of the coarsest topology (the topology with the fewest open sets) under which any element $x \in U$ corresponds to a continuous map on U' (dual space);

b) H is dense in U , with U being a pivotal space, i.e.,

$$H \subset U \equiv U' \subset H' \quad (4.6)$$

where U' and H' are the topological dual spaces (spaces of the continuous and linear functionals) of U and H , respectively;

c) The mapping \mathcal{D} exists, so that its kernel, H_0 is dense in U , such that

$$\text{Ker}(\mathcal{D}) = H_0 \subset H \quad \text{and} \quad H_0 \subset U \equiv U' \subset H_0' \quad (4.7)$$

where the inclusions are dense and continuous.

If two Hilbert space, H and K , have the trace property defined by

conditions 4.5 to 4.7, and associated with them there are the trace operators \mathcal{J}_H and \mathcal{J}_K respectively, such that

$$\begin{aligned}\mathcal{J}_H : H &\rightarrow \partial H; \\ \mathcal{J}_K : K &\rightarrow \partial K\end{aligned}\tag{4.8}$$

then, the sought functions of the problem $B(u, v) : H \times K \rightarrow \mathbb{R}$, where $u \in H$ and $v \in K$, have images at ∂H and ∂K under the operators \mathcal{J}_H and \mathcal{J}_K , respectively.

It can be observed from relation 4.8 that the sought functions of the problem are not all or any function in ∂H and ∂K but only those ones that are images of H and K under the operators \mathcal{J}_H and \mathcal{J}_K , respectively.

Considering the trace property described by relations 4.5 to 4.7, one can define a continuous boundary bilinear form, $b(\cdot, \cdot)$, that is:

$$b(\mathcal{J}_H(u), \mathcal{J}_K(v)) : H \times K \rightarrow \mathbb{R}.\tag{4.9}$$

Taking the bilinear form from the variational boundary-value problem $B(u, v) : H \times K \rightarrow \mathbb{R}$ (Appendix “A”, expression A.21), for the case where $u \in H$ is fixed and $v \in K_0$, one can be expressed by the continuous linear operator $\ell(u)$, such as

$$\ell : H \rightarrow K_0'\tag{4.10}$$

Thus, if there exists such transformation, one can conclude

$$B(u, v) = \langle \ell(u), v \rangle_K, \quad \forall v \in K_0\tag{4.11}$$

where $\ell(u)$ is the operator associated to B and $\langle \cdot, \cdot \rangle_K$ is the duality pairing in $K' \times K$. In this way, the operator ℓ belongs to the space $L(H, K_0')$, i.e., the linear operators space of H in K_0' .

The adjoint problem of (4.11) can be derived when $v \in K$ is fixed and going

through $u \in H_0$, now taking the formal adjoint operator ℓ^* associated to a linear and continuous bilinear form B , we have

$$B(u, v) = \langle \ell^*(v), u \rangle_H, \quad \forall u \in H_0. \quad (4.12)$$

Similarly, ℓ^* belongs to the space $L(K, H_0')$.

We can see in Figure 4.1 the relation among the spaces H and K , the kernel spaces H_0 and K_0 , and the pivotal spaces associated to them $U = U'$ and $V = V'$ as well as the mapping performed by the operators ℓ and ℓ^* whereby the bilinear form $B(u, v)$ depends on.

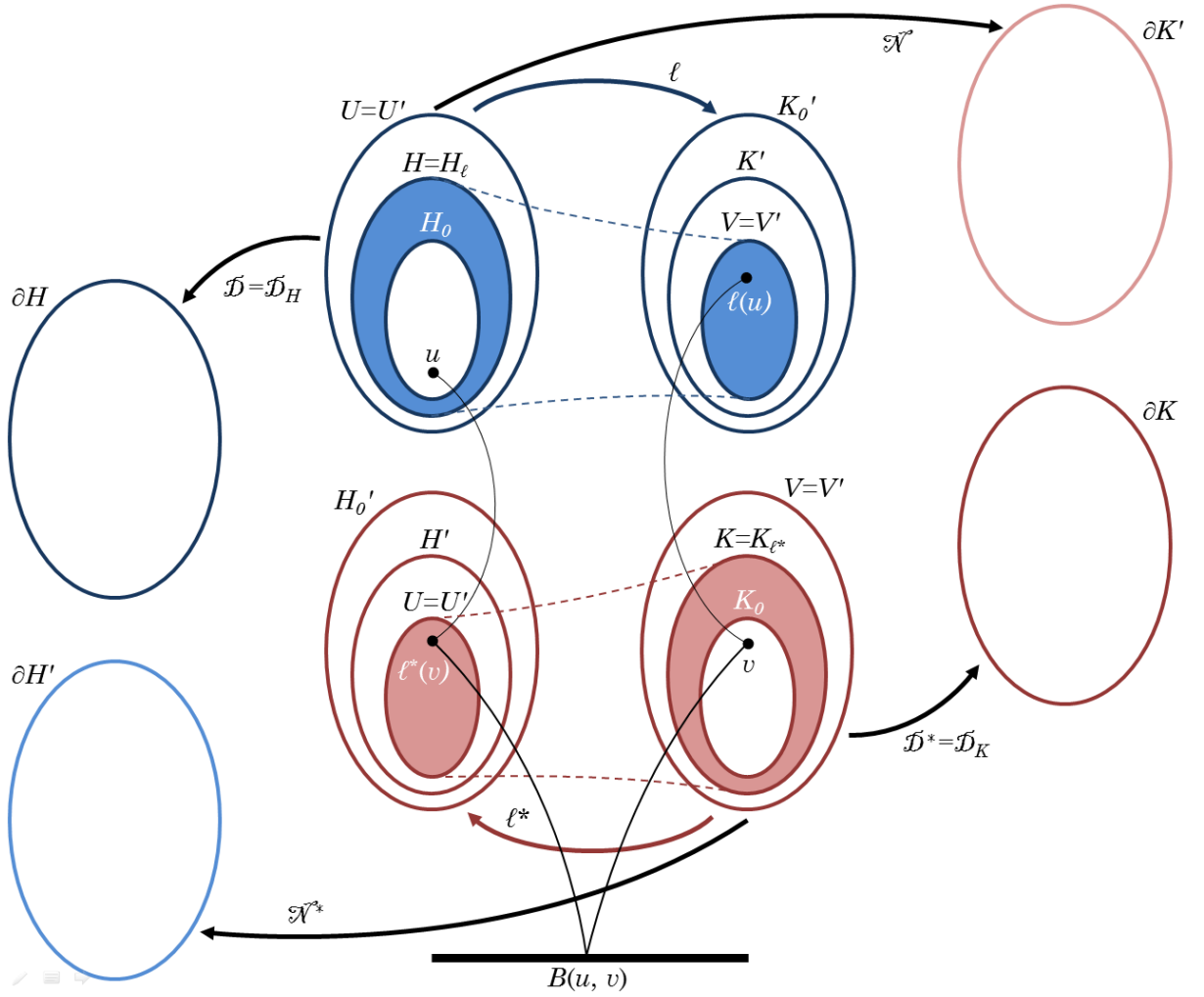


Figure 4.1 – Spaces, differential operators and bilinear forms. **SOURCE:** Adapted from Machado (1992).

In order to establish a generalized reciprocity relation, it is important to observe that the bilinear forms 4.11 and 4.12 are only valid for $u \in H_0$ and $v \in K_0$, that is, they don't take into account the boundary values. They are just included when $u \in H$ and $v \in K$. Moreover, this procedure becomes more general with the introduction of the boundary bilinear forms as defined in expression 4.9 which spread out these boundary types to be analyzed. Taking into account that, it is necessary to define the following subsets

$$H_\ell = \{ u \in H; \ell(u) \in V \}; \quad (4.13)$$

$$K_{\ell^*} = \{ v \in K; \ell^*(v) \in U \}. \quad (4.14)$$

considering $H \subset U \equiv U' \subset H'$ and $K \subset V \equiv V' \subset K'$. Observe that ℓ and ℓ^* are the constraints of the operators appointed in 4.11 and 4.12 to the spaces H_ℓ and K_{ℓ^*} .

In the conditions described in 4.13 and 4.14, it is possible to identify the following univocal operators

$$\mathcal{N} \in L(H_\ell, \partial K) \quad \text{and} \quad \mathcal{N}^* \in L(K_{\ell^*}, \partial H), \quad (4.15)$$

and

$$\mathcal{D} \in L(H, \partial H) \quad \text{and} \quad \mathcal{D}^* \in L(K, \partial K). \quad (4.16)$$

The operators shown in 4.15, \mathcal{N} and \mathcal{N}^* , are the Neumann's generalized operators likewise the ones shown in 4.16, \mathcal{D} and \mathcal{D}^* , are the Dirichlet's generalized operators (trace operators). They are associated to ℓ and ℓ^* , respectively.

Taking those operators defined in 4.15 and 4.16, the bilinear form (it can be seen in Appendix "A" – expression A.21) can be extended to the boundary such as (ODEN; REDDY, 1976):

$$B(u, v) + b(\mathcal{D}(u), \mathcal{D}^*(v)) = (v, \ell(u))_V + \langle \mathcal{N}(u), \mathcal{D}^*(v) \rangle_{\partial K} \quad (4.17)$$

where $u \in H_\ell$ and $v \in K$.

And,

$$B(u, v) + b(\mathcal{D}(u), \mathcal{D}^*(v)) = (\ell^*(v), u)_U + \langle \mathcal{N}^*(v), \mathcal{D}(u) \rangle_{\partial H} \quad (4.18)$$

where $u \in H$ and $v \in K_{\ell^*}$.

The expressions previously presented for the bilinear form $B(\cdot, \cdot)$ are known as “*The Abstract Green's Formulas*”.

So, those expressions 4.17 and 4.18 can be combined since $u \in H_\ell$ and $v \in K_{\ell^*}$, such that:

$$(\ell^*(v), u)_U = (v, \ell(u))_V + \langle \mathcal{N}(u), \mathcal{D}^*(v) \rangle_{\partial K} - \langle \mathcal{N}^*(v), \mathcal{D}(u) \rangle_{\partial H} \quad (4.19)$$

where $u \in H_\ell$ and $v \in K_{\ell^*}$.

The expression 4.19 is known as “*Generalized Green's Form*” for the operator ℓ and it expresses the generalized reciprocity relation between the conditions $\{ u, \mathcal{D}(u), \mathcal{N}(u) \} \in H_\ell \times \partial H \times \partial K'$ and $\{ v, \mathcal{D}^*(v), \mathcal{N}^*(v) \} \in K_{\ell^*} \times \partial K \times \partial H'$ associated to the operators ℓ and ℓ^* , respectively. The duality pairing in ∂K and ∂H represents the term “*Global Bilinear Concomitant*” of the operator ℓ .

4.2.2 The MLGFM Abstract Formulation

The generalized reciprocity relations developed in previous section are used for the purpose of furnishing representations of the differential equation solution relative to the operator ℓ and to the boundary conditions defined by the operators \mathcal{D} and \mathcal{N} . In order to do that, we can choose v as being the fundamental solution of the operator ℓ^* . Here, it is important to clarify that the variables u and v employed in the bilinear form $B(u, v)$ – Appendix “A”, expression

A.21 – usually are related to two different states: a *real* state, where the unknown variables are and an *auxiliary* state, properly chosen. But, other alternatives can be used as fundamental solution aiming to improve the characteristics of regularity of the system (MACHADO, 1992). For example, as mentioned before, choosing v as a suitable Green's Function is the base of the Local Green's Function Method proposed by Horak (1980). On the other hand, this function in MLGFM is set automatically, without its formal knowledge.

An arbitrary boundary-value problem with the operator ℓ in domain and the operators \mathcal{D} and \mathcal{N} on boundary is solved by MLGFM in two interdependent and different steps. The first step is focused on to find a solution in domain whereas the second step is focused on boundary. But for computational implementation aspects, it is possible to work out firstly the solution on boundary and afterwards in domain.

Furthermore, in both cases (STEP 1 and STEP 2) it is employed a “Dirac delta” distribution – $\delta(P, Q)$ – as an excitation. As consequence, one must specify a point Q where the solution of the problem (“field point”) is and a point P where the excitation occurs (“source point”) considering: $Q, P \in \Omega$. The auxiliary state is defined by $v = v(P, Q)$. When we consider the points on boundary $\partial\Omega$, they are identified by the lowercases p and q . Both cases are shown in Figure 4.2.

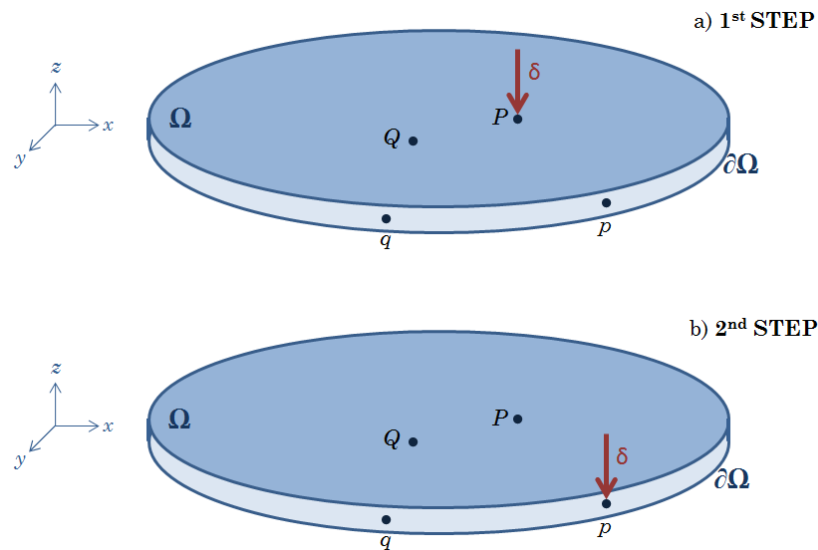


Figure 4.2 – Dirac Delta excitation: a) in domain; b) on boundary. **SOURCE:** Adapted from Machado (1992).

Thus, the two MLGFM steps of solution can be described, such that:

1st STEP: Computation of the domain solution. An auxiliary state of the expression 4.19 is reached by applying the “*Dirac delta*” distribution in domain Ω , so that

$$\ell^*(v(P, Q)) = \delta(P, Q) \quad \text{where } P, Q \in \Omega, \quad (4.20)$$

$$\mathcal{N}^*(v(P, Q)) = 0 \quad \text{where } p \in \partial\Omega. \quad (4.21)$$

To determine the solution in domain interior Ω , the expressions 4.20 and 4.21 can be replaced in 4.19, resulting in

$$u(Q) = (v(P, Q), \ell(u))_V + \langle \mathcal{N}(u), \mathcal{D}^*(v(p, Q)) \rangle_{\partial K}. \quad (4.22)$$

2nd STEP: Computation of the boundary solution. Another auxiliary state of the expression 4.19 is reached by applying the “*Dirac delta*” distribution on boundary $\partial\Omega$, so that

$$\ell^*(v(P, q)) = 0 \quad \text{where } P \in \Omega \text{ and } q \in \partial\Omega, \quad (4.23)$$

$$\mathcal{N}^*(v(p, q)) = \delta(p, q) \quad \text{where } p, q \in \partial\Omega. \quad (4.24)$$

At this time, aiming to determine the solution on boundary interior $\partial\Omega$, the expressions 4.23 and 4.24 can be replaced in 4.19, and identifying the trace operator \mathcal{D} from 4.1, we have

$$\mathcal{D}u(q) = (v(P, q), \ell(u))_V + \langle \mathcal{N}(u), \mathcal{D}^*(v(p, q)) \rangle_{\partial K}. \quad (4.25)$$

The equations 4.22 and 4.25 constitute a system of integral equations that may be used in the solution of problems governed by differential equations defined by operator ℓ and boundary operators \mathcal{D} and \mathcal{N} .

4.3 THE MLGFM VARIATIONAL FORMULATION

One way of performing the discretization of the operators present in integral formulations is to use the variational formulation. It is possible to use other formulations, such as, collocation method or to figure out the Green's functions analytically but using a variational one, the methodology becomes more general and efficient (SILVA, 1988). The variational formulation or "weak formulation" is a weaker one than the conventional formulation since it requires fewer derivatives of u to be in $L_2(\Omega)$ (REDDY, 1986).

Hence, going back to the system of integral equations seen in 4.22 and 4.25, one realizes these representations are not suitable for numerical approximations due to the calculation of the generalized Neumann operator that encompass derivatives of u in trace sense. In order to work around this setback, one introduces a new variable \mathcal{F} defined by

$$\mathcal{F} = \mathcal{N}(u) \in \partial K'. \quad (4.26)$$

Replacing the representation 4.26 into 4.22 and 4.25 and identifying the variable $v(P, Q)$ as the Green's Function $\mathbf{G}(P, Q)$, we have

$$u(Q) = (\mathbf{G}(P, Q), \ell(u))_V + \langle \mathcal{F}, \mathcal{D}^*(\mathbf{G}(p, Q)) \rangle_{\partial K}, \quad (4.27)$$

$$\mathcal{D}u(q) = (\mathbf{G}(P, q), \ell(u))_V + \langle \mathcal{F}, \mathcal{D}^*(\mathbf{G}(p, q)) \rangle_{\partial K} \quad (4.28)$$

where $u \in H_\ell$; $\mathbf{G} \in K_{\ell^*}$; $P, Q \in \Omega$ and $p, q \in \partial\Omega$.

Different types of boundary conditions are included into the formulation by the quantities $\mathcal{D}u(q)$ and \mathcal{F} . In fact, the trace of u on boundary, i.e., $\mathcal{D}u(q)$ takes in directly the Dirichlet (essential) boundary conditions whereas the quantity \mathcal{F} takes in the Neumann (natural) or Cauchy (mixed) boundary conditions. By Cauchy boundary conditions we mean mixed boundary condition: an essential boundary condition is applied on one boundary part and a natural

boundary condition on the other one.

Here, it is important to point out the differences between two classic boundary-value problems for the operator ℓ (with A being a linear differential operator):

1) Dirichlet problem:

Given $f \in V$ and $r \in \partial H$, the problem consists in finding $u \in H_\ell$ such that:

$$\begin{aligned} Au = f \quad \text{or} \quad \ell(u) = f, \\ \mathcal{D}(u) = r. \end{aligned} \tag{4.29}$$

2) Neumann problem:

Given $f \in V$ and $s \in \partial K'$, the problem consists in finding $u \in H_\ell$ such that:

$$\begin{aligned} Au = f \quad \text{or} \quad \ell(u) = f, \\ \mathcal{N}(u) = s. \end{aligned} \tag{4.30}$$

Both classic boundary-value problems can be expressed in a variational way as:

3) Variational Dirichlet problem:

Given $f \in V$ and $r \in \partial H$, the problem consists in finding $u \in H_0$ such that:

$$\begin{aligned} B(u, v) = \ell(v) \quad \text{for } v \in K_0, \\ \ell(v) = (f, v)_V - B(\mathcal{D}^{-1}(r), v) \quad \text{for } v \in K_0. \end{aligned} \tag{4.31}$$

4) Variational Neumann problem:

Given $f \in V$ and $s \in \partial K'$, the problem consists in finding $u \in H$ such that:

$$\begin{aligned} B(u, v) = \ell(v) \quad \text{for } v \in K, \\ \ell(v) = (f, v)_V - \langle s, \mathcal{N}^*(v) \rangle_{\partial K} \quad \text{for } v \in K. \end{aligned} \tag{4.32}$$

According to Oden and Reddy (1976), if \mathcal{D}^{-1} represents the inverse of trace operator \mathcal{D} mapping, then the problems “1” and “3” as well as “2” and “4” are equivalents. In other words, if u is a solution for 4.29 than $(u - \mathcal{D}^{-1}(r))$ is a solution for 4.31 too. That's the same for 4.30 and 4.32. In addition, the opposite is true in both cases.

The existence and uniqueness of a solution is addressed by “*The Generalized Lax-Milgram Theorem*” (REDDY, 1986) – it can also be seen in definitions A.14 to A.18, Appendix “A”. In a distributional approach, it can be noticed that the problem $\ell(u) = f$ is valid in “almost everywhere”, considering $f \in V$, so $u \in H_\ell$.

Now, aiming to develop the MLGFM integral equations of the problem, it is necessary to define more two sets, where all boundary conditions can be represented. Thus, remembering that

$$H_\ell = \{ u \in H; \ell(u) \in V \}, \quad (4.33)$$

$$\partial H_r = \{ u \in \partial H; u = r \text{ in } \partial\Omega_r \}, \quad (4.34)$$

$$\partial K_s' = \{ \mathcal{F} \in \partial K'; \mathcal{F} = s \text{ in } \partial\Omega_s \} \quad (4.35)$$

where

$\partial\Omega_r$ – boundary patch union of $\partial\Omega$ where $\mathcal{D}u$ is specified;

$\partial\Omega_s$ – boundary patch union of $\partial\Omega$ where \mathcal{F} is specified;

$\partial\Omega$ – boundary $\partial\Omega$ is completely defined by $\mathcal{D}u$ and \mathcal{F} .

Finally, the MLGFM variational problem can be now written as:

“Given $f \in V$, seek the answer in domain, $u \in H$, and on boundary, $\mathcal{D}u \in \partial H_r$ and $\mathcal{F} \in \partial K_s'$, considering valid the expressions 4.31 and 4.32, or equivalently, in such a way that expressions 4.27 and 4.28 are met”.

4.4 THE FORMALISM OF THE MLGFM

4.4.1 Integral Equations

The MLGFM is an integral method that is able to solve boundary-value problems expressed by a differential equation system and boundary conditions (as can be seen in Appendix “A” – A.19 and A.20). They can be written as

$$Au = f \quad \text{or} \quad \ell(u) = f, \quad (4.36)$$

$$\mathcal{D}(u) = r \quad \text{on } \partial\Omega_r, \quad (4.37)$$

$$\mathcal{N}(u) = s \quad \text{on } \partial\Omega_s \quad (4.38)$$

where A is a linear differential operator; ℓ , \mathcal{D} and \mathcal{N} are, respectively, the problem, Dirichlet and Neumann differential operators; Ω , $\partial\Omega_r$, $\partial\Omega_s$ are the domain and boundary patches where are specified the Dirichlet and Neumann conditions; f , r and s are the domain Ω excitation and the functions that define the boundary conditions at $\partial\Omega_r$ and $\partial\Omega_s$, respectively.

There exists a unique solution if the problem expressed in 4.36, 4.37 and 4.38 is “*well-posed*”, i.e., the boundary conditions are properly prescribed and the excitation function f is considered sufficiently “*well behaved*”.

In order to determine a fundamental solution for the problem 4.36, it is necessary to solve its adjoint problem, considering as an auxiliary state, the Green's function, $\mathbf{G}(P, Q)$, and as an excitation source, a *Dirac Delta* distribution, $\delta(P, Q)$, applied in domain. Note that ℓ^* is the formal adjoint operator of ℓ , and defining \mathbf{I} as the identity tensor, the adjoint problem can be expressed in the form

$$\ell^* \mathbf{G}(P, Q) = \delta(P, Q) \mathbf{I} \quad P, Q \in \Omega. \quad (4.39)$$

The Green's function $\mathbf{G}(P, Q)$ can be understood as a generalized displacement of an arbitrary point \underline{Q} in a “ \underline{i} ” direction due to a generalized unit load applied upon a point \underline{P} in a “ \underline{j} ” direction, wherein P and $Q \in \Omega$.

Multiplying the expression in 4.36 by $\mathbf{G}(P, Q)^t$, results in

$$\mathbf{G}(P, Q)^t \ell(u(P)) = \mathbf{G}(P, Q)^t f(P). \quad (4.40)$$

Now, multiplying the expression 4.39 by $u(P)^t$, results in

$$u(P)^t \ell^* \mathbf{G}(P, Q) = u(P)^t \delta(P, Q). \quad (4.41)$$

Subtracting from 4.40 the transpose of 4.41, we have

$$\mathbf{G}(P, Q)^t \ell(u(P)) - [\ell^* \mathbf{G}(P, Q)]^t u(P) = \mathbf{G}(P, Q)^t f(P) - u(P) \delta(P, Q) \quad (4.42)$$

It is possible to re-arrange the previous expression as

$$u(P) \delta(P, Q) = \mathbf{G}(P, Q)^t f(P) + \ell^* \mathbf{G}(P, Q)^t u(P) - \mathbf{G}(P, Q)^t [\ell u(P)] \quad (4.43)$$

Placing the coordinates system at point \underline{P} and integrating in domain Ω , we write

$$u(Q) = \int_{\Omega_p} \{ \mathbf{G}(P, Q)^t f(P) + [\ell^* \mathbf{G}(P, Q)]^t u(P) - \mathbf{G}(P, Q)^t [\ell u(P)] \} d\Omega_p \quad (4.44)$$

Now, using the “*Gauss Theorem*”, i.e., integrating by parts successively, in last two terms of the above integrand, we have

$$\begin{aligned} u(Q) = & \int_{\Omega_p} \mathbf{G}(P, Q)^t f(P) d\Omega_p - \int_{\partial\Omega_p} [\mathcal{N}^* \mathbf{G}(p, Q)]^t u(p) d\partial\Omega_p \\ & + \int_{\partial\Omega_p} \mathbf{G}^t(p, Q) [\mathcal{N} u(p)] d\partial\Omega_p \end{aligned} \quad (4.45)$$

where $d\partial\Omega_p$ represents an infinitesimal element of the boundary $\partial\Omega$ at point \underline{p}

and \mathcal{N} , \mathcal{N}^* are the Neumann operators associated to ℓ and ℓ^* , respectively.

As a matter of fact, the equation 4.45 expresses exactly the formulation of the “*Direct Boundary Element Method*” (DBEM) and $\mathbf{G}(P,Q)$ represents (so far) only a fundamental solution of equation 4.45.

The numerical handling of the integrals in 4.45 is complicated again because of the Neumann operator that involves u derivate on boundary. In order to overcome this drawback, the MLGFM uses an auxiliary operator \mathcal{N}' that can be adopted as

$$\mathcal{N}' = \text{diag}(k_1, k_2, \dots, k_n) \quad (4.46)$$

where n is the degrees of freedom number in each nodal point and k_i is a non-zero real constant, $i = 1, 2, \dots, n$.

A physical interpretation of the additional operator \mathcal{N}' was presented by Barbieri (1992) as you can see in Figure 4.3. Mathematically speaking

$$\mathcal{N}' = k_i(x - x_i) \quad (4.47)$$

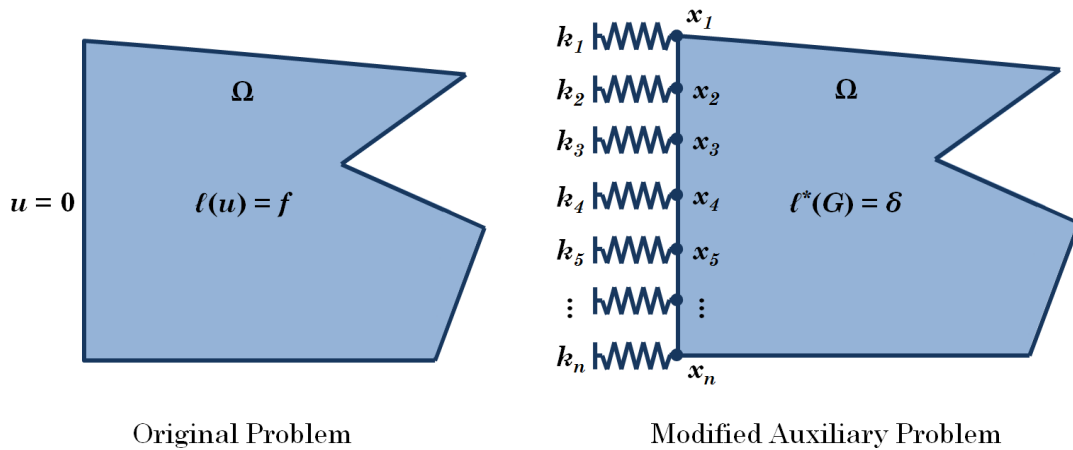


Figure 4.3 – Physical interpretation of the modified auxiliary problem. **SOURCE:** Adapted from Barbieri (1992).

Again, here k_i is a non-zero real constant and x_i are points (finite element mesh nodes) belonging to the boundary where the homogeneous Dirichlet boundary conditions are imposed.

Adding and subtracting in equation 4.45 the following expression

$$\mathbf{G}(p, Q)^t [\mathcal{N}' u(p)] = [\mathcal{N}' \mathbf{G}(p, Q)]^t u(p) \quad (4.48)$$

we write

$$\begin{aligned} u(Q) &= \int_{\Omega_P} \mathbf{G}(P, Q)^t f(P) d\Omega_P - \int_{\partial\Omega_P} [(\mathcal{N}^* + \mathcal{N}') \mathbf{G}(p, Q)]^t u(p) d\partial\Omega_P \\ &\quad + \int_{\partial\Omega_P} \mathbf{G}(p, Q)^t [(\mathcal{N} + \mathcal{N}') u(p)] d\partial\Omega_P \end{aligned} \quad (4.49)$$

Note that with the introduction of the auxiliary operator \mathcal{N}' , if the following boundary condition is satisfied

$$[(\mathcal{N}^* + \mathcal{N}') \mathbf{G}(p, Q)]^t = 0 \quad (4.50)$$

at this moment, by specifying the above boundary condition, the fundamental solution $\mathbf{G}(P, Q)$ will exactly correspond to the “*Green's Function*”!

The expression 4.49 is not suitable for numerical approximations yet because it has derivatives of u in trace sense and its calculation is a really difficult task. In order to work around this setback, one uses the previous variable \mathcal{F} defined by

$$\mathcal{F}(p) = (\mathcal{N} + \mathcal{N}') u(p) \quad (4.51)$$

Replacing 4.50 and 4.51 in 4.49, one finds out the expression for the generalized displacement in domain

$$u(Q) = \int_{\Omega_P} \mathbf{G}(P, Q)^t f(P) d\Omega_P + \int_{\partial\Omega_P} \mathbf{G}(p, Q)^t \mathcal{F}(p) d\partial\Omega_P \quad (4.52)$$

The last expression 4.52 represents the solution of 4.36 in domain Ω . Note

that the integral in last expression 4.52 behaves much better than the expression 4.45 since there is not any derivative of the Green's function $\mathbf{G}(\cdot, \cdot)$ or the variable $\mathcal{F}(\cdot)$. As mentioned before, the equation 4.45 expresses exactly the direct formulation of the "Boundary Element Method" (DBEM) though, for this method, it is usual to develop the integral equations at "field" points \underline{Q} whereas, for this work, the integral equations are developed at "source" points \underline{P} .

Concerning the solution on boundary $\partial\Omega$, a similar process could be developed from 4.36 to 4.52 but, as the involved variables are assumed to belong to Hilbert spaces and these spaces are equipped with the trace property defined by 4.1 to 4.7, it is much simpler directly apply the trace operator to 4.52, resulting in

$$u(q) = \int_{\Omega_P} \mathbf{G}(P, q)^t f(P) d\Omega_P + \int_{\partial\Omega_P} \mathbf{G}(p, q)^t \mathcal{F}(p) d\partial\Omega_P \quad (4.53)$$

Our problem under study is completely defined by equations 4.52 and 4.53. It is important to point out that any kind of approximation was considered which would lead to a reduction in the quality of the results.

4.4.2 Integral Equations Approximation

In this section we will use well-established numerical techniques, such as, FEM and BEM in order to discretize and approximate our problem. With the view to perform the numerical implementation of the MLGFM, two discretizations are needed: a domain one, based on finite elements and a boundary one, based on boundary elements (Figure 4.4). As a matter of fact, the boundary element mesh is taken as the trace of the finite element mesh. The numerical implementation is carried out as following:

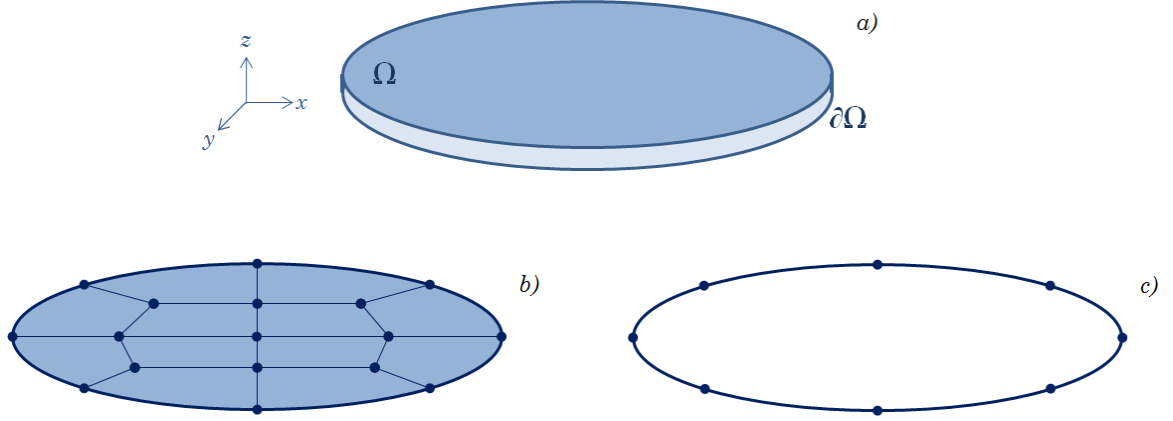


Figure 4.4 – Approximation of a real domain: a) a real domain Ω ; b) the finite elements mesh Ω^k and c) the boundary elements mesh $\partial\Omega^k$. **SOURCE:** Adapted from Machado (1992).

a) Domain Discretization:

In a similar way as in FEM, the real problem domain Ω is constructed by an approximate domain Ω_h , as close the real domain as possible. The approximate domain Ω_h is divided in \underline{nef} sub-domains, i.e., \underline{nef} is the number of finite elements $\overline{\Omega}^k$, such that

$$\Omega \cong \Omega_h = \bigcup_{k=1}^{\underline{nef}} \overline{\Omega}^k. \quad (4.54)$$

Each finite element corresponds to the closure of an open region Ω^k , with its boundary $\partial\Omega^k$, i.e.

$$\overline{\Omega}^k = \Omega^k \cup \partial\Omega^k \quad \text{with } k = 1, 2, \dots, \underline{nef}. \quad (4.55)$$

such that

$$\Omega^k \cap \Omega^j = \emptyset \quad \text{for } k \neq j. \quad (4.56)$$

b) Boundary Discretization:

The boundary is approximated by $\partial\Omega_h$ wherein it is divided in nec boundary intervals, i.e., nec is the number of boundary elements $\partial\Omega^k$. Similarly to the previous case a), we have

$$\partial\Omega_h = \bigcup_{k=1}^{nec} \partial\Omega^k. \quad (4.57)$$

$$\partial\Omega^k = \partial\Omega^k \cup \Gamma^k \quad \text{with } k = 1, 2, \dots, nec. \quad (4.58)$$

$$\partial\Omega^k \cap \partial\Omega^j = \emptyset \quad \text{for } k \neq j. \quad (4.59)$$

where Γ^k is the boundary of $\partial\Omega^k$.

Any domain and boundary approximations can be created through the shape functions ψ_i and ϕ_i , respectively. These functions are defined at local level in each element and they generate the subsets of finite dimension V_h of V , H_h of H and ∂H_h of ∂H where Green's function projections are generated.

c) Variables Approximation:

The variables encompassed in expressions 4.52 and 4.53 can be approximated using the shape functions matrices $\Psi(\cdot)$ and $\Phi(\cdot)$, that is

$$\begin{aligned} u_h(Q) &= \Psi(Q) \mathbf{u}_D & u_h(q) &= \Phi(q) \mathbf{u}_C \\ f_h(P) &= \Psi(P) \mathbf{b} & \tilde{f}_h(p) &= \Phi(p) \mathbf{f} \end{aligned} \quad (4.60)$$

where the variables \mathbf{u}_D , \mathbf{u}_C , \mathbf{b} and \mathbf{f} depict the generalized vectors of nodal displacements in domain and on boundary, the body forces and nodal boundary

reactions, respectively; $\Psi(\cdot)$ and $\Phi(\cdot)$ are the matrices of shape functions in a Green cell. Note that the $\Phi(p)$ is the trace of $\Psi(P)$ as well as $u_h(q)$ is the trace of $u_h(Q)$. Taking this into account, the values of \mathbf{u}_D corresponding to the nodes on boundary of the finite elements mesh overlap to the values of \mathbf{u}_C on boundary elements mesh.

For each element in domain Ω_h , the equation expressed in 4.52 can be rewritten as

$$\Psi(Q)\mathbf{u}_D = \int_{\Omega} \mathbf{G}(P, Q)^t \Psi(P) d\Omega_P \mathbf{b} + \int_{\partial\Omega} \mathbf{G}(p, Q)^t \Phi(p) d\partial\Omega_p \mathbf{f} \quad (4.61)$$

In order to evaluate the nodal displacement values, one can employ the Galerkin Residual Method (the variational boundary-value problem solution method for finite dimensional sets), i.e., taking the projection of $u_h(Q)$ orthogonal to $\Psi(Q)$. Considering that, the last equation can be expressed by

$$\begin{aligned} \int_{\Omega_Q} \Psi(Q)^t \Psi(Q) d\Omega_Q \mathbf{u}_D &= \int_{\Omega} \Psi(Q)^t \int_{\Omega} \mathbf{G}(P, Q)^t \Psi(P) d\Omega_P d\Omega_Q \mathbf{b} \\ &+ \int_{\Omega} \Psi(Q)^t \int_{\partial\Omega} \mathbf{G}(p, Q)^t \Phi(p) d\partial\Omega_p d\Omega_Q \mathbf{f} \end{aligned} \quad (4.62)$$

which may be better represented by

$$\mathbf{A}\mathbf{u}_D = \mathbf{B}\mathbf{f} + \mathbf{C}\mathbf{b} \quad (4.63)$$

where

$$\mathbf{A} = \int_{\Omega} \Psi(Q)^t \Psi(Q) d\Omega_Q \quad (4.64)$$

$$\mathbf{B} = \int_{\partial\Omega} \mathbf{G}_d(p)^t \Phi(p) d\partial\Omega_p \quad (4.65)$$

$$\mathbf{C} = \int_{\Omega} \mathbf{G}_d(P)^t \Psi(P) d\Omega_P \quad (4.66)$$

$$\mathbf{G}_d^t(p) = \int_{\Omega} \boldsymbol{\Psi}(Q)^t \mathbf{G}(p, Q)^t d\Omega_Q \quad (4.67)$$

$$\mathbf{G}_d^t(P) = \int_{\Omega} \boldsymbol{\Psi}(Q)^t \mathbf{G}(P, Q)^t d\Omega_Q \quad (4.68)$$

and where $\mathbf{G}_d(p)$ and $\mathbf{G}_d(P)$ are the projections, at a point p on boundary and P in domain, of the Green's function $\mathbf{G}(\cdot, Q)$, in the space yielded by shape functions ψ_i , respectively.

Now, for each element on boundary $\partial\Omega_h$, the equation expressed in 4.53 can be rewritten as

$$\boldsymbol{\Phi}(q)\mathbf{u}_C = \int_{\Omega} \mathbf{G}(P, q)^t \boldsymbol{\Psi}(P) d\Omega_P \mathbf{b} + \int_{\partial\Omega} \mathbf{G}(p, q)^t \boldsymbol{\Phi}(p) d\partial\Omega_P \mathbf{f} \quad (4.69)$$

Similarly, employing the Galerkin Residual Method (the variational boundary-value problem solution method for finite dimensional sets), i.e., taking the projection of $u_h(q)$ orthogonal to $\boldsymbol{\Phi}(q)$, the boundary equation system is determined, such that

$$\begin{aligned} \int_{\partial\Omega} \boldsymbol{\Phi}(q)^t \boldsymbol{\Phi}(q) d\partial\Omega_q \mathbf{u}_C &= \int_{\partial\Omega} \boldsymbol{\Phi}(q)^t \int_{\Omega} \mathbf{G}(P, q)^t \boldsymbol{\Psi}(P) d\Omega_P d\Omega_q \mathbf{b} \\ &+ \int_{\partial\Omega} \boldsymbol{\Phi}(q)^t \int_{\partial\Omega} \mathbf{G}(p, q)^t \boldsymbol{\Phi}(p) d\partial\Omega_P d\Omega_q \mathbf{f} \end{aligned} \quad (4.70)$$

which may be better represented by

$$\mathbf{D}\mathbf{u}_C = \mathbf{E}\mathbf{f} + \mathbf{F}\mathbf{b} \quad (4.71)$$

where

$$\mathbf{D} = \int_{\partial\Omega} \boldsymbol{\Phi}(q)^t \boldsymbol{\Phi}(q) d\partial\Omega_q \quad (4.72)$$

$$\mathbf{E} = \int_{\partial\Omega} \mathbf{G}_c(p)^t \boldsymbol{\Phi}(p) d\partial\Omega_p \quad (4.73)$$

$$\mathbf{F} = \int_{\Omega} \mathbf{G}_c(P)^t \boldsymbol{\Psi}(P) d\Omega_P \quad (4.74)$$

$$\mathbf{G}_c(p)^t = \int_{\partial\Omega} \boldsymbol{\Phi}(q)^t \mathbf{G}(p, q)^t d\partial\Omega_q \quad (4.75)$$

$$\mathbf{G}_c(P)^t = \int_{\partial\Omega} \boldsymbol{\Phi}(q)^t \mathbf{G}(P, q)^t d\partial\Omega_q \quad (4.76)$$

and where $\mathbf{G}_c(p)$ and $\mathbf{G}_c(P)$ are the projections, at a point p on boundary and P in domain, of the Green's function $\mathbf{G}(\cdot, q)$, in the space yielded by the shape functions ϕ_i , respectively.

The problem is fully solved by expressions 4.63 and 4.71. Note that the matrices \mathbf{A} and \mathbf{D} are easily resolved since they only contain shape functions. The other matrices, \mathbf{B} , \mathbf{C} , \mathbf{E} and \mathbf{F} depend on Green's function projections knowledge whose solution by the MLGFM will be dealt with in next section.

Also, it is important to highlight that the expression 4.71 is similar to the final system obtained by the “*Direct Boundary Element Method*” (DBEM). Depending on the boundary condition, if the displacement is prescribed ($\bar{\mathbf{u}}_c$) or if the “generalized forces” are specified ($\bar{\mathbf{f}}$), it is possible to rearrange the equation system in 4.71 aiming to split the known terms from the unknown ones such that

$$[-\mathbf{E} \quad : \quad \mathbf{D}] \begin{Bmatrix} \mathbf{f} \\ \mathbf{u}_c \end{Bmatrix} = [-\bar{\mathbf{D}} \quad : \quad \bar{\mathbf{E}}] \begin{Bmatrix} \bar{\mathbf{u}}_c \\ \bar{\mathbf{f}} \end{Bmatrix} + \mathbf{F}\mathbf{b} \quad (4.77)$$

4.4.3 The Green's Function Projections Determination

One of the most important steps in MLGFM is the determination of the Green's function projections in sets generated by the interpolation functions ψ_i and ϕ_i whereby the matrices \mathbf{B} , \mathbf{C} , \mathbf{E} and \mathbf{F} can be implemented. The determination of the Green's function projections were proposed by Barcellos and

Silva (1987) and it consists of obtaining these projections involving two distinct steps of solution through FEM such as:

1st STEP: Determination of Green's function projections $\underline{\mathbf{G}}_d(P)$ and $\underline{\mathbf{G}}_d(p)$ corresponding to Green's function $\mathbf{G}(P, Q)$ and $\mathbf{G}(p, Q)$, respectively.

In this step, as derived in section 4.2.2 (The MLGFM Abstract Formulation), applying the “Dirac delta” distribution $\delta(\cdot, \cdot)$ in domain Ω , with $Q \in \Omega$, the expressions 4.20 and 4.21 are solved, considering that the auxiliary state $v = v(\cdot, Q)$ is now defined by the Green's function $\mathbf{G}(\cdot, Q)$ and introducing the additional operator \mathcal{N}' on boundary conditions, as in 4.50, we have

$$\ell^* \mathbf{G}(P, Q)^t = \delta(P, Q) \mathbf{I} \quad \text{where } P, Q \in \Omega, \quad (4.78)$$

$$(\mathcal{N}^{*} + \mathcal{N}') \mathbf{G}(p, Q)^t = 0 \quad \text{where } p \in \partial\Omega \text{ and } Q \in \Omega. \quad (4.79)$$

Multiplying the expression 4.78 by $\Psi(Q)$ and integrate it in domain Ω , we have

$$\ell^* \left(\int_{\Omega} \mathbf{G}(P, Q)^t \Psi(Q) d\Omega_Q \right) = \int_{\Omega} \delta(P, Q) \Psi(Q) d\Omega_Q. \quad (4.80)$$

It can be recognized the projection $\mathbf{G}_d(P)$ in the left side of the equation 4.80, that is

$$\ell^* \mathbf{G}_d(P) = \Psi(P). \quad (4.81)$$

Similarly, adopting the same procedure but now aiming to find out the projection $\mathbf{G}_d(p)$, we have

$$(\mathcal{N}^{*} + \mathcal{N}') \int_{\Omega} \mathbf{G}^t(p, Q) \Psi(Q) d\Omega_Q = 0 \quad (4.82)$$

which is equivalent to

$$(\mathcal{N}^* + \mathcal{N}')\mathbf{G}_d(p) = 0. \quad (4.83)$$

2nd STEP: Determination of Green's function projections $\mathbf{G}_c(p)$ and $\mathbf{G}_c(P)$ corresponding to Green's function $\mathbf{G}(p,q)$ and $\mathbf{G}(P,q)$, respectively.

Here, applying the “*Dirac delta*” distribution $\delta(\cdot, \cdot)$ on boundary $\partial\Omega$, with $q \in \partial\Omega$, the expressions 4.23 and 4.24 are solved, considering that the auxiliary state $v = v(\cdot, q)$ is now defined by the Green's function $\mathbf{G}(\cdot, q)$ and introducing the additional operator \mathcal{N}' on boundary conditions, as in 4.50, we write

$$\ell^* \mathbf{G}(P, q)^t = 0 \quad \text{where } P \in \Omega \text{ and } q \in \partial\Omega, \quad (4.84)$$

$$(\mathcal{N}^* + \mathcal{N}')\mathbf{G}(p, q)^t = \delta(p, q)\mathbf{I} \quad \text{where } p, q \in \partial\Omega. \quad (4.85)$$

Now, multiplying the expression 4.84 by $\Phi(q)$ and integrating it on boundary $\partial\Omega$, such that

$$\ell^* \left(\int_{\partial\Omega} \mathbf{G}(P, q)^t \Phi(q) d\partial\Omega_q \right) = 0. \quad (4.86)$$

Again, the projection $\mathbf{G}_c(P)$ can be recognized in the left side of the equation 4.86, that is

$$\ell^* \mathbf{G}_c(P) = 0. \quad (4.87)$$

Similarly, adopting the same procedure but now aiming to find out the projection $\mathbf{G}_c(p)$, we have

$$(\mathcal{N}^* + \mathcal{N}') \int_{\partial\Omega} \mathbf{G}(p, q)^t \Phi(q) d\partial\Omega_q = \int_{\partial\Omega} \delta(p, q) \Phi(q) d\partial\Omega_q \quad (4.88)$$

which is equivalent to

$$(\mathcal{N}^* + \mathcal{N}') \mathbf{G}_c(p) = \Phi(p). \quad (4.89)$$

A physical interpretation for both two distinct steps of solution through FEM can be seen in Figure 4.5.

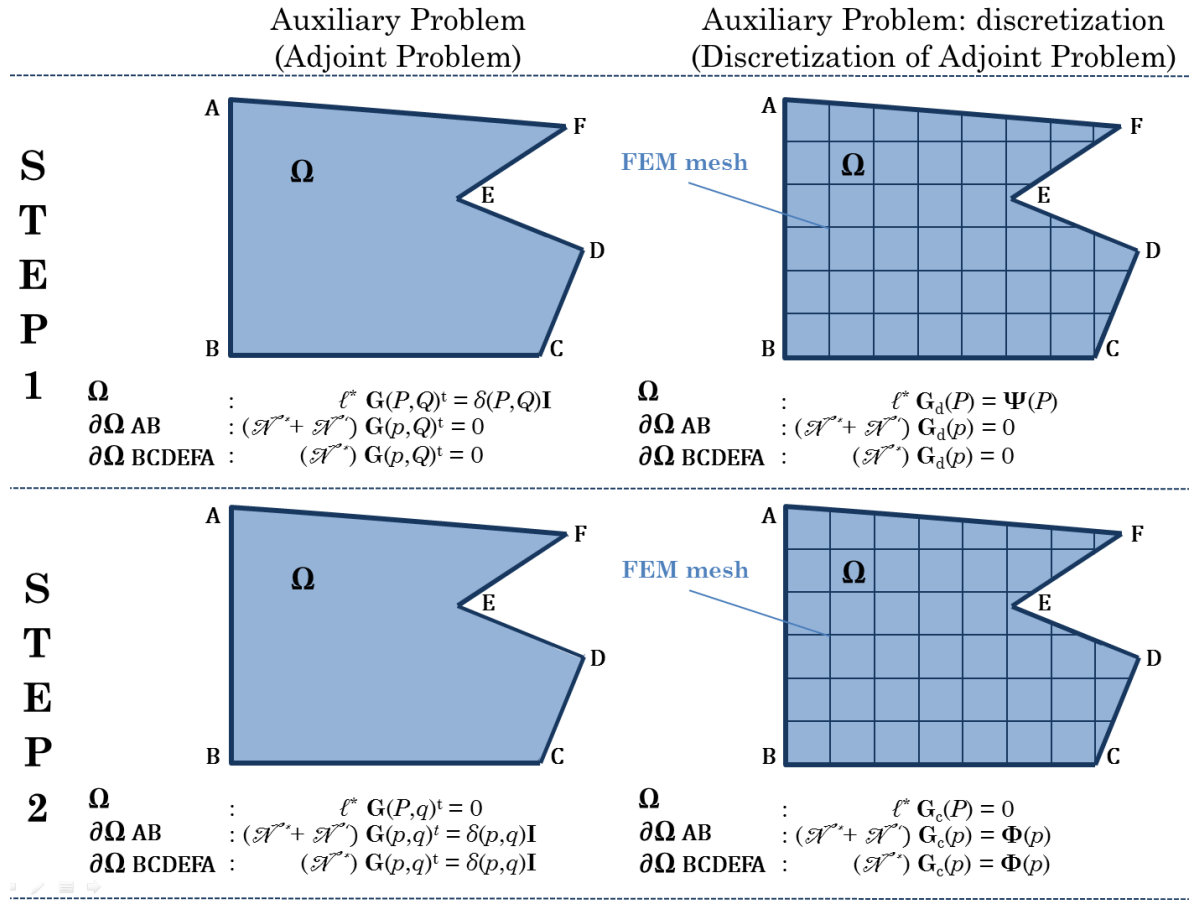


Figure 4.5 – Projections determination: physical interpretation of the solution in two distinct steps (by FEM). **SOURCE:** Adapted from Barbieri (1992).

Note that the right side of expressions 4.81 and 4.89 are the shape functions in domain and on boundary, respectively. It is possible to use the conventional Lagrangian shape function with continuity $C^0(\Omega)$ – space of continuous function up to order “0” (zero) in Ω – or any other continuity

depending on the order of the differential operator of the boundary-value problem to be solved. In conventional MLGFM, it is used Lagrangian shape functions but the scope of this work is exactly to enrich the space of shape functions either using a hierarchical approach (for instance, using Lobatto shape functions) or using different shape functions rather than the polynomial ones.

It is also worth mentioning that the excitation used in both steps is a “Dirac Delta” one $\delta(\cdot, \cdot)$ wherein is much more singular, i.e., if $x, y \in \mathbb{R}^n$, then $\delta(x, y) \in H^m(\Omega)$ where $m = -(n+\epsilon)/2$ and ϵ is a small positive constant. Also, note that $H^{-m}(\Omega) = H_0^m(\Omega)$. As consequence, the Green's function projections calculated in 4.81, 4.83 and 4.87, 4.89 have a smoother and regular behavior than the Green's function $\mathbf{G}(P, Q)$ itself. This simplifies the numerical handling and it is one of the most important reasons of the MLGFM's excellent performance.

The Green's projections can be also expanded by the shape functions ϕ_i and ψ_i used previously, considering that these Green's projections are smooth and continuous functions (MACHADO, 1992). Thus, we have

$$\begin{aligned} \mathbf{G}_d(P) &= \mathbf{\Psi}(P)\mathbf{G}^{DP}, & \mathbf{G}_d(p) &= \mathbf{\Phi}(p)\mathbf{G}^{Dp}, \\ \mathbf{G}_c(P) &= \mathbf{\Psi}(P)\mathbf{G}^{CP}, & \mathbf{G}_c(p) &= \mathbf{\Phi}(p)\mathbf{G}^{Cp} \end{aligned} \quad (4.90)$$

where \mathbf{G}^{DP} , \mathbf{G}^{Dp} , \mathbf{G}^{CP} and \mathbf{G}^{Cp} are the tensors obtained from nodal values of $\mathbf{G}_d(P)$, $\mathbf{G}_d(p)$, $\mathbf{G}_c(P)$ and $\mathbf{G}_c(p)$, respectively.

For self-adjoint operators ($\ell = \ell^*$) it is possible to define a functional $\mathcal{F}(\mathbf{G}_d, \mathbf{G}_c)$ whose extremization via Galerkin–FEM leads to the nodal values mentioned above. This functional may be written such that (BARBIERI, 1992)

$$\mathcal{F}(\mathbf{G}_d, \mathbf{G}_c) = B(\mathcal{J}, \mathcal{J}) - \alpha B_1(\mathbf{G}_d, \mathbf{\Psi}) - \beta B_2(\mathbf{G}_c, \mathbf{\Phi}) + B_3(\mathcal{J}, \mathcal{J}) \quad (4.91)$$

where:

- a) α and β are constants wherein $\alpha=1$ and $\beta=0$ if \mathbf{G}_d is the projection to be calculated minimizing 4.91 otherwise if \mathbf{G}_c is the one to be figured out than $\alpha=0$ and $\beta=1$;
- b) \mathcal{G} corresponds to \mathbf{G}_d or \mathbf{G}_c depending on the case to be calculated;
- c) $B(\mathcal{G}, \mathcal{G})$ is the bilinear form under study depending on the choice of \mathcal{G} (either \mathbf{G}_d or \mathbf{G}_c);
- d) B_1 , B_2 and B_3 are bilinear forms such as

$$B_1(\mathbf{G}_d, \boldsymbol{\Psi}) = \int_{\Omega} \mathbf{G}_d(P) \cdot \boldsymbol{\Psi}(P) d\Omega_p, \quad (4.92)$$

$$B_2(\mathbf{G}_c, \boldsymbol{\Phi}) = \int_{\partial\Omega} \mathbf{G}_c(p) \cdot \boldsymbol{\Phi}(p) d\partial\Omega_p, \quad (4.93)$$

$$B_3(\mathcal{G}, \mathcal{G}) = \frac{1}{2} \int_{\partial\Omega} [\mathcal{N}' \mathcal{G}(p)] \cdot \mathcal{G}(p) d\partial\Omega_p. \quad (4.94)$$

Then, minimizing the functional \mathcal{F} , one finds out the equation system similar to

$$\mathbf{K} \begin{pmatrix} \mathbf{G}^{\text{DP}} & \mathbf{G}^{\text{CP}} \end{pmatrix} = \begin{pmatrix} \mathbf{A} & \mathbf{D} \end{pmatrix} \quad \text{or} \quad [\mathbf{K}] \begin{bmatrix} \mathbf{G}^{\text{DP}} & \mathbf{G}^{\text{CP}} \end{bmatrix} = \begin{bmatrix} \mathbf{A} & \mathbf{D} \end{bmatrix} \quad (4.95)$$

where:

$$\mathbf{K} = \mathbf{K}_{\text{FEM}} + \mathbf{K}' \quad \text{or} \quad [\mathbf{K}] = [\mathbf{K}_{\text{FEM}}] + [\mathbf{K}'] \quad (4.96)$$

- a) $[\mathbf{K}_{\text{FEM}}]$: Finite Element Method standard stiffness matrix;
- b) $[\mathbf{K}']$: matrix whose the boundary operator \mathcal{N}' coefficients are placed and can be represented as a diagonal matrix (as mentioned in 4.46), such that

$$[K'] = \begin{bmatrix} k_1 & & & \\ & k_2 & & \\ & & \ddots & \\ & & & k_i \end{bmatrix} \quad (4.97)$$

- c) \mathbf{A} and \mathbf{D} : matrices resulting from the functional minimization $\mathcal{F}(\mathbf{G}_d, \mathbf{G}_c)$ process which correspond to the matrices of 4.64 and 4.72, respectively.

The coefficients k_i , $i = 1, 2, \dots, n$, are constants with nonzero values where n is the total number of degrees of freedom and with values that do not compromise the final conditioning of the equation system. These coefficients must be specified only where there are homogeneous Dirichlet boundary conditions ($\mathbf{u} = 0$). This restriction can be better understood by observing that this MLGFM additional operator \mathcal{N}' is included only in the bilinear form $B_3(\mathcal{G}, \mathcal{G})$ – expression 4.94 – directly affecting the stiffness matrix (expression 4.96). The values of the nodal resultant vector $\mathbf{f} = (\mathcal{N} + \mathcal{N}')\mathbf{u}_c$ are calculated using the operator \mathcal{N}' : while the first part $\mathcal{N}\mathbf{u}_c$ corresponds to the real reactions and loads, the second one $\mathcal{N}'\mathbf{u}_c$ corresponds to "fictitious" values. The "fictitious" reactions and loads are not included into the equation system since the operator \mathcal{N}' is only introduced on boundary patch wherein Dirichlet conditions are homogeneous ($\mathbf{u} = 0$). Otherwise, it would be necessary a post-processing to extract these "fictitious" quantities from the results. Barbieri (1992) tested the coefficients k_i from $[10^{-11}K_{\max}]$ to $[10^8K_{\max}]$, where $[K_{\max}]$ é the highest value of the standard stiffness matrix diagonal, and it hasn't been found any disturbance in MLGFM. This is a little bit different when enriching the space of shape functions (using Lobatto shape functions – HFEM) or using non-polynomial ones (GFEM). It was tested, in this work, coefficients k_i from $[10^{-25}K_{\max}]$ to $[10^{25}K_{\max}]$ and some disturbance was found out. This subject can affect the condition number of MLGFM matrices and will be better discussed in results chapter.

4.4.4 Matrices Implementation and Equation System Calculation

In this section, it will be established a sequence of steps to figure out the matrices and calculate the unknown nodal values in MLGFM. Going back to the equation system defined by expressions 4.63 ($\mathbf{A}\mathbf{u}_d = \mathbf{B}\mathbf{b} + \mathbf{C}\mathbf{f}$) and 4.71 ($\mathbf{D}\mathbf{u}_c = \mathbf{E}\mathbf{f} + \mathbf{F}\mathbf{b}$), we have:

- a) The matrices \mathbf{A} (expression 4.64) and \mathbf{D} (expression 4.72) are easily figured out because they only contain shape functions matrices;
- b) Once we know \mathbf{G}^{DP} and \mathbf{G}^{CP} nodal values in 4.95, we can automatically calculate \mathbf{G}^{Dp} and \mathbf{G}^{Cp} nodal values by trace property defined by 4.1 to 4.7;
- c) With the Green's tensor projections \mathbf{G}^{CP} and \mathbf{G}^{DP} figured out in last sub item b), the matrices \mathbf{B} in 4.65 and \mathbf{C} in 4.66 can be rewritten, using 4.90, as

$$\mathbf{B} = \int_{\Omega} \boldsymbol{\Psi}(P)^t \boldsymbol{\Psi}(P) d\Omega_p \mathbf{G}^{CP}, \quad (4.98)$$

$$\mathbf{C} = \int_{\Omega} \boldsymbol{\Psi}(P)^t \boldsymbol{\Psi}(P) d\Omega_p \mathbf{G}^{DP}. \quad (4.99)$$

We can readily recognize the matrix \mathbf{A} (4.64) in last expressions 4.98 and 4.99. So, those expressions yield

$$\mathbf{B} = \mathbf{A} \mathbf{G}^{CP} \quad (4.100)$$

$$\mathbf{C} = \mathbf{A} \mathbf{G}^{DP} \quad (4.101)$$

- d) Similarly for the last sub item c) but now for the matrix \mathbf{E} (4.73) we can rewritten, using 4.90, as

$$\mathbf{E} = \int_{\partial\Omega} \boldsymbol{\Phi}(p)^t \boldsymbol{\Phi}(p) d\partial\Omega_p \mathbf{G}^{cp} \quad (4.102)$$

So now, recognizing the matrix \mathbf{D} (4.72) in last expression 4.102 yields

$$\mathbf{E} = \mathbf{D} \mathbf{G}^{cp} \quad (4.103)$$

- e) Considering that the boundary shape functions matrix $\boldsymbol{\Phi}(\cdot)$ correspond to the trace of the domain shape functions matrix $\boldsymbol{\Psi}(\cdot)$, one concludes observing 4.65 and 4.74 that

$$\mathbf{F} = \mathbf{B}^t \quad (4.104)$$

- f) Once we have the matrices \mathbf{D} , \mathbf{E} and \mathbf{F} together with the body forces \mathbf{b} , prescribed forces $\bar{\mathbf{f}}$ and prescribed displacements $\bar{\mathbf{u}}_c$, the equation system 4.77 can be solved and the boundary nodal values in 4.71 ($\mathbf{D} \mathbf{u}_c = \mathbf{E} \mathbf{f} + \mathbf{F} \mathbf{b}$) can be calculated. Afterwards, with all nodal boundary reactions \mathbf{f} calculated, it is possible to replace them in 4.63 ($\mathbf{A} \mathbf{u}_d = \mathbf{B} \mathbf{b} + \mathbf{C} \mathbf{f}$) – in order to determine the domain nodal values. This approach is very fruitful because, using the expressions 4.100 and 4.101, the results in domain are obtained without knowing the inverse of matrix \mathbf{A} , in other words, the domain system equation 4.63 simplifies to

$$\mathbf{u}_d = \mathbf{G}^{cp} \mathbf{f} + \mathbf{G}^{dp} \mathbf{b} \quad (4.105)$$

- g) If the previous procedure to determine the domain nodal values is chosen – described in the sub item f) – it does not necessary to calculate the matrix C since we already know the G^{CP} and G^{DP} values but it is still necessary to determine the matrix B on account of to know F as described in sub item e).

The Figure 4.6 shows a simplified flowchart describing the equation system calculation steps. The complete one can be seen in Appendix “C”.

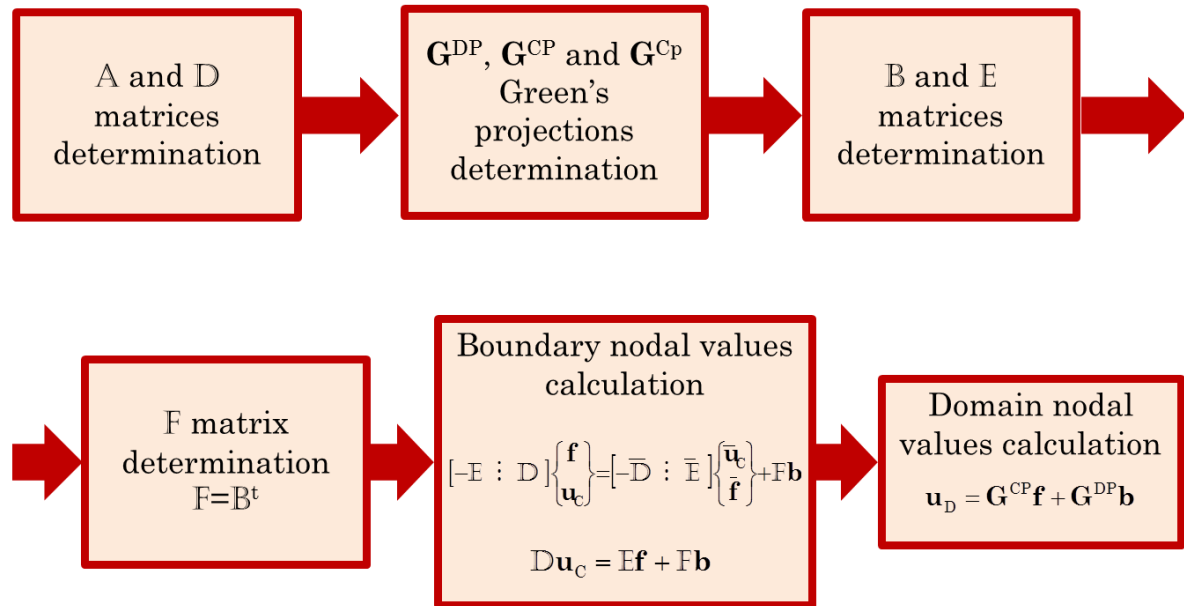


Figure 4.6 – MLGFM equation system: simplified calculation steps flowchart.

Finally, we conclude this chapter pointing out in next parts of this work we will use all concepts described here for the MLGFM formulation and extend them when using enrichment approach. The enrichment techniques employed in MLGFM will be better detailed in next chapter.

Chapter 5

Enriched Modified Local Green's Function Methodology for Elasto Static

5.1 INTRODUCTION

In this chapter, the Enriched Modified Local Green's Function Method (EMLGFM) is presented and its methodology is developed. The EMLGFM formalism for the Elasto Static is formulated from variational principles using the principle of minimum total potential energy in order to identify the problem's differential operator and its formal adjoint. Once identified these differential operators, it is possible to develop a methodology to determine the Green's function projections and their approximation using FEM. An important characteristic of this method is how the MLGFM's matrices are affected for the enriched case and, afterwards, this is further discussed too. In the end, it is examined how to figure out the displacements, reaction forces and stresses using the Enriched Modified Local Green's Function technique.

5.2 EMLGFM FORMALISM TO ELASTO STATIC

In elasticity theory one of the greatest interests is the solution of called *Lamé–Navier* equations of elasticity (REDDY, 2008). This expression represents the equilibrium equations expressed in terms of the displacement field for homogeneous, isotropic and linear media. These equilibrium equations (they can be visualized in Appendix “B”), as applied to solid bodies, can also be formulated by means of variational principles. The principle of minimum total potential energy, for example, can be regarded as a substitute to the equations of equilibrium of elastic bodies. The use of variational principles makes it possible to concentrate in a single functional all of the intrinsic features of the problem at hand: the governing equations, the boundary conditions, initial conditions, constraint conditions, even jump conditions. So, by the principle of minimum total potential energy, the first variation of the total potential energy must be null such that

$$\delta II = \delta U_{SE} + \delta V_{WD} = 0 \quad (5.1)$$

wherein II is the total potential energy, U_{SE} is the strain energy and V_{WD} is the total work done by external forces.

The total strain energy of a body occupying a domain Ω is given by

$$U_{SE} = \frac{1}{2} \int_{\Omega} \sigma_{ij} \varepsilon_{ij} d\Omega \quad (5.2)$$

in which σ_{ij} and ε_{ij} are the components of the stress and strain tensors, respectively.

The total work done by applied external forces is given by

$$V_{WD} = - \left(\int_{\Omega} b_i u_i d\Omega - \int_{\partial\Omega} T_i u_i d\partial\Omega \right) \quad (5.3)$$

in which b_i are the components of the body forces, u_i are the components of the displacement field and T_i are the components of the tractions (surface forces).

If a body is in equilibrium, among all admissible displacement fields “ u ”, the one “ u ” that makes the total potential energy a minimum corresponds to the equilibrium solution, i.e., in Elasto Static, we seek the displacement field $u(\mathbf{x})$ that minimizes the following functional $\mathcal{F}(u)$ that is

$$\mathcal{F}(u) = \frac{1}{2} \int_{\Omega} D_{ijkl} u_{i,j} u_{k,l} d\Omega - \int_{\Omega} b_i u_i d\Omega - \int_{\partial\Omega_2} \bar{T}_i u_i d\partial\Omega - \int_{\partial\Omega_1} T_i \bar{u}_i d\partial\Omega \quad \text{for } \Omega \subset \mathbb{R}^3 \quad (5.4)$$

where it is possible to recognize the first term of the functional as the total strain energy and the remaining terms as the total work done by external forces with $\partial\Omega_1$ being the boundary path where $u_i = \bar{u}_i$ is prescribed and $\partial\Omega_2$ being the boundary path where $T_i = \bar{T}_i$ is prescribed. Here, D_{ijkl} are the elastic stiffness coefficients of the elasticity matrix \mathbf{D} .

The functional $\mathcal{F}(u)$ can be properly rewritten as

$$\mathcal{F}(u) = \frac{1}{2} B(u, u) - \ell(u) \quad (5.5)$$

where $B(\cdot, \cdot)$ is the bilinear form

$$B(u, u) = \int_{\Omega} D_{ijkl} u_{i,j} u_{k,l} d\Omega \quad (5.6)$$

and $\ell(\cdot)$ is the functional

$$\ell(u) = \int_{\Omega} b_i u_i d\Omega + \int_{\partial\Omega_2} \bar{T}_i u_i d\partial\Omega + \int_{\partial\Omega_1} T_i \bar{u}_i d\partial\Omega \quad (5.7)$$

Hence, minimizing $\mathcal{F}(u)$ with respect to the displacement field, one

obtains the elasto static equilibrium equations expressed by

$$G u_{j,kk} + \frac{G}{1-2\nu} u_{k,kj} + b_j = 0 \quad (5.8)$$

with the following boundary conditions

$$\bar{T}_i = \frac{2G\nu}{1-2\nu} u_{k,k} n_i + G(u_{i,j} + u_{j,i}) n_j \text{ in } \partial\Omega_2 \quad \text{or} \quad u_i = \bar{u}_i \text{ in } \partial\Omega_1 \quad (5.9)$$

where n_i is the normal vector components; \bar{u}_i , \bar{T}_i are the prescribed values of the displacement and traction, respectively; G is the shear modulus and ν is the Poisson's ratio.

Observing the Equations 5.8 and 5.9, one can identify the differential operator A and the Neumann operator \mathcal{N} (Figure 5.1) such that

$$\begin{aligned} Au = \ell(u) &= f & \text{in } \Omega \\ \mathcal{N}(u) &= T & \text{on } \partial\Omega \end{aligned} \quad (5.10)$$

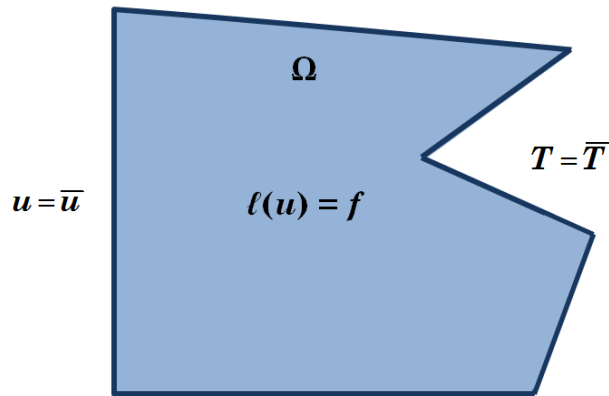


Figure 5.1 – Boundary conditions for an arbitrary domain Ω . **SOURCE:** Adapted from Barbieri (1992).

The sufficient conditions on the associated bilinear forms to guarantee the existence and uniqueness of a solution are addressed by “*The Generalized*

Lax-Milgram Theorem” (REDDY, 1986). The operator ℓ is symmetric, continuous and self-adjoint, i.e., $\ell = \ell^*$. Since ℓ is a self-adjoint operator, the operators ℓ^* and \mathcal{N}^* are also automatically identified (BARBIERI, 1992). Remember (from chapter 4, Figure 4.5), it is necessary to know the adjoint operators from the auxiliary problem in order to determine the Green's functions projections.

Hence, now we know the differential operators, we are in place to figure out the Green's function projections using the methodology described in chapter 4.

5.3 GREEN'S FUNCTION PROJECTIONS DETERMINATION

5.3.1 Green's Matrices General Characteristics

In order to facilitate the comprehension of this section, it is interesting to establish the following parameters:

- $ngln$: number of degrees of freedom per node;
- $nnef$: number of nodes in a finite element;
- $nnec$: number of nodes in a boundary element;
- ntn : total number of finite element nodes;
- $ntnc$: total number of boundary element nodes.

It is also important to distinguish the following displacement vectors:

- **d**: the degrees of freedom per node vector (displacements “x” and “y” in one node);
- **u^e**: the nodal displacement vector of an element;
- **u**: the nodal displacement vector of whole problem.

Such vectors, considering the spaces generated by the finite element, can be expressed as

$$\begin{aligned} \mathbf{d}_j^e &= \{u_{1j}, u_{2j}\}_j^t, & \text{for an element node "j",} \\ \mathbf{d}_j &= \{u_{1j}, u_{2j}\}_j^t, & \text{for whole problem node "j",} \end{aligned} \quad (5.11)$$

$$\begin{aligned} \mathbf{u}_D^e &= \{u_{11}^e, u_{21}^e, \dots, u_{(ngln \times nnef)}^e\}_e^t, & \text{for a domain element "e",} \\ &= \{\mathbf{d}_1^e, \mathbf{d}_2^e, \dots, \mathbf{d}_{nnef}^e\}_j^t, & \text{or} \\ \mathbf{u}_B^e &= \{u_{11}^e, u_{21}^e, \dots, u_{(ngln \times ntnc)}^e\}_e^t, & \text{for a boundary element "e",} \\ &= \{\mathbf{d}_1^e, \mathbf{d}_2^e, \dots, \mathbf{d}_{ntnc}^e\}_j^t, \end{aligned} \quad (5.12)$$

$$\begin{aligned} \mathbf{u}_D &= \{u_1, u_2, \dots, u_{(ngln \times ntn)}\}^t & \text{for the domain whole problem,} \\ &= \{\mathbf{d}_1, \mathbf{d}_2, \dots, \mathbf{d}_{ntn}\}^t, & \text{or} \\ \mathbf{u}_B &= \{u_1, u_2, \dots, u_{(ngln \times ntnc)}\}^t, & \text{for the boundary whole problem,} \\ &= \{\mathbf{d}_1, \mathbf{d}_2, \dots, \mathbf{d}_{ntnc}\}^t. \end{aligned} \quad (5.13)$$

In this way, \mathbf{d} , \mathbf{u}^e and \mathbf{u} are vectors with dimensions: $\mathbf{d}_{[ngln \times 1]}$, $\mathbf{u}_D^e [(nnef \times ngln) \times 1]$ for a domain element or $\mathbf{u}_B^e [(ntnc \times ngln) \times 1]$ for a boundary element and $\mathbf{u}_D [(ntn \times ngln) \times 1]$ for a domain mesh or $\mathbf{u}_B [(ntnc \times ngln) \times 1]$ for a boundary mesh, respectively.

Since the 4-node bilinear quadrilateral element in domain and the 2-node linear element on boundary are utilized in this work, they are considered in next developments.

Therefore, it is possible to approximate the displacement vector in domain \mathbf{u}_D^e for an arbitrary 4-node 2D quadrilateral element such that

$$\mathbf{u}_D^e = \begin{bmatrix} \psi_1^e & 0 & \psi_2^e & 0 & \psi_3^e & 0 & \psi_4^e & 0 \\ 0 & \psi_1^e & 0 & \psi_2^e & 0 & \psi_3^e & 0 & \psi_4^e \end{bmatrix} \{u_{11}^e \ u_{21}^e \ u_{12}^e \ u_{22}^e \ u_{13}^e \ u_{23}^e \ u_{14}^e \ u_{24}^e\}^t \quad (5.14)$$

where ψ_i^e are components of the local shape function matrix Ψ^e in domain and u_{kl}^e is the displacement component of a “ k ” degree of freedom at a local node “ l ”.

The last expression can be generically described as

$$\mathbf{u}_D^e = \Psi^e \mathbf{u}^e \quad (5.15)$$

So, each shape function sub-matrix

$$\Psi_i^e = \begin{bmatrix} \psi_i^e & 0 \\ 0 & \psi_i^e \end{bmatrix} \quad (5.16)$$

related to a degree of freedom has a dimension of $ngln \times ngln$ and the matrix Ψ^e has a dimension of $[ngln \times (ngln \times nnef)]$.

For whole domain, the displacement vector in domain \mathbf{u}_D can be denoted by global shape functions as

$$\mathbf{u}_D = \begin{bmatrix} \psi_1 & 0 & \psi_2 & 0 & \vdots & \psi_{ntn} & 0 \\ 0 & \psi_1 & 0 & \psi_2 & \vdots & 0 & \psi_{ntn} \end{bmatrix} \{u_1 \quad u_2 \quad u_3 \quad \cdots \quad u_{(ngln \times ntn)}\}^t \quad (5.17)$$

or, generically

$$\mathbf{u}_D = \Psi \mathbf{u} \quad (5.18)$$

with Ψ has the dimension of $[ngln \times (ngln \times ntn)]$.

In the case of the 2-node 1D element, the approximate displacement vector on boundary \mathbf{u}_B^e element can be expressed by

$$\mathbf{u}_B^e = \begin{bmatrix} \phi_1^e & 0 & \phi_2^e & 0 \\ 0 & \phi_1^e & 0 & \phi_2^e \end{bmatrix} \{u_{11}^e \quad u_{21}^e \quad u_{12}^e \quad u_{22}^e\}^t \quad (5.19)$$

where ϕ_i^e are components of the local shape function matrix Φ^e on boundary and

u_{kl}^e is the displacement component of a “ k ” degree of freedom at a local node “ l ”.

The last expression can be generically described as

$$\mathbf{u}_B^e = \mathbf{\Phi}^e \mathbf{u}^e \quad (5.20)$$

So, each shape function sub-matrix

$$\mathbf{\Phi}_i^e = \begin{bmatrix} \phi_i^e & 0 \\ 0 & \phi_i^e \end{bmatrix} \quad (5.21)$$

related to a degree of freedom has a dimension of $ngln \times ngln$ and the matrix $\mathbf{\Phi}^e$ has a dimension of $[ngln \times (ngln \times nnec)]$.

For whole domain, the displacement vector on boundary \mathbf{u}_B can be denoted by global shape functions as

$$\mathbf{u}_B = \begin{bmatrix} \phi_1 & 0 \vdots \phi_2 & 0 \vdots & \vdots \phi_{ntn} & 0 \\ 0 & \phi_1 \vdots 0 & \phi_2 \vdots & \vdots 0 & \phi_{ntn} \end{bmatrix} \left\{ \mathbf{u}_1 \quad \mathbf{u}_2 \quad \mathbf{u}_3 \quad \cdots \quad \mathbf{u}_{(ngln \times ntnc)} \right\}^t \quad (5.22)$$

or, generically

$$\mathbf{u}_B = \mathbf{\Phi} \mathbf{u} \quad (5.23)$$

with $\mathbf{\Phi}$ has the dimension of $[ngln \times (ngln \times ntnc)]$.

Remember that the Green's function projection in domain, $\mathbf{G}_d(P)$, is expressed by Equation 4.68, that is

$$\mathbf{G}_d^t(P) = \int_{\Omega} \mathbf{\Psi}(Q)^t \mathbf{G}(P, Q)^t d\Omega_Q \quad (5.24)$$

and the Green's tensor $\mathbf{G}(P, Q)$ has the dimension of $(ngln \times ngln)$.

So, based on the shape function matrix form $\mathbf{\Psi}$ in Equation 5.17, one concludes that the $\mathbf{G}_d(P)$ has the same pattern, i.e.,

$$\mathbf{G}_d(P) = [\mathbf{G}_d^1(P) \quad \vdots \quad \mathbf{G}_d^2(P) \quad \vdots \quad \mathbf{G}_d^3(P) \quad \vdots \quad \dots \quad \vdots \quad \mathbf{G}_d^{ntn}(P)] \quad (5.25)$$

Each sub-matrix $[\mathbf{G}_d^i(P)]$ of Equation (5.25) corresponds to a node in the finite element mesh and it has the dimension of $(ngln \times ngln)$. Consequently, the matrix $\mathbf{G}_d(P)$ has the dimension of $[ngln \times (ngln \times ntn)]$.

Consider a sub-matrix from $\mathbf{G}_d(P)$ in expression (5.25) corresponding to a node “ i ”, i.e., $\mathbf{G}_d^i(P)$. This sub-matrix can be simplified by

$$\mathbf{G}_d^i(P) = [\mathbf{G}_{d1}^i \quad \vdots \quad \mathbf{G}_{d2}^i \quad \vdots \quad \dots \quad \vdots \quad \mathbf{G}_{dngln}^i] \quad (5.26)$$

where \mathbf{G}_{dj}^i is a vector $\{\mathbf{G}_{dj}^i\}$ corresponding to “ j -th” column (or degree of freedom) of $\mathbf{G}_d^i(P)$. It is necessary to go deep in details because the minimization of the functional \mathcal{F} uses the vectors $\{\mathbf{G}_{dj}^i\}$.

It is possible, by similarity, to ascertain the projection $\mathbf{G}_c(P)$ expressed by Equation 4.76 in the space generated by the boundary elements. Aiming doing that, it is necessary to replace from domain shape functions matrix $\mathbf{\Psi}$ to boundary shape functions matrix $\mathbf{\Phi}$ and change the parameter from ntn to $ntnc$, consequently.

Doing so, one concludes that $\mathbf{G}_c(P)$, has a dimension of $[ngln \times (ngln \times ntnc)]$ and it is composed by $ntnc$ sub-matrices with the dimension of $(ngln \times ngln)$, such that

$$\mathbf{G}_c(P) = [\mathbf{G}_c^1(P) \quad \vdots \quad \mathbf{G}_c^2(P) \quad \vdots \quad \mathbf{G}_c^3(P) \quad \vdots \quad \dots \quad \vdots \quad \mathbf{G}_c^{ntnc}(P)] \quad (5.27)$$

In the same way, a sub-matrix $\mathbf{G}_c(P)$ corresponding to a node “ i ” can be given by

$$\mathbf{G}_c^i(P) = [\mathbf{G}_{c1}^i \quad \vdots \quad \mathbf{G}_{c2}^i \quad \vdots \quad \dots \quad \vdots \quad \mathbf{G}_{cngln}^i] \quad (5.28)$$

where $\mathbf{G}_{c_j}^i$ is a vector $\{\mathbf{G}_{c_j}^i\}$ correspond to “ j -th” column (or degree of freedom) of $\mathbf{G}_c^i(P)$ and these vectors are also utilized when minimizing the functional \mathcal{F} .

It will be seen in next section how the Green's function projections can be approximated using the Finite Element Method (FEM).

5.3.2 Green's Function Projections Approximation

Examining the proceedings developed in chapter 4 – section 4.4.3 – to obtain the projections $\mathbf{G}_d(P)$, $\mathbf{G}_d(p)$ and $\mathbf{G}_c(P)$, $\mathbf{G}_c(p)$, we have

1) From the **STEP 1**, aiming to approximate $\mathbf{G}_d(P)$, we write

$$\ell^* \mathbf{G}(P, Q)^t = \delta(P, Q) \mathbf{I} \quad \text{where } P, Q \in \Omega, \quad (5.29)$$

$$(\mathcal{N}^* + \mathcal{N}') \mathbf{G}(p, Q)^t = 0 \quad \text{where } p \in \partial\Omega \text{ and } Q \in \Omega. \quad (5.30)$$

Multiplying the expression 5.29 by $\Psi(Q)$ and integrating it in domain Ω

$$\ell^* \mathbf{G}_d(P) = \Psi(P). \quad (5.31)$$

Similarly, but now for expression 5.30, we have

$$(\mathcal{N}^* + \mathcal{N}') \mathbf{G}_d(p) = 0. \quad (5.32)$$

Then, the Green's function projection in domain, $\mathbf{G}_d(P)$, given by Equation 4.68, can be expressed by

$$\mathbf{G}_d(P) = \int_{\Omega} \begin{bmatrix} G_{11} & G_{12} \\ G_{21} & G_{22} \end{bmatrix} \begin{bmatrix} \psi_1 & 0 & \psi_2 & 0 & \dots & \psi_{ntn} & 0 \\ 0 & \psi_1 & 0 & \psi_2 & \dots & 0 & \psi_{ntn} \end{bmatrix} d\Omega_Q \quad (5.33)$$

which in the Green's tensor $\mathbf{G}(P, Q)$ has the dimension of $(ngln \times ngln)$ and Ψ has the dimension of $[ngln \times (ngln \times ntn)]$. Each G_{ij} term depends on points " P , Q " and each ψ_i component depends on the point " Q ". The last expression can be rewritten as seen in last section

$$\mathbf{G}_d(P) = [\mathbf{G}_d^1(P) \quad \vdots \quad \mathbf{G}_d^2(P) \quad \vdots \quad \mathbf{G}_d^3(P) \quad \vdots \quad \dots \quad \vdots \quad \mathbf{G}_d^{ntn}(P)] \quad (5.34)$$

where

$$\mathbf{G}_d^i(P) = \int_{\Omega} \begin{bmatrix} G_{11}\psi_i \vdots G_{12}\psi_i \\ G_{21}\psi_i \vdots G_{22}\psi_i \end{bmatrix} d\Omega_Q \quad (5.35)$$

and it represents the " i -th" component of the Green's function projection in the finite element space. Using the last expression (Equation 5.35) in Equation 5.31, we write

$$\ell^* \int_{\Omega} \begin{bmatrix} G_{11}\psi_i \vdots G_{12}\psi_i \\ G_{21}\psi_i \vdots G_{22}\psi_i \end{bmatrix} d\Omega_Q = \begin{bmatrix} \psi_i \vdots 0 \\ 0 \vdots \psi_i \end{bmatrix} \quad (5.36)$$

or

$$\ell^* \mathbf{G}_d^i(P) = \begin{bmatrix} \psi_i(P) \vdots 0 \\ 0 \vdots \psi_i(P) \end{bmatrix} \quad \text{where } P, Q \in \Omega. \quad (5.37)$$

Examining the last expression, one concludes the Green's function projection also obey the adjoint problem differential equation with only the difference that the Dirac delta excitation $\delta(P, Q)\mathbf{I}$ is replaced by

$$\begin{bmatrix} \psi_i(P) \vdots 0 \\ 0 \vdots \psi_i(P) \end{bmatrix}. \quad (5.38)$$

This is why the regularity of the projection $\mathbf{G}_d(P)$ is superior when compared to the Green's function $\mathbf{G}(P, Q)$!

The boundary conditions for the expression 5.37 are established from Equation 5.32 such that

$$(\mathcal{N}^* + \mathcal{N}') \mathbf{G}_d^i(p) = 0 \quad \text{where } p \in \partial\Omega. \quad (5.39)$$

Finally, the last step now is to obtain from Equations 5.37 and 5.39 the finite element approximation without knowing the functional in its explicit form. In chapter 4, it was shown the projections \mathbf{G}_d and \mathbf{G}_c can be figured out through a functional minimization $\mathcal{F}(\mathbf{G}_d, \mathbf{G}_c)$ – Equation 4.91 – with four different bilinear forms: $B(\mathcal{J}, \mathcal{J})$, $B_1(\mathbf{G}_d, \mathbf{\Psi})$, $B_2(\mathbf{G}_c, \mathbf{\Phi})$ and $B_3(\mathcal{J}, \mathcal{J})$. The bilinear form under study is $B(\mathcal{J}, \mathcal{J})$ whose it can be developed for \mathbf{G}_d or \mathbf{G}_c depending on the case to be calculated.

Firstly, one defines the differential operator \mathcal{L} as

$$\mathcal{L} = \begin{bmatrix} (\cdot)_{,x} & \vdots & 0 \\ 0 & \vdots & (\cdot)_{,y} \end{bmatrix} \quad (5.40)$$

which in $(\cdot)_{,x}$ and $(\cdot)_{,y}$ represent the partial derivatives of a function in “ x ” and “ y ”, respectively. For the projection $\mathbf{G}_d(P)$, the functional $\mathcal{F}(\mathbf{G}_{d_j}^i)$ can be formulated as (BARBIERI, 1992)

$$\begin{aligned} \mathcal{F}(\mathbf{G}_{d_j}^i) = & \frac{1}{2} \int_{\Omega} [\mathbf{D} \mathcal{L}(\mathbf{G}_{d_j}^i)]^t \mathcal{L}(\mathbf{G}_{d_j}^i) d\Omega - \int_{\Omega} [\mathbf{G}_{d_j}^i]^t \mathbf{W}_j d\Omega + \\ & + \int_{\partial\Omega} [\mathcal{N}'(\mathbf{G}_{d_j}^i)]^t \mathbf{G}_{d_j}^i d\partial\Omega \end{aligned} \quad (5.41)$$

that will be minimized and solved by the Finite Element Method (FEM) to find out the sought Green's function projection. The term $\mathbf{G}_{d_j}^i$ represents the “ j -th”

column of \mathbf{G}_d^i and \mathbf{W}_j , with $j = 1$ and $j = 2$ for $ngln = 2$, is given by

$$\mathbf{W}_1 = \begin{bmatrix} \psi_i(P) \\ 0 \end{bmatrix} \quad \text{and} \quad \mathbf{W}_2 = \begin{bmatrix} 0 \\ \psi_i(P) \end{bmatrix}. \quad (5.42)$$

Consider now the terms \mathbf{G}_{dj}^i . Expanding the components of $\mathbf{G}_d^i(P)$ using the finite element technique, we have

$$\mathbf{G}_d^i(P) = \begin{bmatrix} \psi_1 & 0 & \psi_2 & 0 & \dots & \psi_{ntn} & 0 \\ 0 & \psi_1 & 0 & \psi_2 & \dots & 0 & \psi_{ntn} \end{bmatrix} \begin{bmatrix} g_{11}^{DP} & g_{12}^{DP} & \dots & g_{1(ngln \times ntn)}^{DP} \\ g_{21}^{DP} & g_{22}^{DP} & \dots & g_{2(ngln \times ntn)}^{DP} \end{bmatrix}^t \quad (5.43)$$

or

$$\mathbf{G}_d^i(P) = \begin{bmatrix} gd_{11} & gd_{12} \\ gd_{21} & gd_{22} \end{bmatrix} \quad (5.44)$$

Thus, \mathbf{G}_{dj}^i can be expressed by

$$\begin{aligned} \mathbf{G}_{dj}^i &= \begin{Bmatrix} gd_{1j} \\ gd_{2j} \end{Bmatrix} \\ &= \begin{bmatrix} \psi_1 & 0 & \psi_2 & 0 & \dots & \psi_{ntn} & 0 \\ 0 & \psi_1 & 0 & \psi_2 & \dots & 0 & \psi_{ntn} \end{bmatrix} \{ g_{j1}^{DP} \quad g_{j2}^{DP} \quad \dots \quad g_{j(ngln \times ntn)}^{DP} \}^t \\ &= \mathbf{\Psi}_G \mathbf{G}^{DP^i}_j \end{aligned} \quad (5.45)$$

where $\mathbf{G}^{DP^i}_j$ is the vector $\{ \mathbf{G}^{DP} \}_j^i = \{ g_{j1}^{DP} \quad g_{j2}^{DP} \quad \dots \quad g_{j(ngln \times ntn)}^{DP} \}$ and g_{jk}^{DP} represents the value in the node “ k ” (considering $k = 1, 2, \dots, (ngln \times ntn)$) of the “ j -th” column of the “ i -th” component of the projection $\mathbf{G}_d(P)$.

Taking the last expansion for the projection \mathbf{G}_{dj}^i into the functional $\mathcal{F}(\mathbf{G}_{dj}^i)$ and minimizing it with respect to each component of \mathbf{G}_d^i obtained by

FEM, one achieves the following equation system

$$\mathbf{K} \mathbf{G}^{\text{DP}} = \mathbf{A} \quad \text{or} \quad [\mathbf{K}][\mathbf{G}^{\text{DP}}] = [\mathbf{A}] \quad (5.46)$$

where

$$\mathbf{K} = \mathbf{K}_{\text{FEM}} + \mathbf{K}' \quad \text{or} \quad [\mathbf{K}] = [\mathbf{K}_{\text{FEM}}] + [\mathbf{K}'] \quad (5.47)$$

and:

- a) \mathbf{K}_{FEM} : the Finite Element Method standard matrix;
- b) \mathbf{K}' : matrix whose the boundary operator \mathcal{N}' coefficients are placed and can be represented as a diagonal matrix (as mentioned in Equation (4.46)), such that:

$$\mathbf{K}' = \begin{bmatrix} k_1 & & & & \\ & k_2 & & & \\ & & \ddots & & \\ & & & k_{(2*m-1)} & \\ & & & & k_{2*m} \end{bmatrix} \quad (5.48)$$

which in the index “ m ” means the number of nodes on boundary whose the operator \mathcal{N}' acts.

- c) \mathbf{A} : matrix resulting from the functional minimization $\mathcal{J}(\mathbf{G}_{\text{d}j}^i)$ process which correspond to the matrix of Equation 4.64 and it can be expressed by

$$\mathbf{A} = \int_{\Omega} \begin{bmatrix} \psi_1 & 0 & \psi_2 & 0 & \dots & \psi_{ntn} & 0 \\ 0 & \psi_1 & 0 & \psi_2 & \dots & 0 & \psi_{ntn} \end{bmatrix}^t \begin{bmatrix} \psi_1 & 0 & \psi_2 & 0 & \dots & \psi_{ntn} & 0 \\ 0 & \psi_1 & 0 & \psi_2 & \dots & 0 & \psi_{ntn} \end{bmatrix} d\Omega \quad (5.49)$$

d) The matrix (tensor) \mathbf{G}^{DP} contain nodal values of the Green's function projections, such as:

- $\mathbf{G}^{\text{DP}}_{j,(2i-1)}$: nodal values [$j = 1, \dots, (2 \times ntn)$] of the projection \mathbf{G}_d^i components due to the load ψ_i ($i = 1, \dots, ntn$) in the direction “1”;
- $\mathbf{G}^{\text{DP}}_{j,(2i)}$: nodal values [$j = 1, \dots, (2 \times ntn)$] of the projection \mathbf{G}_d^i components due to the load ψ_i ($i = 1, \dots, ntn$) in the direction “2”;

2) Taking now the **STEP 2**, the same procedure can be done as described in last section but now aiming to find out the projection $\mathbf{G}_c(P)$, replacing the domain shape functions matrix $\mathbf{\Psi}$ by the boundary shape functions matrix $\mathbf{\Phi}$.

Starting by enumerating the Equations 4.84 and 4.85 with the aim to approximate $\mathbf{G}_c(P)$, we write

$$\ell^* \mathbf{G}(P, q)^t = 0 \quad \text{where } P \in \Omega \text{ and } q \in \partial\Omega, \quad (5.50)$$

$$(\mathcal{N}^* + \mathcal{N}') \mathbf{G}(p, q)^t = \delta(p, q) \mathbf{I} \quad \text{where } p, q \in \partial\Omega. \quad (5.51)$$

Multiplying the expression 5.50 by $\mathbf{\Phi}(q)$ and integrating it on boundary $\partial\Omega$, we have

$$\ell^* \mathbf{G}_c(P) = 0. \quad (5.52)$$

Similarly, but now for expression 5.51, one results

$$(\mathcal{N}^* + \mathcal{N}') \mathbf{G}_c(p) = \mathbf{\Phi}(p). \quad (5.53)$$

Then, the Green's function projection in domain, $\mathbf{G}_c(P)$, given by Equation

4.67, can be expressed by that is

$$\mathbf{G}_c(P) = \int_{\Omega} \begin{bmatrix} G_{11} \vdots G_{12} \\ G_{21} \vdots G_{22} \end{bmatrix} \begin{bmatrix} \phi_1 & 0 \vdots \phi_2 & 0 \vdots & \vdots \phi_{ntnc} & 0 \\ 0 & \phi_1 \vdots 0 & \phi_2 \vdots & \vdots 0 & \phi_{ntnc} \end{bmatrix} d\partial\Omega_q \quad (5.54)$$

which in the Green's tensor $\mathbf{G}(P, q)$ has the dimension of $(ngln \times ngln)$ and Φ has the dimension of $[ngln \times (ngln \times ntnc)]$. Each \mathbf{G}_{ij} term depends on points “ p , Q ” and ϕ_i component depends on the point “ q ”. The last expression can be rewritten as

$$\mathbf{G}_c(P) = [\mathbf{G}_c^1(P) \quad \vdots \quad \mathbf{G}_c^2(P) \quad \vdots \quad \mathbf{G}_c^3(P) \quad \vdots \quad \dots \quad \vdots \quad \mathbf{G}_c^{ntnc}(P)] \quad (5.55)$$

where

$$\mathbf{G}_c^i(P) = \int_{\partial\Omega_p} \begin{bmatrix} G_{11}\phi_i \vdots G_{12}\phi_i \\ G_{21}\phi_i \vdots G_{22}\phi_i \end{bmatrix} d\partial\Omega_q \quad (5.56)$$

and it represents the “ i -th” component of the Green's function projection in the finite element space generated by the boundary shape functions. Using the last expression (Equation 5.56) in Equation 5.52, we write

$$\ell^* \int_{\partial\Omega} \begin{bmatrix} G_{11}\phi_i \vdots G_{12}\phi_i \\ G_{21}\phi_i \vdots G_{22}\phi_i \end{bmatrix} d\partial\Omega_q = 0 \quad (5.57)$$

or

$$\ell^* \mathbf{G}_c^i(P) = 0 \quad \text{where } P \in \Omega. \quad (5.58)$$

Examining the last expression, one concludes the Green's function projection also obey the adjoint problem differential equation with only the difference that the Dirac delta excitation $\delta(P, Q)$ is replaced like that

$$\delta(P, Q) \mathbf{I} \quad \text{by} \quad 0 \text{ (zero)} \quad (5.59)$$

It is worth again highlighting that this is the reason why the regularity of the projections $\mathbf{G}_c(P)$ is superior when compared to the Green's tensor $\mathbf{G}(P, q)$!

The boundary conditions for the expression (5.58) are established from Equation (5.53) such that

$$(\mathcal{N}^* + \mathcal{N}') \mathbf{G}_c^i(p) = \begin{bmatrix} \phi_i(p) & 0 \\ 0 & \phi_i(p) \end{bmatrix}. \quad (5.60)$$

In the same way as developed for $\mathbf{G}_d(P)$, it is possible to write the following functional $\mathcal{F}(\mathbf{G}_{c_j}^i)$ to be minimized

$$\begin{aligned} \mathcal{F}(\mathbf{G}_{c_j}^i) = & \frac{1}{2} \int_{\Omega} [\mathbf{D} \mathcal{L}(\mathbf{G}_{c_j}^i)]^t \mathcal{L}(\mathbf{G}_{c_j}^i) d\Omega - \int_{\partial\Omega} [\mathbf{G}_{c_j}^i]^t \mathbf{w}_j d\partial\Omega + \\ & + \int_{\partial\Omega} [\mathcal{N}'(\mathbf{G}_{c_j}^i)]^t \mathbf{G}_{c_j}^i d\partial\Omega \end{aligned} \quad (5.61)$$

that will be solved by finite element method to find out the sought Green's function projection. The term $\mathbf{G}_{c_j}^i$ represents the “ j -th” column of \mathbf{G}_c^i and \mathbf{w}_j , with $j = 1$ and $j = 2$ for $ngln = 2$, is given by

$$\mathbf{w}_1 = \begin{bmatrix} \phi_i(p) \\ 0 \end{bmatrix} \quad \text{and} \quad \mathbf{w}_2 = \begin{bmatrix} 0 \\ \phi_i(p) \end{bmatrix} \quad (5.62)$$

Consider now $\mathbf{G}_{c_j}^i$. Expanding the components of $\mathbf{G}_c^i(P)$ using the finite element technique, we have

$$\mathbf{G}_c^i(P) = \begin{bmatrix} \psi_1 & 0 & \psi_2 & 0 & \dots & \psi_{ntn} & 0 \\ 0 & \psi_1 & 0 & \psi_2 & \dots & 0 & \psi_{ntn} \end{bmatrix} \begin{bmatrix} \mathbf{g}_{11}^{CP} & \mathbf{g}_{12}^{CP} & \dots & \mathbf{g}_{1(ngln \times ntn)}^{CP} \\ \mathbf{g}_{21}^{CP} & \mathbf{g}_{22}^{CP} & \dots & \mathbf{g}_{2(ngln \times ntn)}^{CP} \end{bmatrix}^t \quad (5.63)$$

or

$$\mathbf{G}_c^i(P) = \begin{bmatrix} g_{c_{11}} & g_{c_{12}} \\ g_{c_{21}} & g_{c_{22}} \end{bmatrix}. \quad (5.64)$$

Thus, $\mathbf{G}_{c_j}^i$ can be expressed by

$$\begin{aligned} \mathbf{G}_{c_j}^i &= \begin{Bmatrix} g_{c_{1j}} \\ g_{c_{2j}} \end{Bmatrix} \\ &= \begin{bmatrix} \psi_1 & 0 & \vdots & \psi_2 & 0 & \vdots & \cdots & \vdots & \psi_{ntn} & 0 \\ 0 & \psi_1 & \vdots & 0 & \psi_2 & \vdots & \cdots & \vdots & 0 & \psi_{ntn} \end{bmatrix} \begin{Bmatrix} g_{j1}^{CP} & \vdots & g_{j2}^{CP} & \vdots & \cdots & \vdots & g_{j(ng \ln x ntn)}^{CP} \end{Bmatrix}^t \\ &= \mathbf{\Psi}_G \mathbf{G}_{c_j}^{CPi} \end{aligned} \quad (5.65)$$

where $\mathbf{G}_{c_j}^{CPi}$ is the vector $\{G^{CP}\}_j^i = \{g_{j1}^{CP} \quad \vdots \quad g_{j2}^{CP} \quad \vdots \quad \cdots \quad \vdots \quad g_{jk}^{CP}\}$ and g_{jk}^{CP} represents the value in the node “ k ” (considering $k = 1, 2, \dots, (ng \ln x ntn)$) of the “ j -th” column of the “ i -th” component of the projection $\mathbf{G}_c(P)$.

Taking the last expansion for the projection $\mathbf{G}_{c_j}^i$ into the functional $\mathcal{F}(\mathbf{G}_{c_j}^i)$ and minimizing it with respect to each component of \mathbf{G}_c^i obtained by FEM, one achieves the following equation system

$$\mathbf{K} \mathbf{G}^{CP} = \mathbf{D} \quad \text{or} \quad [\mathbf{K}][\mathbf{G}^{CP}] = [\mathbf{D}] \quad (5.66)$$

where

$$\mathbf{K} = \mathbf{K}_{\text{FEM}} + \mathbf{K}' \quad \text{or} \quad [\mathbf{K}] = [\mathbf{K}_{\text{FEM}}] + [\mathbf{K}'] \quad (5.67)$$

and:

a) \mathbf{K}_{FEM} and \mathbf{K}' are the same matrices calculated previously for \mathbf{G}_d^i ;

- b) \mathbf{D} : matrix resulting from the functional minimization $\mathcal{F}(\mathbf{G}_{cj}^i)$ process which correspond to the matrix of Equation 4.72 and it can be expressed by

$$\mathbf{D} = \int_{\partial\Omega} \begin{bmatrix} \phi_1 & 0 & \phi_2 & 0 & \dots & \phi_{ntnc} & 0 \\ 0 & \phi_1 & 0 & \phi_2 & \dots & 0 & \phi_{ntnc} \end{bmatrix}^t \begin{bmatrix} \phi_1 & 0 & \phi_2 & 0 & \dots & \phi_{ntnc} & 0 \\ 0 & \phi_1 & 0 & \phi_2 & \dots & 0 & \phi_{ntnc} \end{bmatrix} d\partial\Omega \quad (5.68)$$

- c) The matrix \mathbf{G}^{CP} contain nodal values of the Green's function projections, such as:

- $\mathbf{G}_{j,(2i-1)}^{\text{CP}}$: nodal values [$j = 1, \dots, (2 \times ntnc)$] of the projection \mathbf{G}_c^i components due to the load ϕ_i ($i = 1, \dots, ntnc$) in the direction “1”;
- $\mathbf{G}_{j,(2i)}^{\text{CP}}$: nodal values [$j = 1, \dots, (2 \times ntnc)$] of the projection \mathbf{G}_c^i components due to the load ϕ_i ($i = 1, \dots, ntnc$) in the direction “2”;

In the end, the Equations 5.46 and 5.66 can be solved simultaneously, such that

$$\mathbf{K}(\mathbf{G}^{\text{DP}} \quad \mathbf{G}^{\text{CP}}) = (\mathbf{A} \quad \mathbf{D}) \quad \text{or} \quad [\mathbf{K}][\mathbf{G}^{\text{DP}} \quad \mathbf{G}^{\text{CP}}] = [\mathbf{A} \quad \mathbf{D}] \quad (5.69)$$

The values of the projections $\mathbf{G}_d(p)$ and $\mathbf{G}_c(p)$ are traces of the values of the projections $\mathbf{G}_d(P)$ and $\mathbf{G}_c(P)$, respectively, and they can be calculated once the Equation 5.69 is solved.

5.4 MLGFM's MATRICES FOR THE ENRICHED CASE

All developments performed up to now in last sections are valid both for conventional MLGFM and for the enriched case. But, in the case of the enrichment, it is necessary to include in domain variables ($ngln \times ntn$) and on boundary variables ($ngln \times ntnc$) the corresponding new degrees of freedom due to the enrichment that it is named here as $ngle$, in domain and $nglec$, on boundary.

For instance, consider an arbitrary problem discretized with only one element in domain, a 4-node 2D bilinear quadrilateral element with two nodal degrees of freedom and four elements on boundary, a 2-node 1D linear element with also two nodal degrees of freedom as seen in Figure 5.2.

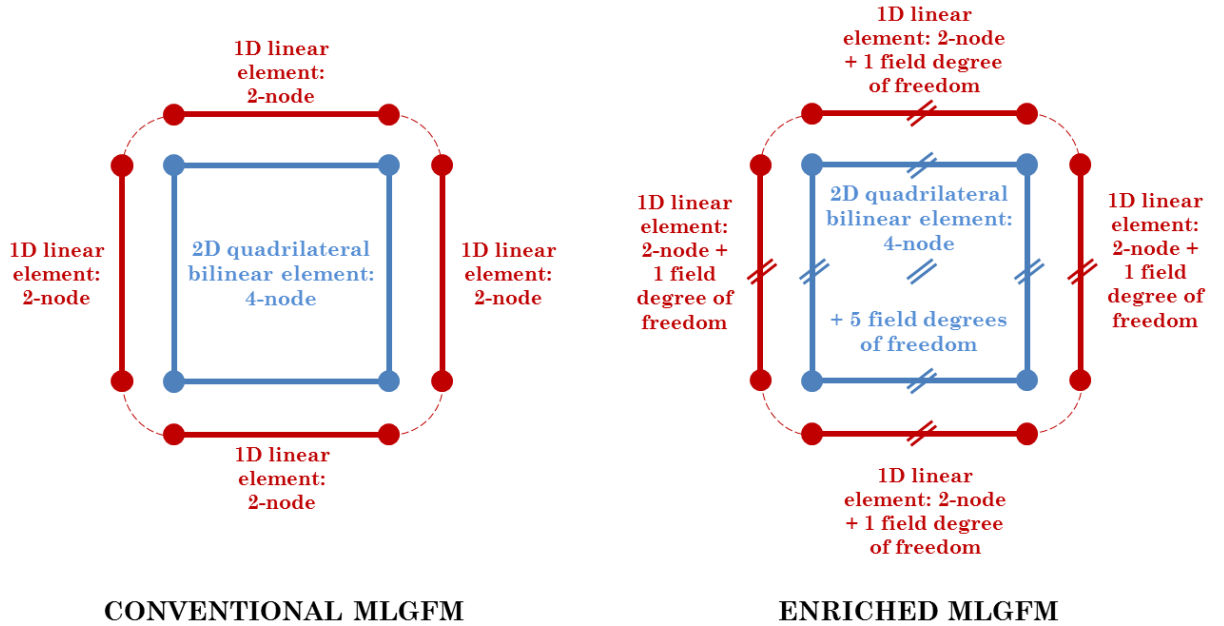


Figure 5.2 – A conventional and enriched MLGFM problem discretized with only 1 finite element in domain and 4 boundary elements on boundary.

It means that one has in domain: $ngln = 2$ and $ntn = 4$ (in this case, $nnef = ntn$) and on boundary: $ngln = 2$ and $ntnc = 8$ (in this case, $nnec = 2$). It is worth quoting each node and field degree of freedom have two degrees of freedom in this work (displacements in “ x ” and “ y ” directions). Also, note that if the same problem

was discretized with four finite elements in the domain mesh, the boundary mesh would have eight boundary elements as seen in Figure 5.3. Both discretized problems in Figure 5.2 and 5.3 possess double nodes at corners commonly used in Boundary Elements Method (BEM). For double nodes, the coordinates of both nodes are the same but the normal vectors differ. Also the type of boundary condition may be different at two nodes (GRILLI; SVENDSEN, 1990).

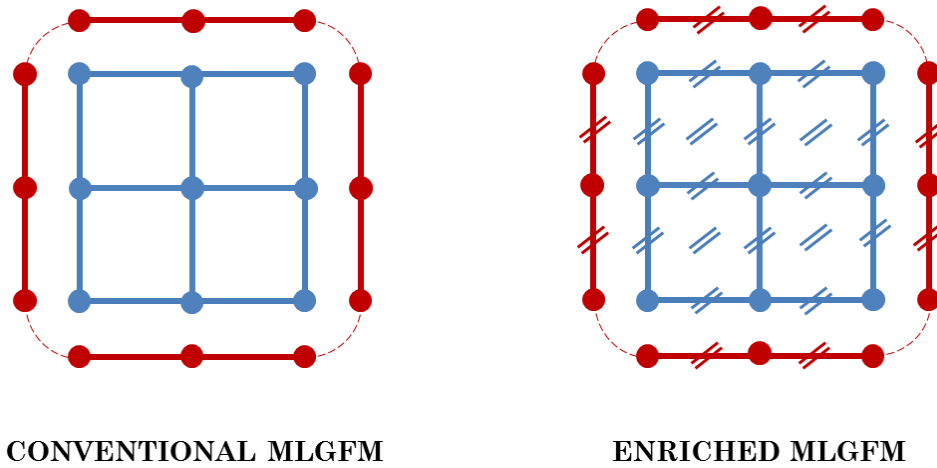


Figure 5.3 – A conventional and enriched MLGFM problem discretized with 4 finite elements in domain and 8 boundary elements on boundary.

But, we will focus on the example exposed here in Figure 5.2 where it is considered only 1 element in domain and 4 elements on boundary. Hence, the standard FEM stiffness matrix $[K_{FEM}]$ has a dimension of $[(ngln \times ntn) \times (ngln \times ntn)]$, i.e., 8×8 . That is the same dimension of the matrices $[G^{DP}]$ and $[A]$. For $[G^{CP}]$, this matrix has the dimension of $[(ngln \times ntn) \times (ngln \times ntnc)]$, i.e., for this problem, 8×16 and the $[D]$ matrix has the dimension of $[(ngln \times ntnc) \times (ngln \times ntnc)]$, i.e., 16×16 .

Considering only a first level of enrichment ($p = 2$ or $le = 1$), for example, the 4-node 2D bilinear quadrilateral element is enriched by 5 new field degrees of freedom ($ngle$) and the 2-node 1D linear element is enriched by 1 new field degree of freedom ($nglec$) as shown in Figure 5.2. Remembering: these nodes and field degrees of freedom must be multiplied by node degrees of freedom (in the case of

this work, it is equals two – displacements in “ x ” and “ y ” directions) to obtain the total number of degrees of freedom – DOF [$ngln \times (ntn+ngle)$].

Thus, the enriched stiffness matrix (K_{ENR} or $[K_{ENR}]$) will have, for this case, a dimension of $\{[ngln \times (ntn+ngle)] \times [ngln \times (ntn+ngle)]\}$, i.e., 18×18 (remember that for this case $nnef = ntn$). And again, that is the same dimension of the matrices $[G^{DP}]$ and $[A]$. For $[G^{CP}]$, this matrix has the dimension of $\{[ngln \times (ntn+ngle)] \times [ngln \times 4x(nnec+nglec)]\}$, i.e., for this problem, 18×12 and the $[D]$ matrix has the dimension of $\{[ngln \times 4x(nnec+nglec)] \times [ngln \times 4x(nnec+nglec)]\}$, i.e., 24×24 . So, as shown in Figure 5.4, there is an enlargement of the stiffness matrix once the finite element mesh is enriched. For the example that we have been explored so far, the dimension is increased from 8×8 to 18×18 .



Figure 5.4 – Standard $[K_{FEM}]$ and enriched $[K_{ENR}]$ stiffness matrix.

An important characteristic of this increase is that: the standard stiffness matrix is a part of the new enriched stiffness matrix, i.e., the enriched stiffness matrix $[K_{ENR}]$ is composed by the standard stiffness matrix $[K_{FEM}]$ plus new

rows and columns related to the enrichment level. This characteristic is not only inherent of the stiffness matrix but for all MLGFM system of matrices once the shape functions spaces are enriched both in domain and on boundary. This fact means that when calculating the Green's functions projections using the finite element space, these projections will be "enriched" as soon as this space is enriched. As the MLGFM is known by precise flow variable values as well as by displacement nodal values, it is expected these values could be even better once enriched. Unfortunately, it is not always the case that this situation happens to the enriched approach and this aspect will be better discussed in results chapter.

5.5 DISPLACEMENTS, REACTION FORCES AND STRESSES CALCULATION

The Modified Local Green's Function Method is able to determine, with high precision, the displacements and reaction forces values on boundary mesh nodal points as previously pointed out. These values can be figured out through the equation system (Equation 4.77) rewritten below

$$\begin{bmatrix} -\mathbf{E} & \mathbf{D} \end{bmatrix} \begin{Bmatrix} \mathbf{f} \\ \mathbf{u}_c \end{Bmatrix} = \begin{bmatrix} -\bar{\mathbf{D}} & \bar{\mathbf{E}} \end{bmatrix} \begin{Bmatrix} \bar{\mathbf{u}}_c \\ \bar{\mathbf{f}} \end{Bmatrix} + \mathbf{F}\mathbf{b} \quad (5.70)$$

Once it is ascertained the boundary nodal unknown values, \mathbf{u}_c and \mathbf{f} , the displacement values connected to the finite element mesh in domain are figured out by the Equation 4.105 rewritten below

$$\mathbf{u}_D = \mathbf{G}^{CP} \mathbf{f} + \mathbf{G}^{DP} \mathbf{b} \quad (5.71)$$

The MLGFM demands the same treatment as FEM when aiming to determine the reaction forces in domain, i.e., it is necessary to calculate the nodal displacement derivatives and, by using the constitutive relationship, the internal

reaction forces can be found out. There is an unavoidable loss of precision when calculating the derivatives even for the MLGFM. But this loss of precision is substantial lower whereas the enriched approach is used.

One important point that deserves to be highlighted is despite the high nodal precision values delivered by the MLGFM, the internal reaction forces can be improved using the sub-region technique suggested by Barbieri (1992). By means of this process, each sub-region corresponds to a “Green’s cell”, i.e., each boundary value of the Green’s cell are the result in domain of the original problem. Hence, the internal reaction forces can be calculated with the same precision as the boundary values of the problem (MENDONÇA, 1995). But, in this work, the sub-region approach is not used and the “Green’s cell” is applied to the whole domain.

For the case of the stresses σ_x , σ_y and σ_{xy} , it is possible to utilize two alternatives. If the sought point is on boundary, the reaction forces are known with high precision. Inverting the elasticity matrix $\mathbf{D} = D_{ijkl}$, one calculates the strain values without loss of precision instead of calculating by the derivative operation. Once the values of the strain are known, the stress values can be figured out using the constitutive relationship. So, the MLGFM can determine stress values with high precision, without using derivative operation.

On the other hand, if the sought point is in domain, it is necessary to use the nodal displacement derivatives in order to obtain strain values and by using the constitutive relationship, the stress values are determined. This is the same process utilized by FEM causing an unavoidable loss of precision as mentioned before. But these results are improved with the enrichment approach.

Now, with all mathematical concepts and the EMLGFM methodology settled down, we are in place to apply it into some solid mechanics applications. This is exactly the topic of the next chapter.

Chapter 6

Enriched Modified Local Green's Function Method Applications for Elasto Static Problems

6.1 INTRODUCTION

In this chapter, the first employment of the Enriched Modified Local Green's Function Method (EMLGFM) is developed and implemented in several examples. It is introduced some general aspects in order to organize certain information like: the type of elements, number of degrees of freedom, Gauss points, specified constraints and numerical platforms (pre- and pos-processing) used in each example. Each application is individually presented and their results are exposed and discussed in its each section. The main objective here is to test and prove the efficiency of this new method. The MLGFM has been successfully used for a long time and the idea of enriching the domain and/or the boundary shape functions space has never been applied up to now. This is the novelty of this work! In order to test it, six different applications have been proposed: a straight cantilever beam, a curved cantilever beam, a thick-walled cylinder, a rectangular plate with a center hole, a rectangular plate with a center crack and an L-shaped domain with a singularity. In each section of the

application, the studied problem is better detailed: their numerical approximation, assumptions and different kind of results. In all applications are visualized excellent numerical results and the great potential of this new technique.

6.2 APPLICATIONS, RESULTS AND DISCUSSIONS

This section presents the first applications of the Enriched Modified Local Green's Function Method (named in this work as "EMLGFM") for a diversity of Elasto Static problems. The main goal of these problems is to verify the efficiency and accuracy of the EMLGFM. Again, it is important to highlight that all applications were held considering only one "Green's cell" for the whole domain (a unicell-multielement approach). The number of finite elements and consequently the boundary elements varies according to the proposed study and play an essential role on the convergence process. In this work, it has been considered a 4-node bilinear quadrilateral element in domain and a 2-node linear element on boundary applied to plane stress and strain problems, with 2 degrees of freedom ($ngln = 2$), i.e., degrees of freedom related to the displacement in "x" and "y" directions. A hierarchical enrichment methodology (HFEM) was adopted using Lobatto shape functions (ŠOLÍN *et al.*, 2004) and its concept extended for GFEM (BABUŠKA; MELENK, 1997).

It is used three different approaches for the first and second application: the domain/boundary enrichment, the domain only enrichment and the boundary only enrichment (3 ways of enriching the MLGFM). For the remaining ones, only one approach is used: the domain/boundary enrichment. There is not any selective process to define which element deserves to be enriched: all elements are enriched in every application. The loading types, boundary conditions, element meshing, geometries and properties are differently given in each application and they are described in each one of them. Double nodes are included into normal discontinuity points (mainly at corners for proposed

examples) and it is shown in each application. The same double-node technique was employed in Barbieri (1992) and Machado (1992) works.

The results from the EMLGFM are compared to the conventional MLGFM using a 4-node bilinear quadrilateral element in domain and a 2-node linear element on boundary, the conventional MLGFM using a 9-node biquadratic quadrilateral element in domain and a 3-node quadratic element on boundary (Figure 6.1), the standard FEM and the analytical solutions. In the case of FEM, a 4-node 2D bilinear quadrilateral is considered. The discretization, results pre- and post-processing are performed by Creo Simulate 2.0[©] in this case (for classic FEM). For MLGFM and EMLGFM, it is used the FORTRAN platform (Fortran PowerStation 4.0[©]).

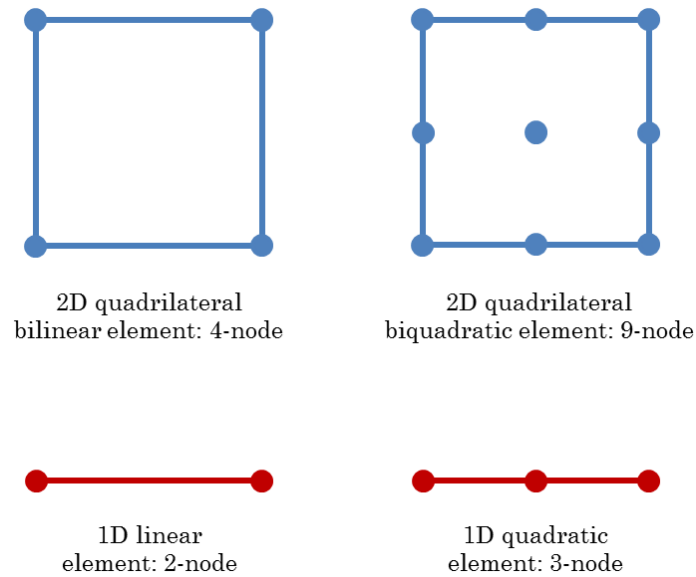





Figure 6.1 – Type of elements used in this work: 2D bilinear and biquadratic as well as 1D linear and quadratic elements.

The boundary conditions are specified in each degree of freedom for the EMLGFM where the value “0” means constraint and “1” means freedom. Remember that when specifying the boundary conditions, they can be prescribed displacement (essential boundary condition) or prescribed generalized forces (natural boundary conditions). For field degrees of freedom generated by enrichment process, they are automatically set null on boundary conditions. The

load distribution rules (applied nodal loads) are the same as described by MacNeal and Harder (1985). Note that the proper way to apply free end load depends on element type. Constraints definition, including their symbols, can be seen in Table 6.1.

Table 6.1 – Boundary conditions: constraint symbols and degree of freedom definition.

BOUNDARY CONDITION	SYMBOL	u_x	u_y
Completely constrained		0	0
Free displacement in the "x" direction		1	0
Free displacement in the "y" direction		0	1

The value of coefficients k_i used in all applications is 1.0^{+10} , remembering these coefficients are included into MLGFM matrix $[K']$ (boundary operator \mathcal{N}').

The numerical integration is a very important aspect when using an enrichment approach specially when increasing the order or level of enrichment. In order to proper compare to the applications and eliminate the numerical integration variable in approximate results, all numerical solutions were calculated with 16 Gauss points in each coordinate direction except by the first straight and curved beam experiments with Lobatto shape functions up to $p = 2$ polynomial order and selective reduced integration (SRI) approach (ZIENKIEWICZ *et al.*, 1971) – better detailed in next two application sections. The minimum number of quadrature points for the Gauss quadrature over quadrilaterals was suggested by Šolín *et al.* (2004) and the minimum number would be 8 for $p = 5$. Here, this value was purposely duplicated. The choice in applying a higher Gauss quadrature is based on the difficulty of the enrichment approach to capture and approximate with accurate precision the shape function values when using lower Gauss point values (STROUBOULIS *et al.*, 2000). This aspect is intensified for non-polynomial shape functions (BARROS, 2002) that is the case of the two last applications where GFEM approach is tested with

MLGFM.

Summarizing then Gauss quadrature points: for the first tests performed in straight and curved beam with $p = 2$, the integration is carried out with 3 Gauss points in each coordinate direction (SRI is an exception case that will be better discussed in next application section, as earlier mentioned). The choice of using only $p = 2$ for these first studies are based on to first check the differences among the following enrichment approaches: domain/boundary, only domain and only boundary. For all other results investigated in next sections, it is used 16 Gauss points in each coordinate direction, i.e., 16 x 16 Gauss quadrature in 2D elements and 16 Gauss quadrature in 1D elements. Only for the last application, a Gauss quadrature points study was also performed, varying the number of points. It was used 3, 16, 48 and 96 Gauss quadrature points in each coordinate direction and concluded a great disturbance only for 3 points for polynomial order above $p = 3$ (and level of enrichment above $le = 2$).

6.2.1 Straight Cantilever Beam

The tensile and bending tests for beams proposed MacNeal and Harder (1985) are taken as reference here in this section. The main goal of these problems is to verify the efficiency of the 2D elements related to the distortion and aspect ratio. The straight cantilever beam is considered in a state of plane stress. The geometric properties are shown for both cases – extension and bending cases – in Figure 6.2.

The solution to the simple case under axial loading (named here as case 1: extension) is well-known and derived from the Hooke's Law

$$\sigma_x = E\varepsilon_x, \quad (6.1)$$

$$\varepsilon_x = \frac{\partial u_x}{\partial x}, \quad (6.2)$$

$$u_x = \int_0^L \frac{P(x)}{A(x)E} dx \quad (6.3)$$

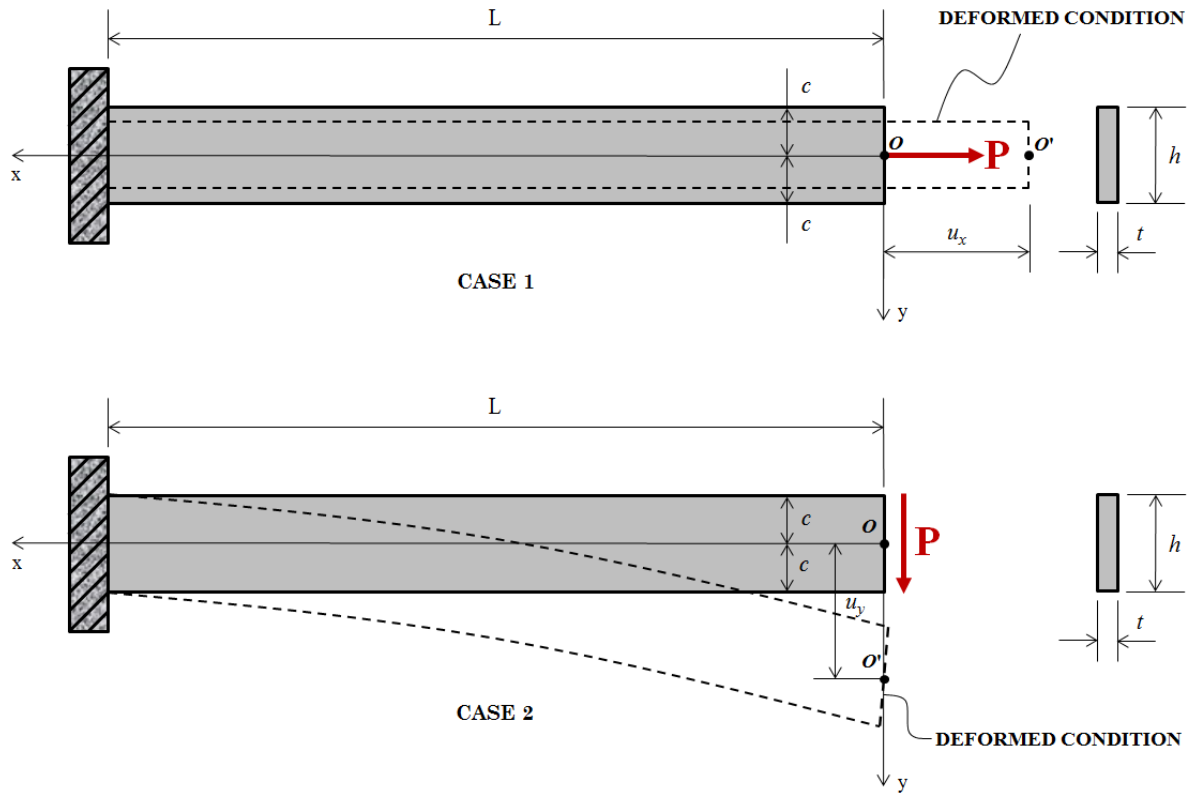


Figure 6.2 – The straight cantilever beam: geometric properties.

For the case where the cross-sectional area and axial load are assumed to be constant, we can rewrite the last equation as

$$u_x = \frac{PL}{AE} \quad (6.4)$$

where “P” is the load, “L” is the length of the bar, “A” is the cross-sectional area and “E” is the elastic modulus.

The solution to the bending problem (named here as case 2: bending) is given in Timoshenko and Goodier (1951) based on use of a stress function solution. The solution for stresses is given by

$$\sigma_x = -\frac{3}{2} \frac{Pxy}{c^3}, \quad (6.5)$$

$$\sigma_y = 0, \quad (6.6)$$

$$\sigma_{xy} = -\frac{3P}{4c} \left[1 - \left(\frac{y}{c} \right)^2 \right] \quad (6.7)$$

where “P” is the applied load and “c” the half-width (height) of the beam.

The solution for displacements under boundary conditions $u_x(L,0) = u_y(L,0) = 0$ and $u_x(L,c) = u_x(L,-c) = 0$ are given by

$$u_x = -\frac{Py(x^2 - L^2)}{2EI} - \frac{\nu Py(y^2 - c^2)}{6EI} + \frac{Py(y^2 - c^2)}{6GI}, \quad (6.8)$$

$$u_y = -\frac{\nu Pxy^2}{2EI} + \frac{P(x^3 - L^3)}{6EI} - \left(\frac{PL^2}{2EI} + \frac{\nu Pc^2}{6EI} + \frac{Pc^2}{3GI} \right) (x - L). \quad (6.9)$$

In the above “E” and “ν” are the elastic modulus and Poisson ratio, “G” is the shear modulus given by $E / [2(1 + \nu)]$ and “I” is the area moment of inertia which is equal to $2tc^3 / 3$ where “t” is a constant beam thickness.

For this solution (case 2), the tractions on the boundaries become (forces on boundary condition)

$$\begin{Bmatrix} T_x \\ T_y \end{Bmatrix} = t \begin{Bmatrix} 0 \\ -\sigma_{xy} \end{Bmatrix} \quad \text{for } x = 0; \quad -c \leq y \leq c, \quad (6.10)$$

$$\begin{Bmatrix} T_x \\ T_y \end{Bmatrix} = t \begin{Bmatrix} \sigma_x \\ \sigma_{xy} \end{Bmatrix} \quad \text{for } x = L; \quad -c \leq y \leq c. \quad (6.11)$$

For the numerical solutions, it is used two meshes: one in domain and another one on boundary, utilizing double node at normal discontinuity as we can see in Figure 6.3.

For each problem, it is chosen the geometry, material properties, boundary conditions, loading, and element meshing shown in Figure 6.4 for FEM solutions. As seen in this figure, case 1 and case 2 are associated to tensile and shear loading, respectively.

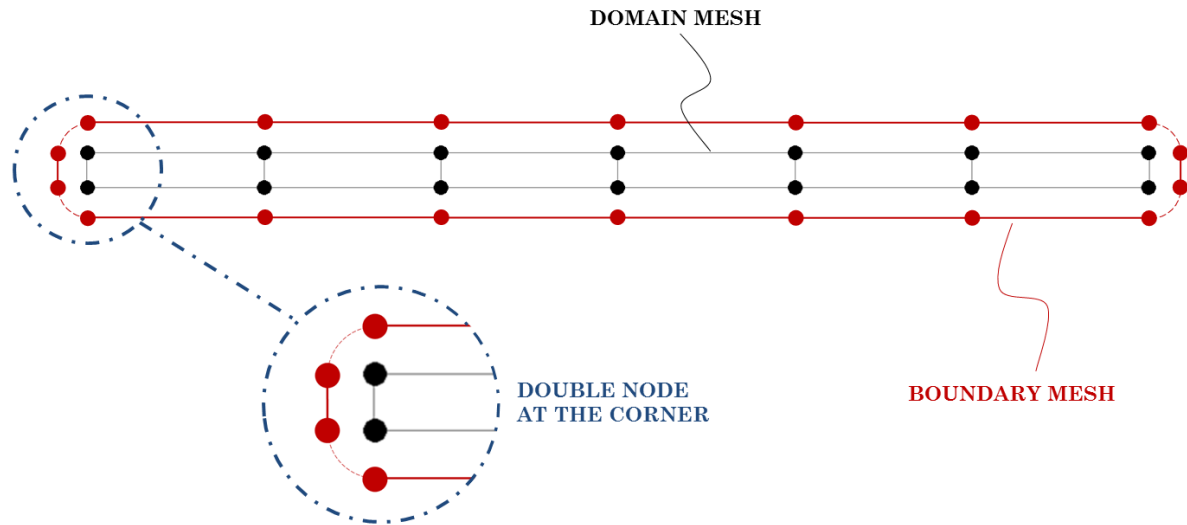


Figure 6.3 – Domain and boundary meshes for straight cantilever beam. Double node considered at corners.

Problem (a) utilizes a regular mesh and problems (b) and (c) use distorted meshes (a trapezoidal and a parallelogram one). In these results, it is used Lobatto shape functions with order $p = 2$ only and the integration is carried out with 3 Gauss points in each direction except by Selective Reduced Integration (SRI) that is better detailed further in this session. The choice of using only $p = 2$ for these studies is based on to first check the differences among the following enrichment approaches: domain and boundary, domain only and boundary only. For all other results investigated in this section (with polynomial order up to $p = 5$), it is used 16 Gauss points in each direction. Since the results are compared against the analytical and classic FEM solutions given by MacNeal and Harder (1985), displacements at point “O” (see Figure 6.2) are computed.

An important aspect of the results is the well-known locking behavior caused by the 2D quadrilateral element (ZIENKIEWICZ *et al.*, 1971). This inherent deficiency of low-order, displacement-assumed plane stress elements was quickly noticed in late 1960s when applied to problems in which in-plane bending was dominant (DOHERTY *et al.*, 1969). Those elements absorbed parasitic shear energy, resulting in over stiffness. The phenomenon was given the name “*shear locking*”. That effect is magnified when the element aspect ratio

becomes larger. As a result, the computed deflections (and associated stresses) could be too small by orders of magnitude, leading to unsafe designs.

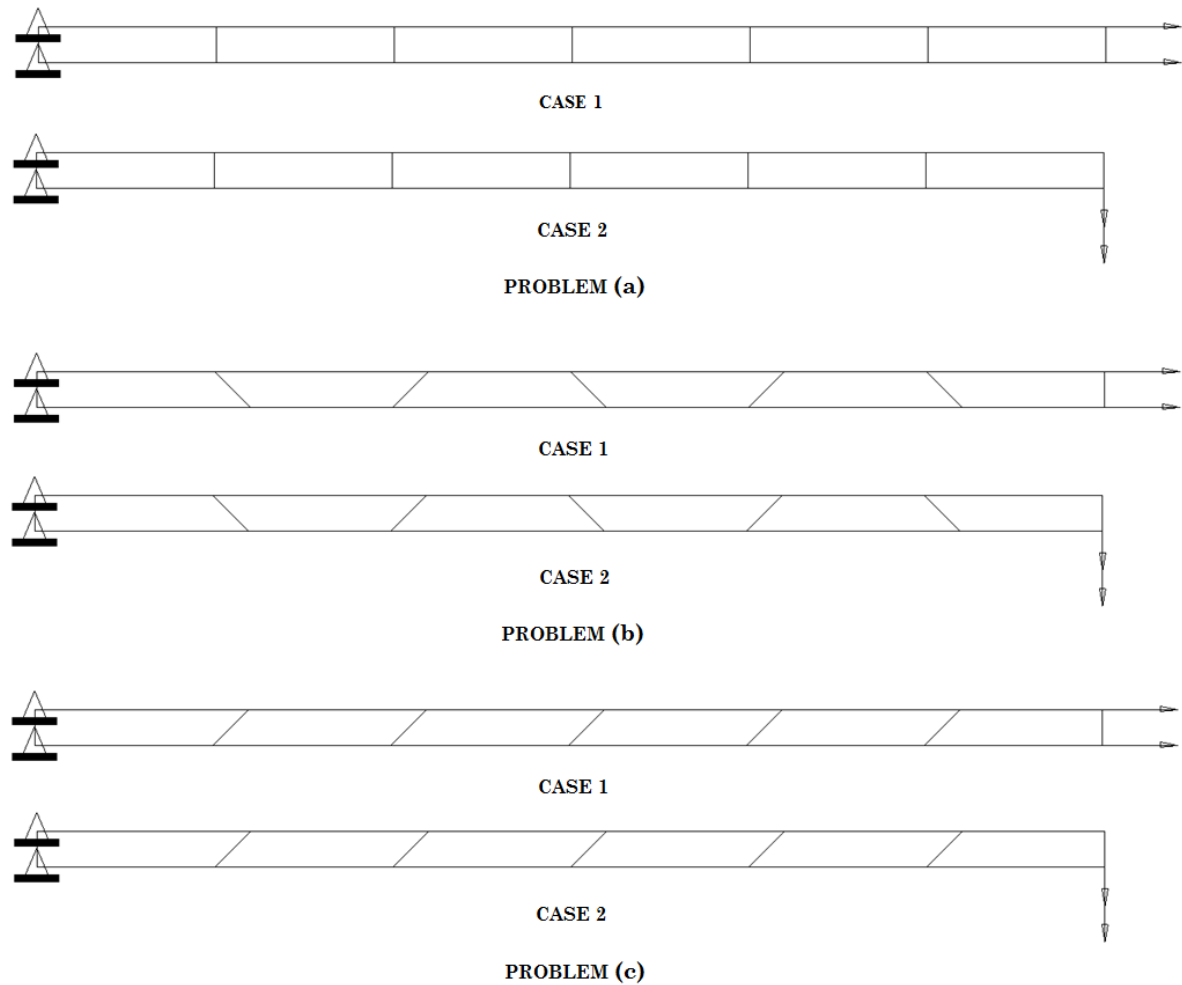


Figure 6.4 – Straight cantilever beam: problem (a) - regular shape elements; problem (b) - trapezoidal shape elements; problem (c) - parallelogram shape elements. Length = 6.0; width (height) = 0.2; depth (thickness) = 0.1; $E = 1.0 \times 10^7$; $\nu = 0.30$; mesh = 6 x 1. Loading: unit forces at free end (tip). Constraint: fixed support.

There are several approaches to alleviate shear locking found in literature but here it is used the modified gauss integration rules and, more specifically, the Selective Reduced Integration (SRI). In this approach, to prevent shear locking, the part of the stiffness matrix associated to shear strain energy has to be evaluated at a single Gauss point as the rest can be dealt with by a full integration scheme. Doing so, the rank (the maximum number of linearly

independent row or column of a matrix) of the stiffness tensor remains full, also preventing spurious zero-energy modes.

So, splitting the plane stress elasticity matrix \mathbf{D} into two parts: a normal strain part \mathbf{D}_ε and a shear strain part \mathbf{D}_γ , we write

$$\mathbf{D} = \begin{bmatrix} D_{11} & D_{12} & 0 \\ D_{21} & D_{22} & 0 \\ 0 & 0 & D_{33} \end{bmatrix} = \begin{bmatrix} D_{11} & D_{12} & 0 \\ D_{21} & D_{22} & 0 \\ 0 & 0 & 0 \end{bmatrix} + \begin{bmatrix} 0 & 0 & 0 \\ 0 & 0 & 0 \\ 0 & 0 & D_{33} \end{bmatrix} = \mathbf{D}_\varepsilon + \mathbf{D}_\gamma \quad (6.12)$$

Thus, the stiffness matrix \mathbf{K} may also be split into a normal strain \mathbf{K}_ε and a shear strain part \mathbf{K}_γ :

$$\mathbf{K} = \int_{\Omega} \mathbf{B}^T \mathbf{D} \mathbf{B} d\Omega = \int_{\Omega} \mathbf{B}^T \mathbf{D}_\varepsilon \mathbf{B} d\Omega + \int_{\Omega} \mathbf{B}^T \mathbf{D}_\gamma \mathbf{B} d\Omega = \mathbf{K}_\varepsilon + \mathbf{K}_\gamma \quad (6.13)$$

where \mathbf{B} is the strain-displacement matrix and \mathbf{D} is the elasticity matrix.

Spurious shear strain terms that appear in the stiffness matrix of the four-node quadrilateral are eliminated by integrating \mathbf{K}_γ using one Gauss point which is located at the element center, while the normal strain contribution is integrated by a 2 x 2 Gauss rule (full integration).

The results displayed in Table 6.2 and Table 6.3 are taken at end of the beam where the maximum displacement occurs as shown in Figure 6.5.

The normalized displacement is taken, for instance in case 2, as $[(u_y)_h / u_y]$ where “ $(u_y)_h$ ” is the displacement of the approximate solution and “ u_y ” is the displacement of the exact solution in “y” direction.

As we can see in displacements results (Table 6.2) and normalized displacement results (Table 6.3), for straight beam at tensile load (extension – case 1), the results presented good approximation compared to the analytical solution even with irregular elements shape – problems (b) and (c). Anyway, it is important to highlight that there is no significant variation among the problems (a), (b) and (c) for all enriched approaches (domain/boundary, only domain and

only boundary). Another important point that deserves to be highlighted is the boundary condition used in MacNeal and Harder (1985) for this test: it is completely clamped in one end of the beam. This assumption avoids Poisson's effect in "y" direction and it can be overcome constraining only one node in both directions and other nodes only in "x" direction. Doing so, the values for case 1 is 100% precise, i.e., no error as seen in Zienkiewicz *et al.* (2005).

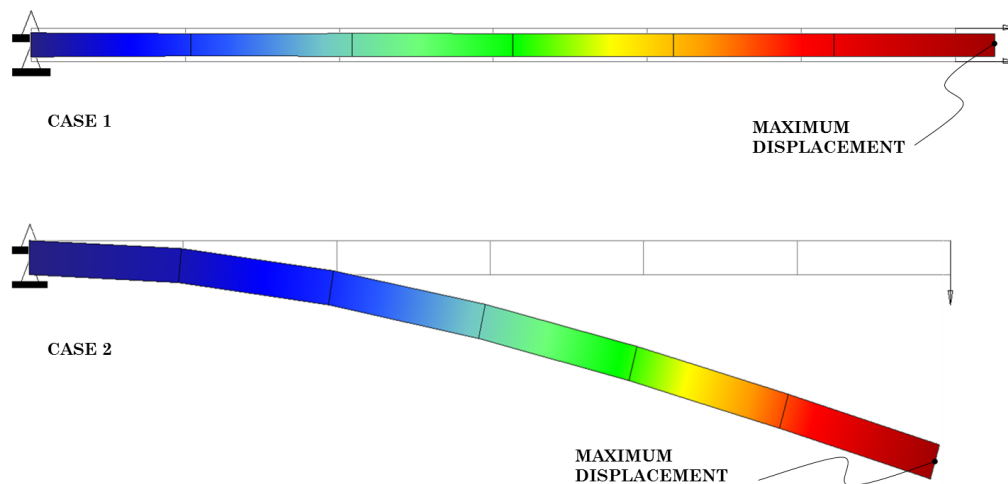


Figure 6.5 – Maximum displacement for cases 1 and 2 due to forces at free end.

On the other hand, for bending load problems (in-plane shear – case 2) applied for straight beam, the results presented a very low variation with domain/boundary enrichment among problems (a), (b) and (c). It is also interesting to notice that the boundary only enrichment approach showed results very close to the conventional 4-node MLGFM. When compared to the plate elements tested by MacNeal and Harder (1985), the results are much better despite the great disturbance visualized for the conventional 4-node MLGFM element (without using SRI). Therefore, the boundary only enrichment approach presents low accuracy for shear problems. Better results are provided by the domain only enrichment approach. However, the EMLGFM reaches the best performance when the domain and boundary enrichment approach is employed. This is an interesting conclusion since the Green's function projections (GFp) are

calculated by FEM procedures, demonstrating it is not enough to enrich only the boundary mesh.

Table 6.2 – Displacements results and analytical solution for straight cantilever beam.

DISPLACEMENT IN DIRECTION OF LOAD FOR STRAIGHT BEAM						
PROBLEM AND TYPE OF ELEMENT				PROBLEM (a): REGULAR	PROBLEM (b): TRAPEZOIDAL	PROBLEM (c): PARALLELLOGRAM
CASE TYPE				CASE 1	CASE 1	CASE 1
TIP LOAD				EXTENSION	EXTENSION	EXTENSION
SOLUTION	ANALYTICAL*			3.00000E-05		
	FEM (QUAD4)*	4-node	p=1	2.98500E-05	2.98800E-05	2.98800E-05
	MLGFM	4-node	p=1	2.98630E-05	2.99270E-05	2.99180E-05
		4-node SRI		2.98640E-05	2.99780E-05	2.99800E-05
		9-node		p=2	2.99430E-05	3.03380E-05
	HFEM EMLGFM 4-node	Domain/ Boundary	p=2	2.99250E-05	2.99170E-05	2.99250E-05
		Only Domain		3.06140E-05	3.06380E-05	3.06140E-05
		Only Boundary		2.98630E-05	2.98390E-05	2.98630E-05

PROBLEM AND TYPE OF ELEMENT				PROBLEM (a): REGULAR	PROBLEM (b): TRAPEZOIDAL	PROBLEM (c): PARALLELLOGRAM
CASE TYPE				CASE 2	CASE 2	CASE 2
TIP LOAD				IN-PLANE SHEAR	IN-PLANE SHEAR	IN-PLANE SHEAR
SOLUTION	ANALYTICAL*			-1.08100E-01		
	FEM (QUAD4)*	4-node	p=1	-9.77220E-02	-7.67510E-03	-8.64800E-03
	MLGFM	4-node	p=1	-1.00880E-02	-2.68600E-03	-3.42740E-03
		4-node SRI		-9.76760E-02	-7.59160E-03	-8.60990E-03
		9-node		p=2	-1.07030E-01	-1.06020E-01
	HFEM EMLGFM 4-node	Domain/ Boundary	p=2	-1.07550E-01	-1.07470E-01	-1.07550E-01
		Only Domain		-1.07550E-01	-1.07460E-01	-1.07550E-01
		Only Boundary		-1.00880E-02	-9.40110E-03	-1.00880E-02

* MacNeal and Harder, 1985.

Table 6.3 – Normalized tip displacements results in direction of load.

NORMALIZED DISPLACEMENT FOR STRAIGHT BEAM							
PROBLEM AND TYPE OF ELEMENT				PROBLEM (a): REGULAR	PROBLEM (b): TRAPEZOIDAL	PROBLEM (c): PARALLELLOGRAM	
CASE TYPE				CASE 1	CASE 1	CASE 1	
TIP LOAD				EXTENSION	EXTENSION	EXTENSION	
SOLUTION	FEM (QUAD4)*	4-node	$p=1$	0.99500	0.99600	0.99600	
	MLGFM	4-node		0.99543	0.99757	0.99727	
		4-node	$p=1$	0.99546	0.99926	0.99934	
		SRI		0.99810	1.01127	1.01043	
	HFEM EMLGFM 4-node	9-node	$p=2$	0.99749	0.99724	0.99749	
		Domain/ Boundary		1.02048	1.02127	1.02048	
		Only Domain	$p=2$	0.99543	0.99465	0.99543	
Only Boundary							

PROBLEM AND TYPE OF ELEMENT				PROBLEM (a): REGULAR	PROBLEM (b): TRAPEZOIDAL	PROBLEM (c): PARALLELLOGRAM	
CASE TYPE				CASE 2	CASE 2	CASE 2	
TIP LOAD				IN-PLANE SHEAR	IN-PLANE SHEAR	IN-PLANE SHEAR	
SOLUTION	FEM (QUAD4)*	4-node	$p=1$	0.90400	0.07100	0.08000	
	MLGFM	4-node		0.09341	0.02487	0.03174	
		4-node	$p=1$	0.90440	0.07027	0.07970	
		SRI		0.99102	0.98167	0.98185	
	HFEM EMLGFM 4-node	9-node	$p=2$	0.99541	0.99413	0.99494	
		Domain/ Boundary		0.99488	0.99406	0.99488	
		Only Domain	$p=2$	0.09332	0.08697	0.09332	
Only Boundary							

A series of analysis has been run with different length-to-height ratio (L/h) considering the loading case type 2 and regular mesh in order to test the shear locking effect due to the element aspect ratio (the ratio of the element longest to smallest dimension), mentioned earlier in this section. The L/h values tested in these analysis vary from $L/h = 5$ to $L/h = 1000$ and results are

expressed both for displacements and stresses in error percentage as shown in Table 6.4 and Table 6.5.

The percentage error here is defined as $(|(u_y)_h - u_y| / u_y) * 100\%$ where “ $(u_y)_h$ ” is the displacement of the approximate solution and “ u_y ” is the displacement of the analytical solution in “y” direction. The stress error measurement follows the same pattern just replacing the displacement variable by stress variable, such as: $(|\sigma_h - \sigma| / \sigma) * 100\%$. The model is discretized with 6 elements and 16 Gauss points in each direction. The results are given for conventional MLGFM with 4 nodes and 9 nodes comparing to the EMLGFM with the polynomial order from $p = 2$ to $p = 5$.

Table 6.4 – Displacement error (%) for different L/h aspect ratio.

DISPLACEMENT (u_y) ERROR (%) IN DIRECTION OF LOAD						
6 ELEM	MLGFM		ENRICHED MLGFM			
	4-node	9-node	4-node			
L/h	$p=1$		$p=2$	$p=3$	$p=4$	$p=5$
5	26.97991%	1.20054%	0.32409%	3.22149%	4.08185%	5.91757%
30	90.66735%	0.98396%	0.54545%	0.03923%	0.21407%	0.23628%
100	99.07348%	1.18271%	0.71999%	0.05955%	0.02905%	0.00430%
1000	99.99064%	1.26258%	0.75258%	0.07583%	0.06933%	0.03808%

Table 6.5 – Stress error (%) for different L/h aspect ratio.

NORMAL STRESS (σ_x) ERROR MEASURED ON BOUNDARY (%)						
6 ELEM	MLGFM		ENRICHED MLGFM			
	4-node	9-node	4-node			
L/h	$p=1$		$p=2$	$p=3$	$p=4$	$p=5$
5	92.34207%	0.00000%	0.00000%	0.00000%	0.00000%	0.00000%
30	90.23669%	0.00000%	0.00000%	0.00000%	0.00000%	0.00000%
100	99.30848%	0.00000%	0.00000%	0.00000%	0.00000%	0.00000%
1000	99.02098%	0.06000%	0.00500%	0.00500%	0.00500%	0.00500%

It is observed the great accuracy of the EMLGFM both for displacement and even more for stress results. An important aspect to note here is that the

EMLGM inherits the excellent results for flux variables from MLGFM. In this case, the flux variable is the stress.

Another important assessment of the overall quality of the approximate solution is the measure of the error in energy norm. When comparing alternative approaches in numerical methods, the error versus the number of degrees of freedom relationship is of interest (and consequently the computational cost), with the error measured in terms of displacements, stresses, stress resultants at specific points, or in terms of energy. It is usual to measure the error in energy norm versus the total number of degrees of freedom (NDOF) as basis for comparison and we shall be concerned with the rate of change of the error in energy with respects those NDOF.

The NDOF can be increased in various ways: uniform mesh refinement (h -refinement), uniform change in polynomial order (p -refinement) or both refinements at the same time (hp -refinement). For the problem studied here, the straight cantilever beam is uniformly refined for the standard FEM and MLGFM characterizing an NDOF increase by an h -refinement (Figure 6.6) but the NDOF for EMLGFM is increased by increasing the hierarchical polynomial order using Lobatto shape functions. Performing such meshes, considering the loading case type 2, it is possible to plot the convergence path as is shown in Figure 6.7. The convergence path is plotted in $\log(e_r)_E$ versus $\log(\text{NDOF})$ curve.

The relative error in energy norm $(e_r)_E$ is defined according to Szabó (1986) as follows

$$(e_r)_E = \sqrt{\frac{|U(\mathbf{u}) - U(\mathbf{u}_h)|}{U(\mathbf{u})}} \quad (6.14)$$

where $U(\mathbf{u})$ is the strain energy of the exact solution and $U(\mathbf{u}_h)$ is the strain energy of the approximate solution.

Numerical strain energy in a displacement formulation can be expressed by (ZIENKIEWICZ *et al.*, 2005)

$$U(\mathbf{u}_a) = \frac{1}{2} \mathbf{u}_a^T \mathbf{K} \mathbf{u}_a \quad (6.15)$$

where the exact value used in this work is found as $U(\mathbf{u}) = 2.000156$.

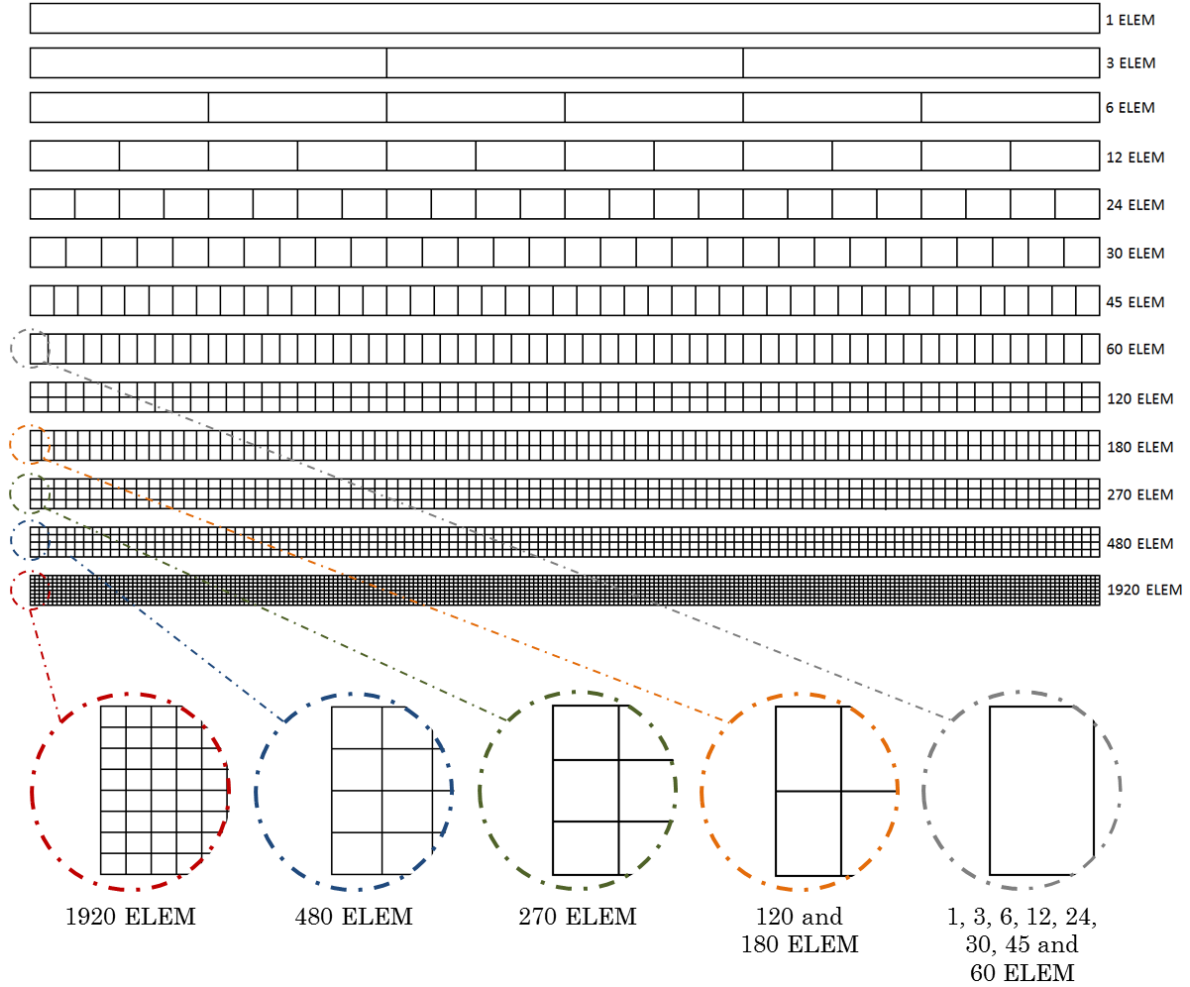


Figure 6.6 – Domain meshes and geometries for different number of elements.

The rate of convergence for 4-node quadrilateral is so slow that is not feasible to control the error of the approximation for lower NDOF values. But using SRI in conventional MLGFM (Selective Reduced Integration) there's clearly an improvement of the results. It is indeed interesting to observe the convergence rate for both 4-node (including the SRI) and 9-node in conventional MLGFM: they have nearly the same curve slope although the error is smaller for

9-node in higher NDOF values. Also note that the 9-node element has not been treated for shear locking. The EMLGFM presents a faster rate of convergence reaching smaller error in energy norm for lower NDOF values than the classic FEM and conventional MLGFM. The slopes of the curves are found as 0.20115 for FEM, 0.20115 for MLGFM 4-node, 0.37268 for MLGFM 4-node using SRI, 0.78242 for MLGFM 9-node and 2.06605 for enriched MLGFM (EMLGFM). The rate of convergence for EMLGFM is 10.27147 times faster than classic FEM.

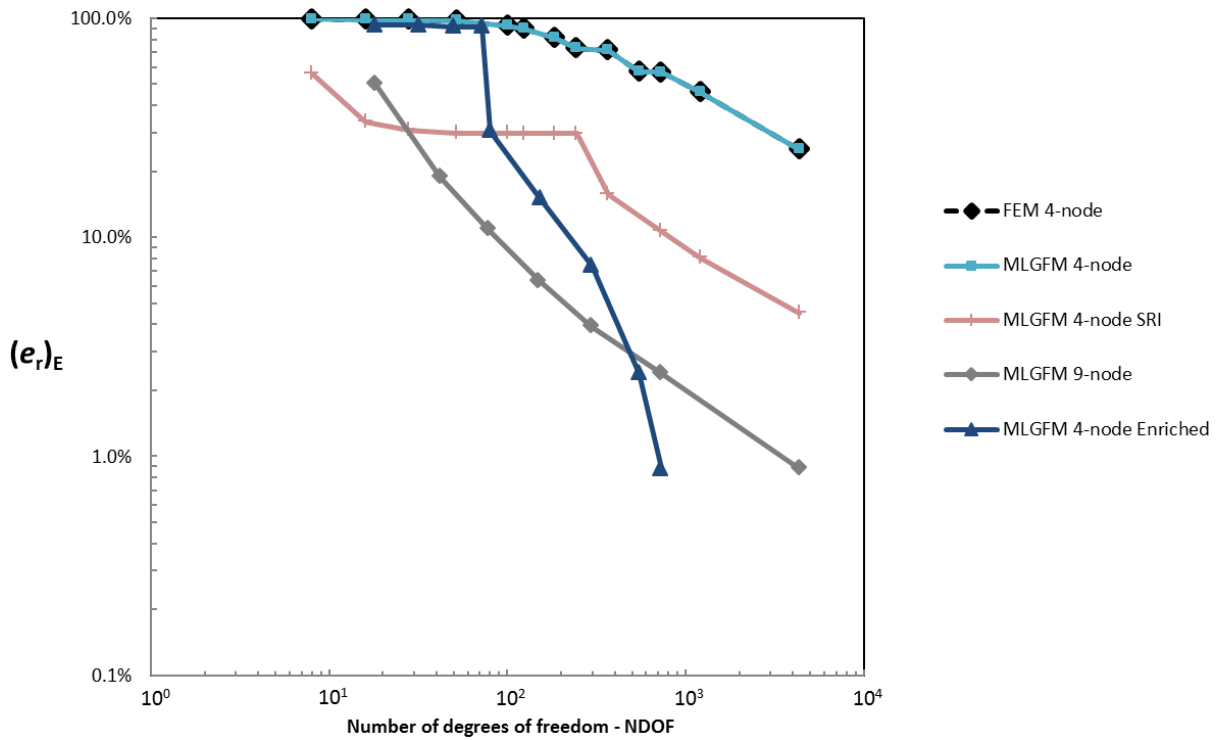


Figure 6.7 – Error in energy norm $(e_r)_E$ for different Degrees of Freedom - DOF (logarithmic scale).

When it comes to the computational cost aspects, the EMLGFM and its predecessor the MLGFM need to figure out firstly Green's function projections in order to compute displacement's solution. So, the computational cost might be increased if this process is singly considered when comparing to other methods, e.g., FEM and BEM. But, the EMLGFM is deemed to be a coarse mesh method, reaching high value precision with relative low degrees of freedom. Anyway, as shown in Table 6.6, the conventional MLGFM, solved with 4-node element,

presents a lower computational cost compared to FEM and same level of solution error. But this is different for the solution by MLGFM 9-node and EMLGFM 4-node where there is an increase of elapsed calculation time but in contrast the precision is significantly higher.

Table 6.6 – Computational cost evaluation versus displacement u_y error.

ELAPSED CALCULATION TIME (seconds) versus DISPLACEMENT u_y ERROR (%)						
Solution Type		Number of Elements: 6 ELEM 12 ELEM 24 ELEM 60 ELEM				
FEM	4-node	Elapsed Time (s)	0.330	0.340	0.340	0.350
MLGFM	4-node	Elapsed Time (s)	0.094	0.109	0.218	0.349
	9-node	Elapsed Time (s)	0.250	0.640	5.160	45.000
HFEM EMLGFM 4-node	$p=2$	Elapsed Time (s)	0.156	0.250	0.874	13.000
	$p=2$ without \mathbf{G}^{DP}	Elapsed Time (s)	0.156	0.218	0.577	8.471
	Time Reduction without \mathbf{G}^{DP} (%)		0,000%	12.800%	33.982%	34.838%
FEM	4-node	Displacement Error (%)	99.074%	96.404%	87.140%	53.859%
MLGFM	4-node	Displacement Error (%)	99.073%	96.404%	87.140%	53.860%
	9-node	Displacement Error (%)	1.183%	0.415%	0.175%	0.078%
HFEM EMLGFM 4-node	$p=2$	Displacement Error (%)	0.720%	0.166%	0.032%	0.003%

If we disregard Green's function projections (\mathbf{GF}_p) figured out in domain (\mathbf{G}^{DP}), the computational cost sharply decreases. In this example, it is possible to do that due to the absence of body forces. Comparing the EMLGFM $p = 2$ without \mathbf{G}^{DP} (Green's projections calculated in domain) against the EMLGFM $p = 2$ with \mathbf{G}^{DP} (in this example, projections related to body forces are zero as previously

mentioned), we have a reduction of computational cost of 12.800% for 12 elements, 33.982% for 24 elements and 34.839% for 60 elements. And we have 0.000% for 6 elements.

A very important property of a numerical solution that measures an ill-conditioning of a matrix $[K]$ is known as the “*condition number*”, denoted here by $\text{cond}(K)$. The condition number of a matrix measures the sensitivity of the solution of a system of linear equations to errors in the data. It gives an indication of the accuracy of the results from matrix inversion and the linear equation solution. Values of $\text{cond}(K)$ near 1 indicate a well-conditioned matrix. A large condition number warns that a numerical solution may contain appreciable error. Bazán (2003) describes the number $\|K\| \|K^{-1}\|$ as the condition number $\text{cond}(K)$ and in the case of 2-norm condition number, it is given by the ratio of the largest singular value of K to the smallest.

This is exactly the values calculated by Matlab (MATHWORKS, 2012) and used in this work shown in Table 6.7. The values of the condition number are taken from the stiffness matrix $[K]$. There is an increase on the condition number once raising the polynomial order. But the numerical results as discussed in this section are not substantially affected by that. This aspect may not be so significant in the example explored here but it gains relevant importance in the last application especially for GFEM combined with MLGFM.

Table 6.7 – Condition number study for straight cantilever beam

CONDITION NUMBER: $\text{cond}(K)$				
Application: Problem: Case type: Number of elements:				Straight Beam Regular Case 2 6 elements
SOLUTION	MLGFM	4-node	$p=1$	1.35850E+05
			$p=2$	2.85130E+05
	HFEM	4-node	$p=3$	2.99340E+05
	EMLGFM		$p=4$	4.04610E+05
			$p=5$	4.04710E+05

Concluding this section, it is also important to highlight another aspect quite cited by Barbieri (1992) and Machado (1992) and further reinforced by Maldaner (1993): values of k_i , the components of the diagonal matrix $[K']$ whose the boundary operator \mathcal{N}' coefficients are placed, were firstly tested from $\pm 10^{-6}$ to $\pm 10^6$ and they demonstrated an insensitive characteristics for the analysis results. But the value of k_i can tightly contribute to the condition number.

This condition is exacerbated for the enriched approach as we can see on Table 6.7. Some tests changing the value of k_i from $\pm 10^{-25}$ to $\pm 10^{+25}$ were performed for EMLGFM with different polynomial orders (from $p = 2$ to $p = 5$) and the analysis results are not as insensitive as pointed out by Barbieri (1998a). The disturbance noted here may be assigned to the fact that all elements are equally enriched in the mesh both in domain and on boundary. There is no especial treatment for Dirichlet boundary condition when domain is enriched coupled to boundary conditions applied to boundary mesh or even an element selective enrichment. Only on boundary mesh, Dirichlet boundary conditions for enriched degrees of freedom are set null. Also, none preconditioner, such as the incomplete Cholesky-Conjugate Gradient Method (KERSHAW, 1978) was used in studied examples. This subject is not deeper investigated in this work and deserves to be better explored in future developments. The enrichment on the Dirichlet boundary condition can affect the EMLGFM matrices conditioning as well as the inappropriate k_i values. This subject is not deeper investigated in this work and deserves to be better explored in future developments.

6.2.2 Curved Cantilever Beam

MacNeal and Harder (1985) also proposed a curved cantilever beam application where combinations of the principal deformation modes are evoked by a single in-plane shear load at the tip. This circular beam is modeled in a state of plane stress as for straight beam. The geometric properties are shown in Figure

6.8. The solution to the problem is also given in Timoshenko and Goodier (1951) based on use of a stress function. The solution for stresses is given by

$$\sigma_r = \frac{P}{N} \left[r + \frac{a^2 b^2}{r^3} - \frac{a^2 + b^2}{r} \right] \sin \theta, \quad (6.16)$$

$$\sigma_\theta = \frac{P}{N} \left[3r - \frac{a^2 b^2}{r^3} - \frac{a^2 + b^2}{r} \right] \sin \theta, \quad (6.17)$$

$$\sigma_{r\theta} = -\frac{P}{N} \left[r + \frac{a^2 b^2}{r^3} - \frac{a^2 + b^2}{r} \right] \cos \theta \quad (6.18)$$

where $N = a^2 - b^2 + (a^2 + b^2) \log b/a$. The solution for displacements is given by

$$u_r = \frac{P}{NE} \{J \sin \theta + L \cos \theta\} - K \sin \theta, \quad (6.19)$$

$$u_\theta = \frac{P}{NE} \{M \cos \theta - N \sin \theta\} - K \cos \theta \quad (6.20)$$

where

$$\begin{aligned} J &= \frac{1}{2} (1-3\nu) r^2 - \frac{a^2 b^2 (1+\nu)}{2r^2} - (a^2 + b^2) (1-\nu) \log r, \\ L &= (a^2 + b^2) (\theta - \pi), \\ M &= \frac{1}{2} (5+\nu) r^2 - \frac{a^2 b^2 (1+\nu)}{2r^2} + (a^2 + b^2) (1-\nu) \log r - (1+\nu), \\ N &= (a^2 + b^2) (\theta - \pi) \end{aligned} \quad (6.21)$$

and where for $u_r(a, \pi/2) = 0$ we have

$$K = \frac{P}{NE} \left[\frac{1}{2} (1-3\nu) a^2 - \frac{b^2 (1+\nu)}{2} - (a^2 + b^2) (1-\nu) \log a \right]. \quad (6.22)$$

As previously described in this text, “ E ” and “ ν ” are the elastic modulus and Poisson ratio; “ a ” and “ b ” are the inner and outer radii, respectively (see Figure 6.8).

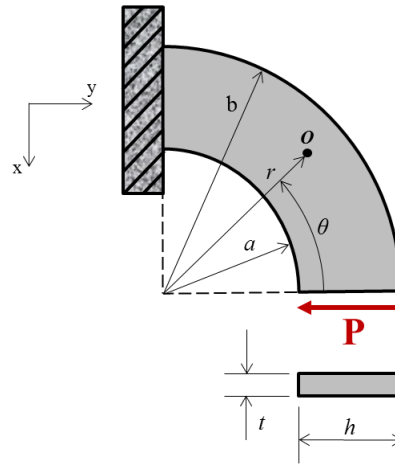


Figure 6.8 – The curved beam: geometric properties.

The radial displacement u_r for $\theta = 0$ for this solution is given by

$$u_r(r,0) = -\frac{\pi P}{EN} (a^2 + b^2) \quad (6.23)$$

As in straight beam application, it is used two meshes: one in domain and another one on boundary, utilizing double node at normal discontinuity as we can see in Figure 6.9.

For this application, the geometry, material properties, boundary conditions, loading, and element meshing are given as in Figure 6.10. Again, it is used Lobatto shape functions with order $p = 2$ only, 3 Gauss points in each direction (except by SRI, as previous described) and the results are given in terms of displacement values in order to compare to the analytical and FEM solutions given by MacNeal and Harder (1985). The bending load is applied at end of the beam where the maximum displacement occurs (Figure 6.11).

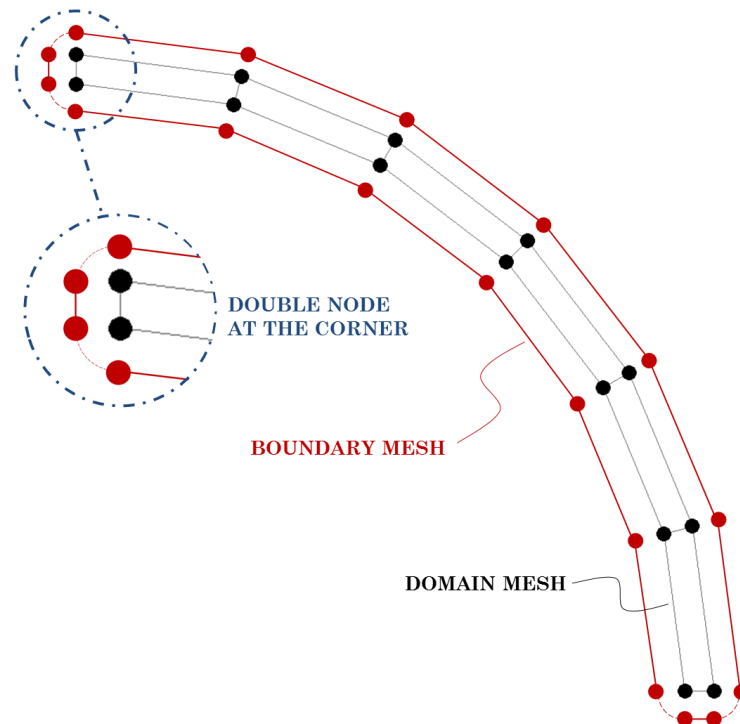


Figure 6.9 – Domain and boundary meshes for curved beam. Double node considered at corners.

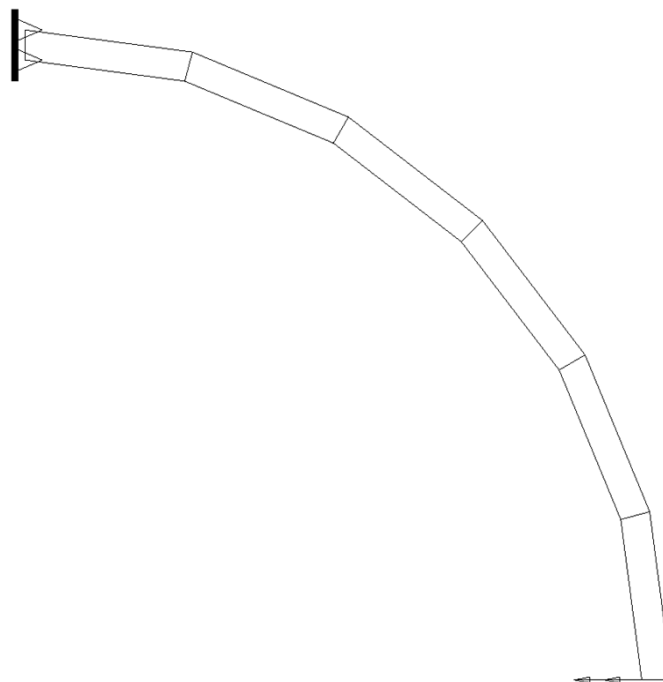


Figure 6.10– Curved beam: inner radius = 4.12; outer radius = 4.32; arc = 90°; depth (thickness) = 0.1; $E = 1.0 \times 10^7$; $\nu = 0.25$; mesh = 6 x 1. Loading: unit forces at free end (tip). Constraint: fixed support.

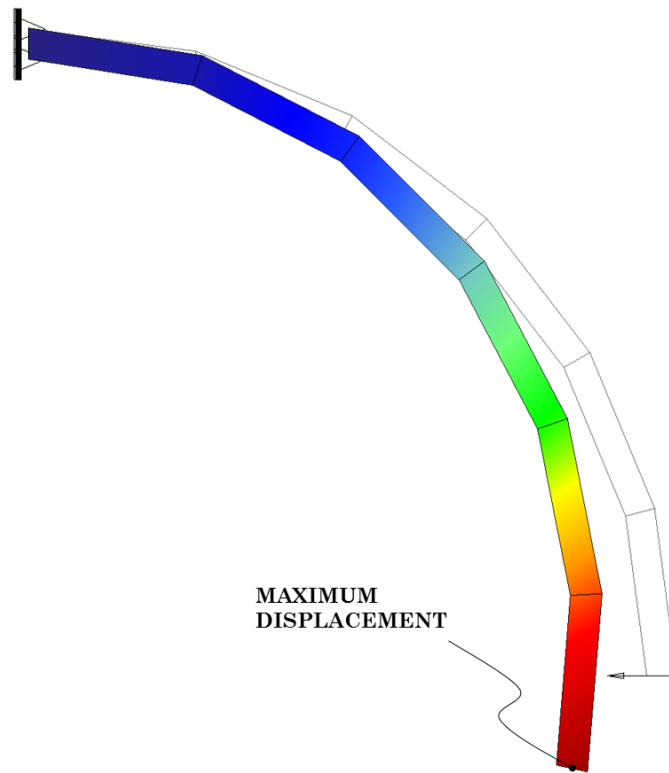


Figure 6.11– Maximum displacement for case 2 due to forces at free end.

The results for curved beam in-plane shear are shown in Table 6.8 (displacement results) and Table 6.9 (normalized displacement results).

Note also that the element shape is not quite rectangular for this application, which will test the effect of slight irregularity too. It can be seen that the EMLGFM with domain/boundary enrichment demonstrates high accuracy as well as the enrichment in domain only. Boundary enrichment only gives poor result. For classic FEM, the displacement error percentage is below 10% (in this case, 6.466%) with an elapsed time calculation of 1.150 seconds only with 1704 degrees of freedom (DOF). On the other hand, the EMLGFM reaches best displacement value for domain/boundary approach presenting only 1.532% of error with an elapsed time calculation of 0.202 seconds. It represents an error improvement of 4.220 times in displacement value compared to classic FEM using only 78 DOF in EMLGFM against 1702 DOF in classic FEM.

Table 6.8 – Displacements results, error (%) and elapsed time (s) for curved beam.

DISPLACEMENT IN DIRECTION OF LOAD FOR CURVED BEAM							
SOLUTION	TIP LOAD: IN-PLANE SHEAR			DOF (Domain)	u_y	Error (%)	Elapsed Time (s)
	ANALYTICAL*			-	-8.73400E-02	-	-
	FEM (QUAD4)*	4-node	$p=1$	28*	-6.41380E-03	92.65651%	0.280
				76	-1.46957E-02	83.17417%	0.360
				222	-5.42841E-02	37.84742%	0.360
				576	-6.69930E-02	23.29627%	0.390
				1704	-8.16925E-02	6.46609%	1.150
	MLGFM	4-node	$p=1$	28	-6.41373E-03	92.65659%	0.156
		4-node SRI	$p=2$	28	-1.85100E-02	78.80696%	0.218
		9-node		78	-7.72510E-02	11.55141%	0.250
	HFEM	Domain/ Boundary	$p=2$	78	-8.86784E-02	1.53240%	0.202
	EMLGFM	Only Domain		78	-8.86877E-02	1.54305%	0.203
	4-node	Only Boundary		28	-6.41323E-03	92.65717%	0.190

* MacNeal and Harder, 1985.

Table 6.9 – Normalized tip displacements results in direction of load.

NORMALIZED DISPLACEMENT FOR CURVED BEAM					
SOLUTION	TIP LOAD: IN-PLANE SHEAR			DOF (Domain)	$(u_y)_h/u_y$
	FEM (QUAD4)*	4-node	$p=1$	28*	0.07344
				76	0.16825
				222	0.62153
				576	0.76704
				1704	0.93534
	MLGFM	4-node	$p=1$	28	0.07343
		4-node SRI	$p=2$	28	0.21193
		9-node		78	0.88449
	HFEM EMLGFM 4-node	Domain/ Boundary	$p=2$	78	1.01532
		Only Domain		78	1.01543
		Only Boundary		28	0.07343

* MacNeal and Harder, 1985.

6.2.3 Thick-Walled Cylinder

In this section, the thick-walled cylinder problem is used to test the EMLGFM. This application is also proposed by MacNeal and Harder (1985). The geometric properties are shown in Figure 6.12. The analytical solution to the problem is also given in Timoshenko and Goodier (1951). The solution for stresses is given by

$$\sigma_r = \frac{\alpha^2 p_a}{b^2 - \alpha^2} \left(1 - \frac{b^2}{r^2} \right), \quad (6.24)$$

$$\sigma_\theta = \frac{\alpha^2 p_a}{b^2 - \alpha^2} \left(1 + \frac{b^2}{r^2} \right) \quad (6.25)$$

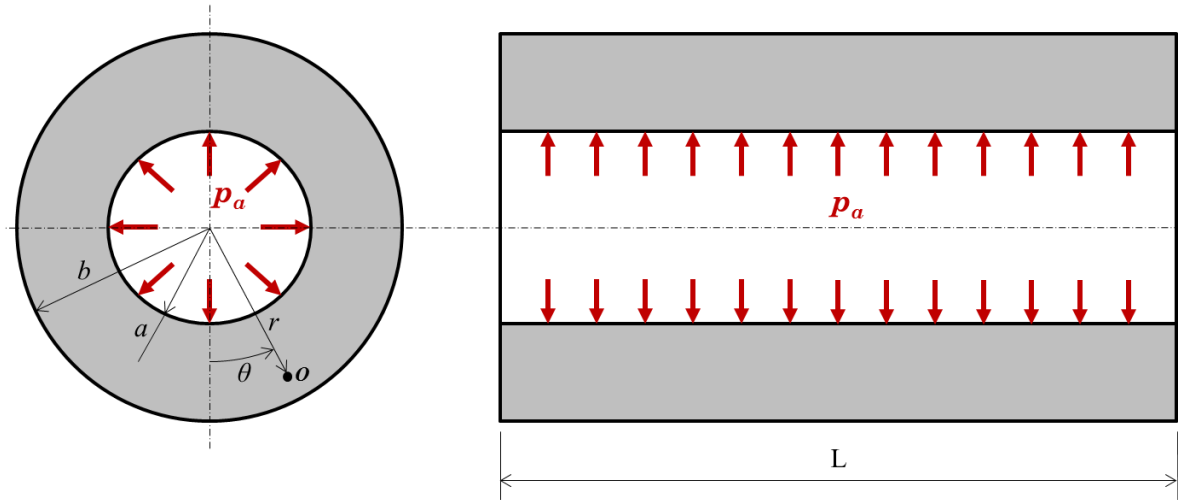


Figure 6.12– The thick-walled cylinder: geometric properties.

and the radial displacement u_r is given by

$$u_r = \frac{(1+\nu)\alpha^2 p_a}{E(b^2 + \alpha^2)} \left[\frac{b^2}{r} + (1-2\nu)r \right] \quad (6.26)$$

where “ p_a ” is the internal pressure.

Note that a plane strain condition is assumed here which, along with the radial symmetry, confines the material in all but the radial direction and intensifies the numerical difficulty caused by near incompressibility (Poisson's ratio increasing next to 0.5). For this example and all other ones from now on, it is only used the enrichment approach domain/boundary. Four levels of enrichment (polynomial order) are used here (from $p = 2$ to $p = 5$) and 16 Gauss points in each direction. Its geometry, mesh and properties are showed in Figure 6.13. Only a quarter of the model is discretized with symmetry considered at vertical and horizontal axis, similarly as suggested by Barbieri (1992).

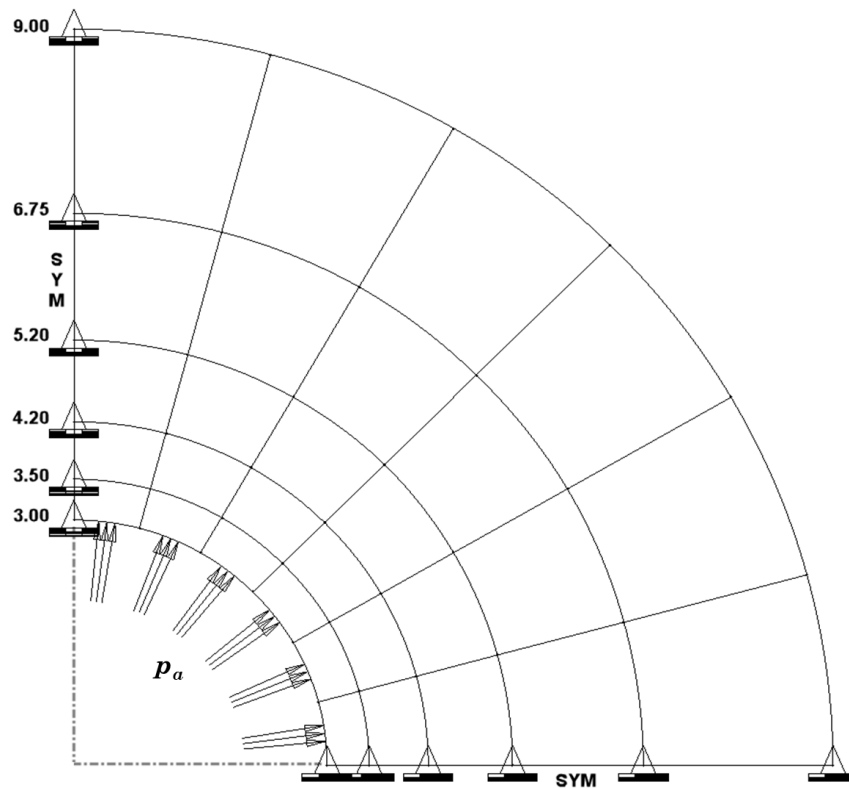


Figure 6.13– Thick-walled cylinder. Inner radius = 3.0; outer radius = 9.0; thickness = 1.0; $E = 1000$; $\nu = 0.49, 0.499, 0.4999$; plane strain condition; mesh = 5 x 6. Loading: unit pressure at inner radius.

As for all discretized problems of MLGFM employed in this work, two meshes are considered: one in domain and another one on boundary, utilizing double node at normal discontinuity as we can see in Figure 6.14.

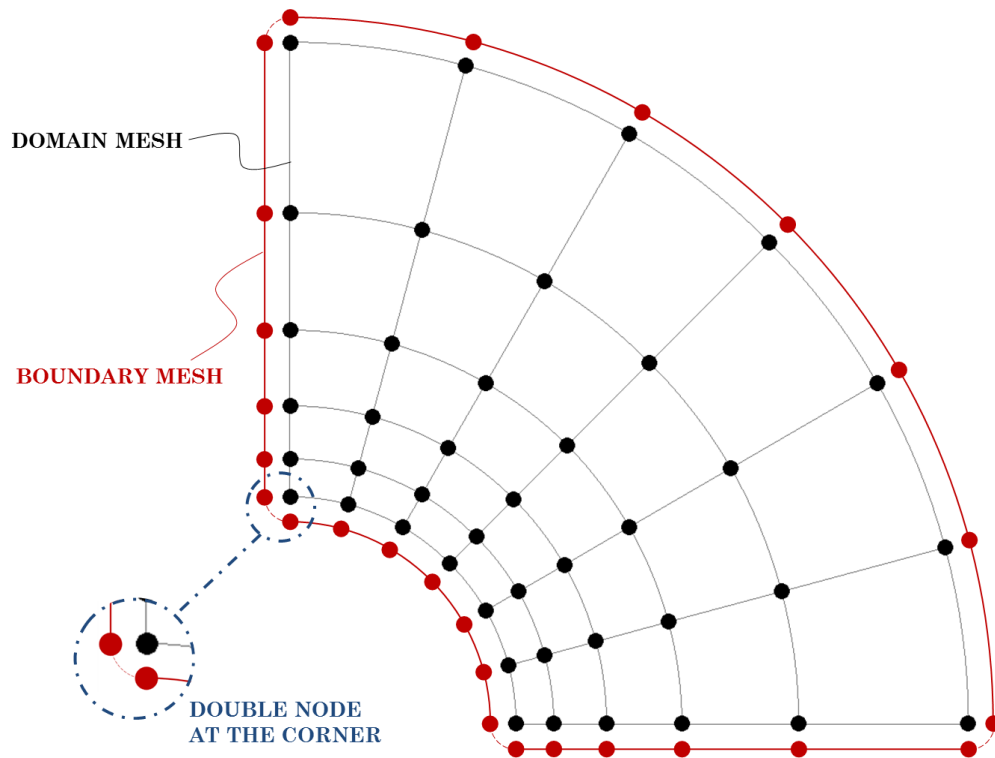


Figure 6.14— Domain and boundary meshes for thick-walled cylinder. Double node considered at corners.

The displacement results displayed in Table 6.10 are taken at the inner radius maximum displacement as seen in Figure 6.15.

In Table 6.10 (displacements results) and Table 6.11 (normal stress results), it is clearly verified that the classic FEM 4-node element $p = 1$ cannot represent well both displacements and stresses without a good mesh refinement and integration treatment due to locking. Locking behavior was also observed by MacNeal and Harder (1985) when using classic FEM. The 9-node MLGFM element shows good results for displacements, but such results degrade as the Poisson's ratio approaches 0.5. Percent errors are 0.13095%, 1.30430% and 11.60342% for 0.49, 0.499 and 0.4999, respectively. On the other hand, the EMLGFM presents better results, and they improve with increasing polynomial order as expected. Percent errors for $p = 5$ are 0.72938%, 0.74938% and 0.75341% for 0.49, 0.499 and 0.4999, respectively.

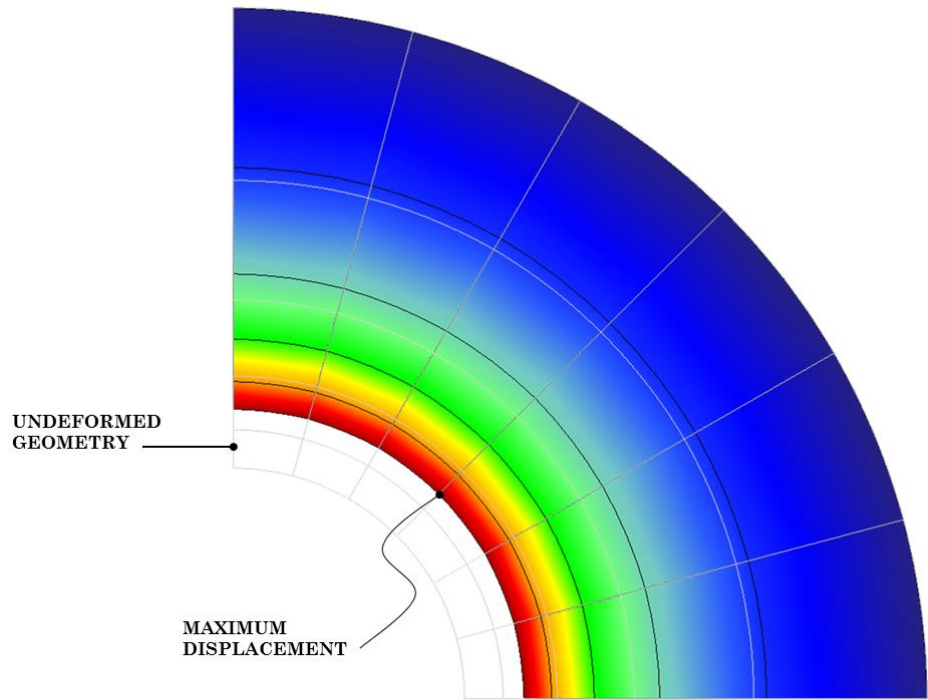


Figure 6.15– Thick-walled cylinder: undeformed and deformed geometry with the maximum displacement representation.

Table 6.10 – Thick-walled cylinder displacement results for different Poisson's ratio values.

RADIAL DISPLACEMENT for $r = 3.0$						
Poisson's Ratio				$\nu = 0.49$	$\nu = 0.499$	$\nu = 0.4999$
SOLUTION	ANALYTICAL*			0.00503993	0.00506025	0.00506227
	FEM	4-node	DOF = 84	0.00428952	0.00182865	0.00027089
			$p=1$ DOF = 608	0.00494317	0.00420622	0.00166638
			DOF = 2300	0.00502180	0.00481745	0.00335309
	MLGFM	4-node SRI	$p=1$ DOF = 84	0.00423479	0.00180640	0.00026766
			$p=1$ DOF = 84	0.00425165	0.00181331	0.00026860
			$p=2$ DOF = 286	0.00503330	0.00499420	0.00447490
	HFEM EMLGFM	4-node	$p=2$ DOF = 286	0.00496845	0.00494931	0.00484208
			$p=3$ DOF = 608	0.00498654	0.00500047	0.00499993
			$p=4$ DOF = 1050	0.00499756	0.00501670	0.00501851
			$p=5$ DOF = 1612	0.00500314	0.00502228	0.00502416

* MacNeal and Harder, 1985.

Table 6.11 – Thick-walled cylinder normal stress results for different radial positions.

NORMAL STRESS σ_r for $\nu = 0.49$											
Radius Value					9.000	6.750	5.200	4.200	3.500	3.000	
SOLUTION	ANALYTICAL				0.250	0.347	0.499	0.699	0.952	1.250	
	FEM	4-node	$p=1$	DOF = 84	0.318	0.560	0.566	0.850	1.236	2.623	
				DOF = 608	0.113	0.433	0.647	0.580	1.111	1.998	
				DOF = 2300	0.184	0.396	0.584	0.783	1.053	1.617	
	MLGFM	4-node SRI	$p=1$	DOF = 84	0.282	0.515	0.515	0.737	0.601	2.681	
					0.272	0.512	0.517	0.735	0.624	2.605	
				9-node	$p=2$	DOF = 286	0.255	0.355	0.508	0.710	0.969
	HFEM EMLGFM	4-node	$p=2$	DOF = 286	0.213	0.346	0.485	0.685	0.915	1.316	
				$p=3$	DOF = 608	0.223	0.344	0.484	0.685	0.905	1.362
				$p=4$	DOF = 1050	0.235	0.347	0.483	0.685	0.929	1.324
$p=5$				DOF = 1612	0.238	0.348	0.482	0.683	0.933	1.315	

Results for normal stresses at different radial positions for $\nu = 0.49$ are poor when the problem is modeled by classic FEM 4-node $p = 1$ and by MLGFM 4-node as values in Table 6.11 demonstrate. Note that MLGFM 9-node presents excellent stress results accuracy that are continuously improved for the EMLGFM 4-node from $p = 2$ to $p = 5$. Better results are obtained when the polynomial order is 5 as expected. Percent errors for this last model are nearly 2.999% in average against 2.449% for MLGFM 9-node.

6.2.4 Rectangular Plate with a Center Hole

In this section, a rectangular plate with a center hole and thickness “ t ” is used to test the EMLGFM. The geometric properties are shown in Figure 6.16.

The plate is modeled by a finite quarter plate and treated as plane stress (Figure 6.17). The analytical solution to the problem is again provided by Timoshenko and Goodier (1951) to solve two-dimensional problems by means of polar coordinates.

The solution for stresses is given by

$$\sigma_r = \frac{\sigma}{2} \left(1 - \frac{a^2}{r^2} \right) + \frac{\sigma}{2} \left(1 + \frac{3a^2}{r^4} - \frac{4a^2}{r^2} \right) \cos 2\theta, \quad (6.27)$$

$$\sigma_\theta = \frac{\sigma}{2} \left(1 + \frac{a^2}{r^2} \right) - \frac{\sigma}{2} \left(1 + \frac{3a^2}{r^4} \right) \cos 2\theta, \quad (6.28)$$

$$\sigma_{r\theta} = -\frac{\sigma}{2} \left(1 - \frac{3a^2}{r^4} + \frac{2a^2}{r^2} \right) \sin 2\theta. \quad (6.29)$$

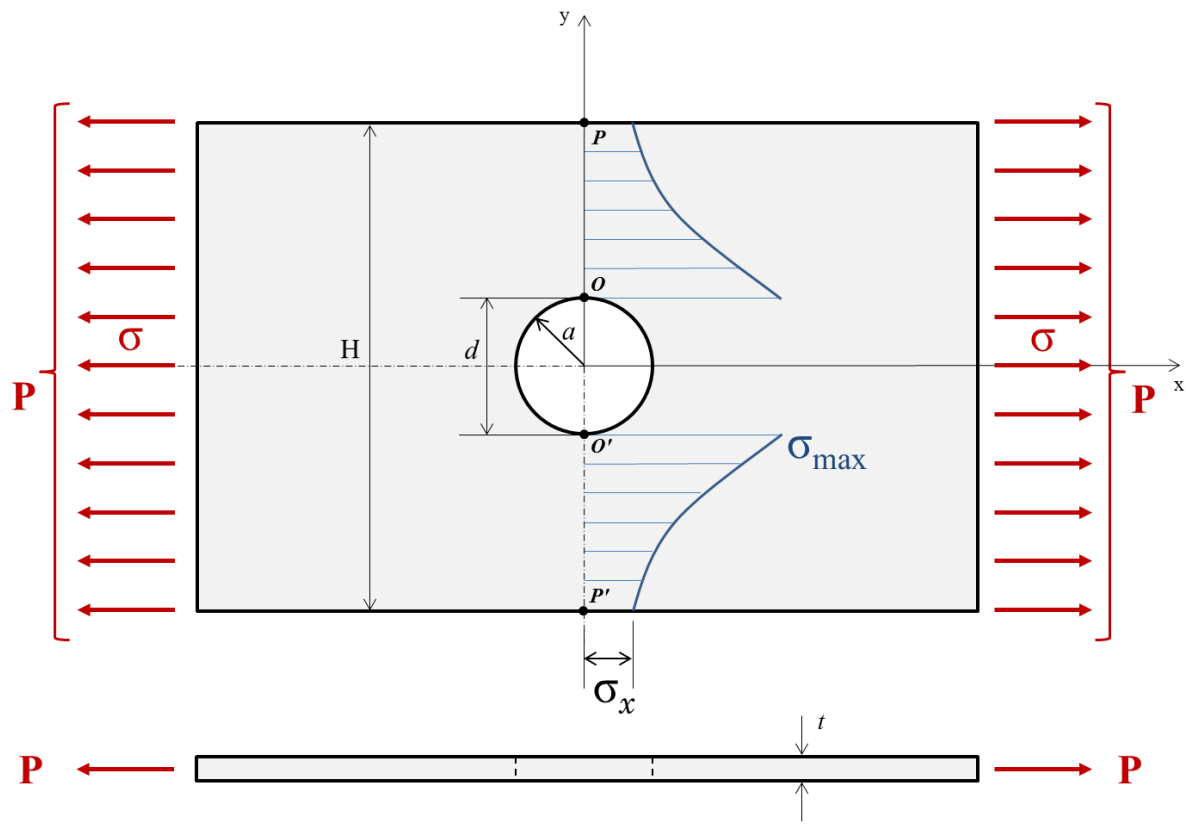


Figure 6.16— Tension plate with a center hole application: geometric properties.

These equations can be expressed in Cartesian coordinates such that

$$\sigma_x = \sigma_r \cos^2 \theta + \sigma_\theta \sin^2 \theta - 2\sigma_{r\theta} \sin \theta \cos \theta, \quad (6.30)$$

$$\sigma_y = \sigma_r \sin^2 \theta + \sigma_\theta \cos^2 \theta + 2\sigma_{r\theta} \sin \theta \cos \theta, \quad (6.31)$$

$$\sigma_{xy} = (\sigma_r - \sigma_\theta) \sin \theta \cos \theta + 2\sigma_{r\theta} (\cos^2 \theta - \sin^2 \theta) \quad (6.32)$$

where r and θ are defined in Figure 6.17.

The nominal stress (gross cross sectional area: cross section far from the circular hole as the reference stress) is defined by

$$\sigma = \frac{P}{Ht} = \sigma_{nom} \quad (6.33)$$

as well as the net stress (net cross sectional area: on the cross section at the hole, which is formed by removing the circular hole from the gross cross section) is expressed by

$$\sigma_n = \frac{P}{(H-d)t}, \quad (6.34)$$

$$\sigma_{max} = \sigma_O. \quad (6.35)$$

Usually, the stress concentration factor is “ K_{tg} ”, for which the reference stress is based on gross cross-sectional area, or “ K_{tn} ”, for which the reference stress is based on net cross-sectional area. For a two-dimensional plate with a single hole (Figure 6.16), we have

$$K_{tg} = \frac{\sigma_{max}}{\sigma} \quad (6.36)$$

where “ K_{tg} ” is the stress concentration factor based on gross stress, “ σ_{max} ” is the maximum stress, at the edge of the hole, “ σ ” is the stress on gross section far from the hole, and

$$K_{tn} = \frac{\sigma_{max}}{\sigma_n} \quad (6.37)$$

where “ K_{tn} ” is the stress concentration factor based on net (nominal) stress and “ σ_n ” is the net stress $[\sigma / (1 - d/H)]$, with “ d ” the hole diameter and “ H ” the width of plate as in Figure 6.16.

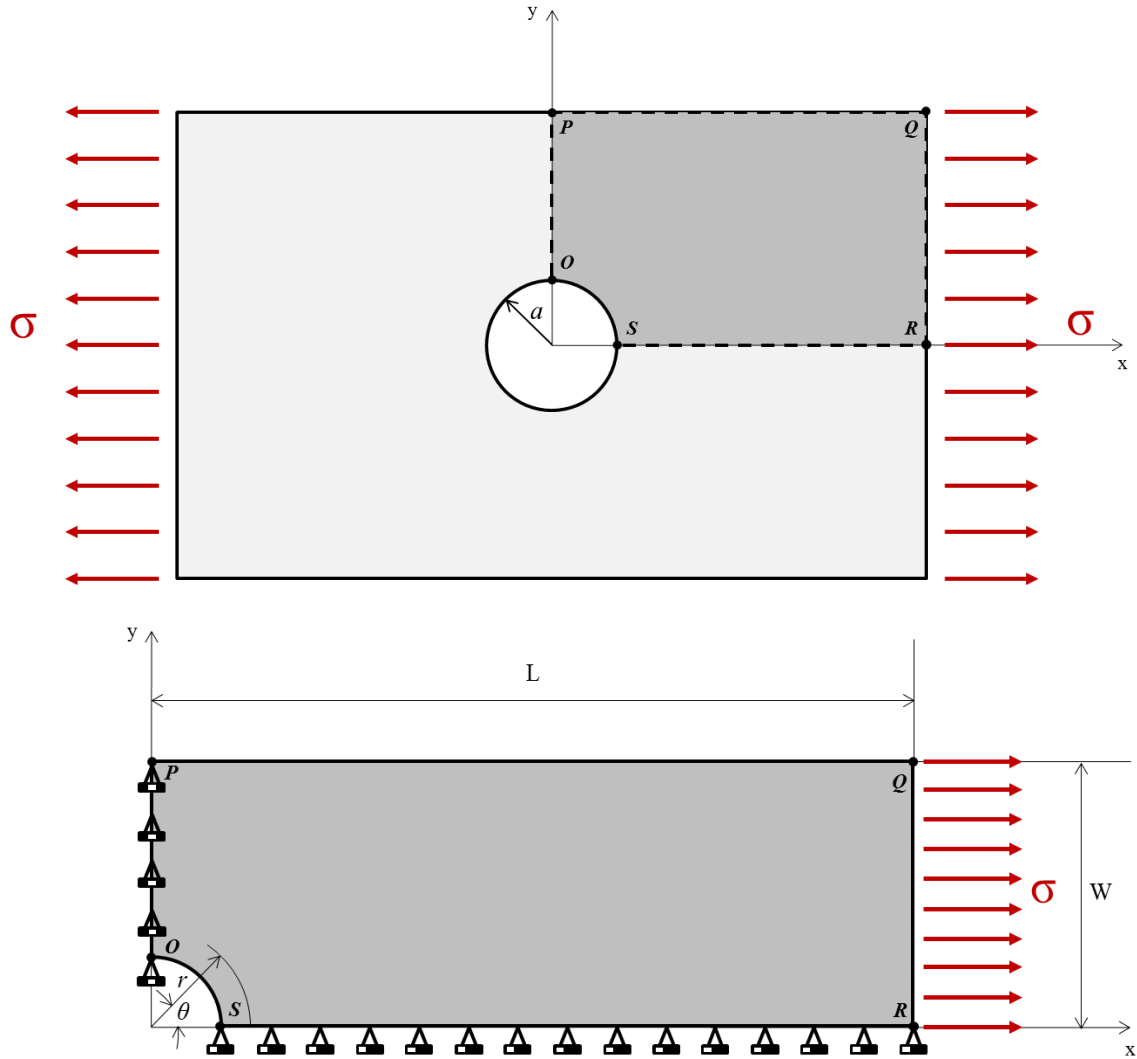


Figure 6.17– The rectangular plate with a center hole boundary condition, geometry and properties: $a=1$; $W = H/2 = 4$; $L = 28$; $E = 1.0 \times 10^5$; $\nu = 0.3$; $\sigma = 10$.

From the foregoing,

$$K_{tn} = K_{tg} \left(1 - \frac{d}{H} \right) = K_{tg} \frac{\sigma}{\sigma_n} \quad \text{or} \quad K_{tg} = \frac{\sigma_n}{\sigma} K_{tn} . \quad (6.38)$$

For the tension case of a finite-width thin plate with a circular hole, according to Pilkey and Pilkey (2008) values of “ K_{tn} ” for $d/H \leq 0.5$ can be expressed by

$$K_{tn} = 2 + 0.284\left(1 - \frac{d}{H}\right) - 0.600\left(1 - \frac{d}{H}\right)^2 + 1.32\left(1 - \frac{d}{H}\right)^3 \quad (6.39)$$

This is exactly the analytical expression used here to compare the stress concentration factor K_{tn} against numerical values $(K_{tn})_h$. The maximum stress “ σ_{\max} ” extracted from the numerical solution in order to calculate the stress concentration factor $(K_{tn})_h$ using Equation 6.37 is shown in Figure 6.18 for a coarse mesh. The employed value is pointed out in the figure as “*stress concentration*”.

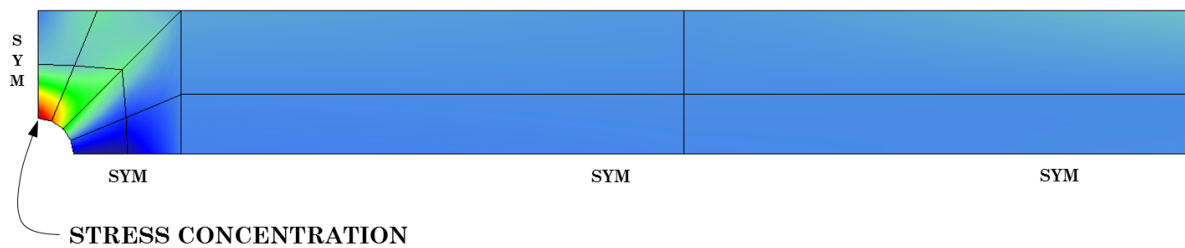


Figure 6.18– The rectangular plate with a center hole: stress field representation for coarse mesh.

It is employed here two FEM meshes: a coarse one with 12 elements and a refined one with 672 elements as seen in Figure 6.19. A mesh refinement is necessary in this application since the numerical model was not able to accurately capture the stress values in a very coarse mesh when using classic FEM.

For the EMLGFM, the model’s discretization utilizes double node at normal discontinuity as displayed in Figure 6.20.

The error percentage shown in Table 6.12 is again figured out by the expression $[|(K_{tn})_h - K_{tn}| / K_{tn}] * 100\%$, where $(K_{tn})_h$ is the approximate stress

concentration factor and K_{tn} is the analytical stress concentration factor.

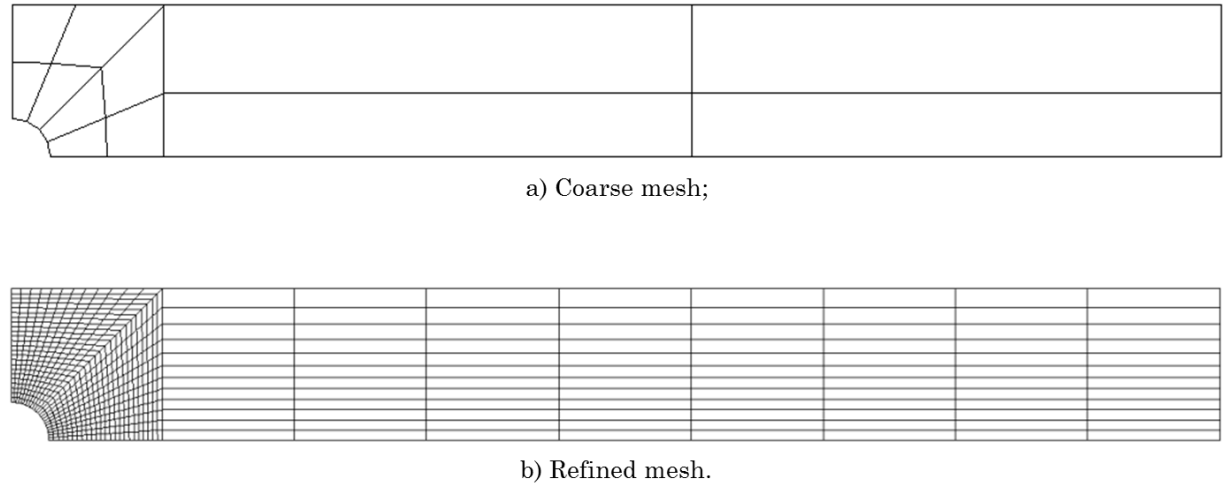


Figure 6.19– FEM meshes: a) coarse and b) refined.

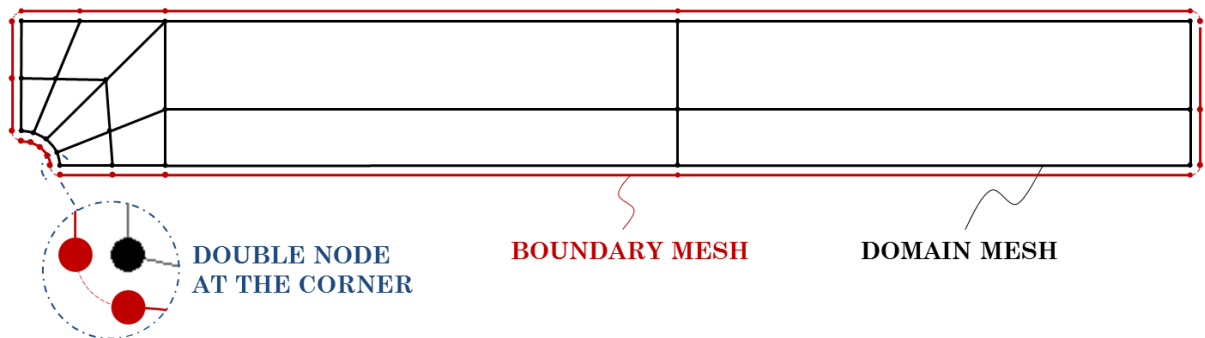


Figure 6.20– Domain and boundary meshes for the rectangular plate with a center hole. Coarse mesh: a quarter of the domain. Double node considered at corners.

The results in Table 6.12 demonstrate high precision values once EMLGM increases the polynomial order. It reaches the best for polynomial order $p = 5$ as expected. Once again, note that the EMLGFM needs to calculate Green's function projections (GFp) and this requires a certain amount of time (seen in Table 6.12 as well). If we again disregard Green's function projections (GFp) figured out in domain (G^{DP}), the computational cost sharply decreases. In this example, we also can neglect them due to the absence of body forces. Comparing EMLGFM from $p = 2$ to $p = 5$, the elapsed calculation time strongly reduces

reaching 74.128% of reduction for $p = 5$ with a K_{tn} error of 0.061%.

Table 6.12 – Stress Concentration Factor Comparison for Lobatto Shape Functions.

STRESS CONCENTRATION FACTOR: K_{tn}								
Solution	FEM 4-node		MLGFM 9-node	HFEM EMLGFM 4-node				
Number of Domain's Elements	12	672	12	12				
Number of Domain's DOF	42	1458	130	42	130	266	450	682
Polynomial Order	$p=1$		$p=2$	$p=1$	$p=2$	$p=3$	$p=4$	$p=5$
Analytical K_{tn}	2.432		2.432	2.432				
Numerical K_{tn} : $(K_{tn})_h$	1.629	2.463	2.508	3.238	2.734	2.718	2.562	2.431
Error (%)	33.013%	1.243%	3.093%	33.106%	12.409%	11.725%	5.337%	0.061%
Elapsed Time (s)	0.250	0.670	0.967	0.125	0.265	0.874	3.323	13.447
Elapsed Time without G^{DP}	-	-	-	-	0.187	0.452	1.045	3.479
Time Reduction (%)	-	-	-	-	29.434%	48.284%	68.553%	74.128%

None selective enrichment in elements near the stress concentration was taken into account in this application. All elements were regularly enriched. A selective approach and special domain Dirichlet boundary condition can be better investigated in future works.

6.2.5 Rectangular Plate with a Center Crack

In this application, the goal is to calculate the stress intensity factor (SIF) – K_I for center-cracked plate with thickness “ t ”. It is considered the plane strain

state and geometry is modeled as a quarter of the domain (Figure 6.21).

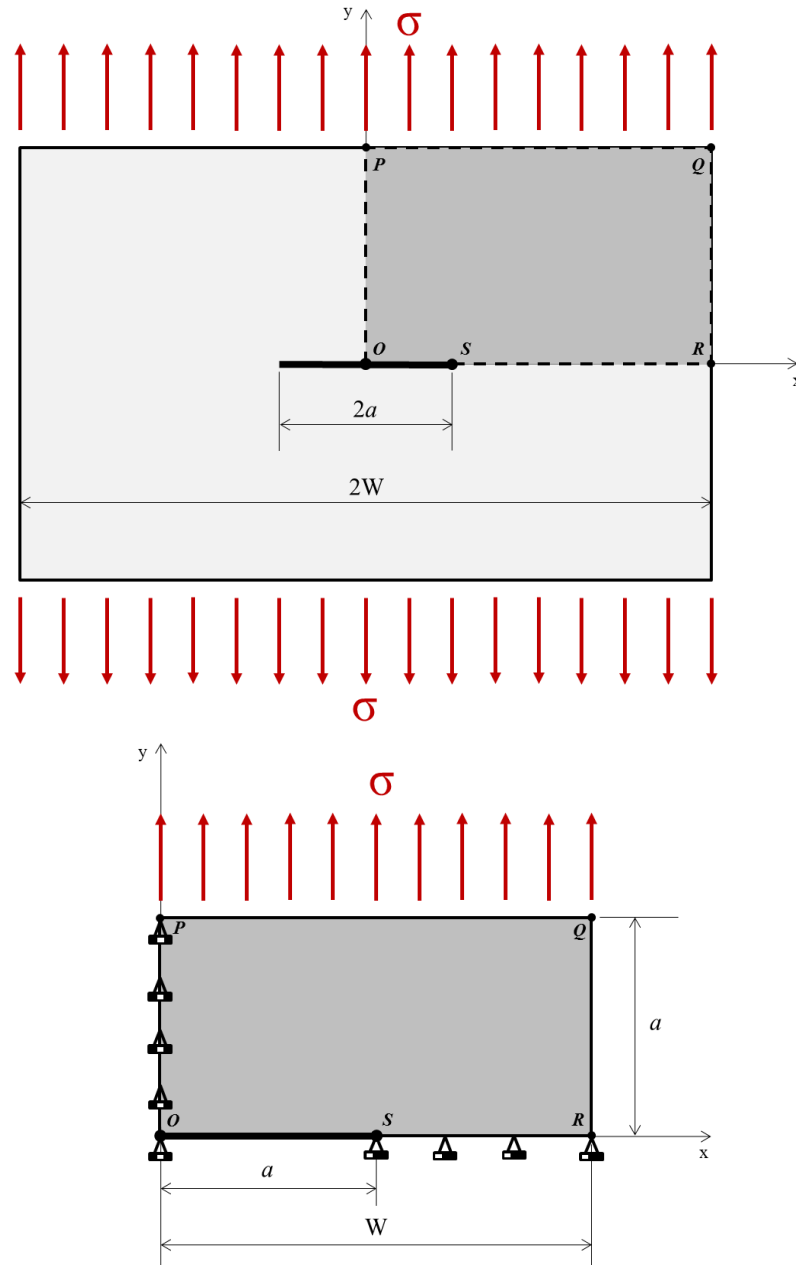


Figure 6.21– The rectangular plate with a center crack: geometric properties $a = 7$ and $W = 14$.

Here, a geometric progression close to the crack tip is taken similar to the Szabó (1986) work for graded mesh applied for L-shaped elastic body example.

The mesh is composed by 62 elements with symmetric boundary conditions. The mesh geometry and properties are also shown in Figure 6.22.

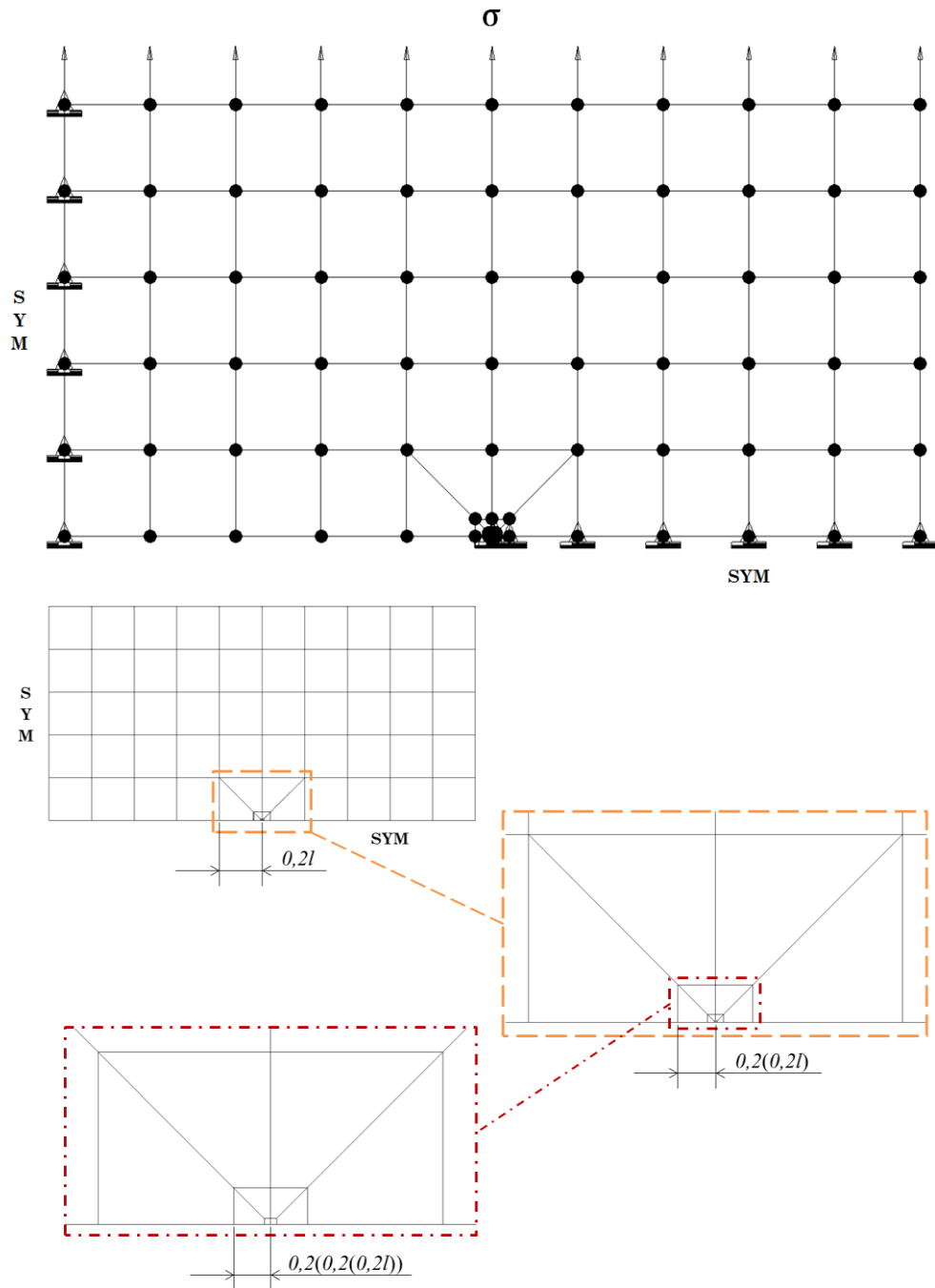


Figure 6.22– The rectangular plate with a center crack boundary conditions, geometry and properties: $l = 1.4$; $E = 1.0 \times 10^5$; $\nu = 0.3$; state of plane strain; graded mesh = 62 elements. Loading: $\sigma = 10$.

Two meshes are considered in the discretized model: one in domain and another one on boundary, utilizing double node at normal discontinuity as we can see in Figure 6.23.

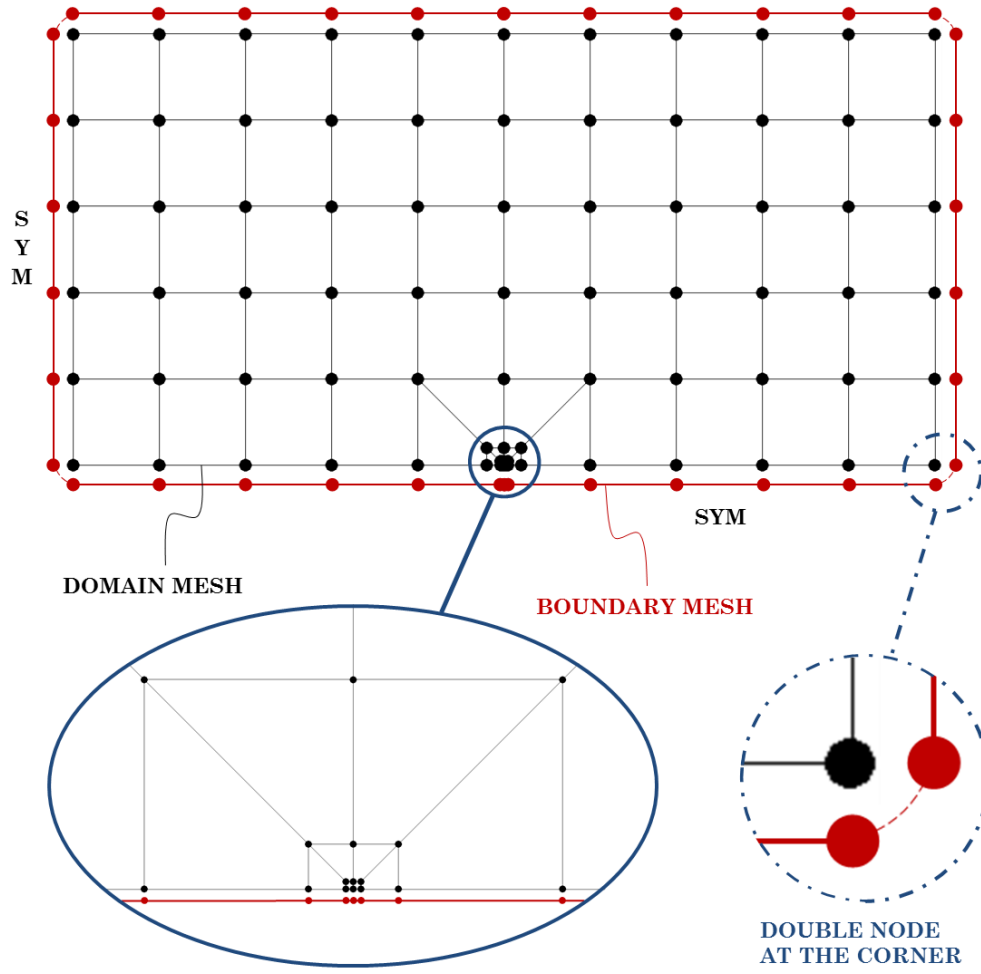


Figure 6.23– Domain and boundary meshes for the rectangular plate with a center crack. Mesh: a quarter of the domain with graded mesh at the crack tip. Double node considered at corners.

The stress field ahead of a crack tip for mode I is given by Anderson (2005) as following

$$\sigma_x = \frac{K_I}{\sqrt{2\pi r}} \cos\left(\frac{\theta}{2}\right) \left[1 - \sin\left(\frac{\theta}{2}\right) \sin\left(\frac{3\theta}{2}\right) \right], \quad (6.40)$$

$$\sigma_y = \frac{K_I}{\sqrt{2\pi r}} \cos\left(\frac{\theta}{2}\right) \left[1 + \sin\left(\frac{\theta}{2}\right) \sin\left(\frac{3\theta}{2}\right) \right], \quad (6.41)$$

$$\sigma_{xy} = \frac{K_I}{\sqrt{2\pi r}} \sin\left(\frac{\theta}{2}\right) \cos\left(\frac{\theta}{2}\right) \cos\left(\frac{3\theta}{2}\right) \quad (6.42)$$

where r and θ are defined in Figure 6.24.

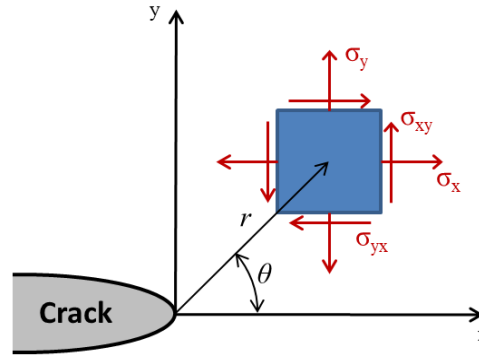


Figure 6.24– Definition of the coordinate axis ahead of a crack tip.

Now, considering the mode I singular field on the crack plane, with $\theta = 0$. Then, the stresses in “x” and “y” directions can be expressed by

$$\sigma_x = \sigma_y = \frac{K_I}{\sqrt{2\pi r}} \quad (6.43)$$

or for K_I

$$K_I = \sigma_x \sqrt{2\pi r} = \sigma_y \sqrt{2\pi r} . \quad (6.44)$$

Observe in Figure 6.25 both undeformed and deformed geometry after loading as well as the stress distribution close to the stress singularity. Stresses values are extracted to nodes at $\theta = 0$ near to the singularity shown in Figure 6.25. With plot of K_I as a function of r expressed in Equation 6.44, stress intensity factor (SIF) K_I at the crack tip ($r = 0$) can be determined by extrapolating. This numerical method used for SIF calculation is known in literature as “*Stress Extrapolation Method*” (HAN *et al.*, 2015). One way of using the extrapolation method to numerically determine stress intensity factor K_I from stresses is presented by Zafošnik and Fajdiga (2016). This is the approach adopted in this work.

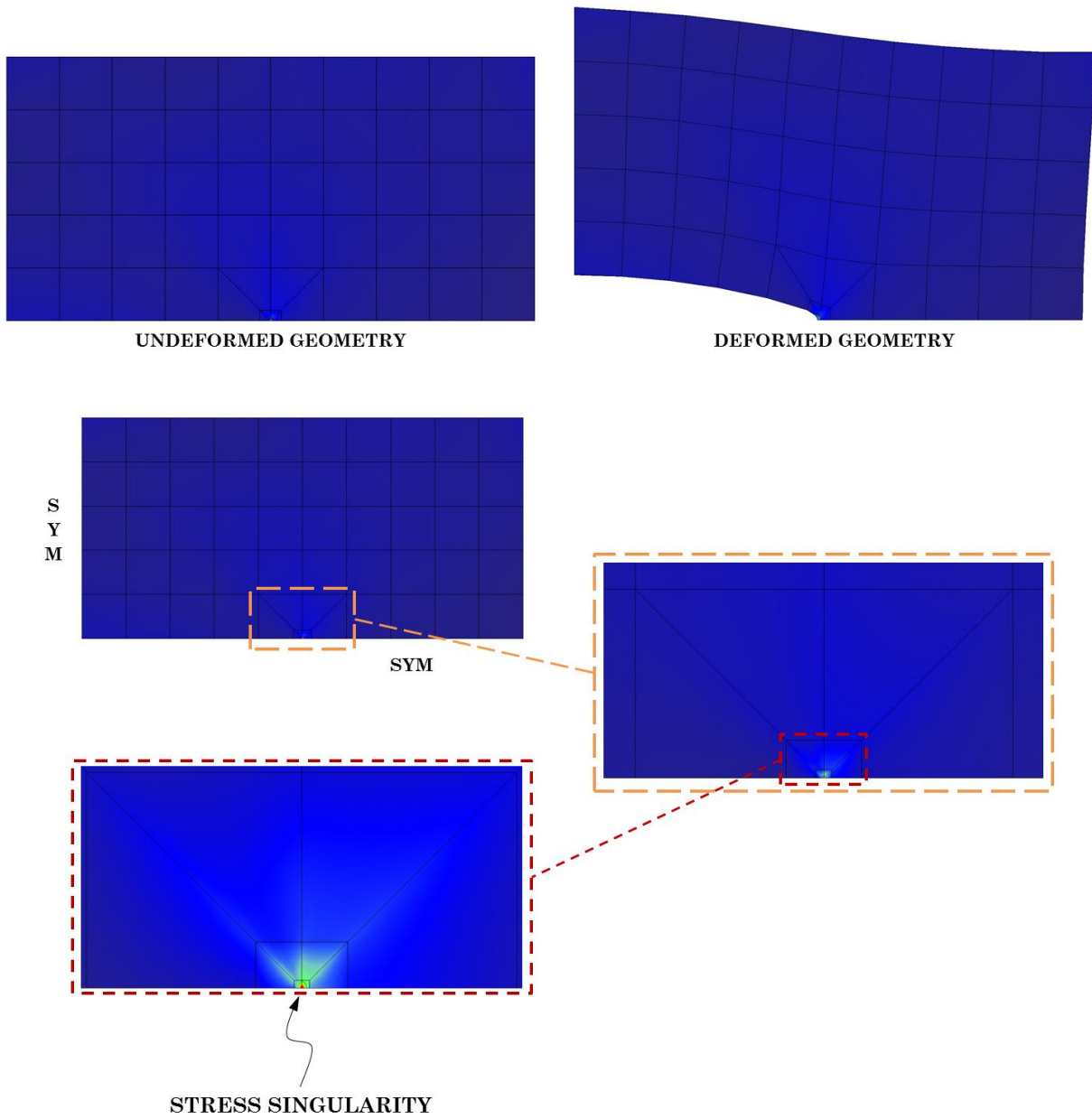


Figure 6.25– The rectangular plate with a center crack: stress field representation.

Numerical results $(K_I)_h$ as well as analytical solution K_I can be seen on Tables 6.13 and 6.14. The analytical solution is also given by Anderson (2005)

$$K_I = \sigma \sqrt{\pi a} \left[\sec \left(\frac{\pi a}{2W} \right)^{1/2} \right] \left[1 - 0.025 \left(\frac{a}{W} \right)^2 + 0.06 \left(\frac{a}{W} \right)^4 \right] \quad (6.45)$$

which in “ a ” and “ W ” are the crack radius and half of plate width, respectively.

Table 6.13 – Stress Intensity Factor Comparison.

STRESS INTENSITY FACTOR (SIF) – K _I					
SOLUTION	ANALYTICAL*			78.67004	
	FEM	4-node	<i>p</i> =1	72.46553	
	MLGFM	4-node	<i>p</i> =1	80.42065	
		9-node		79.62214	
	Type of enrichment			HFEM	GFEM
	EMLGFM	4-node	<i>p</i> =2 or <i>le</i> =1	77.58708	80.34232
			<i>p</i> =3 or <i>le</i> =2	78.07879	77.81671
			<i>p</i> =4 or <i>le</i> =3	78.23411	78.18159
<i>p</i> =5 or <i>le</i> =4			78.31137	78.29197	

*Anderson, 2005

Table 6.14 – Stress Intensity Factor Comparison: error (%).

STRESS INTENSITY FACTOR (SIF) – K_I : ERROR (%)					
SOLUTION	FEM	4-node	$p=1$	7.88675%	
	MLGFM	4-node	$p=1$	2.22526%	
		9-node		1.21025%	
	Type of enrichment			HFEM	GFEM
	EMLGFM	4-node	$p=2$ or $le=1$	1.37658%	2.12570%
			$p=3$ or $le=2$	0.75156%	1.08469%
			$p=4$ or $le=3$	0.55412%	0.62087%
			$p=5$ or $le=4$	0.45592%	0.48058%

The results present an excellent conformity both using Lobatto shape functions (HFEM) and trigonometric shape functions (GFEM) once polynomial order and level of enrichment are incremented. It is interesting to observe that, at lower levels of enrichment, HFEM approach shows a slightly better response compared to GFEM approach but the difference is not so significant under higher levels of enrichment. The error percentage shown in Table 6.14 is also worked out by the expression $[|(K_I)_h - K_I| / K_I] * 100\%$, where $(K_I)_h$ is the approximate stress intensity factor and K_I is the analytical stress intensity factor. The stress σ_y behavior against distance r from crack tip is plotted in Figure 6.26.

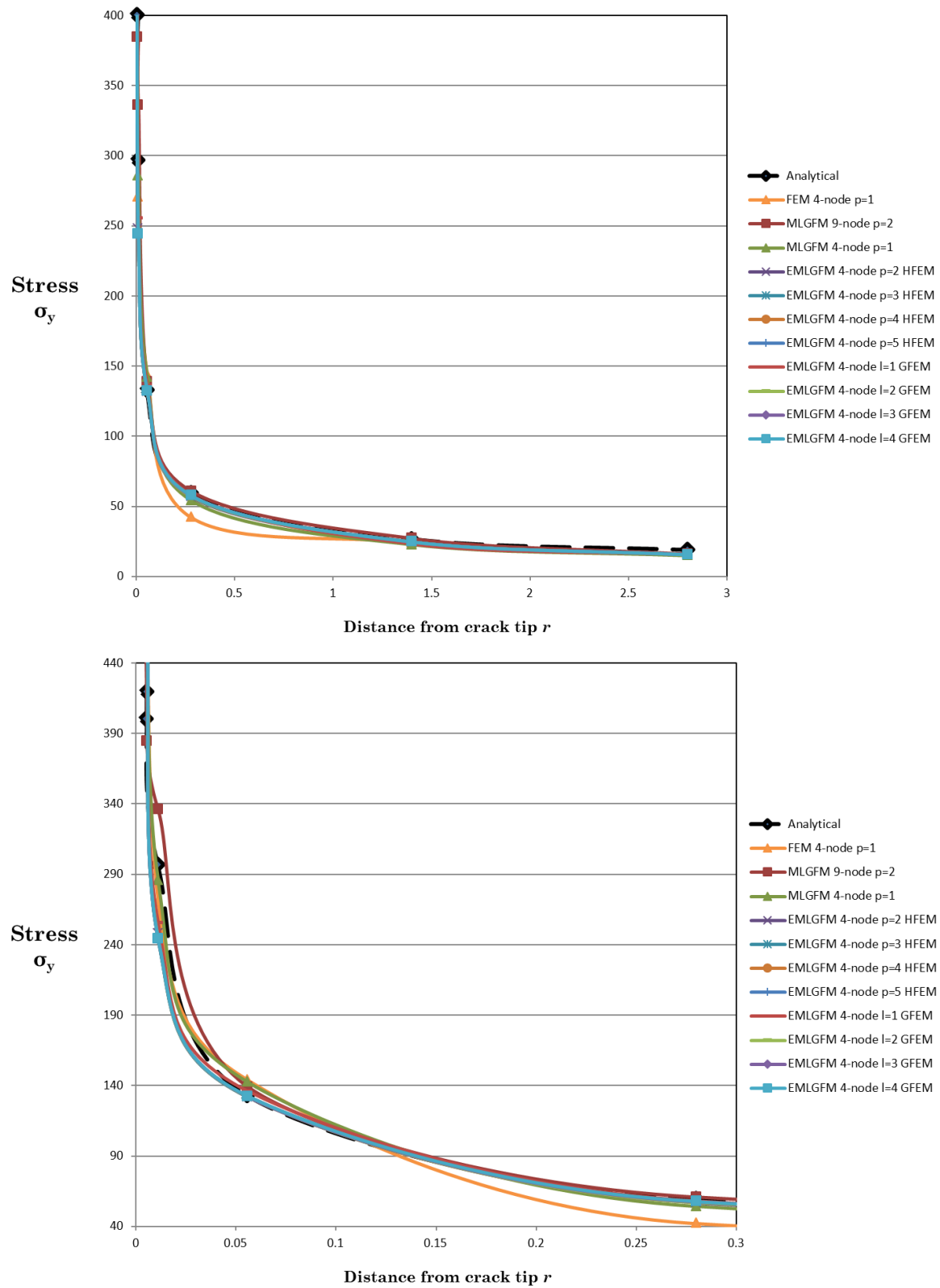


Figure 6.26– Stress distribution along singular side: Stress σ_y versus distance r from Crack tip.

The lower picture is a zoom of the upper one in. As we can see, all approaches present the same behavior with higher stresses moving towards to stress singularity ($r = 0$). Stresses values for conventional MLGFM and EMLGFM present conservative behavior next to the singularity but it is softened as long as the distance from crack tip gets longer. For classic FEM, the values are even conservatives for all measures of r . There are some variations of classic FEM, conventional MLGFM 4-node and 9-node compared to analytical values but not so evidenced in EMLGFM approach. For all EMLGFM polynomial order and level of enrichment, they present exactly same curve pattern.

6.2.6 L-Shaped Domain with a Singularity

It is considered the problem of an L-shaped plane elastic body of thickness “ t ” loaded by the tractions associated with the following stress field (SZABÓ, 1986)

$$\sigma_x = K_I \lambda_I r^{\lambda_I-1} [(2 - Q_I(\lambda_I + 1)) \cos(\lambda_I - 1)\theta - (\lambda_I - 1) \cos(\lambda_I - 3)\theta], \quad (6.46)$$

$$\sigma_y = K_I \lambda_I r^{\lambda_I-1} [(2 + Q_I(\lambda_I + 1)) \cos(\lambda_I - 1)\theta + (\lambda_I - 1) \cos(\lambda_I - 3)\theta], \quad (6.47)$$

$$\sigma_{xy} = K_I \lambda_I r^{\lambda_I-1} [(\lambda_I - 1) \sin(\lambda_I - 3)\theta + Q_I(\lambda_I + 1) \sin(\lambda_I - 1)\theta] \quad (6.48)$$

where (r, θ) is the polar coordinate system shown in Figure 6.27, “ K_I ” is a generalized stress-intensity factor (considered here in this section as $K_I = 1$), $\lambda_I = 0.544483737$ and $Q_I = 0.543075579$.

The stress field in the last equation corresponds to the first term of the symmetric part of the expansion of the elasticity solution in the neighborhood of the corner “O” shown in Figure 6.27, in other words, the Mode-I term of the asymptotic expansion of displacement “ u ” about the re-entrant corner. Therefore, the analytical solution is known.

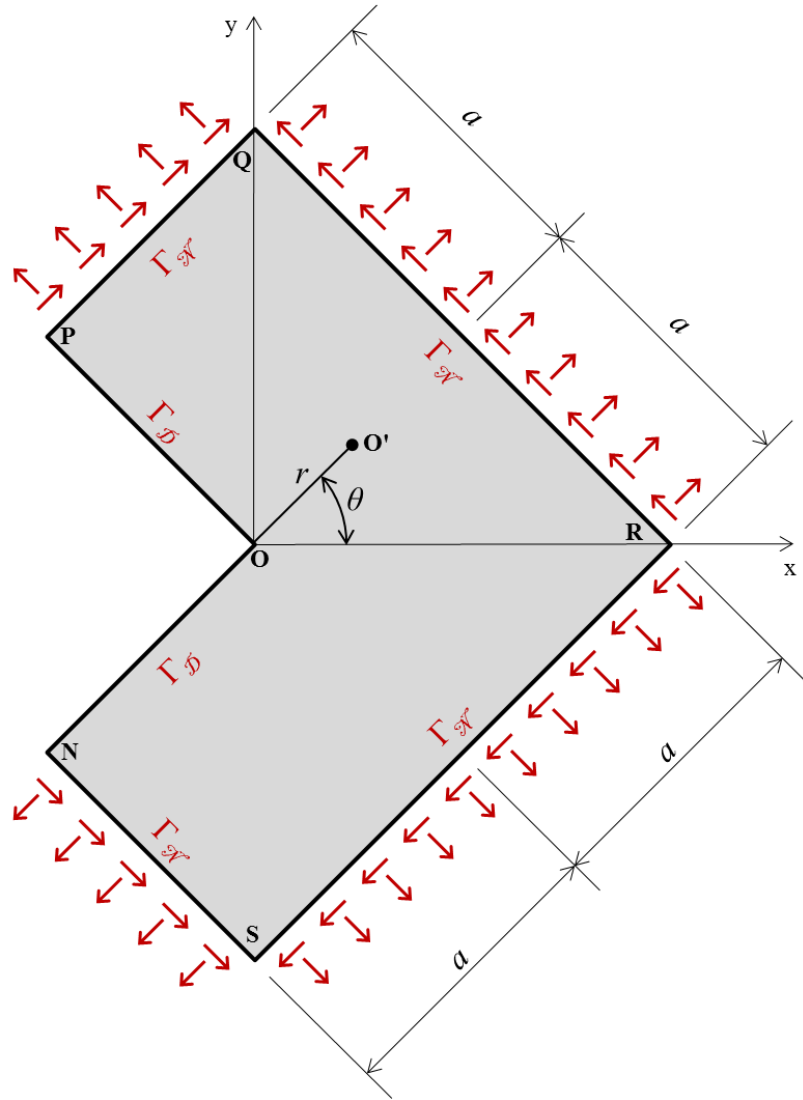


Figure 6.27– The L-shaped domain geometric and boundary condition definition: $a = 1$.

Specifically, the components of “ u ” in the coordinate system shown in Figure 6.27 are

$$u_x = \frac{K_I}{2G} r^{\lambda_I} [(\kappa - Q_I(\lambda_I + 1)) \cos \lambda_I \theta - \lambda_I \cos(\lambda_I - 2)\theta], \quad (6.49)$$

$$u_y = \frac{K_I}{2G} r^{\lambda_I} [(\kappa + Q_I(\lambda_I + 1)) \sin \lambda_I \theta + \lambda_I \sin(\lambda_I - 2)\theta] \quad (6.50)$$

where “ G ” is the modulus of rigidity (shear modulus), and “ κ ” depends on Poisson’s ration “ ν ” only. For plane strain, the following relation is valid:

$\kappa = 3 - 4\nu$ (SZABÓ, 1986). We have assumed plane strain condition and $\nu = 0.3$ therefore $\kappa = 1.8$.

Once computed the tractions ($\Gamma_{\mathcal{N}}$) from the stress field expressed by the Equations 6.46, 6.47 and 6.48 which exactly satisfies the equilibrium and compatibility equations and the stress-free conditions along the re-entrant corner ($\Gamma_{\mathcal{D}}$), it is expected the stress singularity seen in Figure 6.28.

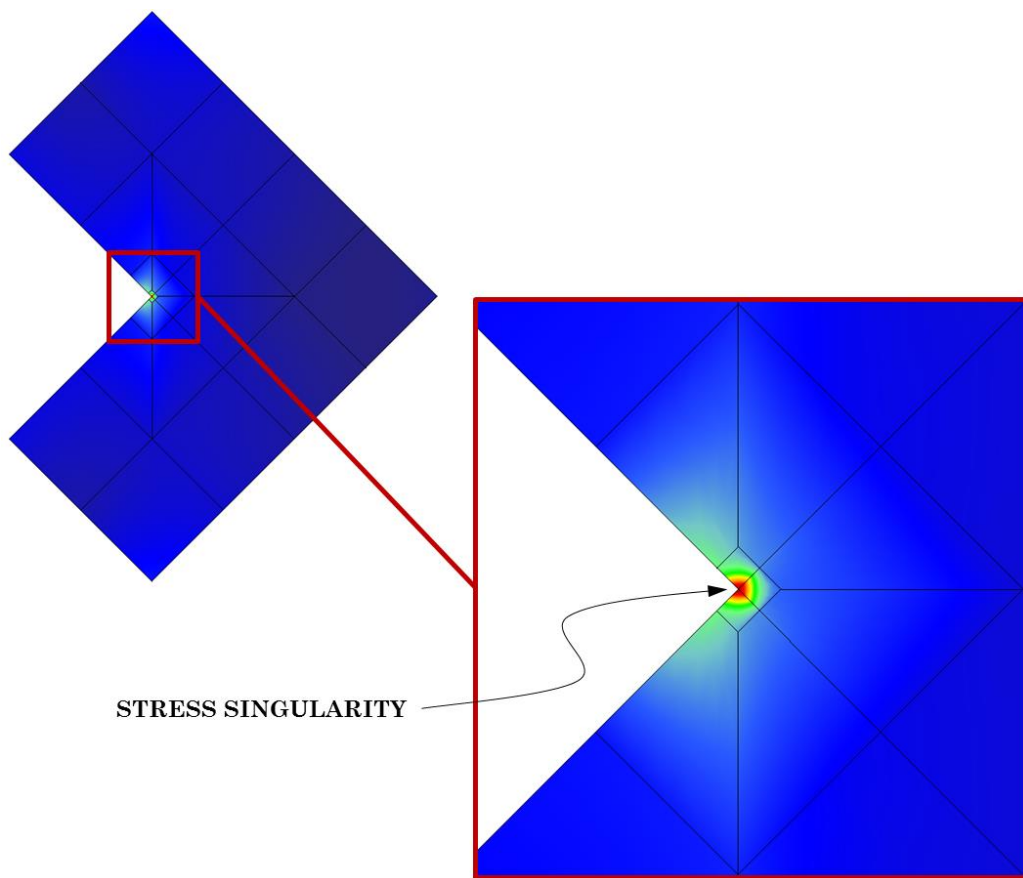


Figure 6.28— The L-shaped domain: stress field representation with the stress singularity at the re-entrant corner.

Two meshes are considered in the discretized model: one in domain and another one on boundary, utilizing double node at normal discontinuity as we can see in Figure 6.29 and 6.30. It is used a uniform mesh (Figure 6.29) and a graded mesh (Figure 6.30) for this application. The meshes boundary conditions, properties and graded geometry are shown in Figures 6.31 and 6.32.

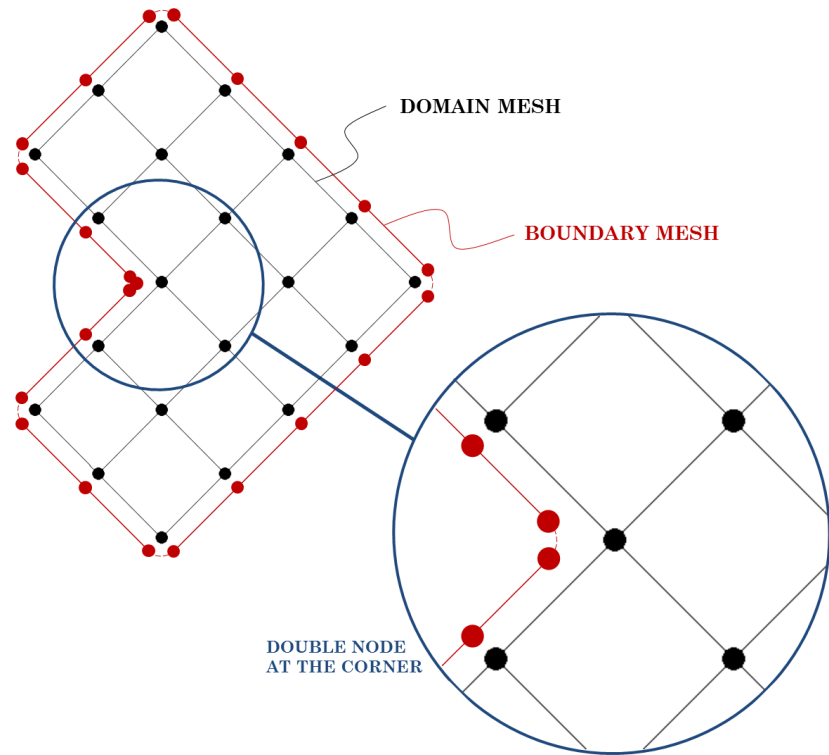


Figure 6.29– Domain and boundary meshes for the L-shaped domain: uniform mesh. Double node considered at corners including the re-entrant corner.

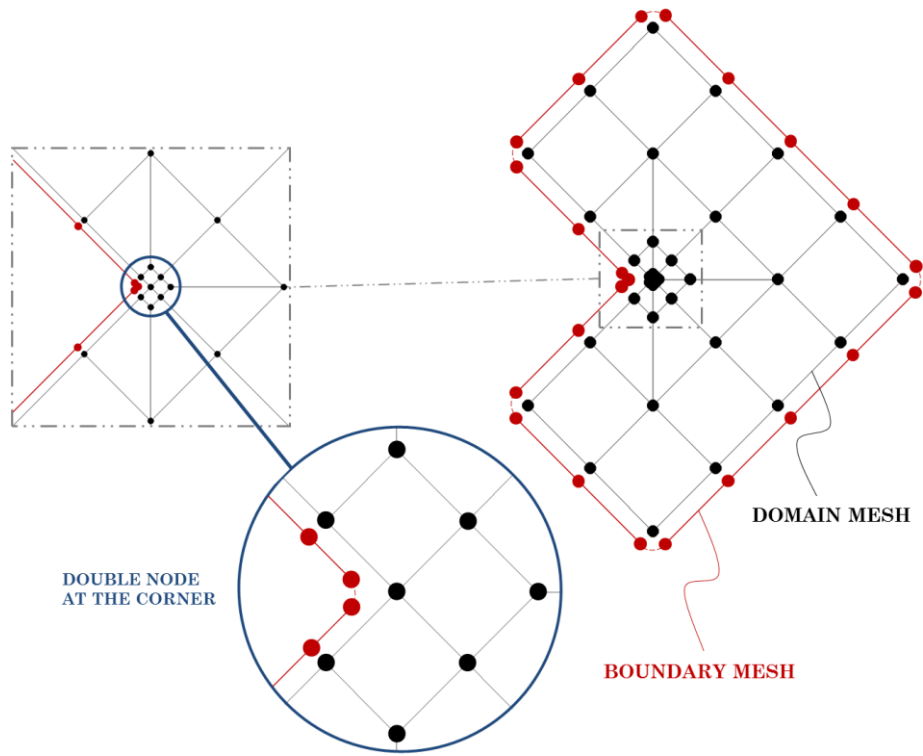


Figure 6.30– Domain and boundary meshes for the L-shaped domain: graded mesh. Double node considered at corners including the re-entrant corner.

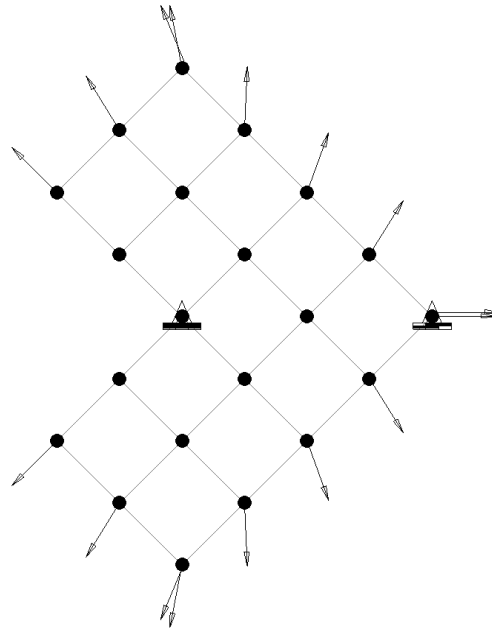


Figure 6.31– The L-shaped domain: boundary condition, $E = 1.0 \times 10^5$; $\nu = 0.3$; plane strain condition; uniform mesh = 12 elements. Loading: tractions computed from Equations 6.46 to 6.48 applied on boundary mesh nodes.

There are a series of values computed from Table 6.15 to 6.20. They are divided in the following way: from Table 6.15 to 6.18 we have a displacement “u” comparison and from Table 6.19 to 6.20 a stress comparison (σ_x , σ_y or σ_{xy}). The values shown in these tables are chosen in domain mesh and on boundary mesh in order to express values both near and far from the stress singularity.

The values of the polar coordinates (r , θ) are seen in each table as well as the type of mesh: uniform or graded. The resultant displacement is given by

$$u = \sqrt{(u_x)^2 + (u_y)^2} \quad (6.51)$$

and the analytical displacement components “x” and “y” are calculated by Equations 6.49 and 6.50.

The analytical stress values are computed by Equations 6.46, 6.47 and 6.48. Due to the intrinsic characteristic of the graded mesh, there are nearest nodes from the re-entrant corner and these values are shown on the tables but there are not correspondent uniform mesh values in order to compare to and

because of that the uniform mesh values are omitted in these cases.

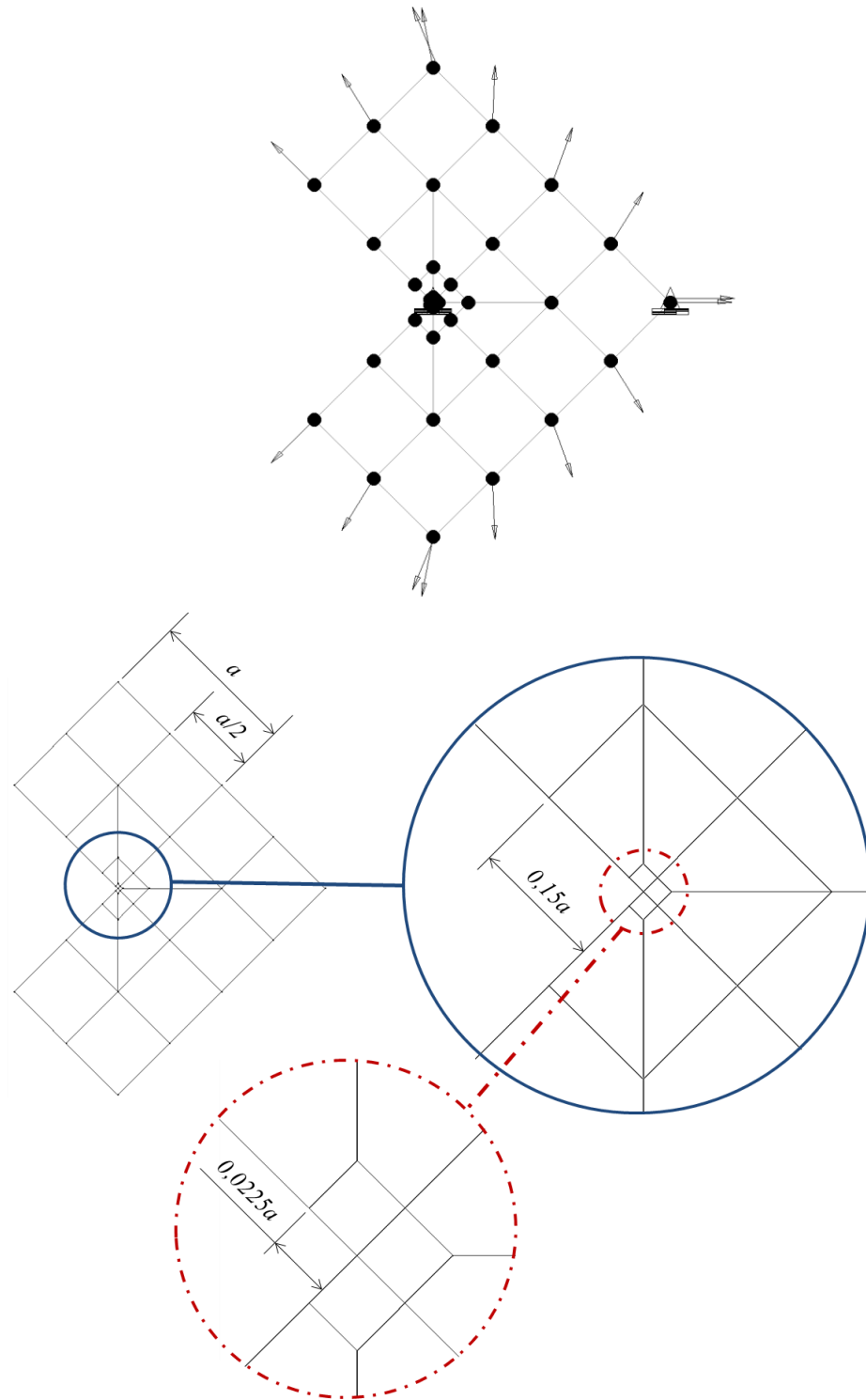


Figure 6.32– The L-shaped domain: boundary condition, $a = 1.0$; $E = 1.0 \times 10^5$; $\nu = 0.3$; plane strain condition; graded mesh = 24 elements. Loading: tractions computed from Equations 6.46 to 6.48 applied on boundary mesh nodes.

Table 6.15 – Resultant displacement results for uniform and graded meshes in domain.

RESULTANT DISPLACEMENT u IN DOMAIN							
Radius r Angle θ Type of Mesh #				0.70711 -90°		0.02250 45°	0.03182 -90°
				UNIFORM	GRADED	GRADED	GRADED
SOLUTION	ANALYTICAL			2.00640E-05		1.45445E-06	3.70777E-06
	FEM	4-node	$p=1$	2.77620E-05	3.79414E-05	5.01866E-06	8.20539E-06
	MLGFM	4-node	$p=1$	2.77620E-05	1.70006E-05	9.89720E-07	3.08319E-06
		9-node	$p=2$	1.71670E-05	–	1.17096E-06	3.38650E-06
	HFEM EMLGFM	4-node	$p=2$	1.72812E-05	1.98414E-05	1.21579E-06	3.40211E-06
			$p=3$	1.85336E-05	2.02973E-05	1.30106E-06	3.59869E-06
			$p=4$	1.90739E-05	2.03888E-05	1.35539E-06	3.66377E-06
			$p=5$	1.93844E-05	2.04344E-05	1.38701E-06	3.70534E-06
	GFEM EMLGFM	4-node	$le=1$	1.74455E-05	1.91330E-05	1.36960E-06	3.54420E-06
			$le=2$	1.83252E-05	2.02182E-05	1.29167E-06	3.57530E-06
			$le=3$	1.91198E-05	2.03447E-05	1.36781E-06	3.62261E-06
			$le=4$	1.77219E-05	2.04293E-05	1.38290E-06	3.70002E-06

Table 6.16 – Resultant displacement results for uniform and graded meshes on boundary.

RESULTANT DISPLACEMENT u ON BOUNDARY						
Radius r Angle θ Type of Mesh #				0.50000 135°		0.02250 135°
				UNIFORM	GRADED	GRADED
SOLUTION	ANALYTICAL			2.49572E-05		4.61202E-06
	MLGFM	4-node	$p=1$	1.83592E-05	2.14746E-05	4.09230E-06
		9-node	$p=2$	2.20168E-05	–	4.46178E-06
	HFEM EMLGFM	4-node	$p=2$	2.20593E-05	2.46434E-05	4.37781E-06
			$p=3$	2.36629E-05	2.51583E-05	4.57764E-06
			$p=4$	2.40073E-05	2.52272E-05	4.61881E-06
			$p=5$	2.43317E-05	2.52699E-05	4.65904E-06
	GFEM EMLGFM	4-node	$le=1$	2.29243E-05	2.40844E-05	4.55954E-06
			$le=2$	2.34408E-05	2.50784E-05	4.56082E-06
			$le=3$	2.40692E-05	2.52414E-05	4.63344E-06
			$le=4$	3.06029E-05	2.52665E-05	4.65523E-06

The error percentage shown in Tables 6.17 and 6.18 is worked out by the

expression $[(u)_h - u] / u * 100\%$.

Table 6.17 – Resultant displacement results for uniform and graded meshes in domain: error (%).

RESULTANT DISPLACEMENT u ERROR (%) IN DOMAIN							
		Radius r	Angle θ	0.70711 -90°		0.02250 45°	0.03182 -90°
		Type of Mesh	#	UNIFORM	GRADED	GRADED	GRADED
SOLUTION	FEM	4-node	$p=1$	38.36749%	89.10251%	245.05614%	121.30264%
	MLGFM	4-node	$p=1$	38.36749%	15.26804%	31.95215%	16.84514%
		9-node	$p=2$	14.43857%	–	19.49112%	8.66488%
	HFEM EMLGFM	4-node	$p=2$	13.86919%	1.10926%	16.40865%	8.24384%
			$p=3$	7.62744%	1.16286%	10.54622%	2.94177%
			$p=4$	4.93461%	1.61925%	6.81063%	1.18678%
			$p=5$	3.38701%	1.84633%	4.63651%	0.06550%
	GFEM EMLGFM	4-node	$le=1$	13.05054%	4.63993%	5.83379%	4.41151%
			$le=2$	8.66630%	0.76858%	11.19199%	3.57269%
			$le=3$	4.70572%	1.39937%	5.95651%	2.29674%
			$le=4$	11.67309%	1.82106%	4.91917%	0.20896%

Table 6.18 – Resultant displacement results for uniform and graded meshes on boundary: error (%).

RESULTANT DISPLACEMENT u ERROR (%) ON BOUNDARY						
		Radius r	Angle θ	0.50000 135°		0.02250 135°
		Type of Mesh	#	UNIFORM	GRADED	GRADED
SOLUTION	MLGFM	4-node	$p=1$	26.43736%	13.95422%	11.26884%
		9-node	$p=2$	11.78165%	–	3.25767%
	HFEM EMLGFM	4-node	$p=2$	11.61130%	1.25714%	5.07830%
			$p=3$	5.18587%	0.80605%	0.74549%
			$p=4$	3.80584%	1.08215%	0.14705%
			$p=5$	2.50631%	1.25287%	1.01941%
	GFEM EMLGFM	4-node	$le=1$	8.14559%	3.49723%	1.13795%
			$le=2$	6.07589%	0.48554%	1.11027%
			$le=3$	3.55807%	1.13878%	0.46445%
			$le=4$	12.84989%	1.23929%	0.93675%

Table 6.19 – Stress values for uniform and graded meshes in domain.

STRESS VALUES IN DOMAIN									
SOLUTION	Radius r			0.70711					
	Angle θ			-90°					
	Type of Mesh #			UNIFORM			GRADED		
	Stress σ			σ_x	σ_y	σ_{xy}	σ_x	σ_y	σ_{xy}
	ANALYTICAL			0.33961	1.58530	0.54136	0.33961	1.58530	0.54136
	FEM	4-node	$p=1$	0.50000	2.80870	1.07169	0.64832	3.65266	1.20105
	MLGFM	4-node	$p=1$	0.53400	1.87100	0.41360	0.31550	1.71500	0.22710
		9-node	$p=2$	0.75720	0.93960	0.65400	–	–	–
	HFEM EMLGFM	4-node	$p=2$	0.41390	1.83700	0.49690	0.34100	1.80600	0.55070
			$p=3$	0.32390	1.52500	0.59600	0.27470	1.58700	0.50630
			$p=4$	0.38990	1.64400	0.51230	0.35260	1.53600	0.51500
			$p=5$	0.35970	1.78000	0.52970	0.30850	1.54900	0.51890
	GFEM EMLGFM	4-node	$le=1$	0.34010	1.40600	0.51700	0.32270	1.48400	0.49620
			$le=2$	0.34840	1.38300	0.60530	0.40490	1.65500	0.57240
			$le=3$	0.39590	1.66400	0.50860	0.35100	1.59200	0.51850
			$le=4$	0.36680	1.80200	0.52810	0.37480	1.59700	0.54100

STRESS VALUES IN DOMAIN									
SOLUTION	Radius r			0.02250			0.03182		
	Angle θ			45°			-90°		
	Type of Mesh #			GRADED			GRADED		
	Stress σ			σ_x	σ_y	σ_{xy}	σ_x	σ_y	σ_{xy}
	ANALYTICAL			2.84597	8.64205	0.40766	1.39464	6.51021	2.22317
	FEM	4-node	$p=1$	1.87498	12.71200	2.96095	2.03775	11.28030	4.81076
	MLGFM	4-node	$p=1$	2.01000	8.61300	1.04100	2.07100	4.00600	3.31000
		9-node	$p=2$	–	–	–	2.18600	0.24140	2.41400
	HFEM EMLGFM	4-node	$p=2$	1.99900	8.89600	0.14060	0.29470	4.99400	2.60700
			$p=3$	2.23100	8.62000	0.54630	1.20700	6.11500	2.15500
			$p=4$	2.60200	9.13800	0.43490	1.25900	6.47400	2.43700
			$p=5$	3.06400	9.20500	0.39280	1.21100	6.58800	2.39700
	GFEM EMLGFM	4-node	$le=1$	1.86100	7.34300	0.35670	1.03300	5.19100	2.71100
			$le=2$	2.80200	8.44000	0.36120	1.29800	5.68300	2.49200
			$le=3$	2.60200	8.83600	0.43170	1.24600	6.12100	2.48600
			$le=4$	2.57600	8.86000	0.54380	1.20100	6.53600	2.08000

The error percentage shown in Table 6.20 is figured out by the expression

$[|(\sigma)_h - \sigma| / \sigma] * 100\%$ (σ_x , σ_y or σ_{xy} , depending on the case) where $(\cdot)_h$ means the approximate solution.

Table 6.20 – Stress error (%) for uniform and graded meshes in domain.

STRESS ERROR (%) IN DOMAIN									
		Radius	r	0.70711					
		Angle	θ	-90°					
		Type of Mesh	#	UNIFORM			GRADED		
		Stress	σ	σ_x	σ_y	σ_{xy}	σ_x	σ_y	σ_{xy}
SOLUTION	FEM	4-node	$p=1$	47.23%	77.17%	97.96%	90.90%	130.41%	121.86%
	MLGFM	4-node	$p=1$	57.24%	18.02%	23.60%	7.10%	8.18%	58.05%
		9-node	$p=2$	122.96%	40.73%	20.81%	–	–	–
	HFEM EMLGFM	4-node	$p=2$	21.88%	15.88%	8.21%	0.41%	13.92%	1.73%
			$p=3$	4.63%	3.80%	10.09%	19.11%	0.11%	6.48%
			$p=4$	14.81%	3.70%	5.37%	3.83%	3.11%	4.87%
			$p=5$	5.92%	12.28%	2.16%	9.16%	2.29%	4.15%
	GFEM EMLGFM	4-node	$le=1$	0.15%	11.31%	4.50%	4.98%	6.39%	8.34%
			$le=2$	2.59%	12.76%	11.81%	19.23%	4.40%	5.73%
			$le=3$	16.58%	4.96%	6.05%	3.36%	0.42%	4.22%
			$le=4$	8.01%	13.67%	2.45%	10.36%	0.74%	0.07%

STRESS ERROR IN DOMAIN									
		Radius	r	0.02250			0.03182		
		Angle	θ	45°			-90°		
		Type of Mesh	#	GRADED			GRADED		
		Stress	σ	σ_x	σ_y	σ_{xy}	σ_x	σ_y	σ_{xy}
SOLUTION	FEM	4-node	$p=1$	34.12%	47.10%	626.33%	46.11%	73.27%	116.39%
	MLGFM	4-node	$p=1$	29.37%	0.34%	155.36%	48.50%	38.47%	48.89%
		9-node	$p=2$	–	–	–	56.74%	96.29%	8.58%
	HFEM EMLGFM	4-node	$p=2$	29.76%	2.94%	65.51%	78.87%	23.29%	17.27%
			$p=3$	21.61%	0.26%	34.01%	13.45%	6.07%	3.07%
			$p=4$	8.57%	5.74%	6.68%	9.73%	0.56%	9.62%
			$p=5$	7.66%	6.51%	3.66%	13.17%	1.20%	7.82%
	GFEM EMLGFM	4-node	$le=1$	34.61%	15.03%	12.50%	25.94%	20.27%	21.94%
			$le=2$	1.55%	2.34%	11.40%	6.93%	12.71%	12.09%
			$le=3$	8.57%	2.24%	5.90%	10.66%	5.98%	11.82%
			$le=4$	9.49%	2.52%	33.40%	13.88%	0.40%	6.44%

The results for displacement present good conformity both using Lobatto shape functions (HFEM) and trigonometric shape functions (GFEM). It is visualized in this application some disturbance in values for GFEM approach. This aspect is attenuated in the graded mesh but, anyhow, it evidences when dealing with trigonometric shape functions, it is really important to observe how the EMLGFM matrices conditioning and integration treatment are affected. A Gauss quadrature points study was performed for this application. It was used 3, 16, 48 and 96 Gauss points in each coordinate direction. From 16 Gauss points on, there are no differences. But for 3 Gauss points, it is not possible to compute reasonable values from $p = 3$ or $le = 2$ on.

Another attribute that should be pointed out is the fact of GFEM employed here is different compared to Arndt (2009) applied in his study: each level of enrichment is not added “in group” with the enriched shape functions for left and right covering being added at the same time. Here, each enriched shape function corresponds to a level of enrichment and it doesn't matter if this enriched function measures up a left or right covering of the element. The enrichment “in groups” is not the object of study in this work but it should be better investigated in future ones.

Concerning stress values, the first part of the Tables 6.19 and 6.20 compares to uniform mesh values against graded mesh values (decimal digits has been restricted in order to better accommodate the tables). It is interesting to note that the values are slightly better for the graded mesh in both cases HFEM and GFEM approaches. Observing only the graded mesh and the closest node to the stress singularity, HFEM approach is slightly better than GFEM approach applied to the MLGFM. The same observation about this phenomenon can be enumerated here as discussed previously for the displacement case. It is worth remembering how the condition number can affect an equation system (see Table 6.22).

When it comes to stresses plotted against distance of the singularity, the values shown in Figures 6.33 and 6.34 are extracted from mesh domain nodes at $\theta = 0$.

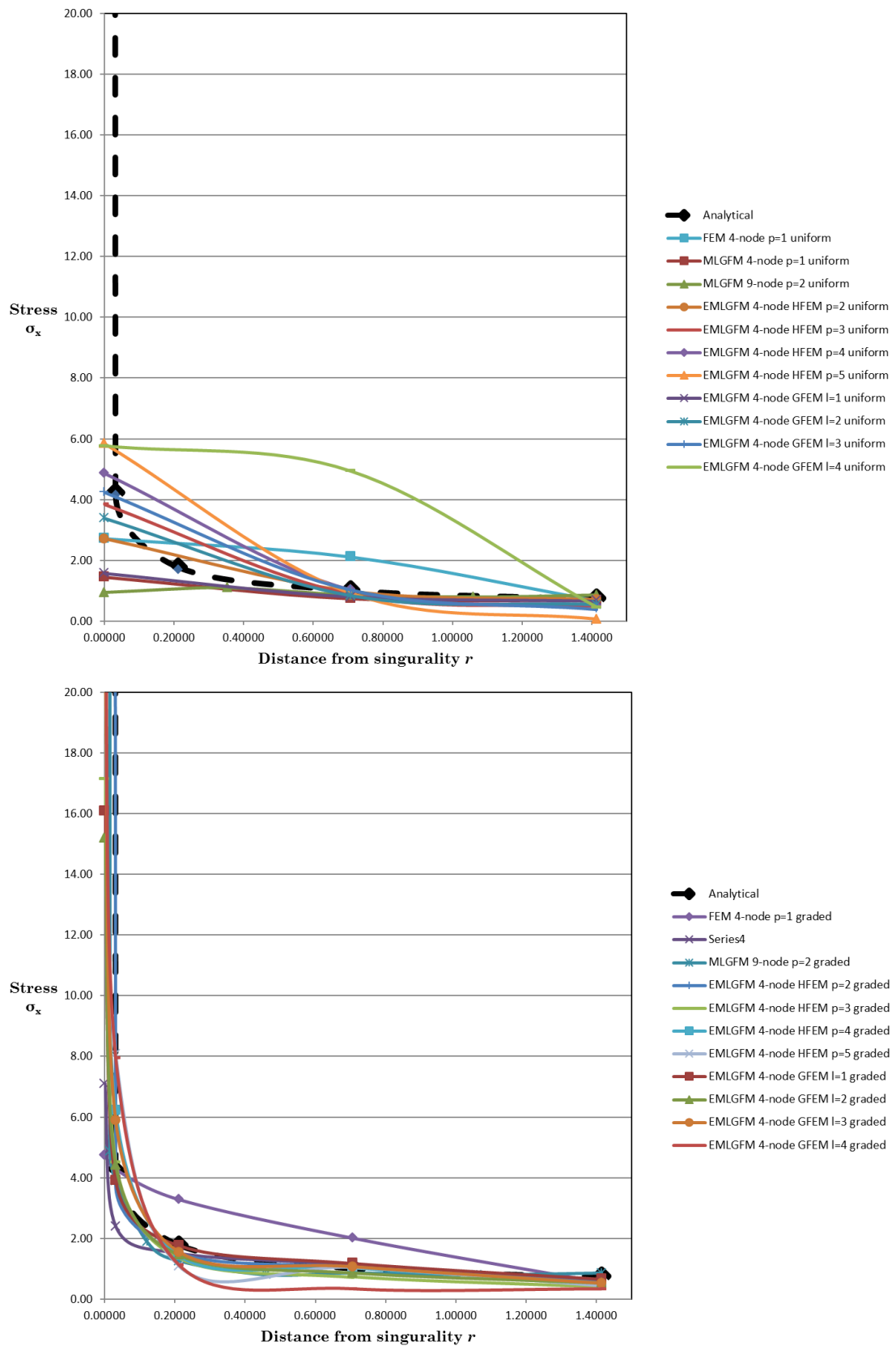


Figure 6.33— Stress curve: stress σ_x versus distance r from stress singularity for uniform and graded meshes.

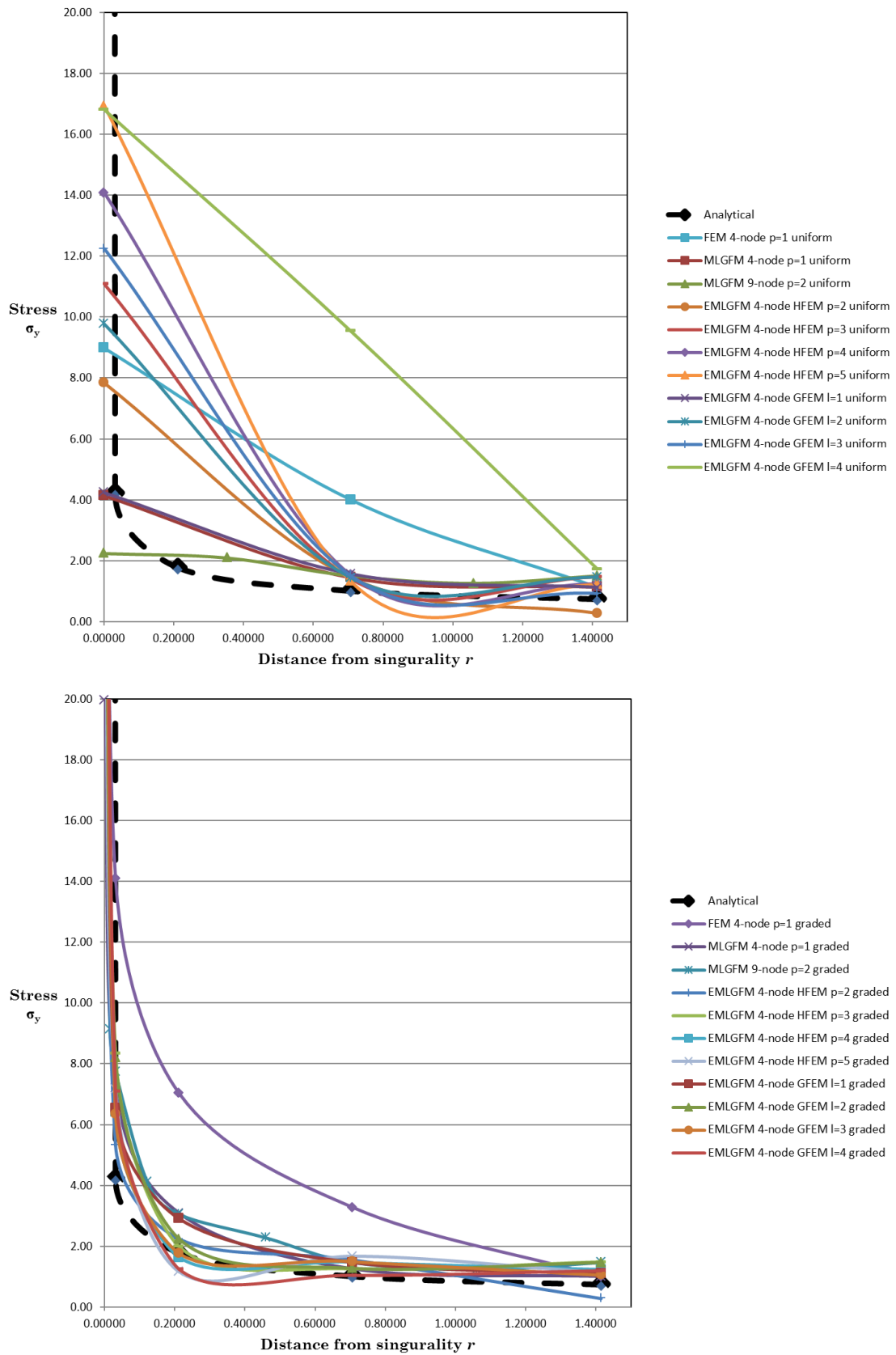


Figure 6.34— Stress curve: stress σ_y versus distance r from stress singularity for uniform and graded meshes.

It is clearly seen how poor is the uniform mesh for this kind of problem using only 12 elements. There is a significant improvement using graded mesh but, for GFEM approach at $le = 4$, the values are a little bit degraded. Remember those values are calculated by FEM procedures and they present similar accuracy as classic FEM. This situation may be overcome when using the “multi-cell – multi-element” MLGFM approach, i.e., the division of the problem into several “Green’s cells”, allowing the results of very precise stresses inside the mesh. Anyhow, for graded mesh, all curves show same decaying pattern.

Now, observe the numerical error values of the generalized stress-intensity factor K_I exposed in Table 6.21. Note those values are calculated by Equations 6.49 and 6.50 and extrapolated to $r = 0$ using “*Displacement Extrapolation Method*” (HAN *et al.*, 2015). Again, the extrapolation method to numerically determine stress intensity factor K_I presented by Zafošnik and Fajdiga (2016) is adopted here. The displacements are extracted from boundary nodes of the graded mesh.

Table 6.21 – K_I error (%) calculated from displacements on boundary: graded mesh.

NUMERICAL $(K_I)_h$ ERROR (%)					
Displacement direction				u_x	u_y
SOLUTION	MLGFM	4-node	$p=1$	35.09952%	10.19168%
		9-node		25.61469%	1.59704%
	HFEM EMLGFM	4-node	$p=2$	22.77459%	2.96872%
			$p=3$	12.73410%	0.55346%
			$p=4$	9.49882%	1.16566%
			$p=5$	6.29349%	1.68135%
	GFEM EMLGFM	4-node	$le=1$	30.41035%	5.01159%
			$le=2$	14.07152%	0.27070%
			$le=3$	10.31149%	0.97377%
			$le=4$	6.58542%	1.63098%

The error percentage displayed in Table 6.21 is also worked out by the expression $[|(K_I)_h - K_I| / K_I] * 100\%$, where $(K_I)_h$ is the approximate stress intensity factor and K_I is the analytical stress intensity factor, in the case here, $K_I = 1$.

Interesting to observe both HFEM and GFEM approaches produce lesser error once the polynomial order or level of enrichment are increased as expected. The conventional MLGFM 9-node presents excellent results when calculating $(K_I)_h$ by displacement u_y as well as EMLGFM in both approaches: HFEM and GFEM.

Wrapping up the application section, it is intriguing to note how GFEM approach is affected by the condition number expressed in Table 6.22. There is a substantial difference between the uniform and graded meshes but even more relevant comparing the differences in higher orders for GFEM approach. Considering that the selected enriched shape function is appropriated and representative for the studied problem, alternatives to improve the matrix conditioning such as the incomplete Cholesky-Conjugate Gradient Method (KERSHAW, 1978) may upgrade the numerical results in both cases: HFEM and GFEM approaches applied to the MLGFM. This subject is not studied and it is suggested to be better detailed in future works.

Table 6.22 – Condition number for K matrix.

CONDITION NUMBER: cond(K)					
Problem: Case type: Number of elements:				L-shaped domain	
				UNIFORM 12 elements	GRADED 24 elements
SOLUTION	MLGFM	4-node	$p=1$	2.89780E+04	2.27140E+03
			$p=2$	3.50650E+04	2.50430E+05
		4-node	$p=3$	3.51420E+04	2.54000E+05
			$p=4$	3.51500E+04	2.54480E+05
			$p=5$	3.51530E+04	2.54650E+05
	GFEM EMLGFM	4-node	$le=1$	3.26960E+04	2.31630E+05
			$le=2$	3.67980E+04	2.69250E+05
			$le=3$	2.71390E+06	1.38390E+08
			$le=4$	1.31090E+07	1.03190E+08

Chapter 7

Conclusions and Recommendations for Future Work

7.1 SUMMARY

This work presented the first attempt to enrich the Modified Local Green's Function Method using a Hierarchical Finite Element Method (HFEM) approach as well as a Generalized Finite Element (GFEM) approach. In order to do so, for the Hierarchical Finite Element approach, it is employed the Lobatto shape functions whereas for the Generalized Finite Element is exploited trigonometric functions suggested firstly by Arndt (2009) and improved by Torii (2012). These trigonometric shape functions are also related to the analytical solution. Also, it is imperative to highlight all EMLGFM applications used only one “green cell”, i.e., one cell for the whole domain (unicell-multielement approach).

It has been exposed a deep literature review focusing on FEM and its extensions in HFEM and GFEM concepts as well as in MLGFM. It has also been dedicated a particular chapter for the enriched methods exploring the Hierarchical Finite Element (HFEM) and the Generalized Finite Element Method (GFEM) as well as a dedicated chapter for the Modified Local Green's Function Method (MLGFM). In there, the mathematical formulation for each

approach has been showed focusing afterwards in how to enrich MLGFM shape functions space.

When it concerns the applications employed in this work aiming to investigate EMLGFM, it is firstly important to mention the words expressed by Prof. Roberto Dalledone Machado (MACHADO, 1992): “When Barcellos and Silva (1987) idealized the Modified Local Green's Function Method (MLGFM), they realized that they were dealing with a powerful computational analysis tool to solve mechanical problems. This new instrument, however, needed to be better investigated in order to prove its potential”. After 30 years of their proposal, it is possible and secure to say that this tool was successfully investigated and tested in a wide range of engineering problems, such that already quoted in this text but again referred to: potential problems, 2D and 3D elasticity problems, fracture mechanics problems, composite laminate problems, damage and its evolution problems and others. And now, its formulation has been improved with the new advances in Finite Element techniques.

It has been chosen a very simple 2D plane stress elasto static problem to start with: the straight cantilever beam. Starting with that, a wide investigation for this first example was applied. Firstly, a study was performed considering a Hierarchical Finite Element approach using Lobatto shape functions with order $p = 2$ only. The main objective was to test the differences among enriching only the domain, only the boundary and both at the same time without changing the polynomial order. It has been proved that “the complete enrichment”, i.e., enriching both shape function spaces in domain and on boundary, provided the best results. Also, for problem primarily dominated by shear, EMLGFM demonstrated its superiority. In other studies performed for this application, it was employed polynomial order from $p = 2$ to $p = 5$. So, when it comes to the aspect ratio (L/h), EMLGFM could keep good values for different displacement values of L/h but the best performance was achieved for stress values, as expected. It is worth mentioning that MLGFM had already presented excellent results for flow variables as stresses but it seems that this characteristic was accentuated for EMLGFM. Also, in this application, a convergence rate study was executed demonstrating good performance and faster convergence than the other

compared methods. A computational cost analysis was presented for this application with polynomial order $p = 2$, focusing on the time reduction when disregarding \mathbf{G}^{DP} since this example does not present body forces. And, concluding the study of this application, it was verified how the matrix conditioning is affected when the polynomial order is increased.

For the second application, it has been chosen the curved cantilever beam in plane stress state. It is an interesting study since the element shape is slightly irregular. In this analysis, it was only considered Lobatto shape functions of order $p = 2$. Again, EMLGFM showed excellent results.

For the third application, an impressive case of near incompressibility was investigated using the thick-walled cylinder study in a plane strain condition, using Lobatto shape functions of polynomial order from $p = 2$ to $p = 5$. In this study, EMLGFM really proved to be remarkable, keeping excellent displacement results for different Poisson's ratio, showing again high accuracy for stress values and improving its results when increasing the polynomial order.

For the fourth application, a rectangular plate with a center hole loaded by tractions was modeled in plane stress state, using Lobatto shape functions of polynomial order from $p = 2$ to $p = 5$. This specific case produces a stress concentration in the end border of the hole. It was also performed a computational cost analysis but here varying the polynomial order from $p = 2$ to $p = 5$. There was a strong reduction in calculation elapsed time when \mathbf{G}^{DP} was not calculated, being really accentually for $p = 5$. In this case, EMLGFM could extract the stress concentration factor " K_{tn} " with better precision when compared to the other studied methods.

For the fifth application, a rectangular plate with a center crack loaded by tractions was discretized in plane strain condition, using Lobatto shape functions of polynomial order from $p = 2$ to $p = 5$ and trigonometric enriched functions of level $le = 1$ to $le = 4$. This is also a tough example to be studied since the singularity at the tip crack is more accentuated. But EMLGFM presented excellent results both for Hierarchical Finite Element and for Generalized Finite Element approaches. It has been possible to predict the stress intensity factor (K_I) with a small error percentage.

And for the sixth and last application, a L-shaped domain with singularity loaded by tractions was tested in plane strain state, using Lobatto shape functions of polynomial order from $p = 2$ to $p = 5$ and trigonometric enriched functions of level $le = 1$ to $le = 4$. A Gauss quadrature points study was performed, varying the number of points from 3 to 96 Gauss points in each coordinate direction and concluded a great disturbance only for 3 Gauss points. This example showed good results but evidenced one more time the situation about the condition number. It is interesting to observe that the condition number is worse when using a graded mesh and even worse for trigonometric functions in higher levels of enrichment.

Observing the examples used in this work, naturally some conclusions and recommendations can be mentioned. One of them is the Modified Local Green's Function Method (MLGFM) can be considered as a "coarse mesh method", since, with few elements in the discretization, a high degree of results accuracy is reached and it also presents high rates of convergence. This characteristic is intensified in the Enriched Modified Local Green's Function Method (EMLGFM). So, it is natural to think of using it in adaptive procedures in future works.

Another point that could be better studied is the "sub-regions" or "Green's cells" subject. Throughout this work, a single "cell" (unicell-multielement approach) was used to discretize the problem, consisting of a finite element mesh in domain, and another one associated with the boundary, by means of boundary elements. This approach may limit the studies of MLGFM and EMLGFM to linear problems with coarse meshes, extracting precise flow variables only on boundary. The division of the problem into several "cells", with well-established boundary conditions among them, will allow the results of very precise stresses in a sub-region boundary, corresponding to the domain interior of the problem. The original Silva's model (SILVA, 1988) for MLGFM and the sub-regional treatment studied by Mendonça (1995), Barbieri and Machado (2015) represent alternatives that deserve to be implemented.

Allied to the "multicell" approach and adaptive procedures, it would be interesting to test singular problems using GFEM^{gl} like exposed by Gupta *et al.*

(2012). Or even test GFEM with “multiscale” approach (MS-GFEM) suggested by Friderikos *et al.* (2017) in fracture mechanics problems. Even more it has been employed the C^k formulation proposed by Duarte *et al.* (2006) and this might be tested in MLGFM too.

An important point to consider here is this work explored only 1D linear (2-node) and 2D bilinear (4-node quadrilateral) elements with Lagrange shape functions as PoU. The concepts exposed here can be applied to other kind of elements, such that, 1D quadratic (3-node) and 2D quadratic (9-node) elements, serendipity, cubic, and so on as well as other kind of elements, e.g., a triangular type. Also, different types of PoU can be explored, e.g., Shepard and trigonometric functions, among others.

There is a huge lane for EMLGFM when it concerns its enrichment process. The concepts used in this text are based on the formulation proposed by Šolín *et al.* (2004) but other formulation can be adapted to MLGFM. Also, it has been exploited the enrichment by Lobatto shape functions and trigonometric shape functions. There are a lot of other possible shape functions both using as partition of unity and enrichment functions to be explored and tested in EMLGFM. And an abundant levels of enrichment to be employed too.

Having mentioned that, it is relevant to emphasize how important is the condition number and computational cost for MLGFM and even more for EMLGFM. There is a considerable computational cost in calculating the Green's function projections. Since these functions are figured out using extensions of the stiffness matrix, it is imperative to keep the condition number as lower as possible. One way of doing that would be using the stable GFEM – SGFEM treatment in EMLGFM (BABUŠKA *et al.*, 2017). Also, MLGFM and EMLGFM are implemented in the FORTRAN platform. New methods, programming languages could be exploited now here, improving EMLGFM algorithm.

And, finally wrapping up this conclusion, this is just the beginning for the Enriched Modified Local Green's Function Method. All above comments can be extended to other important and vital applications in solid mechanics, such as, Midlin's plate, laminate composite, free-vibration problems, dynamic problem using transient analysis, buckling, nonlinear problems, and damages and so on.

References

ABDELAZIZ, Y.; HAMOUINE, A. A survey of the extended finite element. **Computers and Structures**, v. 86, n. 11–12, p. 1141–1151, 2008.

ALVES, M. M. **Método da Partição na Análise de Múltiplas Fissuras**, Thesis (Doutorado em Engenharia de Estruturas), Universidade de São Paulo, São Carlos, Brasil, 2010..

ALVES, P. D. **Estratégia Global-Local Aplicada ao Método dos Elementos Finitos Generalizados**. Dissertation (Mestre em Engenharia de Estruturas), Universidade Federal de Minas Gerais, Belo Horizonte, Brasil, 2012.

AMORIM, D. L. N. DE F. **Formulações Híbridas e Mistas para o Método dos Elementos Finitos Generalizados: Aplicação à Mecânica do Dano**. Dissertation (Mestre em Engenharia de Estruturas), Universidade de São Paulo, São Carlos, 2012..

ANDERSON, T. L. **Fracture Mechanics: Fundamentals and Applications**. 3rd ed. Boca Raton, FL: CRC Taylor & Francis Group, 2005.

ARAGÓN, A. M.; DUARTE, C. A.; GEUBELLE, P. H. Generalized finite element enrichment functions for discontinuous gradient fields. **International Journal for Numerical Methods in Engineering**, v. 10, p. 1–6, 2008.

ARAGÓN, A. M.; SIMONE, A. The Discontinuity-Enriched Finite Element Method. **International Journal for Numerical Methods in Engineering**, v. 112, n. 11, p. 1589–1613, 2017.

ARGÔLO, H. S. D. DE. **Emprego de Formulações Não-Convencionais de Elementos Finitos na Análise Linear Bidimensional de Sólidos com Múltiplas Fissuras**. Dissertation (Mestre em Engenharia de Estruturas), Universidade de São

Paulo, São Carlos, Brasil, 2010.

ARNDT, M.; MACHADO, R. D.; HECKE, M. B. The composite element method applied to free vibration analysis of trusses and beams. **Applied Numerical Mathematics**, v. 47, n. 2, p. 59–73, 2003.

ARNDT, M. **O Método dos Elementos Finitos Generalizado aplicado à Análise de Vibrações Livres de Estruturas Reticuladas**. Thesis (Doutorado em Métodos Numéricos em Engenharia), Universidade Federal do Paraná, Curitiba, Brasil, 2009.

ARNDT, M.; MACHADO, R. D.; SCREMIN, A. An adaptive generalized finite element method applied to free vibration analysis of straight bars and trusses. **Journal of Sound and Vibration**, v. 329, n. 6, p. 659–672, 2010.

ARNDT, M.; MACHADO, R. D.; SCREMIN, A. The Generalized Finite Element Method Applied to Free Vibration of Framed Structures. **Advances in Vibration Analysis Research**, , n. c, p. 187–212, 2011.

ARNDT, M.; MACHADO, R. D.; SCREMIN, A. Accurate assessment of natural frequencies for uniform and non-uniform Euler-Bernoulli beams and frames by adaptive generalized finite element method. **Engineering Computations**, v. 33, n. 5, p. 1586–1609, 2016.

ARNDT, M.; TORII, A. J.; MACHADO, R. D.; SCREMIN, A. Generalized Finite Element Method for Vibration Analysis of Bars. **Proceedings of 10th World Congress on Computational Mechanics**. Blucher Mechanical Engineering Proceedings. . v. 1, 2014.

BABUŠKA, I.; CALOZ, G.; OSBORN, J. E. Special Finite Element Methods for a Class of Second Order Elliptic Problems with Rough Coefficients. **SIAM Journal on Numerical Analysis**, v. 31, n. 4, p. 945–981, 1994.

BABUŠKA, I.; IHLENBURG, F.; PAIK, E. T.; SAUTER, S. A. A Generalized Finite Element Method for solving the Helmholtz equation in two dimensions with minimal pollution. **Computer Methods in Applied Mechanics and Engineering**, v. 128, n. 3–4, p. 325–359, 1995.

BABUŠKA, I.; MELENK, J. M. The partition of unity method, Int. **J. Numer. Methods Engrg.**, v. 40, n. 4, p. 727–758, 1997.

BABUŠKA, I.; ZHANG, Z. The partition of unity method for the elastically supported beam. **Computer Methods in Applied Mechanics and Engineering**, v. 152, n. 1–2, p. 1–18, 1998.

BABUŠKA, I.; SAUTER, S. A. Is The Pollution Effect of the FEM Avoidable for the Helmholtz Equation Considering High Wave Numbers? **SIAM Journal on Numerical Analysis**, v. 42, n. 3, p. 451–484, 2000.

BABUŠKA, I.; BANERJEE, U.; OSBORN, J. E. On principles for the selection of shape functions for the Generalized Finite Element Method. **Computer Methods in Applied Mechanics and Engineering**, v. 191, n. 49–50, p. 5595–5629, 2002.

BABUŠKA, I.; BANERJEE, U.; OSBORN, J. E. Survey of meshless and generalized finite element methods: A unified approach. **Acta Numerica**, v. 12, n. July 2003, p. 1–125, 2003.

BABUŠKA, I.; BANERJEE, U.; OSBORN, J. E. Generalized Finite Element Methods — Main Ideas, Results and Perspective. **International Journal of Computational Methods**, v. 1, n. 1, p. 67–103, 2004.

BABUŠKA, I. M.; NISTOR, V.; TARFULEA, N. Approximate and low regularity Dirichlet boundary conditions in the generalized finite element method. **Mathematical Models and Methods in Applied Sciences**, v. 17, n. 12, p. 2115–2142, 2007a.

BABUŠKA, I.; BANERJEE, U.; OSBORN, J. E. Superconvergence in the generalized finite element method. **Numerische Mathematik**, v. 107, n. 3, p. 353–395, 2007b.

BABUŠKA, I.; NISTOR, V.; TARFULEA, N. Generalized finite element method for second-order elliptic operators with Dirichlet boundary conditions. **Journal of Computational and Applied Mathematics**, v. 218, n. 1, p. 175–183, 2008.

BABUŠKA, I.; LIPTON, R. Optimal Local Approximation Spaces for Generalized Finite Element Methods with Application to Multiscale Problems. **Multiscale Modeling & Simulation**, v. 9, n. 1, p. 373–406, 2011.

BABUŠKA, I.; BANERJEE, U. Stable Generalized Finite Element Method (SGFEM). **Computer Methods in Applied Mechanics and Engineering**, v. 201–204, p. 91–111, 2012.

BABUŠKA, I.; BANERJEE, U.; KERGRENE, K. Strongly stable generalized finite element method: Application to interface problems. **Computer Methods in Applied Mechanics and Engineering**, v. 327, p. 58–92, 2017.

BARBIERI, R.; BARCELLOS, C.S. Solution of the potential problem by the modified local green's function method (MLGFM). **Proceedings of XI COBEM – Brazilian Congress of Mechanical Engineering**, São Paulo, 1991a.

BARBIERI, R.; BARCELLOS, C. S. A Modified Local Green's Function Technique for the Mindlin's Plate Model. **Proceedings of XIII BEM Conference**, Tulsa, USA, p. 551-565, 1991b.

BARBIERI, R. **Desenvolvimento e Aplicação do Método da Função de Green Local Modificado (MLGFM) para Problemas do Meio Contínuo**, Thesis (Doutorado em Engenharia Mecânica), Universidade Federal de Santa Catarina, Brasil, 1992.

BARBIERI, R.; MACHADO, R. D.; FILIPPIN, C. G.; BARCELLOS, C. S. O método da função de green local modificado (MLGFM) aplicado a problemas da mecânica do contínuo: Parte i – elasto estática. **Proceedings of XIII CILAMCE - Cong. Ibero Latino-Americano sobre Métodos Computacionais para Engenharia**, Porto Alegre, 1992.

BARBIERI, R.; BARCELLOS, C. S. Non-Homogeneous Field Potential Problems Solution by the Modified Local Green's Function Method (MLGFM). **Engineering Analysis with Boundary Elements**, UK, v.11, n.1, p. 9-15, 1993a.

BARBIERI, R.; BARCELLOS, C. S. Mindlin's Plate Solutions by the MLGFM. **Proceedings of XV BEM - International Conference on Boundary Element Method**, Albuquerque, USA, v.2, p.149-164, 1993b.

BARBIERI, R.; NOEL, A. T.; BARCELLOS, C. S. A green's function approach to shell analysis. **Proceedings of BEM XV - International Conference on Boundary Element Methods** 2, p. 179–194, 1993a.

BARBIERI, R.; BARCELLOS, C. S.; MACHADO, R. D.; FILIPPIN, C. G. O Método da Função de Green Local Modificado (MLGFM) aplicado Placa de Mindlin. **Proceedings of Congresso Brasileiro de Engenharia Mecânica**, Brasília. Anais do XII COBEM,

1993b.

BARBIERI, R.; MUÑOZ, R. P. A.; MACHADO, R. D. Modified Local Green's Function Method (MLGFM) Part I. Mathematical background and formulation. **Engineering Analysis with Boundary Elements**, v. 22, n. 2, p. 141–151, 1998.

BARBIERI, R.; MUÑOZ, R. P. A. Modified Local Green's Function Method (MLGFM) Part II. Application for accurate flux and traction evaluation. **Engineering Analysis with Boundary Elements**, v. 22, n. 2, p. 153–159, 1998.

BARBIERI, R.; MACHADO, R. D. The Local Formulation for the Modified Green's Function Method. **Latin American Journal of Solids and Structures**, v. 12, n. 5, p. 883–904, 2015.

BARCELLOS, C. S.; SILVA, L. H. M. Elastic membrane solution by a modified local Green's function method. In Brebbia CA, Venturini editors, W.S. **Proceedings of the international conference on boundary element technology**, Southampton, UK of Applied Mechanics, v. 69, i. 3, p. 145–59, 1987.

BARCELLOS, C. S.; BARBIERI, R.. Solution of singular potential problems by the modified local green's function method (MLGFM), **Proceedings of XIII BEM Conference**, Ed. Brebbia, C.A., 1991.

BARCELLOS, C. S.; BARBIERI, R.; MACHADO, R. D.; FILIPPIN, C. G. Método modificado da função de green local (MLGFM) - uma nova alternativa para a solução de problemas da mecânica - parte i: Descrição do método. **Proceedings of 7o SIBRAT - Simpósio Brasileiro Sobre Tubulações e Vasos de Pressão**, Florianópolis, 1992a.

BARCELLOS, C. S.; BARBIERI, R.; MACHADO, R. D.; FILIPPIN, C. G. Método modificado da função de green local (MLGFM) - uma nova alternativa para a solução de problemas da mecânica - parte ii: Aplicações. **Proceedings of 7o SIBRAT - Simpósio Brasileiro Sobre Tubulações e Vasos de Pressão**, Florianópolis, 1992b.

BARCELLOS, C. S.; BARBIERI, R.; MUÑOZ, R. P. A.; MEIRA, J. A. D. A comparison of the modified local green's function method (MLGFM) and the finite element method (FEM) for some problems in 3-D elasticity. **Proceedings of XVI CILAMCE - Congresso Ibero Latino Americano de Métodos Computacionais para a Engenharia**, Curitiba, p. 80-89, 1995.

BARCELLOS, C. S. DE; MENDONÇA, P. DE T. R.; DUARTE, C. A. A C^k continuous generalized finite element formulation applied to laminated Kirchhoff plate model. **Computational Mechanics**, v. 44, n. 3, p. 377–393, 2009.

BARROS, F. B. **Métodos sem malha e método dos elementos finitos generalizados em Análise Não-Linear de Estruturas**. Thesis (Doutorado em Engenharia de Estruturas), Universidade de São Paulo, São Carlos, Brasil, 2002.

BARROS, F. B.; PROENÇA, S. P. B.; DE BARCELLOS, C. S. Generalized finite element method in structural nonlinear analysis - a p-adaptive strategy. **Computational Mechanics**, v. 33, n. 2, p. 95–107, 2004.

BARROS, F. B.; DE BARCELLOS, C. S.; DUARTE, C. A. P-Adaptive C^k generalized finite element method for arbitrary polygonal clouds. **Computational Mechanics**, v. 41, n. 1, p. 175–187, 2007.

BARROS, F. B.; DE BARCELLOS, C. S.; DUARTE, C. A.; TORRES, D. A. F. Subdomain-based error techniques for generalized finite element approximations of problems with singular stress fields. **Computational Mechanics**, v. 52, n. 6, p. 1395–1415, 2013.

BATHE, K. J. **Finite Element Procedures**, Prentice Hall, Upper Saddle River, N. J. , 1996.

BAZÁN, F. S. V. Autovalores de Polinômios Matriciais: Sensibilidade, Computação e Aplicação. [S.l.: s.n.], ISBN 85-244-0206-7, 2003.

BECKER, E. B.; CAREY, G. F.; ODEN, J. T. **Finite Elements: An Introduction, Volume I**. Prentice-Hall, Inc., 1981.

BELYTSCHKO, T.; LU, Y. Y.; GU, L. Crack propagation by element-free Galerkin methods. **Engineering Fracture Mechanics**, v. 51, n. 2, p. 295–315, 1995.

BELYTSCHKO, T.; GRACIE, R.; VENTURA, G. A review of extended/generalized finite element methods for material modeling. **Modelling and Simulation in Materials Science and Engineering**, v. 17, n. 4, 2009.

BENVENUTI, E. An effective XFEM with equivalent eigenstrain for stress intensity factors of homogeneous plates. **Computer Methods in Applied Mechanics and Engineering**, v. 321, p. 427–454, 2017.

BESLIN, O.; NICOLAS, J. A hierarchical functions set for predicting very high order plate bending modes with any boundary conditions. **Journal of Sound and Vibration**, v. 202, n. 5, p. 633–655, 1997.

BREBBIA, C. A.; DOMINGUEZ, J. **Boundary Elements An Introductory Course**. 2nd Ed ed. WIT Press/Computational Mechanics Publications, 1992.

BREBBIA, C. A.; TELLES, J. C. F.; WROBEL, L. C. **Boundary Element Techniques: Theory and Applications in Engineering**. Springer-Verlag Berlin, Heidelberg, 1984

BURNS, T. J. **The partial current balance method: A local Green's function technique for the numerical solution of multidimensional neutron diffusion problems**. Thesis (Doctor of Philosophy), University of Illinois, Urbana, USA, 1975.

CAMPION, S. D.; JARVIS, J. L. An investigation of the implementation of the p-version finite element method. **Finite Elements in Analysis and Design**, v. 23, p. 1- 21, 1996.

CANALES, D.; LEYGUE, A.; CHINESTA, F. Vademecum-based GFEM (V-GFEM): optimal enrichment for transient problems. **International Journal for Numerical Methods in Engineering**, v. 108, p. 971–989, 2016.

CERVELIN, D. **Método dos Elementos Finitos Generalizado: Desenvolvimento e Aplicação em Análise Não-Linear Utilizando Elemento de Pórtico Espacial de Alta Ordem**. Dissertation (Mestre em Engenharia), Pontifícia Universidade Católica do Paraná, Curitiba, Brasil, 2014.

CHEN, K.; LI, Q.; LU, J.; WRIGHT, S. J. Randomized sampling for basis functions construction in generalized finite element methods. **Report**, 2018.

CHESSA, J.; BELYTSCHKO, T. A local space-time discontinuous finite element method. **Computer Methods in Applied Mechanics and Engineering**, v. 195, n. 13–16, p. 1325–1343, 2006.

CIARLET, P. G. Basic Error Estimates for Elliptic Problems. **Handbook of numerical analysis: Volume II; Finite Element Methods (Part 1)**, v. 11, n. Part 1, 1991.

CRAMER, H.; RUDOLPH, M.; STEINL, G.; WUNDERLICH, W. A hierarchical adaptive finite element strategy for elastic–plastic problems. **Computers & Structures**, v. 73, n. 1–5, p. 61–72, 1999.

DAUX, C.; MOES, N.; DOLBOW, J.; SUKUMAR, N.; BELYTSCHKO, T. Arbitrary branched and intersecting cracks with extended finite element method. **International Journal for Numerical Methods in Engineering**, v. 48, n. 12, p. 1741–1760, 2000.

DE, S.; BATHE, K. J. The method of finite spheres with improved numerical integration. **Computers and Structures**, v. 79, n. 22–25, p. 2183–2196, 2001.

DEUFLHARD, P.; LEINEN, P.; YSERENTANT, H. Concepts of an adaptive hierarchical finite element code. **IMPACT of Computing in Science and Engineering**, v. 1, n. 1, p. 3–35, 1989.

DOHERTY, W.P.; WILSON, E.L.; TAYLOR, R.L. Stress analysis of axi-symmetric solids using higher-order quadrilateral finite elements, **Structural Engineering Laboratory Report No. SESM 69-3**, University of California, Berkeley, 1969.

DUARTE, C. A.; ODEN, J. T. Hp clouds a meshless method to solve boundary-value problems. **Texas Institute for Computational and Applied Mathematics**, TICAM Report 95-05, 1995.

DUARTE, C. A. **The HP Cloud Method**. Thesis (Doctor of Philosophy), University of Texas at Austin, 1996.

DUARTE, C. A.; ODEN, J. T. An h-p adaptive method using clouds. **Computer Methods in Applied Mechanics and Engineering**, v. 139, n. 1–4, p. 237–262, 1996a.

DUARTE, C. A.; ODEN, J. T. H-p Clouds - An h-p Meshless Method. **Numerical Methods for Partial Differential Equations**, v. 12, n. 6, p. 673–705, 1996b.

DUARTE, C. A.; BABUŠKA, I.; ODEN, J. T. Generalized finite element methods for three-dimensional structural mechanics problems. **Computers and Structures**, v. 77, n. 2, p. 215–232, 2000.

DUARTE, C. A.; HAMZEH, O. N.; LISZKA, T. J.; TWORZYDLO, W. W. **A generalized finite element method for the simulation of three-dimensional dynamic crack propagation**. *Computer Methods in Applied Mechanics and Engineering*, v. 190, n. 15–17, p. 2227–2262, 2001.

DUARTE, C. A.; BABUSKA, I. Mesh independent p-orthotropic enrichment using the generalized finite element method. **International Journal for Numerical Methods**

in **Engineering**, , n. 0, p. 1–16, 2002.

DUARTE, C. A.; LISZKA, T. J.; TWORZYDLO, W. W.; WESTERMANN, T. A. The Generalized Finite Element Method - Improving Finite Elements Through Meshless Technology. **Civil Engineering Studies, Structural Research Series n. 639**, Report, 2005a.

DUARTE, C.; MIGLIANO, D.; BECKER, E. A Technique to Combine Meshfree-and Finite Element-Based Partition of Unity Approximations. **Civil Engineering Studies, Structural Research Series no 638**, Report, 2005b.

DUARTE, C. A.; KIM, D. J.; QUARESMA, D. M. Arbitrarily smooth generalized finite element approximations. **Computer Methods in Applied Mechanics and Engineering**, v. 196, n. 1–3, p. 33–56, 2006.

DUARTE, C. A.; LISZKA, T. J.; TWORZYDLO, W. W. Clustered generalized finite element methods for mesh unrefinement, non-matching and invalid meshes. **International Journal for Numerical Methods in Engineering**, v. 69, n. 11, p. 2409–2440, 2007a.

DUARTE, C. A.; RENO, L. G.; SIMONE, A. A high-order generalized FEM for through-the-thickness branched cracks. **International Journal for Numerical Methods in Engineering**, v. 72, n. 3, p. 325–351, 2007b.

DUARTE, C. A.; KIM, D.-J.; BABUŠKA, I. A global-local approach for the construction of enrichment functions for the generalized FEM and its application to propagating three-dimensional cracks. **ECCOMAS Thematic Conference on Meshless Methods**, p. 1–26, 2007c.

DUARTE, C. A.; KIM, D. J. Analysis and applications of a generalized finite element method with global-local enrichment functions. **Computer Methods in Applied Mechanics and Engineering**, v. 197, n. 6–8, p. 487–504, 2008.

ENGELS, R. Finite element modeling of dynamic behavior of some basic structural members. **Journal of Vibration and Acoustics**, v. 114, n. 1, p. 3–9, 1992.

EVANGELISTA, F.; ROESLER, J. R.; DUARTE, C. A. Two-scale approach to predict multi-site cracking potential in 3-D structures using the generalized finite element method. **International Journal of Solids and Structures**, v. 50, n. 13, p. 1991–2002,

2013.

FILIPPIN, C. G. **Desenvolvimento e aplicação do método da função de green local modificado à equação de helmholtz**. Dissertation (Mestre em Engenharia Mecânica), Universidade Federal de Santa Catarina, Florianópolis, Brasil, 1992.

FILIPPIN, C.G., BARBIERI, R., BARCELLOS, C.S. Numerical results for h- and p-convergences for the modified local green's function method. **Proceedings of 14th International Conference Boundary Element Technology**, USA, 1992a.

FILIPPIN, C.G., BARBIERI, R., MACHADO, R. D., BARCELLOS, C.S. The modified local green's function method (MLGFM) applied to continuum mechanics problems: part III – helmholtz equation problems. **Proceedings of XIII CILAMCE – Latin American Congress on Computational Methods for Engineering**, Porto Alegre, Brazil, 1992b.

FILIPPIN, C.G., BARBIERI, R., MACHADO, R. D., BARCELLOS, C.S. The modified local green's function method (MLGFM) as a computational tool for free vibration problems. Brazilian Acoustic Society – SOBRAC – Acoustic and Vibrations Magazine, Vol. 11, 1992c.

FILIPPIN, C. G.; MACHADO, R. D.; BARBIERI, R., MUNOZ R., P. A.; BARCELLOS, C. S. Aplicação do Método da Função de Green Local Modificado em Problemas de Vibração Livre de Membranas e Cavidades Acústicas. **Proceedings of – Congresso Brasileiro de Engenharia Mecânica**, Brasília. Anais do XII COBEM, 1993.

FILLMORE, T. B.; DUARTE, C. A. A hierarchical non-intrusive algorithm for the generalized finite element method. **Advanced Modeling and Simulation in Engineering Sciences**, v. 5, n. 1, p. 2, 2018.

FORTTRAN, **Fortran PowerStation 4.0**. Microsoft Developer Studio, 1994-95.

FRIDERIKOS, O.; BARANGER, E.; LADEVÈZE, P. Multiscale GFEM with superposition of crack enrichment functions driven by finite fracture mechanics: Theory, first computation and open problems. **Composite Structures**, v. 164, p. 145–157, 2017.

GANESAN, N.; ENGELS, R. C. Hierarchical Bernoulli-Euler finite elements. **Computers & Structures**, v. 43, n. 2, p. 297–304, 1992.

GARCIA, O. A. **Elementos Finitos Generalizados na Análise Estática de Placas e**

Cascas. Thesis (Doutor em Engenharia Mecânica), Universidade Federal de Santa Catarina, Florianópolis, Brasil, 2003.

GARZON, J.; GUPTA, V.; SIMONE, A.; DUARTE, C. A. Bridging scales with a generalized finite element method. **Procedia IUTAM**, v. 3, p. 172–191, 2012.

GARZON, J.; O'HARA, P.; DUARTE, C. A.; BUTTLAR, W. G. Improvements of Explicit Crack Surface Representation and Update within the Generalized Finite Element Method with Application to Three-Dimensional Crack Coalescence. **International Journal for Numerical Methods in Engineering**, v. 0, p. 1–44, 2010.

GÓIS, W. **Método dos Elementos Finitos Generalizados em Formulação Variacional Mista**. Dissertation (Mestre em Engenharia de Estruturas), Universidade de São Paulo, São Carlos, Brasil, 2004.

GÓIS, W. **Elementos Finitos Híbridos e Híbrido-Mistos de Tensão com Enriquecimento Nodal**, Thesis (Doutor em Engenharia de Estruturas), Universidade de São Paulo, São Carlos, Brasil, 2009.

GRACIE, R.; VENTURA, G.; BELYTSCHKO, T. A new fast finite element method for dislocations based on interior discontinuities. **International Journal for Numerical Methods in Engineering**, v. 69, p. 423–441, 2007.

GRILLI, S. T.; SVENDSEN, I. A. Corner problems and global accuracy in the boundary element solution of nonlinear wave flows. **Engineering Analysis with Boundary Elements**, v. 7, n. 4, p. 178–195, 1990.

GUO, B.; BABUŠKA, I. The h-p version of the finite element method - Part 1: The basic approximation results. **Computational Mechanics**, v. 1, n. 1, p. 21–41, 1986.

GUPTA, P.; PEREIRA, J. P.; KIM, D. J.; DUARTE, C. A.; EASON, T. Analysis of three-dimensional fracture mechanics problems: A non-intrusive approach using a generalized finite element method. **Engineering Fracture Mechanics**, v. 90, p. 41–64, 2012.

GUPTA, V.; KIM, D.-J.; DUARTE, C. A. Extensions of the Two-Scale Generalized Finite Element Method To Nonlinear Fracture Problems. **International Journal for Multiscale Computational Engineering**, v. 11, n. 6, p. 581–596, 2013a.

GUPTA, V.; DUARTE, C. A.; BABUŠKA, I.; BANERJEE, U. A stable and optimally

convergent generalized FEM (SGFEM) for linear elastic fracture mechanics. **Computer Methods in Applied Mechanics and Engineering**, v. 266, n. NOVEMBER, p. 23–39, 2013b.

GUPTA, P.; DUARTE, C. A. Simulation of non-planar three dimensional hydraulic fracture propagation. **International Journal for Numerical and Analytical Methods in Geomechanics**, v. 38, p. 1397–1430, 2014.

GUPTA, V.; DUARTE, C. A.; BABUŠKA, I.; BANERJEE, U. Stable GFEM (SGFEM): Improved conditioning and accuracy of GFEM/XFEM for three-dimensional fracture mechanics. **Computer Methods in Applied Mechanics and Engineering**, v. 289, n. February, p. 355–386, 2015.

GUPTA, P.; DUARTE, C. A. Coupled formulation and algorithms for the simulation of non-planar three-dimensional hydraulic fractures using the generalized finite element method. **International Journal for Numerical and Analytical Methods in Geomechanics**, v. 40, n. 10, p. 1402–1437, 2016a.

GUPTA, V.; DUARTE, C. A. On the enrichment zone size for optimal convergence rate of the Generalized/Extended Finite Element Method. **Computers and Mathematics with Applications**, v. 72, n. 3, p. 481–493, 2016b.

GUPTA, P.; DUARTE, C. A.; DHANKHAR, A. Accuracy and robustness of stress intensity factor extraction methods for the generalized/eXtended Finite Element Method. **Engineering Fracture Mechanics**, v. 179, p. 120–153, 2017.

GUPTA, P.; DUARTE, C. A. Coupled hydromechanical-fracture simulations of nonplanar three-dimensional hydraulic fracture propagation. **International Journal for Numerical and Analytical Methods in Geomechanics**, v. 42, n. 1, p. 143–180, 2018.

HAN, Q.; WUANG, Y.; YIN, Y.; WANG, D. Determination of stress intensity factor for mode I fatigue crack based on finite element analysis, **Engineering Fracture Mechanics**, v. 138, p. 118-126, 2015.

HAZARD, L.; BOUILLARD, P. Structural dynamics of viscoelastic sandwich plates by the partition of unity finite element method. **Computer Methods in Applied Mechanics and Engineering**, v. 196, n. 41–44, p. 4101–4116, 2007.

HEIDEBRECHT, A. C.; SMITH, B. S. Approximate analysis of tall wall-frame

structures. **Journal of the Structural Division**, ASCE, Vol. 99 No. 2, pp. 199-221, (1973).

HENNING, P.; PERSSON, A. A multiscale method for linear elasticity reducing Poisson locking. **Computer Methods in Applied Mechanics and Engineering**, v. 310, p. 156–171, 2016.

HOUMAT, A. An alternative hierarchical finite element formulation applied to plate vibrations. **Journal of Sound and Vibration**, v. 206, n. 2, p. 201–215, 1997.

HORAK, W. C. **Local Green's function techniques for the solution of heat conduction and incompressible fluid flow problems**. Urbana, University of Illinois, (Ph.D. Thesis), 1980.

HORAK, W. C.; DORNING, J. J. A Course-Mesh Method For Heat Flow Analysis Based Upon The Use of Locally-Defined Green's Functions. **Numerical Methods in Thermal Problems**, Vol 2, Pineridge Press, Swansea, UK, 1981.

HUGHES, T. J. R.; COTTRELL, J. A.; BAZILEVS, Y. Isogeometric analysis: CAD, finite elements, NURBS, exact geometry and mesh refinement. **Computer Methods in Applied Mechanics and Engineering**, v. 194, n. 39–41, p. 4135–4195, 2005.

IDELSOHN, S. R.; OÑATE, E. To mesh or not to mesh. That is the question... **Computer Methods in Applied Mechanics and Engineering**, v. 195, n. 37–40, p. 4681–4696, 2006.

IQBAL, M.; GIMPERLEIN, H.; MOHAMED, M. S.; LAGHROUCHE, O. An a posteriori error estimate for the generalized finite element method for transient heat diffusion problems Muhammad. **International Journal for Numerical Methods in Engineering**, v. 110, p. 1103–1118, 2017.

KANT, T; PANDYA, B. N. A simple finite element formulation of higher order theory for unsymmetrically laminated composite plates. **Composite Structures**, v. 9, p. 215-246, 1988.

KERGRENE, K.; BABUŠKA, I.; BANERJEE, U. Stable Generalized Finite Element Method and associated iterative schemes; application to interface problems. **Computer Methods in Applied Mechanics and Engineering**, v. 305, p. 1–36, 2016.

KERSHAW, D. S.. The incomplete Cholesky-Conjugate Gradient Method for the Iterative Solution of Systems of Linear Equations, **Journal of Computational Physics** **26**, p. 43-65, 1978.

KHOEI, A. R.; ANAHID, M.; SHAHIM, K. An extended arbitrary Lagrangian-Eulerian finite element method for large deformation of solid mechanics. **Finite Elements in Analysis and Design**, v. 44, n. 6–7, p. 401–416, 2008.

KIM, D. J.; DUARTE, C. A.; PEREIRA, J. P. Analysis of Interacting Cracks Using the Generalized Finite Element Method With Global-Local Enrichment Functions. **Journal of Applied Mechanics**, v. 75, n. 5, p. 51107, 2008.

KIM, D. J.; DUARTE, C. A.; PROENCA, S. P. Generalized finite element method with global-local enrichments for nonlinear fracture analysis. **Mechanics of Solids in Brazil**, Brazilian Society of Mechanical Sciences and Engineering, 2009a.

KIM, D. J.; PEREIRA, J. P. A.; DUARTE, C. A. Analysis of Three-Dimensional Fracture Mechanics Problems : A Two-Scale Approach Using Coarse Generalized FEM Meshes. **International Journal Of Numerical Methods In Engineering**, p. 1–33, 2009b.

KIM, D. J.; PEREIRA, J. P.; DUARTE, C. A. Analysis of three-dimensional fracture mechanics problems: A two-scale approach using coarse-generalized FEM meshes. **International Journal for Numerical Methods in Engineering**, v. 81, n. 3, p. 335–365, 2010.

KIM, D. J.; DUARTE, C. A.; SOBH, N. A. Parallel simulations of three-dimensional cracks using the generalized finite element method. **Computational Mechanics**, v. 47, n. 3, p. 265–282, 2011.

KIM, D. J.; DUARTE, C. A.; PROENCA, S. P. A generalized finite element method with global-local enrichment functions for confined plasticity problems. **Computational Mechanics**, v. 50, n. 5, p. 563–578, 2012.

KIM, D. J.; HONG, S. G.; DUARTE, C. A. Generalized finite element analysis using the preconditioned conjugate gradient method. **Applied Mathematical Modelling**, v. 39, n. 19, p. 5837–5848, 2015.

KIM, J.; DUARTE, C. A. A new generalized finite element method for two-scale simulations of propagating cohesive fractures in 3-D. **International Journal for**

Numerical Methods in Engineering, v. 104, p. 1139–1172, 2015.

KIM, J.; SIMONE, A.; DUARTE, C. A. Mesh refinement strategies without mapping of nonlinear solutions for the generalized and standard FEM analysis of 3-D cohesive fractures. **International Journal for Numerical Methods in Engineering**, v. 109, n. 2, p. 235–258, 2017.

KOMIJANI, M.; GRACIE, R. An enriched finite element model for wave propagation in fractured media. **Finite Elements in Analysis and Design**, v. 125, n. April 2016, p. 14–23, 2017.

LAZZARI, E. DE. **A NURBS-enhanced Finite Element Method**. Dissertation (Master of Science), Delft University of Technology, The Netherlands, 2017.

LEMAITRE, J. **A Course on Damage Mechanics**, Cambridge University Press, Springer-Verlag, New York, 1992.

LEUNG, A. Y. T.; AU, F. T. K. Spline finite elements for beam and plate. **Computers and Structures**, v. 37, n. 5, p. 717–729, 1990.

LEUNG, A.; CHAN, J. Fourier p-element for the analysis of beams and plates. **Journal of Sound and Vibration**, v. 212, n. 1, p. 179–185, 1998.

LEUNG, A. Y. T.; ZHU, B. Fourier p-elements for curved beam vibrations. **Thin-Walled Structures**, v. 42, n. 1, p. 39–57, 2004.

LINS, R. M. **Estimadores de Erro a Posteriori Baseado em Recuperação do Gradiente para o Método dos Elementos Finitos Generalizados**. (Mestre em Engenharia Mecânica), Universidade de São Paulo, São Carlos, Brasil, 2011.

LISZKA, T. J.; DUARTE, C. A. M.; TWORZYDLO, W. W. hp-Meshless cloud method. **Computer Methods in Applied Mechanics and Engineering**, v. 139, n. 1–4, p. 263–288, 1996.

LIU, B.; XING, Y.; WANG, W.; YU, W. Thickness-shear vibration analysis of circular quartz crystal plates by a differential quadrature hierarchical finite element method. **Composite Structures**, v. 131, p. 1073–1080, 2015.

LIU, B.; ZHAO, L.; FERREIRA, A.J.M.; XING, Y.F.; NEVES, A.M.A.; WANG, J.

Analysis of viscoelastic sandwich laminates using a unified formulation and a differential quadrature hierarchical finite element method. **Composite Part B**, v. 110, p. 185–192, 2017a.

LIU, B.; LU, S.; WU, Y.; XING, Y. Three dimensional micro/macro-mechanical analysis of the interfaces of composites by a differential quadrature hierarchical finite element method. **Composite Structures**, v. 176, p. 654–663, 2017b.

LIU, C.; LIU, B.; ZHAO, L.; A differential quadrature hierarchical finite element method and its applications to vibration and bending of Mindlin plates with curvilinear domains. **International Journal for Numerical Methods in Engineering**, v. 109, n. 2, p. 174–197, 2016a.

LIU, C.; LIU, B.; KANG, T.; XING, Y. Micro/macro-mechanical analysis of the interface of composite structures by a differential quadrature hierarchical finite element method. **Composite Structures**, v. 154, p. 39–48, 2016b.

LIU, C.; LIU, B.; XING, Y. In-plane vibration analysis of plates in curvilinear domains by a differential quadrature hierarchical finite element method. **Meccanica**, v. 52, n. 4–5, p. 1017–1033, 2017c.

LU, Z. R.; LAW, S. S. Discussions on “composite element method for vibration analysis of structure”. **Journal of Sound and Vibration**, v. 305, n. 1–2, p. 357–361, 2007.

MACHADO, R. D. **Desenvolvimento do Método Modificado da Função de Green Local para a Solução de Placas Laminadas de Materiais Compostos**. Thesis (Doutor em Engenharia Mecânica), Universidade Federal de Santa Catarina, Florianópolis, Brasil, 1992.

MACHADO, R. D.; BARBIERI, R.; BARCELLOS, C. S.; FILIPPIN, C. G. O método da função de green local modificado (MLGFM) aplicado a problemas da mecânica do contínuo: Parte ii - placas ortotrópicas laminadas. **Proceedings of XIII CILAMCE - Cong. Ibero Latino-Americano sobre Métodos Computacionais para Engenharia**, Porto Alegre, 1992.

MACHADO, R. D.; BARCELLOS, C. S. A first modified local green's function method approach to orthotropic laminated plates. **Proceedings of CADCOMP-92, Computer Aided Design for Composite Materials Conference**. Ed. Brebbia, C. A., Newark,

USA, 1993.

MACHADO, R. D.; BARBIERI, R.; FILIPPIN, C. G.; BARCELLOS, C. S. Análise Comparativa Entre o MEF e o MLGFM Para a Solução de Placas Laminadas de Materiais Compostos. **Proceedings of XII COBEM – Congresso Brasileiro de Engenharia Mecânica**, Brasília. Anais do XII COBEM, 1993.

MACHADO, R. D.; FILHO, J. E. A.; SILVA, M. P. DA. Stiffness loss of laminated composite plates with distributed damage by the modified local Green's function method. **Composite Structures**, v. 84, n. 3, p. 220–227, 2008.

MACHADO, R. D.; JR, A. T.; SILVA, M. P. DA; BARBIERI, R. Progressive Stiffness Loss Analysis of Symmetric Laminated Plates due to Transverse Cracks Using the MLGFM. In: D. Y. Gan (Org.); **Continuum Mechanics – Progress in Fundamentals and Engineering Applications**, InTech, 2012.

MACHADO, R. D.; BARBIERI, R.; SILVA, M. P. DA; JUNIOR, A. T.; GIUSTINA, E. D. The MLGFM Applied to Laminated Composite Plates. **Proceedings of XXXIV Iberian Latin-American Congress on Computational Methods in Engineering - CILAMCE**. ABMEC, Pirenópolis, GO, Brazil, November 10-13, 2013.

MACNEAL, R. H.; HARDER, R. L. A proposed standard set of problems to test finite element accuracy. **Finite Elements in Analysis and Design** 1, p. 3–20, 1985.

MAHDINEJAD, N.; MOTA, H. O.; SILVA, E. J.; ADRIANO, R. Improvement of System Quality in a Generalized Finite Element Method Using Discrete Curvelet Transform. **IEEE Transactions on Magnetics**, v. 53, n. 6, p. 2–5, 2017.

MALAGÜ, M.; BENVENUTI, E.; DUARTE, C. A.; SIMONE, A. One-dimensional nonlocal and gradient elasticity: Assessment of high order approximation schemes. **Computer Methods in Applied Mechanics and Engineering**, v. 275, p. 138–158, 2014.

MALDANER, M., BARCELLOS, C.S. 2D fracture mechanical problems analysis by the modified local green's function method". **Proceedings of XIII CILAMCE – Latin American Congress on Computational Methods for Engineering**, Porto Alegre, Brazil, 1992.

MALDANER, M. **Obtenção do Fator de Intensidade de Tensão pelo Método da**

Função de Green Local Modificado. Dissertation (Mestre em Engenharia Mecânica), Universidade Federal de Santa Catarina, Florianópolis, Brasil, 1993.

MALDANER, M.; BARCELLOS, C. S. O Fator Intensidade de Tensão Obtido pelo Método da Função de Green Local Modificado Utilizando Elementos de Trinca. **Proceedings of XIV CILAMCE, Anais do 14o Congresso Ibero-Latino-Americano de Métodos Computacionais em Engenharia**, São Paulo, SP, 1993.

MALDANER, M.; BARBIERI, R.; BARCELLOS, C. S. Quarter-Point e o Método da Função de Green Local Modificado. **Proceedings of IEV 93, Anais da Conferência Internacional sobre Avaliação de Integridade e Extensão de Vida de Equipamentos Industriais**, Pouso Alto, MG, 1993.

MANGINI, M. **Método dos Elementos Finitos Generalizados para Análise de Estruturas em Casca de Revolução.** Dissertation (Mestre em Engenharia de Estruturas), Universidade de São Paulo, São Carlos, Brasil, 2006.

MATACHE, A. M.; BABUŠKA, I.; SCHWAB, C. Generalized p-FEM in homogenization. **Numerische Mathematik**, v. 86, n. 2, p. 319–375, 2000.

MATHWORKS, **MATLAB R2012b**. Natick, MA: The Mathworks Inc., 2012.

MATOS, J. O. D.; DONADON, M. V.; CASTRO, S. G. P. Aeroelastic behavior of stiffened composite laminated panel with embedded SMA wire using the hierarchical Rayleigh–Ritz method. **Composite Structures**, v. 181, p. 26–45, 2017.

MAZZOCHI, R.; SUAREZ, O. A. G. DE; ROSSI, R.; SILVA NETO, J. M. Generalized Finite Element Method To Approach Forced and Free Vibration in Elastic 2D Problems. 22nd International Congress of Mechanical Engineering. **Anais ABCM**, 2013..

MAZZUCATO, A. L.; NISTOR, V.; QU, Q. Quasi-optimal rates of convergence for the Generalized Finite Element Method in polygonal domains. **Journal of Computational and Applied Mathematics**, v. 263, p. 466–477, 2014.

MEIRA, J. A. D. DE. **Desenvolvimento e Aplicação do Método da Função de Green Local Modificado (MLGFM) para Solução de Problemas da Elastostática Tridimensional.** Dissertation (Mestre em Engenharia Mecânica), Universidade Federal de Santa Catarina, Florianópolis, Brasil, 1994.

MELENK, J. M. **On Generalized Finite Element Methods**. Thesis (Doctor of Philosophy), University of Maryland, USA, 1995.

MELENK, J. M.; BABUŠKA, I. The partition of unity finite element method: Basic theory and applications. **Computer Methods in Applied Mechanics and Engineering**, v. 139, n. 96, p. 289–314, 1996.

MENDONÇA, P. T. R. **Computation of Secondary Variables by a Modified Local Green's Function Method**. PhD thesis, University of Minnesota, USA, 1995.

MESCHKE, G.; LEONHART, D. A Generalized Finite Element Method for hydro-mechanically coupled analysis of hydraulic fracturing problems using space-time variant enrichment functions. **Computer Methods in Applied Mechanics and Engineering**, v. 290, p. 438–465, 2015.

MUNOZ R., P. A.; FILIPPIN, C. G.; BARCELLOS, C. S. O Método da Função de Green Local Modificado Aplicado ao Problema de Vibração Livre de Placa de Mindlin. **Proceedings of – Congresso Brasileiro de Engenharia Mecânica**, Brasília. Anais do XII COBEM, 1993.

MUÑOZ, R. P. A. **Desenvolvimentos na Aplicação do Método da Função de Green Local Modificado a Problemas de Placa de Mindlin**. Dissertation (Mestre em Engenharia Mecânica), Universidade Federal de Santa Catarina, Florianópolis, Brasil, 1994.

MUÑOZ R., P. A.; BARCELLOS, C. S. Solução do problema de vibração livre de placas de mindlin com o método da função de green local modificado. **Proceedings of VI Congreso Nacional de Ingenieria Mecanica**, Ed. Pontificie Universidad Católica do Chile, p. 223-238, 1994a.

MUÑOZ R., P. A.; BARCELLOS, C. S. Análise comparativa do desempenho do método da função de green local modificado frente ao método dos elementos finitos para a solução de problemas de flexão e vibração livre de placas de mindlin. **Proceedings of XV CILAMCE, anais do 15º Congresso Ibero-Latino-Americano sobre Métodos Computacionais em Engenharia**, Ed. Escola de Engenharia da UFMG, p. 767-776, 1994b.

MUÑOZ R., P. A.; VAZ JUNIOR, M. Flux evaluation in anisotropic heat conduction

using the Modified Local Green's Function Method (MLGFM): Comparative studies. **Materials Science Forum**, v. 553, p. 100–105, 2007.

MUROTANI, K.; YAGAWA, G.; CHOI, J. B. Adaptive finite elements using hierarchical mesh and its application to crack propagation analysis. **Computer Methods in Applied Mechanics and Engineering**, v. 253, p. 1–14, 2013.

NAJAFI, A. R.; SAFDARI, M.; TORTORELLI, D. A.; GEUBELLE, P. H. A gradient-based shape optimization scheme using an interface-enriched generalized FEM. **Computer Methods in Applied Mechanics and Engineering**, v. 296, p. 1–17, 2015.

NAJAFI, A. R.; SAFDARI, M.; TORTORELLI, D. A.; GEUBELLE, P. H. Shape optimization using a NURBS-based interface-enriched generalized FEM. **International Journal for Numerical Methods in Engineering**, v. 111, n. 10, p. 927–954, 2017.

NALLIM, L. G.; OLLER, S.; OÑATE, E.; FLORES, F. G. A hierarchical finite element for composite laminated beams using a refined zigzag theory. **Composite Structures**, v. 163, p. 168–184, 2017.

NICOLAZZI, L. C.; BARCELLOS, C. S.; FANCELLO, E. A.; DUARTE, C. A. M. Generalized boundary element method for galerkin boundary integrals. **Engineering Analysis with Boundary Elements**, v. 29, n. 5, p. 494–510, 2005.

NIRSCHL, G. C. **Método dos Elementos Finitos e Técnicas de Enriquecimento da Aproximação Aplicados à Análise de Tubos Cilíndricos e Cascas Esféricas**. Dissertation (Mestre em Engenharia de Estruturas), Universidade de São Paulo, São Carlos, Brasil, 2005.

NISTOR, I.; PANTALÉ, O.; CAPERAA, S. Numerical implementation of the eXtended Finite Element Method for dynamic crack analysis. **Advances in Engineering Software**, v. 39, n. 7, p. 573–587, 2008.

O'HARA, P.; DUARTE, C. A.; EASON, T. Generalized finite element analysis of three-dimensional heat transfer problems exhibiting sharp thermal gradients. **Computer Methods in Applied Mechanics and Engineering**, v. 198, n. 21–26, p. 1857–1871, 2009.

O'HARA, P.; DUARTE, C. A.; EASON, T. Transient analysis of sharp thermal gradients using coarse finite element meshes. **Computer Methods in Applied Mechanics and**

Engineering, v. 200, n. 5–8, p. 812–829, 2011.

O'HARA, P.; DUARTE, C. A.; EASON, T.; GARZON, J. Efficient analysis of transient heat transfer problems exhibiting sharp thermal gradients. **Computational Mechanics**, v. 51, n. 5, p. 743–764, 2013.

ODEN, J.T.; REDDY, J.N. **An Introduction to the Mathematical Theory of Finite Elements**. John-Wiley & Sons, 1976.

ODEN, J. T.; DUARTE, C. A. Cloud, Cracks and FEMs. **Report**, The University of Texas at Austin, USA, 1997.

ODEN, J. T.; DUARTE, C. A. M.; ZIENKIEWICZ, O. C. A new cloud-based hp finite element method. **Computer Methods in Applied Mechanics and Engineering**, 1998.

OZER, H.; DUARTE, C. A.; AL-QADI, I. L. Formulation and implementation of a high-order 3-D domain integral method for the extraction of energy release rates. **Computational Mechanics**, v. 49, n. 4, p. 459–476, 2012.

PARK, K.; PEREIRA, J. P.; DUARTE, C. A.; PAULINO, G. H. Integration of singular enrichment functions in the generalized/extended finite element method for three-dimensional problems. **International Journal for Numerical Methods in Engineering**, v. 78, n. 10, p. 1220–1257, 2009.

PEANO, A. Hierarchies of conforming finite elements for plane elasticity and plate bending. **Computers and Mathematics with Applications**, v. 2, n. 3–4, p. 211–224, 1976.

PEREIRA, J. P. A. **Extração de Fatores de Intensidade de Tensão Utilizando a Solução do Método dos Elementos Finitos Generalizados**. Dissertation (Mestre em Engenharia de Estruturas), Universidade de São Paulo, São Carlos, Brasil, 2004.

PEREIRA, J. P.; DUARTE, C. A. Extraction of stress intensity factors from generalized finite element solutions. **Engineering Analysis with Boundary Elements**, v. 29, n. 4, p. 397–413, 2005.

PEREIRA, J. P.; DUARTE, C. A.; GUOY, D.; JIAO, X. hp-Generalized FEM and crack surface representation for non-planar 3-D cracks. **International Journal for**

Numerical Methods in Engineering, v. 77, n. 5, p. 601–633, 2009a.

PEREIRA, J. P.; DUARTE, C. A.; JIAO, X.; GUOY, D. Generalized finite element method enrichment functions for curved singularities in 3D fracture mechanics problems. **Computational Mechanics**, v. 44, n. 1, p. 73–92, 2009b.

PEREIRA, J. P.; DUARTE, C. A.; JIAO, X. Three-dimensional crack growth with hp-generalized finite element and face offsetting methods. **Computational Mechanics**, v. 46, n. 3, p. 431–453, 2010.

PEREIRA, J. P. A.; KIM, D. J.; DUARTE, C. A. A two-scale approach for the analysis of propagating three-dimensional fractures. **Computational Mechanics**, v. 49, n. 1, p. 99–121, 2012.

PIEDEDE NETO, D. **On the Generalized Finite Element Method in Nonlinear Solid Mechanics Analyses**. Thesis (Doctor in Science), University of São Paulo, São Carlos, Brazil, 2013.

PILKEY, W. D.; PILKEY, D. F. **Peterson's Stress Concentration Factors**. 3rd ed. WILEY, 2008.

PINHEIRO, D. C. C.; BARROS, F. B.; PITANGUEIRA, R. L. S.; PENNA, S. S. High regularity partition of unity for structural physically non-linear analysis. **Engineering Analysis with Boundary Elements**, v. 83, n. July, p. 43–54, 2017.

PLEWS, J. A.; DUARTE, C. A. Generalized finite element approaches for analysis of localized thermo-structural effects. **International Journal for Numerical Methods in Engineering**, v. 104, n. 6, p. 408–438, 2015a.

PLEWS, J. A.; DUARTE, C. A. Bridging multiple structural scales with a generalized finite element method. **Proceedings of the 2011 American Control Conference**, v. 102, p. 180–201, 2015b.

RAMOS, A. C.; ARAGÓN, A. M.; SOGHRATI, S.; GEUBELLE, P. H.; JEAN-FRANÇOISMOLINARI. A new formulation for imposing Dirichlet boundary conditions on non-matching meshes Aurelia. **International Journal for Numerical Methods in Engineering**, v. 103, p. 430–444, 2015.

RAUEN, M.; MACHADO, R. D.; ARNDT, M. Isogeometric analysis of free vibration of

framed structures: comparative problems. **Engineering Computations**, v. 34, n. 2, p. 377–402, 2017.

REDDY, B. D. **Functional Analysis and Boundary-Value Problems: An Introductory Treatment**. Longman Scientific & Technical, UK, 1986.

REDDY, J. N. **An Introduction to Continuum Mechanics**. Cambridge University Press, Cambridge, UK, 2008.

RIBEIRO, P. Hierarchical finite element analyses of geometrically non-linear vibration of beams and plane frames. **Journal of Sound and Vibration**, v. 246, n. 2, p. 225–244, 2001.

SANTANA, W. C. **Um Método Robusto de Elementos Finitos Generalizados Aplicado à Mecânica da Fratura**. Thesis (Tese de Doutorado, Programa de Pós-Graduação em Engenharia Mecânica da PUC-Rio, Pontifícia Universidade Católica do Rio de Janeiro, Rio de Janeiro, Brasil, 2004.

SATO, F. M. **Numerical Experiments with Stable Versions of the Generalized Finite Element Method**. Dissertation (Master in Science), Universtiy of São Paulo, São Carlos, Brazil, 2017.

SCHWEITZER, M. A. Multilevel particle-partition of unity method. **Computer Methods in Applied Mechanics and Engineering**, v. 198, p. 1260–1272, 2009. Elsevier B.V. Disponível em: <<http://dx.doi.org/10.1016/j.cma.2008.01.009>>. .

SERDOUN, S.; CHERIF, S. H. Free vibration analysis of composite and sandwich plates by alternative hierarchical finite element method based on Reddy's C 1 HSDT. **Journal of Sandwich Structures & Materials**, v. 18, n. 4, p. 501–528, 2016.

SHABIR, Z.; VAN DER GIESSEN, E.; DUARTE, C. A.; SIMONE, A. The role of cohesive properties on intergranular crack propagation in brittle polycrystals. **Modelling and Simulation in Materials Science and Engineering**, v. 19, n. 3, 2011.

SHANG, H. Y. **Análise Dinâmica Elastoplástica de Problemas da Mecânica de Sólidos via Métodos Enriquecidos de Elementos Finitos**. Thesis (Doutor em Engenharia Mecânica), Pontifícia Universidade Católica do Paraná, Curitiba, Brasil, 2014.

SHANG HSU, Y. Enriched finite element methods for Timoshenko beam free vibration analysis. **Applied Mathematical Modelling**, v. 40, n. 15–16, p. 7012–7033, 2016.

SHANG, H. Y.; MACHADO, R. D.; ABDALLA FILHO, J. E. Dynamic analysis of Euler-Bernoulli beam problems using the Generalized Finite Element Method. **Computers and Structures**, v. 173, n. September, p. 109–122, 2016.

SHANG, H. Y.; MACHADO, R. D.; ABDALLA FILHO, J. E.; ARNDT, M. Numerical analysis of plane stress free vibration in severely distorted mesh by Generalized Finite Element Method. **European Journal of Mechanics, A/Solids**, v. 62, p. 50–66, 2017.

SILLEM, A.; SIMONE, A.; SLUYS, L. J. The Orthonormalized Generalized Finite Element Method-OGFEM: Efficient and stable reduction of approximation errors through multiple orthonormalized enriched basis functions. **Computer Methods in Applied Mechanics and Engineering**, v. 287, p. 112–149, 2015.

SILVA, L. H. M. E. **Novas Formulações Integrais para Problemas da Mecânica**. Thesis (Doutor em Engenharia Mecânica), Universidade Federal de Santa Catarina, Florianópolis, Brasil, 1988.

SILVA, M. P. DA. **Análise do Dano em Laminados Compostos pelo MLGFM**. Dissertation (Mestre em Engenharia Mecânica), Pontifícia Universidade Católica do Paraná, Curitiba, Brasil, 2004.

SILVA, M. P. DA; MACHADO, R. D.; FILHO, J. E. A. Analysis of Laminated Composite Plates with Transverse Cracks by MLGFM Solution. **Proceedings of XVIII COBEM - International Congress of Mechanical Engineering - ABCM**. Ouro Preto; Brazil, 2005.

SILVA, M. P. DA; ABDALLA, F. J. E.; SHANG, H. Y.; MACHADO, R. D. Enriched Modified Local Green's Function Method Applied to Elasto Static Problemas. **Proceedings of 24th COBEM - International Congress of Mechanical Engineering - ABCM**. Curitiba, Brazil, 2017a.

SILVA, M. P. DA; MACHADO, R. D.; ABDALLA, F. J. E. Enriched Methods Allied to Modified Local Green's Function Method for Elasto Static Problems. **Proceedings of XXXVIII Iberian Latin-American Congress on Computational Methods in Engineering - CILAMCE, ABMEC**. Florianópolis, Brazil, 2017b.

SIMONE, A.; DUARTE, C. A.; VAN DER GIESSEN, E. A Generalized Finite Element Method for polycrystals with discontinuous grain boundaries. **International Journal for Numerical Methods in Engineering**, v. 67, n. 8, p. 1122–1145, 2006.

SOGHRATI, S.; ARAGÓN, A.; DUARTE, C. A.; GEUBELLE, P. H. An interface-enriched generalized FEM for problems with discontinuous gradient field. **International Journal for Numerical Methods in Engineering**, v. 89, n. 8, p. 991–1008, 2011.

SOGHRATI, S.; GEUBELLE, P. H. A 3D interface-enriched generalized finite element method for weakly discontinuous problems with complex internal geometries. **Computer Methods in Applied Mechanics and Engineering**, v. 217–220, p. 46–57, 2012.

SOGHRATI, S.; ARAGÓN, A. M.; ARMANDO DUARTE, C.; GEUBELLE, P. H. An interface-enriched generalized FEM for problems with discontinuous gradient fields. **International Journal for Numerical Methods in Engineering**, v. 89, n. 8, p. 991–1008, 2012.

SOGHRATI, S.; NAJAFI, A. R.; LIN, J. H. Computational analysis of actively-cooled 3D woven microvascular composites using a stabilized interface-enriched generalized finite element method. **International Journal of Heat and Mass Transfer**, v. 65, p. 153–164, 2013.

SOGHRATI, S.; DUARTE, C. A.; GEUBELLE, P. H. An adaptive interface-enriched generalized FEM for the treatment of problems with curved interfaces. **International Journal for Numerical Methods in Engineering**, v. 102, p. 1352–1370, 2015.

ŠOLÍN, P.; SEGETH, K.; DOLEZEL, I. **Higher-Order Finite Element Methods**. Boca Raton, FL: Chapman & Hall/CRC, 2004.

SON, H.; PARK, J.; KIM, H.; LEE, Y. H.; KIM, D.-J. Generalized finite element analysis of high-rise wall-frame structural systems. **Engineering Computations**, v. 34, n. 1, p. 189–210, 2017.

SOUZA, C. O. DE. **Formulação Híbrida-Trefftz com Enriquecimento Seletivo: Aplicação a Problemas Bidimensionais da Elasticidade**. Dissertation (Mestre em Engenharia de Estruturas), Universidade de São Paulo, São Carlos, Brasil, 2008.

STROUBOULIS, T.; BABUŠKA, I.; COPPS, K. The design and analysis of the

Generalized Finite Element Method. **Computer Methods in Applied Mechanics and Engineering**, v. 181, n. 1–3, p. 43–69, 2000.

STROUBOULIS, T.; COPPS, K.; BABUŠKA, I. The generalized finite element method. **Computer Methods in Applied Mechanics and Engineering**, v. 190, n. 32–33, p. 4081–4193, 2001.

STROUBOULIS, T.; ZHANG, L.; BABUŠKA, I. Generalized finite element method using mesh-based handbooks: Application to problems in domains with many voids. **Computer Methods in Applied Mechanics and Engineering**, v. 192, n. 28–30, p. 3109–3161, 2003.

STROUBOULIS, T.; BABUŠKA, I.; HIDAJAT, R. The generalized finite element method for Helmholtz equation: Theory, computation, and open problems. **Computer Methods in Applied Mechanics and Engineering**, v. 195, n. 37–40, p. 4711–4731, 2006a.

STROUBOULIS, T.; ZHANG, L.; WANG, D.; BABUŠKA, I. A posteriori error estimation for generalized finite element methods. **Computer Methods in Applied Mechanics and Engineering**, v. 195, p. 852–879, 2006b.

STROUBOULIS, T.; HIDAJAT, R.; BABUŠKA, I. The generalized finite element method for Helmholtz equation. Part II: Effect of choice of handbook functions, error due to absorbing boundary conditions and its assessment. **Computer Methods in Applied Mechanics and Engineering**, v. 197, n. 5, p. 364–380, 2008.

SUKUMAR, N.; MOES, N.; MORAN, B.; BELYTSCHKO, T. Extended finite element method for three-dimensional crack modelling. **International Journal for Numerical Methods in Engineering**, v. 48, n. November 1999, p. 1549–1570, 2000.

SUKUMAR, N.; CHOPP, D. L.; MOËS, N.; BELYTSCHKO, T. Modeling holes and inclusions by level sets in the extended finite-element method. **Computer Methods in Applied Mechanics and Engineering**, v. 190, n. 46–47, p. 6183–6200, 2001.

SZABÓ, B. A. Mesh design for the p-version of the finite element method. **Computer Methods in Applied Mechanics and Engineering**, v. 55, n. 1–2, p. 181–197, 1986.

TAN, M. H. Y.; SAFDARI, M.; NAJAFI, A. R.; GEUBELLE, P. H. A NURBS-based interface-enriched generalized finite element scheme for the thermal analysis and design of microvascular composites. **Computer Methods in Applied Mechanics and**

Engineering, v. 283, p. 1382–1400, 2015.

TAN, M. H. Y.; NAJAFI, A. R.; PETY, S. J.; WHITE, S. R.; GEUBELLE, P. H. Gradient-based design of actively-cooled microvascular composite panels. **International Journal of Heat and Mass Transfer**, v. 103, p. 594–606, 2016.

TASSINI, J. A. **Análise da Perda Progressiva da Rigidez em Laminados Devido a Trincas Transversais na Matriz**. Dissertation (Mestre em Engenharia Mecânica), Pontifícia Universidade Católica do Paraná, Curitiba, Brasil, 2005.

TAYLOR, R. L.; ZIENKIEWICZ, O. C.; OÑATE, E. A hierarchical finite element method based on the partition of unity. **Computer Methods in Applied Mechanics and Engineering**, v. 152, n. 1–2, p. 73–84, 1998.

TESSLER, A.; DI SCIUVA, M.; GHERLONE, M. Refinement of Timoshenko beam theory for composite and sandwich beams using zigzag kinematics. **Technical Publication 215086, National Aeronautics and Space Administration**, 2007.

TIAN, R. Extra-dof-free and linearly independent enrichments in GFEM, **Computer Methods in Applied Mechanics and Engineering**, v. 266, p. 1–22, 2013.

TIAN, R.; WEN, L. Improved XFEM—An extra-dof free, well-conditioning, and interpolating XFEM, **Computer Methods in Applied Mechanics and Engineering**, v. 285, p. 639–658, 2015.

TIMOSHENKO, S.; GOODIER, J. N. **Theory of Elasticity**. 2nd ed. New York: McGraw-Hill Book Company, Inc., 1951.

TORII, A. J. **Análise Dinâmica com o Método dos Elementos Finitos Generalizado**. Thesis (Doutor em Engenharia Mecânica), Universidade Federal do Paraná, Curitiba, Brasil, 2012.

TORII, A. J.; MACHADO, R. D. Structural dynamic analysis for time response of bars and trusses using the generalized finite element method. **Latin American Journal of Solids and Structures**, v. 9, n. 3, p. 309–337, 2012.

TORII, A. J.; MACHADO, R. D.; ARNDT, M. GFEM for modal analysis of 2D wave equation. **Engineering Computations**, v. 32, n. 6, p. 1779–1801, 2015.

TORRES, I. F. R. **Desenvolvimento e Aplicação do Método dos Elementos Finitos Generalizados em Análise Tridimensional Não-Linear de Sólidos**. Thesis (Doutor em Engenharia de Estruturas), Universidade de São Paulo, São Carlos, Brasil, 2003.

TORRES, D. A. F.; DE BARCELLOS, C. S.; MENDONÇA, P. DE T. R. Effects of the smoothness of partitions of unity on the quality of representation of singular enrichments for GFEM/XFEM stress approximations around brittle cracks. **Computer Methods in Applied Mechanics and Engineering**, v. 283, p. 243–279, 2015.

TUNCER, O.; SHANKER, B.; KEMPEL, L. C. Discontinuous galerkin inspired framework for vector generalized finite-element methods. **IEEE Transactions on Antennas and Propagation**, v. 62, n. 3, p. 1339–1347, 2014.

WANG, X. Q.; PHILIPOT, G. P.; PEREZ, R. A.; MIGNOLET, M. P. Locally enhanced reduced order modeling for the nonlinear geometric response of structures with defects. **International Journal of Non-Linear Mechanics**, v. 101, p. 1–7, 2018.

WEINHARDT, P. O.; DEBELLA, L.B.C.; ARNDT, M.; MACHADO, R. D. GFEM stabilization techniques applied to dynamic analysis of non-uniform section bars. **Latin American Journal of Solids and Structure – LAJSS** (accepted for publication), 2018.

WEN, L.; TIAN, R. Improved XFEM: Accurate and robust dynamic crack growth simulation. **Computer Methods in Applied Mechanics and Engineering**, v. 308, p. 256–285, 2016.

WU, J.; ZHU, Z. J.; SZMELTER, J.; ZIENKIEWICZ, O. C. Error estimation and adaptivity in navier-stokes incompressible flows, *Computational Mechanics*, v. 6(4), p. 259–270, 1990.

WU, J. Y.; LI, F. B. An improved stable XFEM (Is-XFEM) with a novel enrichment function for the computational modeling of cohesive cracks. **Computer Methods in Applied Mechanics and Engineering**, v. 295, p. 77–107, 2015.

XIAO, Q. Z.; KARIHALOO, B. L. Implementation of hybrid crack element on a general finite element mesh and in combination with XFEM. **Computer Methods in Applied Mechanics and Engineering**, v. 196, n. 13–16, p. 1864–1873, 2007.

YANG, Z. J.; ZHANG, Z. H.; LIU, G. H.; OOI, E. T. An h-hierarchical adaptive scaled boundary finite element method for elastodynamics. **Computers and Structures**, v. 89,

n. 13–14, p. 1417–1429, 2011.

YU, Z.; GUO, X.; CHU, F. A multivariable hierarchical finite element for static and vibration analysis of beams. **Finite Elements in Analysis and Design**, v. 46, n. 8, p. 625–631, 2010.

ZAFOSŃNIK, B.; FAJDIGA, G. Determining stress intensity factor KI with extrapolation method, **Tehnički vjesnik - Technical gazette**, v.23, n.6, p. 1673-1678, 2016.

ZENG, P. Composite Element Method for Vibration Analysis of Structure, Part I: Principle And C^0 Element (Bar). **Journal of Sound and Vibration**, v. 218, n. 4, p. 619–658, 1998.

ZHANG, K.; JIN, J. M.; GEUBELLE, P. H. A 3-D interface-enriched generalized FEM for electromagnetic problems with nonconformal discretizations. **IEEE Transactions on Antennas and Propagation**, v. 63, n. 12, p. 5637–5649, 2015.

ZHANG, K.; NAJAFI, A. R.; JIN, J.-M.; GEUBELLE, P. H. An interface-enriched generalized finite element analysis for electromagnetic problems with non-conformal discretizations Kedi. **International Journal of Numerical Modelling Electronic Networks Devices and Fields**, v. 29, p. 265–279, 2016a.

ZHANG, L. **Generalized Finite Element Method for Multiscale Analysis**. Thesis (Doctor of Philosophy), Texas A&M University, USA, 2003.

ZHANG, Q.; BANERJEE, U.; BABUŠKA, I. Higher order stable generalized finite element method. **Numerische Mathematik**, v. 128, n. 1, p. 1–29, 2014.

ZHANG, S.; ZHANG, X.; WANG, H. Forward Solver in Magnetoacoustic Tomography with Magnetic Induction by Generalized Finite-Element Method. **IEEE Transactions on Magnetics**, v. 52, n. 3, p. 3–6, 2016b.

ZHAO, J.; HOU, Y.; SONG, L. Modified intrinsic extended finite element method for elliptic equation with interfaces. **Journal of Engineering Mathematics**, v. 97, n. 1, p. 147–159, 2016.

ZIENKIEWICZ, O.C.; TAYLOR, R.L.; TOO, J.M. Reduced integration technique in general analysis of plates and shells. **International Journal for Numerical Methods in Engineering**, Vol. 3, p. 275-90, 1971.

ZIENKIEWICZ, O. C.; DE, J. P.; KELLY, D. W. The hierarchical concept in finite element analysis. **Computers and Structures**, v. 16, n. 1–4, p. 53–65, 1983.

ZIENKIEWICZ, O. C.; TAYLOR, R. L.; ZHU, J. Z. **The Finite Element Method: Its Basis and Fundamentals, Sixth edition**. 6th ed. Elsevier Butterworth-Heinemann, 2005.

Appendix A

A.1 SOME TOPICS IN FUNCTIONAL ANALYSIS

A set is any well-defined collection of objects. For example, the set of real numbers \mathbb{R} consists of all rational as well as irrational numbers. It is convenient to think of \mathbb{R} as represented by an infinitely long line, each point on the line being a real number. We define \mathbb{R}^n to be the set of all ordered n -tuples of real numbers, such that

$$\mathbb{R}^n = \{ \mathbf{x} = (x_1, x_2, \dots, x_n): x_i \in \mathbb{R}, i = 1, 2, \dots, n \}. \quad (\text{A.1})$$

When working in two dimensions, for instance, we can use an alternative notation like $\mathbf{x} = (x, y)$ or $\mathbf{x} = (x_1, x_2)$ in \mathbb{R}^2 .

A subset Ω of \mathbb{R}^n is an open set if every point of Ω is an interior point and connected if every pair of points in Ω can be connected by a curve entirely in Ω . We define the closure $\overline{\Omega}$ of a set $\Omega \subset \mathbb{R}^n$ to be the union of Ω and all its limit points.

A function $f(x)$ on an interval I of the real line is continuous at a point $x_0 \in I$ if, given any positive number α , no matter how small, it is possible to find a positive number β such that

$$|f(x) - f(x_0)| < \alpha \quad \text{whenever} \quad |x - x_0| < \beta. \quad (\text{A.2})$$

An arbitrary space U is called a vector space (or linear space) if it has an operation $+$ called addition, an operation of multiplication by a scalar, and satisfies the following axioms

VS1. for all $u, v \in U$, and scalars α, β , $\alpha u + \beta v$ is also a member of U ;

- VS2. $u + v = v + u$ and $u + (v + w) = (u + v) + w$ for all $u, v, w \in U$;
- VS3. there is an element 0 of U called the zero element that has the property $u + 0 = u$ for all $u \in U$;
- VS4. for every $u \in U$ there is an element $-u$ that satisfies $u + (-u) = 0$; then by the difference $u - v$ we understand $u + (-v)$;
- VS5. $(\alpha\beta)u = \alpha(\beta u)$ for all scalars α, β and for all $u \in U$;
- VS6. $(\alpha + \beta)u = \alpha u + \beta u$, and $\alpha(u + v) = \alpha u + \alpha v$ for all scalars α, β and for all $u, v \in U$;
- VS7. $1 \cdot u = u$.

A subspace H of a vector space U is a subset of U that is also a vector space.

If the space U is a vector space then the inner product (u, v) of $u, v \in U$ is an operation that satisfies the following axioms, for all $u, v, w \in U$ and $\alpha, \beta \in \mathbb{R}$, such as

- IP1. $(u, v) \in \mathbb{R}$;
- IP2. $(v, u) = (u, v)$ (the operation is symmetric);
- IP3. $(\alpha u + \beta v, w) = \alpha(u, w) + \beta(v, w)$ (linearity);
- IP4. $(u, u) \geq 0$ and $(u, u) = 0$ if $u = 0$ (positive-definiteness).

Two members u, v of an inner product space U are said to be orthogonal if $(u, v) = 0$.

Given a vector space U , a norm $\| \cdot \|$ on U is an operation that satisfies the following axioms for any members u, v of U , and scalars α :

- N1. $\|u\| \in \mathbb{R}$;
- N2. $\|u\| \geq 0$ and $\|u\| = 0$ if $u = 0$ (positive-definiteness);
- N3. $\|\alpha u\| = |\alpha| \|u\|$ (positive homogeneity);
- N4. $\|u + v\| \leq \|u\| + \|v\|$ (triangle inequality).

A vector space U with a norm $\|\cdot\|$ defined on it is called a normed space.

An inner product generates a norm according to $\|\cdot\| = (u, u)^{1/2}$.

A sequence $\{u_n\}$ in a subset H of a normed space U is convergent if there is a member $u \in H$ for which, given any $\alpha > 0$, a number N can be found such that

$$\|u_n - u\| < \alpha \quad \text{for all } n > N. \quad (\text{A.3})$$

We write $\lim_{n \rightarrow \infty} \|u_n - u\| = 0$ or $\lim_{n \rightarrow \infty} u_n = u$, the limit of the sequence.

A sequence $\{u_n\}$ in a subset H of a normed space U is called a Cauchy sequence if

$$\lim_{m, n \rightarrow \infty} \|u_m - u_n\| = 0 \quad (\text{A.4})$$

or, more formally, if for any given $\alpha > 0$ there exists a number N such that

$$\|u_m - u_n\| < \alpha \quad \text{whenever } m, n > N. \quad (\text{A.5})$$

A subset H of a normed space U is complete if every Cauchy sequence in H converges to an element of U . A subset H of a normed space U is said to be dense in U if the closure of H is U , that is, $\bar{H} = U$. We define the closure \bar{H} of an open set H to be the union of H and all of its limit points, as previously described.

A complete normed space is called a Banach space; a complete inner product space is called a Hilbert space. Since every inner product defines a norm, every Hilbert space is a Banach space.

An operator or map T from a set H to a set K is a rule whereby an element u of H is mapped or transformed to an element v of K . It is possible to write

$$T : H \rightarrow K, \quad Tu = v \text{ (or } T(u) = v) \quad \text{for } u \in H \text{ and } v \in K. \quad (\text{A.6})$$

In this case, H is called the domain of T , written $D(T)$ and $R(T)$, the range

of T , consists of all those elements of K that are images of members of H , i.e.

$$R(T) = \{ v : v \in K, Tu = v \text{ for some } u \in H \}. \quad (\text{A.7})$$

An operator T is injective (one-to-one) if every element of the range of T is mapped to by at most one element of the domain. It is surjective (onto) if every element of the range of T is mapped to by at least one element of the domain, i.e., $R(T) = K$, and T is said to map H onto K . It is bijective (one-to-one and onto or one-to-one correspondence) if every element of the range of T is mapped to by exactly one element of the domain.

A linear operator T is an operator whose domain H is a vector space, and for which

$$T(\alpha u + \beta v) = \alpha T(u) + \beta T(v) \quad \text{for all } u, v \in H \text{ and } \alpha, \beta \in \mathbb{R}. \quad (\text{A.8})$$

A linear operator $T : H \rightarrow K$ where H and K are normed spaces is bounded if

$$\|Tu\| < M\|u\| \quad \text{for all } u \text{ in } H \text{ and for some } M > 0. \quad (\text{A.9})$$

The set of all linear operators from H to K forms a linear space, which we denote by $L(H, K)$.

A linear functional ℓ on a vector space H is defined to be any linear operator that maps elements of H to \mathbb{R} . The space of bounded linear functionals on H is called the dual space of H , and is denoted by H' . That is: $H' = L(H, \mathbb{R})$. For any $\ell \in H'$, we have

$$\|\ell(u)\| = |\ell(u)| \leq M\|u\| \quad \text{for all } u \in H \text{ and for some } M > 0. \quad (\text{A.10})$$

This expression states that ℓ is bounded and hence continuous.

We often write $\langle \ell, u \rangle$ instead of the usual $\ell(u)$ where $\langle \cdot, \cdot \rangle$ denotes duality pairing.

The Riesz Representation Theorem states that considering a Hilbert space H and a bounded linear functional ℓ on H , then there exists a unique element u in H such that

$$\langle \ell, v \rangle = (v, u) \quad \text{for all } v \in H, \text{ with } \|\ell\| = \|u\|. \quad (\text{A.11})$$

Considering that H and K are vector spaces, a bilinear form $B : H \times K \rightarrow \mathbb{R}$ is defined to be an operator with the properties:

$$B(\alpha u + \beta w, v) = \alpha B(u, v) + \beta B(w, v) \quad \text{for } u, w \in H \text{ and } v \in K, \quad (\text{A.12})$$

$$B(u, \alpha v + \beta w) = \alpha B(u, v) + \beta B(u, w) \quad \text{for } u \in H \text{ and } v, w \in K \quad (\text{A.13})$$

where α and β are real numbers.

Suppose that we are given a bilinear form $B : H \times K \rightarrow \mathbb{R}$, where now H and K are normed linear spaces. If there is a positive number $M > 0$ such that:

$$|B(u, v)| \leq M \|u\|_H \|v\|_K \quad \text{for all } u \in H, v \in K. \quad (\text{A.14})$$

then B is called a continuous bilinear form. This is an important conclusion for problems to be “*well-posed*” or “*well-conditioned*”.

Given a bilinear form $B : H \times H \rightarrow \mathbb{R}$, where H is an inner product space, we say that B is *H-elliptic* (or coercive) if there exists a constant $\alpha > 0$ such that

$$B(u, u) \geq \alpha \|u\|_H^2 \quad \text{for all } u \in H. \quad (\text{A.15})$$

The relation A.15 presented above is known as “strongly coercive”.

As quoted by Oden & Reddy (1976): “Important extensions of the theory of variational boundary-value problems can be made by introducing a notion of coerciveness more general than those defined by strongly coercive”. Then, by “weakly coercive” we mean:

$$\inf_{u \in H} \sup_{v \in K} |B(u, v)| \geq \alpha > 0, \quad (\text{A.16})$$

$$\|u\|_H = 1, \quad \|v\|_K \leq 1, \quad (\text{A.17})$$

$$\sup_{u \in H} |B(u, v)| > 0 \quad \text{para } \forall v \in K \text{ e } v \neq 0. \quad (\text{A.18})$$

Naturally, a strongly coercive is a particular case of a weakly coercive.

Now, we have enough mathematical definitions to inquire whether or not solutions to a given variational problem exist and if, so, whether it is unique. What are the conditions on the associated bilinear forms sufficient to guarantee the existence and uniqueness of a solution? “*The Generalized Lax-Milgram Theorem*” addresses and answers this question, using the propositions A.14 – *continuity* – and propositions A.15 to A.18 – *coercivity*.

And what is a variational boundary-value problem? And, before that, what is a boundary-value problem? Why are these concepts so important in this work? This is the scope of next sections.

A.2 BOUNDARY-VALUE PROBLEMS (BVP)

Several physical phenomena can be modeled by differential equations involving unknown functions and their derivatives. A boundary-value problem (BVP) for a given differential equation consists of finding a solution of the given differential equation subject to a given set of boundary conditions (BCs). A boundary condition is a prescription some combinations of values of the unknown solution and its derivatives at more than one point. So, a typical problem involves finding a function u which satisfies a partial differential equation (PDE) of order $2m$ in a domain Ω such that:

$$\text{PDE:} \quad Au = f \quad \text{in } \Omega \subset \mathbb{R}^n, \quad (\text{A.19})$$

$$\text{BCs:} \quad B_k u = g_k \quad \text{on } \partial\Omega \text{ with } 0 \leq k \leq m-1 \quad (\text{A.20})$$

where A is a linear differential operator of order $2m$, $\{B_k\}_{k=0}^{m-1}$ are the linear differential operators on boundary whereas f and g_k , the “nonhomogeneous” part of (A.19) and (A.20), are prescribed functions. The domain Ω is an open bounded set where the problem is defined with a smooth boundary such that $\partial\Omega = \partial\Omega_1 \cup \partial\Omega_2 \cup \dots \cup \partial\Omega_m$ (REDDY, 1986).

A central question of the theory of elliptic boundary-value problems relates to the conditions under which one may expect a unique solution of the Equation A.19 to exist. This question is addressed by “*The Generalized Lax-Milgram Theorem*” as previously quoted in last section. But if a solution exists then it is equally important to know something about the regularity or smoothness of this solution. In other words, if the Equation A.19 has a solution u that belongs to a Hilbert space $H^{s+2m}(\Omega)$, “ s ” being an integer greater than or equal to $2m$, a good idea of how smooth the solution is will be given when establishing the largest value of “ $s+2m$ ” for which $u \in H^{s+2m}(\Omega)$. Note that if $u \in H^{s+2m}(\Omega)$, the Au or f term is in $H^s(\Omega)$ since A is a differential operator of order $2m$. Remember that $H^m(\Omega)$ is the Sobolev space of functions with derivatives up to order “ m ” and square integrable in Lebesgue sense $L_2(\Omega)$.

However, the Sobolev space like $H^m(\Omega)$ are spaces with infinite dimension which makes the search of an analytical solution u for the problem of Equation A.19 rather laborious, and in some cases impossible. It is precisely in this context that the proposal of replacing the space where the solution of the problem is being sought by a subspace of approximation of finite dimension becomes evident. In this context, it should be good to re-written the expressions A.19 and A.20 in such way we could “weaken” this search and “broaden” this concept. This is exactly the essence of the “variational boundary-value problems” to be explored in next section.

A.3 VARIATIONAL BOUNDARY-VALUE PROBLEMS (VBVP)

The concept of a boundary-value problem can be broadened by introducing the idea of variational boundary-value problem. The variational formulation is a weaker one than the conventional formulation since it requires fewer derivatives of u to be in $L_2(\Omega)$.

A boundary-value problem, as former described, can be re-written as a variational boundary-value problem (VBVP) such as: find a function u which belongs to a Hilbert space H and which satisfies the equation:

$$B(u, v) = \ell(v) \quad \forall v \in K. \quad (\text{A.21})$$

Here B is a bilinear form and ℓ a linear functional:

$$B : H \times K \rightarrow \mathbb{R} \quad \text{and} \quad \ell : K \rightarrow \mathbb{R} \quad (\text{A.22})$$

as previously described in functional analysis section.

The space K is called “space of admissible functions” and it is defined as (REDDY, 1986)

$$K = \{ v \in H^m(\Omega) : v \text{ satisfies all essential boundary conditions} \} \quad (\text{A.23})$$

and $2m$ being the order of a boundary-value problem differential operator with the following conditions

- a. Essential (or Dirichlet) boundary conditions are given by order $< m$;
- b. Natural (or Neumann) boundary conditions are given by order $\geq m$.

To fix this idea, consider the simple second-order differential equation in two dimensions:

$$Au \equiv -\frac{\partial}{\partial x} \left[a_{11}(x, y) \frac{\partial u(x, y)}{\partial x} \right] - \frac{\partial}{\partial y} \left[a_{22}(x, y) \frac{\partial u(x, y)}{\partial y} \right] + a_0(x, y)u(x, y) = f(x, y),$$

$$(x, y) \in \Omega \subset \mathbb{R}^2 \quad \text{and} \quad u(x, y) = 0 \text{ for } (x, y) \in \partial\Omega. \quad (\text{A.24})$$

Suppose that the coefficients a_{11} , a_{22} , a_0 are in $C^\infty(\overline{\Omega})$ and that they are such in Equation A.24 is a regularly elliptic boundary-value problem of order 2. Consider the case in which $f \in H^0(\Omega)$. Then, there exists a solution u of Equation A.24 and that it is in $H^2(\Omega)$ or, more specifically, a subspace of $H^2(\Omega)$ containing functions v such that $Av \in H^0(\Omega)$.

Next, consider an alternate boundary-value problem that closely resembles the expression A.24: find u such that $\forall v \in H_0^1(\Omega)$:

$$\int_{\Omega} \left(a_{11} \frac{\partial u}{\partial x} \frac{\partial v}{\partial x} + a_{22} \frac{\partial u}{\partial y} \frac{\partial v}{\partial y} + a_0 uv \right) dx dy = \int_{\Omega} f v dx dy \quad (\text{A.25})$$

The expression A.25 is referred to a *variational boundary-value problem*. Obviously, it suggests that weaker conditions may be required of the solution than that suggested by Equation A.24; second derivatives in A.24, whereas only integrals of first derivatives appear in A.25. This leads us to the following observations:

- a. Every solution of Equation A.24 is also a solution of A.25. This can be seen by multiplying both sides of the expression A.24 by a test function w and integrating by parts;
- b. Judging from the smoothness of u needed in order that Equation A.25 make sense, the solution of A.25 need be only in $H_0^1(\Omega)$. However, $H^2(\Omega)$ is densely embedded in $H^1(\Omega)$, so it is possible that these two solutions, one to A.24 and one to A.25, are the same. Actually, the expressions A.24 and A.25 are equivalent, and it makes sense to say that the solution to A.24 is an element $u \in H^2(\Omega) \cap H_0^1(\Omega)$ (ODEN; REDDY, 1976);

- c. The term “variational boundary-value problem” arises from the fact that the Equation A.25 is precisely the condition for the vanishing of the first variation of a quadratic functional which corresponds to the Equation A.24 in sense of the classical calculus of variations.

Thus, the variational formulation contains all the information found in the conventional formulation and more: it is able to work in a larger space ($H^2(\Omega) \subset H^1(\Omega) \subset H^0(\Omega) = L_2(\Omega)$) and also to consider very irregular data, e.g., distributional differential equations.

There are a plenty of methods to solve a boundary-value problems and find approximate solutions, such as, Finite Difference Method (FDM), Finite Volume Method (FVM), Finite Element Method (FEM), Boundary Element Method (BEM) and others. Regardless of the importance of the Finite Difference Method (FDM) and Finite Volume Method (FVM) for the solution of physics problems, this text will confine itself to briefly commenting only the Finite Element Method (FEM), the Boundary Element Method (BEM) and the Modified Local Green’s Function Method (MLGFM) on items that follow and discussing some mathematical details when necessary for the understandings of future topics in later chapters.

A.4 APPROXIMATED METHODS FOR BOUNDARY-VALUE PROBLEMS

Except for a few problems involving very simple partial derivative equations and geometries, it is quite impossible (as far as is known) to obtain exact solutions to most boundary-value problems in either the conventional or variational formulations. But, do not despair ourselves! There are available many goods methods for finding approximate solutions. Some of these are based on the conventional formulation, for example, finite difference methods, while others, such as Galerkin method, can be also conceived on a variational formulation (Weighted Residual).

A Variational Method approximation is based on the minimization of a

functional, as previously mentioned in last sections. The process of finding stationarity with respect to trial function parameters is an old one and is associated with the names of Rayleigh and Ritz (ZIENKIEWICZ *et al.*, 2005).

Another methods developed to obtain approximate solution to the differential equations are the Weighted Residual Methods where it starts with an estimate of the solution and demand that its weighted average error is minimized. One of the most widely employed method of this kind is “The Galerkin Method”.

The basic idea behind the Galerkin Method is an extremely simple one. Consider the variational boundary-value problem (VBVP) as in expression A.21 of finding $u \in K$, where K is a subspace of a Hilbert space H . The difficulty in trying to solve the last mentioned expression lies with the fact that K is a very large space (infinite-dimensional), with the result that it is impossible (as far as is known) to set up a logical procedure for finding the solution. But if the space K from the VBVP is replaced by an approximate space K_h with the following properties

$$K_h \subset K, \text{span}\{\phi_i\}_{i=1}^N = K_h \quad (\text{A.26})$$

where ϕ_i are few linearly independent functions (basis functions) that define K_h and $N = \dim V^h$.

The index h is a parameter that lies between 0 and 1, and whose magnitude gives some indication of how close K_h is to K ; h is related to the dimension of K_h , and as the number N of basis functions chosen gets larger, h gets smaller. In the limit, as $N \rightarrow \infty$, $h \rightarrow 0$ and we would like to choose $\{\phi_i\}$ in such a way that K_h will approach K .

Having defined the space K_h , one poses the VBVP in K_h instead of in K . That is, find a function $u_h \in K_h$ that satisfies

$$B(u_h, v_h) = \ell(v_h) \quad \forall v_h \in K_h. \quad (\text{A.27})$$

This is the essence of the Galerkin Method. In order to solve for u_h , one simply note that both u_h and v_h must be linear combination of the basis functions of K_h , so that

$$u_h = \sum_{i=1}^N \alpha_i \phi_i, \quad v_h = \sum_{j=1}^N b_j \phi_j \quad (\text{A.28})$$

Of course, since v_h is arbitrary, so are the coefficients b_k . Substituting the Equation A.28 in A.27 and using the fact that B is bilinear and ℓ is linear then

$$\sum_{i=1}^N \sum_{j=1}^N B(\phi_i, \phi_j) \alpha_i b_j = \sum_{j=1}^N \ell(\phi_j) b_j \quad (\text{A.29})$$

or, more concisely,

$$\sum_{j=1}^N b_j \left(\sum_{i=1}^N K_{ij} \alpha_i - F_j \right) = 0 \quad (\text{A.30})$$

where

$$K_{ij} = B(\phi_i, \phi_j) \quad \text{and} \quad F_j = \ell(\phi_j) \quad (\text{A.31})$$

are, respectively an $N \times N$ matrix and an N -tuple (vector). Note that K_{ij} and F_j can be evaluated in practice since ϕ_i are known functions and the forms of B and ℓ are also known.

Since the coefficients b_j are arbitrary, it follows that the Equation A.30 will only hold if the term in brackets is zero. The problem has been reduced to one of solving the set of simultaneous linear equations

$$\sum_{i=1}^N K_{ij} \alpha_i = F_j, \quad \text{for } j = 1, 2, \dots, N. \quad (\text{A.32})$$

Once the last equations are solved, the approximate solution u_h can be found from the first of Equations A.28.

In practical situations the determination of suitable basis functions for use in the Galerkin method can be extremely difficult, especially in cases for which the domain does not have a simple shape. The finite element method overcomes this difficulty by providing a systematic means for generating basis functions on domains of fairly arbitrary shape.

A.4.1 The Finite Element Method

Idealized during the 1950s, the Finite Element Method (FEM) can be understood as a general technique of constructing approximate solutions to boundary-value problems. The method involves dividing the solution domain into a finite number of simple subdomains, the "finite elements", connected to each other by the nodal points, and employs variational concepts to approximate the solution over all elements, for arbitrary boundary conditions. The overall solution is obtained by adding up the local contributions of each element. For linear elliptic problems the method leads to a system of linear equations, generally symmetrical, in the form of a band, and which can be well exploited by several numerical techniques. The combination of all these factors has led to its application in almost all areas of physics, and today, undoubtedly, is the most widespread and used method (ODEN; REDDY, 1976; ODEN; CAREY, 1983).

According to Ciarlet (1991) and Šolín *et al.* (2004), a finite element in \mathbb{R}^n is a triad $\mathcal{K} = (K_h^e; P; \Sigma)$, where

- K_h^e is a closed subset of \mathbb{R}^n with a nonempty interior and a Lipschitz-continuous boundary;
- P_p is a finite-dimensional space of real-valued functions defined over the set K_h^e of dimension $N = \dim(P_p)$;
- Σ is a set of N_p linear forms ζ_i , $1 \leq i \leq N_p$, defined over the space P_p and,

by definition, it is assumed that the set Σ is P_p -unisolvent, in the following sense:

given any real scalars α_i , $1 \leq i \leq N_p$, there exists a unique function $l \in P_p$ that satisfies

$$\zeta_i(l) = \alpha_i \quad \text{for } 1 \leq i \leq N_p, \quad (\text{A.33})$$

in particular

$$\zeta_j(l_i) = \delta_{ij} \quad \text{for } 1 \leq j \leq N_p, \quad (\text{A.34})$$

and the following identity holds

$$l = \sum_{i=1}^{N_p} \zeta_i(l) l_i \quad \text{for all } l \in P_p. \quad (\text{A.35})$$

Here δ_{ij} is the standard “*Kronecker delta*” (for discrete cases), $\delta_{ij} = 1$ if $i = j$ and $\delta_{ij} = 0$ otherwise.

The linear forms ζ_i , $1 \leq i \leq N_p$, are called the *degrees of freedom* of the finite element, and the functions l_i , $1 \leq i \leq N_p$, are called the *basis functions* of the finite element.

The basis functions are also called the *shape functions* in engineering literature. The set K_h^e itself is often called a *finite element*. What makes the method especially attractive is the fact that these basis functions are piecewise polynomials that are non-zero only a relatively small part of the domain Ω .

Once the finite element space K_h is constructed, it can be used in the Galerkin Method to obtain an approximate solution. In this context, FEM clearly appears as a methodology to generate approximation spaces, and the approximate solution is effectively obtained using the Galerkin Method. Other methods besides the Galerkin Method may be used to obtain the approximate solution once the approximate space has been built. Some examples of alternatives are the Least Square Method and the Collocation Method (ZIENKIEWICZ *et al.*, 2005).

A.4.2 The Boundary Element Method

The Boundary Element Method (BEM) is an integral technique that has been employed in several applications. Although integral methods were known since the end of the 19th century, BEM has been boosted only after the introduction of Finite Element Method discretization techniques in late 1960s. In this method, only the boundary is discretized through pieces called "boundary elements", connected together by the nodal points. The solution in domain is due to a process of integration on boundary, being this one of the advantages of the BEM compared to FEM, since the dimension of the problem is reduced, decreasing the data volume and the size of the matrices. Thus, the BEM becomes highly recommended in problems where the domain discretization is complex, for example, in three-dimensional analyzes. In contrast, their matrices are not generally sparse, which does not favor the use of techniques usually employed in FEM, such as "band" or "sky-line" storage.

The Boundary Element Method is also efficient in solving singular problems, e.g., fracture mechanics, in treatment of infinite domains, and, unlike FEM, allows the use of discontinuous elements, which, in many problems, is interesting. Its major disadvantage is that it depends on the explicit knowledge of a fundamental solution appropriate to the problem, which restricts it only to cases where such solution is available, or where it can be determined by dual reciprocal techniques (BREBBIA, 1992). For this reason, some mechanical problems have not yet been adequately solved by the BEM, such as shells with any curvature and some problems involving non-homogeneous media, such as laminate composite materials. In addition, some integrals in the process are singular, requiring special numerical techniques (MACHADO, 1992).

A.4.3 The Modified Local Green's Function Method

The Modified Local Green's Function Method (MLGFM) is an integral

method that brings together three different techniques: the Finite Element Method (FEM), the Boundary Element Method (BEM) and the Green's Function Method (GFM). Idealized at the end of the 1980s by Barcellos e Silva (1987), MLGFM uses FEM as a residual process to locally approximate the "Green's Function projections" on the space generated by the finite elements, and then employs the values of these projections, equivalent to a "fundamental solution", in a boundary integral system, solved by the "Direct Boundary Element Method" (DBEM). The resulting system of equations, in domain and on boundary, involves sufficiently regular integrals, which can be solved by conventional numerical integration techniques.

Several applications have already been performed through MLGFM and there is a reserved chapter – chapter 4 – to discuss it. The MLGFM is a very accurate method, even with coarse meshes, which allows small volume of data supplied to a computer program. By using established techniques of Finite Elements and Boundary Elements, the discretization of the problem is quite simple. Analogously to a hybrid method, both the primary variables, such as the displacements and temperatures, and dual variables, such as flow and stresses, are equally precise. It is also observed a nodal super convergence of the results, which makes this method endorsed to adaptive processes. Among all the properties of the MLGFM, the most significant is the automatic determination of the fundamental solution of the problem, even in cases where it is not explicitly known. It really represents an excellent alternative for the Boundary Element Method to be extended to new fields of application (BARBIERI, 1992; MACHADO, 1992). This is exactly what this work does!

Appendix B

B.1 ELASTO STATIC CLASSIC RELATIONS

In elasticity theory one of the greatest interests is the solution of called *Lamé–Navier* equations of elasticity (REDDY, 2008). This expression represents the equilibrium equations expressed in terms of the displacement field for homogeneous, isotropic and linear media such that

$$(\lambda + G)\nabla(\nabla \cdot \mathbf{u}) + G\nabla^2 \mathbf{u} + \mathbf{b} = 0 \quad (\text{B.36})$$

or in index notation

$$(\lambda + G)u_{j,ji} + Gu_{i,jj} + b_i = 0 \quad (\text{B.37})$$

where \mathbf{u} is the displacement vector

$$\mathbf{u} = \begin{Bmatrix} u_x \\ u_y \\ u_z \end{Bmatrix} \quad (\text{B.38})$$

and \mathbf{b} is the body force vector

$$\mathbf{b} = \begin{Bmatrix} b_x \\ b_y \\ b_z \end{Bmatrix} \quad (\text{B.39})$$

whereas ∇ is the differential operator *nabla* or *del*, λ and G are the classic *Lamé* constants related to the *Young's Modulus*, E and *Poisson's ratio*, ν given by

$$\lambda = \frac{\nu E}{(1+\nu)(1-2\nu)} \quad (\text{B.40})$$

and

$$G = \frac{E}{2(1+\nu)}. \quad (\text{B.41})$$

In order to have a “*well-posed*” problem it is necessary to set out the domain and its geometry and also to prescribe the boundary conditions in a proper way.

The boundary value problems of elasticity can be classified into three types on the basis of the nature of specified boundary conditions, such as

- TYPE I. Boundary value problems in which if all specified boundary conditions are of the prescribed displacement type like

$$\mathbf{u} = \bar{\mathbf{u}}(x) \quad \text{on } \partial\Omega \quad (\text{B.42})$$

where $\partial\Omega$ is the boundary of the domain Ω .

- TYPE II. Boundary value problems in which if all specified boundary conditions are of the prescribed traction type like

$$\mathbf{T} = \bar{\mathbf{T}}(x) \quad \text{on } \partial\Omega \quad (\text{B.43})$$

where \mathbf{T} is the traction vector in a point $x \in \partial\Omega$ and possess a normal vector \mathbf{n} in almost every points.

- TYPE III. Boundary value problems in which if all specified boundary conditions are of the mixed type

$$\mathbf{u} = \bar{\mathbf{u}}(x) \quad \text{on } \partial\Omega_{\mathcal{D}} \quad \text{and} \quad \mathbf{T} = \bar{\mathbf{T}}(x) \quad \text{on } \partial\Omega_{\mathcal{H}} \quad (\text{B.44})$$

where $\partial\Omega_{\mathcal{D}} \cup \partial\Omega_{\mathcal{N}} = \partial\Omega$. Most practical problems fall into the category of boundary value problems of Type III.

The traction vector is related to the stress tensor by

$$\bar{\mathbf{T}}(x) = \boldsymbol{\sigma} \cdot \mathbf{n} \quad (\text{B.45})$$

wherein is defined by the generalized Hooke's law (in index notation)

$$\sigma_{ij} = \lambda \varepsilon_{mm} \delta_{ij} + 2G \varepsilon_{ij} \quad (\text{B.46})$$

which in

$$\varepsilon_{ij} = \frac{1}{2} (u_{i,j} + u_{j,i}) \quad (\text{B.47})$$

$$\delta_{ij} = \begin{cases} 0 & \text{if } i \neq j \\ 1 & \text{if } i = j \end{cases} \quad (\text{B.48})$$

where $(\cdot)_{,j}$ denotes partial derivative with respect to the “ j ” coordinate of the reference coordinate system, ε_{ij} is the components of the strain tensor and σ_{ij} is the components of the stress tensor.

The Equation B.46 can be properly rewritten as

$$\sigma_{ij} = D_{ijkl} \varepsilon_{kl} \quad (\text{B.49})$$

which in

$$D_{ijkl} = \frac{2G\nu}{1-2\nu} \delta_{ij} \delta_{kl} + G(\delta_{ik} \delta_{jl} + \delta_{il} \delta_{jk}) \quad (\text{B.50})$$

and D_{ijkl} are called elastic stiffness coefficients or, in matrix representation, the elasticity matrix \mathbf{D} .

There exists a class of problems in elasticity, due to geometry, boundary

conditions, and external applied loads, has their solutions (i.e., displacements and stresses) not dependent on one of the coordinates. Such problems are called *plane elasticity problems* (plane strain and plane stress problems). The discussion here is limited to isotropic materials.

B.1.1 Plane Strain Problems

The plane strain problems are characterized by the displacement field

$$u_x = u_x(x, y), \quad u_y = u_y(x, y), \quad u_z = 0 \quad (\text{B.51})$$

where (u_x, u_y, u_z) denote the components of the displacement vector \mathbf{u} in the (x, y, z) coordinate system.

The displacement field from expression B.51 results in the following strain field:

$$\varepsilon_{xz} = \varepsilon_{yz} = \varepsilon_z = 0, \quad (\text{B.52})$$

$$\varepsilon_x = \frac{\partial u_x}{\partial x}, \quad 2\varepsilon_{xy} = \frac{\partial u_x}{\partial y} + \frac{\partial u_y}{\partial x}, \quad \varepsilon_y = \frac{\partial u_y}{\partial y}. \quad (\text{B.53})$$

Clearly, the body is in a state of plane strain. For an isotropic material, the stress components and stress-strain relations are given by

$$\sigma_{xz} = \sigma_{yz} = 0, \quad \sigma_z = \nu(\sigma_x + \sigma_y), \quad (\text{B.54})$$

$$\begin{Bmatrix} \sigma_x \\ \sigma_y \\ \sigma_{xy} \end{Bmatrix} = \frac{E}{(1+\nu)(1-2\nu)} \begin{bmatrix} 1-\nu & \nu & 0 \\ \nu & 1-\nu & 0 \\ 0 & 0 & \frac{(1-2\nu)}{2} \end{bmatrix} \begin{Bmatrix} \varepsilon_x \\ \varepsilon_y \\ 2\varepsilon_{xy} \end{Bmatrix}. \quad (\text{B.55})$$

The equations of equilibrium of three-dimensional linear elasticity, with the body-force components

$$b_z = 0, \quad b_x = b_x(x, y), \quad b_y = b_y(x, y) \quad (\text{B.56})$$

reduce to the following two plane-strain equations

$$\frac{\partial \sigma_x}{\partial x} + \frac{\partial \sigma_{xy}}{\partial y} + b_x = 0, \quad (\text{B.57})$$

$$\frac{\partial \sigma_{xy}}{\partial x} + \frac{\partial \sigma_y}{\partial y} + b_y = 0. \quad (\text{B.58})$$

The boundary conditions are either the stress type

$$\begin{aligned} T_x &= \sigma_x n_x + \sigma_{xy} n_y = \bar{T}_x \\ T_y &= \sigma_{xy} n_x + \sigma_y n_y = \bar{T}_y \end{aligned} \quad \text{on } \partial\Omega_{\mathcal{H}} \quad (\text{B.59})$$

or the displacement type

$$u_x = \bar{u}_x, \quad u_y = \bar{u}_y \quad \text{on } \partial\Omega_{\mathcal{D}}. \quad (\text{B.60})$$

Here (n_x, n_y) denote the components (or direction cosines) of the unit normal vector \mathbf{n} on boundary $\partial\Omega$, \bar{T}_x and \bar{T}_y are the components of the specified traction vector, and \bar{u}_x and \bar{u}_y are the components of specified displacement vector. Only one element of each pair, (u_x, T_x) and (u_y, T_y) , may be specified (prescribed) at a boundary point.

B.1.2 Plane Stress Problems

A state of plane stress is defined as one in which the following stress field exists

$$\sigma_{xz} = \sigma_{yz} = \sigma_z = 0, \quad u_z = 0,$$

$$\sigma_x = \sigma_x(x, y), \quad \sigma_y = \sigma_y(x, y), \quad \sigma_{xy} = \sigma_{xy}(x, y). \quad (\text{B.61})$$

The stress-strain relations of a plane stress state are

$$\begin{Bmatrix} \sigma_x \\ \sigma_y \\ \sigma_{xy} \end{Bmatrix} = \frac{E}{1-\nu^2} \begin{bmatrix} 1 & \nu & 0 \\ \nu & 1 & 0 \\ 0 & 0 & \frac{(1+\nu)}{2} \end{bmatrix} \begin{Bmatrix} \varepsilon_x \\ \varepsilon_y \\ 2\varepsilon_{xy} \end{Bmatrix} \quad (\text{B.62})$$

The equations of equilibrium as well as boundary conditions of a plane stress problem are the same as those listed in Strain State Problem section – from Equations B.57 to B.58.

Appendix C

C.1 THE EMLGFM ALGORITHM FLOWCHART

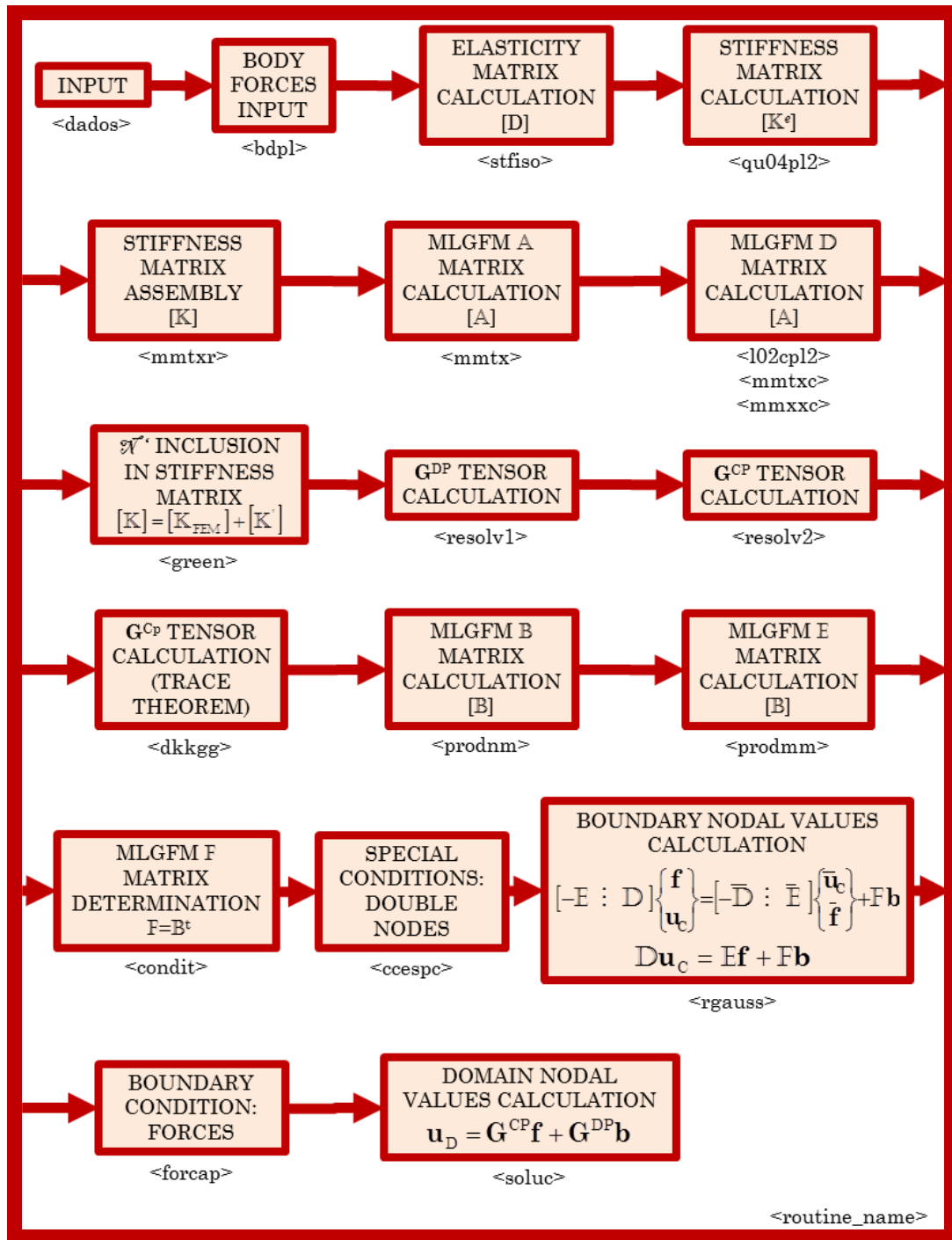


Figure C.1 – EMLGFM approximate solution implementation.